“Deciphering Stromal Dysregulations in Clonal Hematopoiesis and Myelodysplasia”

Dissertation

zur Erlangung des Grades

“Doktor der Naturwissenschaften”

im Promotionsfach Biochemie

Am Fachbereich Chemie, Pharmazie,

Geografie und Geowissenschaften

der Johannes Gutenberg-Universität Mainz

Kevin Woods

Geboren am 03.09.1993 in Mainz

Mainz, 2023

1. Gutachter: Prof. Dr. med. Matthias Theobald

2. Gutachter: Prof. Dr. Dirk Schneider

Tag der mündlichen Prüfung: 30.05.2023

Curriculum Vitae

Personal Details

Name:	Kevin Keith Woods
Address:	Am Fort Elisabeth 35, 55131 Mainz
E-Mail:	kwoods@gmx.de
Date and place of Birth:	03.09.1993, Mainz
Nationality:	German

Education

04/2019–today	**PhD studies in Biochemistry** at the Department of Chemistry, Pharmacy, Geography and Geosciences, Johannes Gutenberg-University Mainz Guezguez Laboratory at the German Consortium for Translational Cancer Research (DKTK), Mainz/Frankfurt 3. Medical Clinic and Policlinic, University Hospital Mainz Title: "Deciphering Stromal Dysregulations in Clonal Hematopoiesis and Myelodysplasia"
11/2017–02/2018	Erasmus research internship at the Institute of Molecular Science (ICMol) in Valencia
10/2016–03/2019	**Master of Science** in Biomedical Chemistry at the Johannes Gutenberg-University Mainz **Master thesis** on "Stromal Regulation of Therapeutic Response in Prostate Cancer"
10/2012–09/2016	**Bachelor of Science** in Biomedical Chemistry at the Johannes Gutenberg-University Mainz **Bachelor thesis** on "Base Excision Repair Enzymes in Granulocytes

Summary

Myelodysplastic neoplasms (MDS) are a group of hematological malignancies affecting White Blood Cell (WBC) differentiation, most commonly arising in the elderly population. If left untreated, patients can suffer from dysplasia (abnormal WBC called blasts) and cytopenia (low number of normal WBC), resulting in infections and heavy bleeding. The causes for this inefficient hematopoiesis are recurrent mutations in Hematopoietic Stem and Progenitor Cells (HSPC) that cause clonal expansion, genomic instability, and ineffective differentiation.

Recently, Clonal Hematopoiesis of Indeterminate Potential (CHIP) has been recognized as a premalignant stage that precedes MDS onset. CHIP carriers show clonal hematopoiesis, often without adverse effects or hematological symptoms. The dominant Hematopoietic Stem Cell (HSC) founding clone often shows mutations in the same epigenetic regulator genes that are found in MDS (e.g., DNMT3A, TET2), but only rarely mutations in oncogenes. Mutation favors the growth of this clone, slowly displacing the progeny of other HSPCs (clonal evolution). While this clonal hematopoiesis does not have adverse effects in most patients, an approximately 40% higher risk for cardiovascular disease was noted. In addition, people with CHIP have a yearly chance of 0.5% to 1% to progress to MDS or Acute Myeloid Leukemia (AML), underlining the importance of understanding this condition as a potential clinical biomarker in the elderly. To identify the underlying causes for progression from CHIP to MDS or AML, we need to reexamine the locus of inefficient hematopoiesis, i.e., the bone marrow microenvironment or niche.

The bone marrow niche describes the cradle of hematopoiesis, the microenvironment of HSPC in the bone marrow. These stem and progenitor cells are not isolated but are in close contact with regulatory stromal cells and immune cells that secrete factors for quiescence, self-renewal and homing on one hand, and proliferation, differentiation, and mobilization on the other.

The aim of this thesis was the morphological, cellular, and molecular characterization of the HSC niche in human CHIP and MDS bone marrow samples. This was achieved using multiplexed immunofluorescence spatial imaging of human and murine bone marrow samples as well as single cell RNA sequencing of patient-matching human bone marrow aspirate.

Summary

Imaging studies of the human bone marrow in CHIP samples showed trends toward higher sinusoidal content but were inconclusive for other stromal populations. Using a high Variant Allele Frequency (VAF) CHIP mouse model (DNMT3A^{R878H}), a significant remodeling of the BM by expansion of sinusoids and adipogenic MSC as well as an accumulation of Treg was detected. The findings were supported by the detection of an adipogenic transcriptional bias as well as the emergence of a stress-induced MSC subset in human CHIP-MSC in scRNA seq studies. These cell populations were connected to inflammatory and angiogenic processes that were present on a transcriptional level in stromal and T cells, supported by the emergence of several specialized T cell populations that are typical for chronic inflammation. Together, the changes in the BM microenvironment in CHIP are the result of chronic inflammatory processes, which promote angiogenesis, MSC differentiation bias and subsequent adipogenesis. As a result, HSC support is diminished, increasing the risk of stress hematopoiesis-related acquisition of somatic mutations that lead to the development of MDS.

MDS samples showed morphological alterations in bone marrow cellularity, sinusoidal vessel density and increased MSC density. This was accompanied by a reduction of immunoregulative Treg. Single cell RNA sequencing of stromal cells revealed the prevalence of the same stress-induced MSC subset that was found in CHIP donors and a shift toward osteogenic and osteochondrogenic differentiation of MSC. T lymphocytes were shifted toward cytotoxic T cell subsets, and gene set enrichment analysis revealed higher metabolic activation states, alterations in T helper differentiation pathways and increased inflammatory potential of several subsets. The inflammatory and pro-angiogenic processes at play were reproduced by an *in vitro* model of MSC and MDS blasts, highlighting the importance of this axis for stroma remodeling and MDS emergence.

Zusammenfassung

Myelodysplastische Neoplasien (MDS) sind bösartige Erkrankungen des blutbildenden Systems, welche die Differenzierung von Leukozyten beeinträchtigen und meist ältere Menschen betreffen. Unbehandelt leiden Betroffene meist unter Dysplasien (charakterisiert durch die Präsenz abnormer Leukozyten im Knochenmark, sogenannter Blasten) und Zytopenien (verminderte Konzentration von Zellen im Blut), was oft zu Infektionen oder unkontrollierten Blutungen führt. Grund für diese ineffiziente Hämatopoese sind Mutationen in Hämatopoetischen Stamm- und Progenitorzellen (HSPC), die klonale Expansion, genomische Instabilität und ineffektive Differenzierung induzieren.

Kürzlich wurde klonale Hämatopoese von unbestimmtem Potenzial (engl. Clonal Hematopoiesis of Indeterminate Potential, CHIP) als prämaligne Vorstufe von MDS erkannt. CHIP-Träger weisen klonale Hämatopoese auf, ohne dabei hämatologische Symptome zu zeigen. Der dominante Hämatopoetische Stammzell(engl. Hematopoietic Stem Cell, HSC)-Klon zeigt oft Mutationen in den gleichen Genen für epigenetische Kontrollproteine, die auch in MDS zu finden sind (z.B. DNMT3A und TET2), jedoch selten in Onkogenen. Dies resultiert im Wachstum des Klons, wodurch dessen Nachkommen langsam die anderer HSCs verdrängen (klonale Evolution). Diese klonale Hämatopoese hat zwar keine direkten nachteiligen Effekte, dennoch zeigen CHIP-Träger ein um 40% erhöhtes Risiko für kardiovaskuläre Krankheiten und ein Risiko von 0,5–1% pro Jahr, MDS oder Akute Myeloische Leukämie (AML) zu entwickeln, was die Signifikanz von CHIP als potenziellem klinischem Biomarker in der älteren Bevölkerung unterstreicht. Um die zugrundeliegenden Ursachen des Fortschreitens von CHIP zu MDS/AML zu verstehen, muss der Blick auf den Ursprung der ineffizienten Hämatopoese gerichtet werden, die Knochenmarksmikroumgebung („Nische“), welche die Mikroumgebung von HSPC im Knochenmark beschreibt. HSPC liegen nicht isoliert vor, sondern sind in engem Kontakt mit regulatorischen Stroma- und Immunzellen, welche einerseits Faktoren für die Quieszenz, Selbsterneuerung und Rekrutierung ins Knochenmark, und andererseits Faktoren für Proliferation, Differenzierung und Mobilisierung sekretieren.

Ziel dieser Dissertation ist die morphologische, zelluläre und molekulare Charakterisierung der HSC-Nische von CHIP- und MDS-Knochenmarksproben. Dies wurde durch multiplex-fluoreszierende immunhistochemische Färbungen von menschlichen und murinen Knochenmarksbiopsaten, sowie durch Einzelzell-RNA-

Sequenzierung (scRNA Seq) von dazugehörigen menschlichen Knochenmarksaspiraten erreicht.

Die Bildgebungsstudien von menschlichen CHIP-Knochenmarksproben zeigten Tendenzen zu mehr sinusoiden Blutgefäßen, jedoch waren die Ergebnisse anderer Stromapopulationen nicht aussagekräftig. Durch Zuhilfenahme eines Mausmodells für CHIP mit hoher Allelfrequenz ($DNMT3A^{R878H}$) konnte eine signifikante Umformung des Knochenmarks, gekennzeichnet durch Expansion von Sinusoiden und adipogenen MSC sowie durch Akkumulation von regulatorischen T-Zellen (Treg), festgestellt werden. Diese Befunde wurden bekräftigt durch die Detektion eines adipogenen Differenzierungsbias sowie das Auftreten einer stressinduzierten MSC-Subpopulation in menschlichen CHIP-Trägern in scRNA Seq-Studien. Diese Zellpopulationen konnten inflammatorischen und angiogenen Prozessen zugeordnet werden, welche auf transkriptionellem Level in Stroma- und T-Zellen vorhanden waren. Zudem waren verschiedene spezialisierte T-Zell-Populationen, die in chronischen Entzündungsbildern auftreten, präsent. Zusammengenommen sind die Veränderungen in der Knochenmarksnische das Resultat chronischer entzündlicher Prozesse, was zu Angiogenese, Differenzierungsbias von MSC und subsequent gesteigerter Adipogenese führt. Dadurch wird die Unterstützung von HSC vermindert, was das Risiko einer Stresshämatopoese-induzierten Ansammlung somatischer Mutationen erhöht und die Entwicklung von MDS auslösen kann.

MDS-Proben wiesen morphologische Veränderungen in der Zellularität und der Dichte des sinusoidalen Netzwerks sowie eine Expansion von MSC auf; gleichzeitig war die Häufigkeit von Treg vermindert. ScRNA Seq von Stromazellen zeigte die gleiche stressinduzierte MSC-Subpopulation, die auch in CHIP-Trägern auftrat, sowie einen Wechsel hin zu osteogener und osteochondrogener Differenzierung von MSC. T-Lymphozyten wiesen vermehrt zytotoxische Populationen auf, und eine Genexpressionsanalyse identifizierte erhöhte metabolische Prozesse, Veränderung in der Differenzierung von T-Helferzellen sowie verstärktes proinflammatorisches Potenzial mehrerer Subpopulationen. Diese inflammatorischen und angiogenen Prozesse wurden durch ein *in-vitro*-Modell von MSC und MDS-Blasten reproduziert, was die Wichtigkeit der MSC-MDS-Achse für die Veränderungen in der Knochenmarksnische und die Entstehung von MDS unterstreicht.

List of abbreviations

AKT	**Protein Kinase B**
AML	Acute Myeloid Leukemia
Angpt1	Angiopoietin 1
ANOVA	Analysis of Variance
ASXL1	Additional Sex Combs-Like 1
BCAM	Basal Cell Adhesion Molecule
BM	Bone Marrow
BMAT	Bone Marrow Adipose Tissue
BMC	Bone Marrow Cellularity
BMP	Bone Morphogenetic Protein
BSA	Bovine Serum Albumin
C/EBP	CCAAT-Enhancer-Binding proteins
CALCRL	Calcitonin Receptor-Like
CAR	CXCL12-Abundant Reticular
CCUS	Clonal Cytopenia of Undetermined Significance
CD	Cluster of Differentiation
CHIP	Clonal Hematopoiesis of Indeterminate Potential
CLP	Common Lymphoid Progenitor
CM	Conditioned Medium
CMP	Common Myeloid Progenitor
COL	Collagen
CRP	C-Reactive Protein
CXCL	Chemokine (C-X-C motif) Ligand
CXCR	Chemokine (C-X-C motif) Receptor
DAPI	4′,6-Diamidino-2-phenylindole
DBE	Dibenzyl Ether
DCM	Dichloromethane
DEG	Differentially Expressed Genes
DMSO	Dimethyl Sulfoxide
DNA	Desoxyribonucleic Acid
DNMT	DNA Methyltransferase
ECM	Extracellular Matrix
EDTA	Ethylenediaminetetraacetic Acid
EGF	Epidermal Growth Factor
EGF(R)	Epidermal Growth Factor (Receptor)
EV	Extracellular Vesicles
FACS	Flow Cytometry-Assisted Cell Sorting
FFPE	Formalin-Fixed, Paraffin Embedded
FGF	Fibroblastic Growth Factor
FSH	Follicle-Stimulating Hormone
g	Relative centrifugal force
G-CSF	Granulocyte Colony Stimulating Factor
GFAP	Glial-Fibrillary Associated Protein
GFP	Green Fluorescent Protein
GM-CSF	Granulocyte-Macrophage Colony Stimulating Factor
GMP	Granulocyte-Monocyte Progenitor
GSEA	Gene Set Enrichment Analysis
h	Hour(s)
H…K…	Histone … Lysine …
HGF	Hepatocyte Growth Factor
HIER	Heat-Induced Epitope Retrieval
HMA	Hypomethylating Agents
hPlt	Human Platelet Lysate
HR	Higher-Risk
HSC	Hematopoietic Stem Cell
HSP	CD4/CD8 Heat-Shock Protein stimulated
HSPC	Hematopoietic Stem and Progenitor Cell
IDH1, 2	Isocitrate Dehydrogenase (NADP+) 1, 2
IF	Immunofluorescence
IFN	Interferon
IGF1	Insulin-like growth factor 1
IL(R)	Interleukin (Receptor)
IPSS-R	International Prognostic Point System Revised
IR	Intermediate-Risk
IRAK4	Interleukin-1 Receptor-Associated Kinase 4
JAK2	Janus Kinase 2

KRAS	Kirsten Rat Sarcoma Virus
LEPR	Leptin Receptor
LFQ	Label-Free Quantitation
LMPP	Lymphoid-Primed Multipotent Progenitor
Log2FC	Log_2 of Fold Change
LR	Lower-Risk
LT	Long Term
MAIT	Mucosal Associated Invariant T cell
MAPK	Mitogen-Activated Protein Kinase
MAPK/ERK	Ras-Raf-MEK-ERK pathway
MDS	Myelodysplastic Neoplasms
MeOH	Methanol
MEP	Megakaryocyte-Erythroid Progenitor
MIP-1a	Macrophage Inflammatory Protein-1a
MK	Megakaryocyte
MPP	Multipotent Progenitors
MSC	Mesenchymal Stromal Cell
n	Technical replicates
N	Biological replicates
NFκB	Nuclear factor kappa-light-chain-enhancer of activated B cells
NK	Natural Killer
NLRP3	NLR family pyrin domain containing 3
NPM1	Nucleophosmin 1
NRAS	Neuroblastoma RAS viral oncogene homolog
NRP1	Neuropilin 1
ns	not significant
OB	Osteoblast
OPN	Osteopontin
OSM	Oncostatin M
OSX	Osterix
P/S	Penicillin/Streptomycin
PAI-1	Plasminogen Activator Inhibitor-1
PBS	Phosphate Buffered Saline
PDGF	Platelet-Derived Growth Factor
PDGF-R	Platelet-Derived Growth Factor Receptor
PFA	Paraformaldehyde
PI3K	Phosphoinositide 3-Kinase
polyI:C	Polyinosinic:polycytidylic acid
PPARy	Peroxisome Proliferator-Activated Receptor gamma
PPM1D	Protein Phosphatase, Mg2+/Mn2+ Dependent 1D
PTH	Parathyroid Hormone
PTwH0.5	PBS-Tween (0.5%)
RAMP1	Receptor Activity Modifying Protein 1
RNA	Ribonucleic Acid
ROI	Region of Interest
ROS	Reactive Oxygen Species
RUNX2	Runt-related transcription factor 2
SASP	Senescence-Associated Secretory Profile
SCF	Stem Cell Factor
scRNA seq	Single Cell RNA Sequencing
SCT	Stem Cell Transplantation
SDF-1	Stromal-Derived Factor 1
SF3B1	Splicing Factor 3b Subunit 1
SN	Sympathetic Neuron
SNS	Sympathetic Nervous System
SPARC	Secreted Protein Acidic and Rich in Cysteine
SRSF2	Serine and arginine Rich Splicing Factor 2
ST	Short Term
Tcm	Central Memory T cell
Tem	Effector Memory T cell
TET2	Tet methylcytosine dioxygenase 2
TGF-β	Transforming Growth Factor β
TH	Tyrosine Hydroxylase
Th	Helper T cell
TNFα	Tumor Necrosis Factor α
TP53	Tumor Protein P53

List of abbreviations

TPO	Thrombopoietin
Treg(s)	Regulatory T cell(s)
UEA-1	Ulex Europaeus Agglutinin-1
UMAP	Uniform Manifold Approximation and Projection
VAF	Variant Allele Frequency
VCAM1	Vascular Cell Adhesion Molecule 1
VEGF(R)	Vascular Endothelial Growth Factor (Receptor)
WBC	White Blood Cell
WHO	World Health Organization

Table of content

Table of content

1 Introduction

1.1 Hematopoiesis and the hematopoietic niche

1.1.1 The anatomy of the bone marrow

Bone Marrow (BM) is the site of hematopoiesis in mammals and is primarily located in the skeleton, especially in large bones (Travlos 2006), such as the femur and the iliac crest. There are two types of BM (termed “red” and “yellow”), characterized by appearance, composition, and function. While constitutive hematopoiesis occurs in the red marrow, yellow marrow is primarily composed of adipocytes (known as Bone Marrow Adipose Tissue, BMAT) and is thought to confer no hematologic activity. The latter however is important for bone metabolism and Hematopoietic Stem Cell (HSC) regulation (Li et al. 2019), which is addressed in more detail in chapter 1.3.4. After an injury, it can become active and transform into red marrow, a process called reconversion. The balance of both types of BM changes during aging: in children, only red marrow is present, but yellow marrow takes over quickly and becomes dominant in adult and aged individuals. In long bones like the femur, yellow BM is located in the diaphysis in the center of the bone and extends with age axially and peripherally, while red marrow is located in the femoral head in adults. The ratio of yellow and red bone marrow is reflected in the overall Bone Marrow Cellularity (BMC). The cellularity changes from 40–60% in young adults to 20–40% in older people, where the bone cavity is filled by bone marrow adipocytes (Longo 2008). Different skeletal sites change to varying extents; while the femur cellularity is heavily affected during aging, the BMC of pelvis and sternum is steadier (Figure 1). This alteration during aging influences the cellular composition of the niche (Matteini et al. 2021).

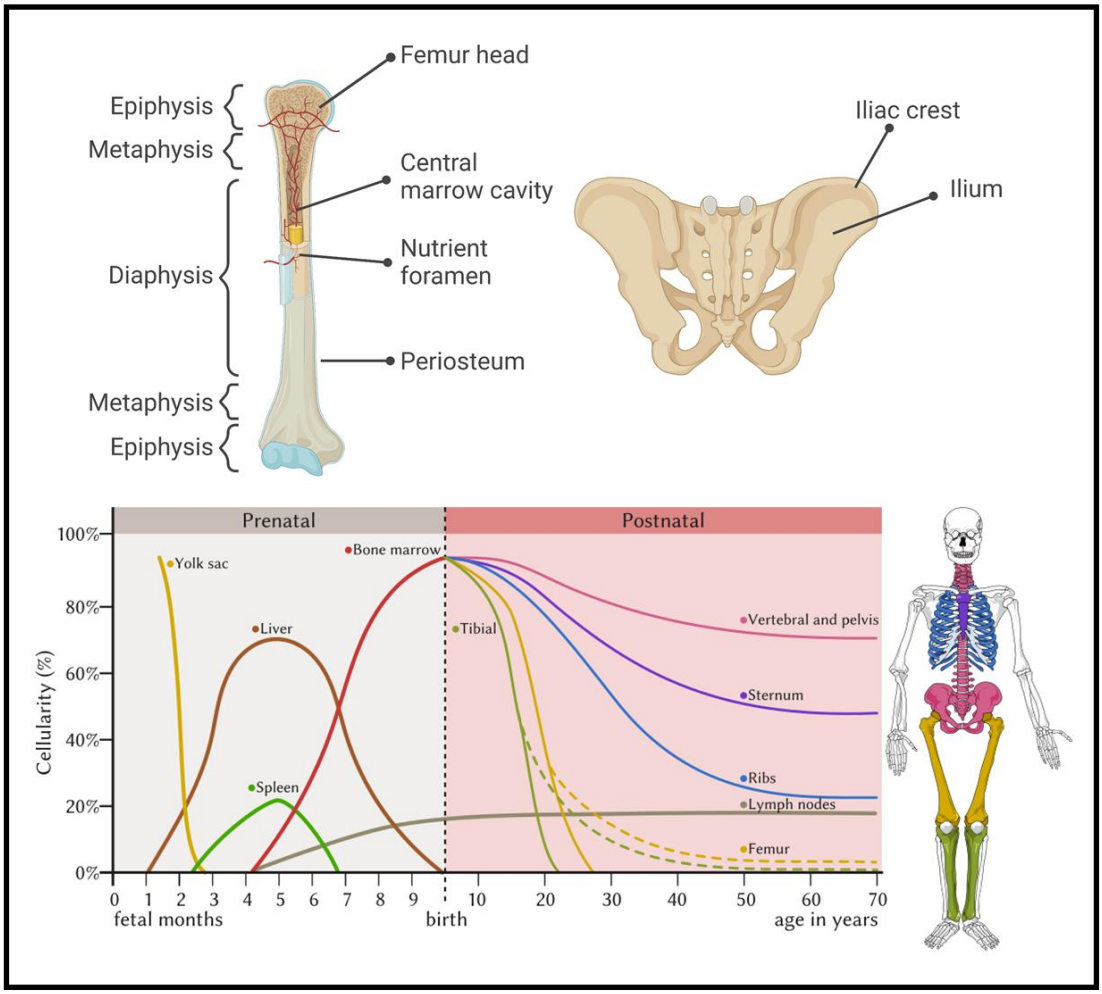

Figure 1: Anatomical sites of hematopoiesis in adult humans. Top: Anatomical structure of the femur and the pelvis. Bottom: Changes in bone marrow cellularity for different bones during the human lifespan. Figure was created with Biorender.com.

1.1.2 Hematopoiesis

Hematopoiesis is a continuous process where HSC self-renew, form, and replenish blood and immune cells. In adults, hematopoiesis occurs mainly in the bone marrow of long and flat bones like femur, tibia, sternum and pelvis, although the final maturation step for immune cells occurs in secondary locations, such as the spleen, thymus or lymph nodes (Lee et al. 2019). Over the last two decades, mouse models have been developed as a gold standard in stem cell biology that allowed to understand and delineate HSC regenerative properties via serial engraftment studies. These studies have identified two distinct HSC populations, which self-renew but exhibit Long (LT, longer than 3–4 months)- or Short-Term (ST, up to 1 month) reconstitution capacity (Adolfsson et al. 2001; Cheng et al. 2020). According to the classical hierarchical hematopoiesis model, which is based on

flow cytometry characterization and fractionation of cell populations by surface marker expression, ST-HSC produce Multipotent Progenitors (MPP), that can differentiate into two paths toward either Lymphoid-primed Multipotent Progenitors (LMPP) or Common Myeloid Progenitors (CMP). CMPs can give rise to Megakaryocyte-Erythroid Progenitors (MEP), which form erythrocytes and megakaryocytes, or Granulocyte-Macrophage Progenitors (GMP), which produce neutrophils and granulocytes. GMP can also be delineated from LMPP, which are also responsible for the formation of Common Lymphoid Progenitors (CLP) and the lymphoid lineage (NK cells, B cells, T cells) (Boiko and Borghesi 2012). HSC and committed progenitor populations can be combined into a common cell entity, referred to as Hematopoietic Stem and Progenitor Cells (HSPC).

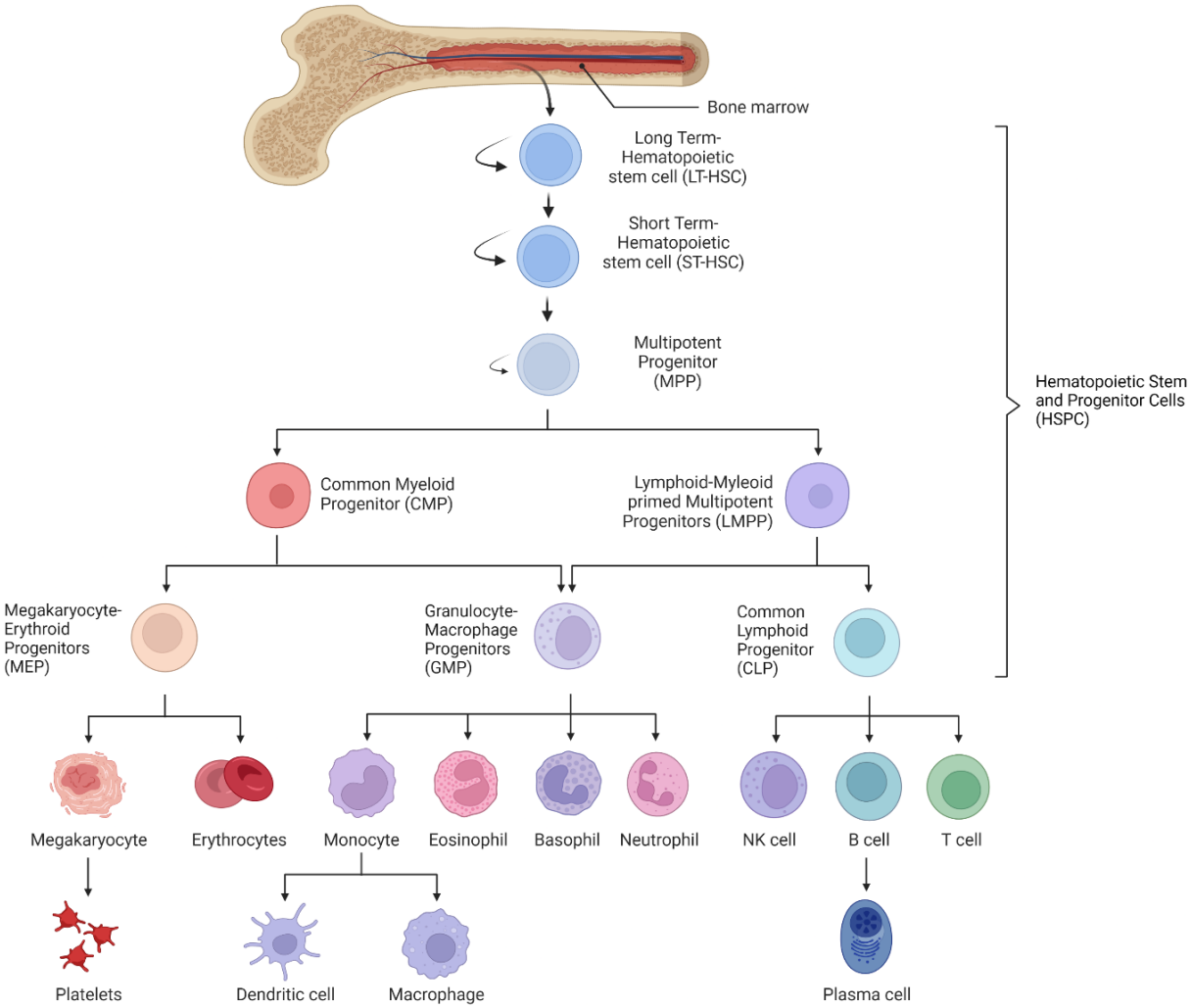

Figure 2: Schematic hematopoietic tree with HSC on top of the hierarchy, differentiating into HSPC populations. These in turn give rise to mature progeny (Boiko and Borghesi 2012). Figure created with Biorender.com.

The classic hierarchical model for hematopoiesis has been recently revised due to the emergence of single-cell RNA sequencing (scRNA seq) approaches that showed the lineage commitment as a more nuanced and continuous process rather than discrete steps

towards differentiation, and HSC priming at a much earlier stage in hematopoiesis than previously thought (Haas et al. 2018; Macaulay et al. 2016).

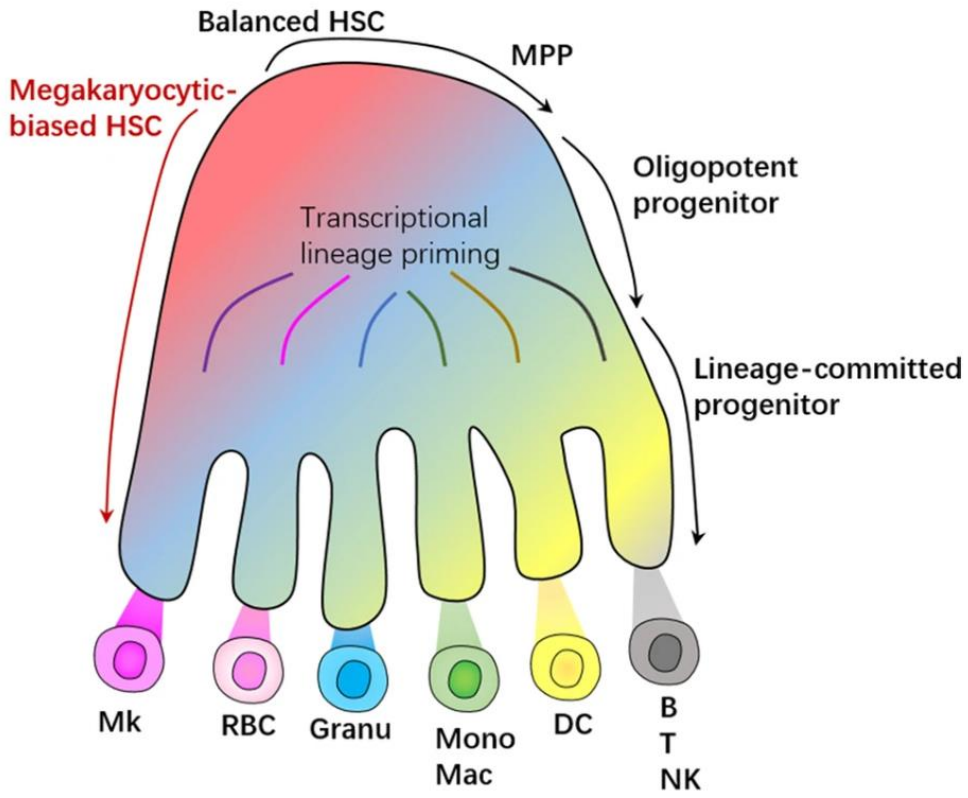

Figure 3: Waddington landscape model of HSC "continuum" differentiation with earlier priming of HSC towards lineage differentiation (Zhang et al. 2022a). Mk: Megakaryocyte, RBC: Red Blood Cell, Granu: Granulocyte, Mono: Monocyte, Mac: Macrophage. DC: Dendritic Cells.

Nevertheless, the classical model still provides valuable information about distribution of progenitors, lineage bias, and functional defects in HSPC. This is important when alterations in hematopoiesis occur, for instance while an organism ages.

1.1.3 Clonal hematopoiesis

During aging, somatic mutations occur and accumulate in all tissues in the human body (Szilard 1959), also in LT-HSC, which in humans proliferate at a rate of approximately once every 40 weeks (Catlin et al. 2011). Some of these mutations confer a growth advantage, leading to the expansion of a single HSC or progenitor clone and its progeny. This expansion, termed Clonal Hematopoiesis of Indeterminate Potential (CHIP) is not pathologic, although it is associated with a 40% increased risk for cardiovascular disease and a 0.5–1% risk per year of development of hematologic malignancies, such as Myelodysplastic Neoplasms (MDS) or Acute Myeloid Leukemia (AML) (Steensma et al.

2015; Libby et al. 2019; Jaiswal et al. 2017). Another non-malignant state called Clonal Cytopenia of Undetermined Significance (CCUS) can be discerned from CHIP by presence of peripheral cytopenias without dysplasia while still showing clonal hematopoiesis of MDS-related mutations (Valent 2019). The malignant potential of both conditions has been proposed for the revised WHO classification of MDS, wherein CHIP and CCUS are listed as myeloid precursor lesions, highlighting their contribution to MDS emergence (Gondek and DeZern 2020). Additionally, health care managers consider the creation of specialty clinics for assessment and counseling of patients with clonal hematopoiesis (Bolton et al. 2020). At the molecular level, most mutated genes in CHIP are of somatic and heterozygous origin and often affect epigenetic modifier-, RNA splicing- or DNA damage response genes (Table 1). The Variant Allele Frequency (VAF), which is the frequency of the mutant variant in the whole allele pool, must be > 2% to be termed CHIP, translating to substantial clonal expansion of mutant HSPC. This threshold was set by technical limitations and does not confer any biological effects (Steensma et al. 2015).

Table 1: Frequent CHIP driver mutations (Marnell et al. 2021) and their prevalence in a cohort of 4,229 CHIP individuals (Bick et al. 2020).

Affected gene	Function	Group	Prevalence in CHIP cohorts	Mutation consequence
DNMT3A	*De-novo* DNMA methyltransferase	Epigenetic modifiers	58.5%	Loss of function, hypomethylation at differentially methylated regions (Russler-Germain et al. 2014)
TET2	Catalyzes 5-mC to 5-hmC	Epigenetic modifiers	20%	Loss of function, global hypermethylation (Ferrone et al. 2020)
ASXL1	Chromatin modifier	Epigenetic modifier	8%	Loss of function or truncated protein with gain-of-function, H3K27me3 loss (Abdel-Wahab et al. 2012; Inoue et al. 2013)
JAK2	Downstream mediator of cytokine receptor signaling, upstream of TET2 signaling	Signal transduction, inflammatory response	3.2%	Missense, altered signaling, cytokine hypersensitivity, oncostatin M secretion into BMME (Chen and Mullally 2014)

PPM1D	Downstream of p53, negatively regulates p38 MAPK signaling	DNA damage response	3.8%	Truncated protein, increased resistance to apoptosis (Genovese et al. 2014; Hsu et al. 2018)
TP53	Regulates cell cycle arrest, DNA repair, metabolism changes	DNA damage response	1.9%	Missense, increase in H3K27me3, leading to increased self-renewal and differentiation (Chen et al. 2019)
SF3B1	mRNA spliceosome complex components	RNA splicing	2%	Aberrant splicing, resulting in reduced protein and gene expression (Darman et al. 2015)
SRSF2	mRNA spliceosome complex components	RNA splicing	2%	Altered protein structure (Meggendorfer et al. 2012)

The most commonly mutated gene in CHIP, DNMT3A, is a *de novo* methyltransferase that is essential for DNA methylation during mammalian development (Okano et al. 1999). Its active form is heterotetrameric, consisting of DNMT3A and DNMT3L, where DNMT3L stabilizes and stimulates the catalytically active DNMT3A. The most frequent mutation, the hotspot somatic mutation R882H, prevents the binding of DNMT3L, instead leading to the formation of large DNMT3A oligomers with lowered methyltransferase activity and altered flanking sequence preferences. This results in overall hypomethylation at differentially methylated regions, but can also lead to strong hypo- and hypermethylation depending on the binding site (Emperle et al. 2018; Nguyen et al. 2019). The prevalence of this mutation in CHIP, MDS and AML and the increased attention it received led to more comprehensive preclinical research through the generation of mouse models carrying the R878H mutation, which is equivalent in terms of mutation consequence to the R882H mutation in humans (Guryanova et al. 2016; Loberg et al. 2019). These models are inducible heterozygous mutants within the HSPC compartment, recapitulating CHIP with a DNMT3A^{R882H} VAF of 50%, well above the normal range of VAF in individuals, which is most often around 2–10% (Hecker et al. 2021).

1.2 Myelodysplastic neoplasms

Myelodysplastic neoplasms are a group of heterogeneous bone marrow disorders, accompanied by anemia, ineffective hematopoiesis and a risk of progression to AML (Friedrich and Kosmider 2022), which occur primarily in the elderly population. They are

characterized by a defect in maturation of the erythro-myeloid lineage that can lead to an accumulation of morphologically altered immature cells, so-called blasts, in the bone marrow. This blood dysregulation results in cytopenias, especially anemia, neutropenia and thrombocytopenia (Sekeres and Taylor 2022). MDS cells are derived from HSPC that acquired somatic mutations, which lead to differentiation block and aberrant proliferation, thereby outcompeting wild-type HSPC (Elias et al. 2014). These mutations include epigenetic regulators (e.g. DNMT3A, TET2, ASXL1, IDH1, IDH2), splicing factors (e.g. SF3B1, SRSF2), regulators of transcription (e.g. NPM1, TP53) and signaling molecules (e.g. NRAS, KRAS, FLT3) (Fenaux and Adès 2013) and thus share the mutational background of both CHIP and CCUS. Since the 2016 edition, the WHO has defined seven MDS subtypes, based on number of dysplasias, cytopenias, morphological changes such as ring-sideroblasts, percentage of blasts in the bone marrow and cytogenetics (Ming Hong and Guangsheng He 2017). In 2022, this classification was revised and now includes eight subtypes, with more emphasis on the cytogenetics of the disease (see annex Table 15, Table 16 for more detail). For instance, SF3B1-mutated MDS is now considered a low-risk subtype, characterized by ring-sideroblasts and generally favorable outcome (Zhang et al. 2022b).

For clinical management, MDS are stratified based on the Revised International Prognostic Scoring System (IPSS-R) into low risk, Intermediate Risk (IR-1 and IR-2), and high risk MDS. This score is a point-based system that encompasses bone marrow blast infiltration, cytogenetics and cytopenias displayed by the patient (see annex chapter 9.1.2 for detailed description) (Bejar 2013).

Higher risk MDS (HR-MDS, entail IR-2 and high risk-MDS) patients have significantly higher chances of developing AML, a worse five-year survival chance and are in consequence treated more intensively, for instance with hypomethylating agents (HMA, e.g. azacitidine, decitabine), allogeneic Stem Cell Transplantation (SCT) or sometimes chemotherapy (anthracyclines + cytarabine) (Fenaux and Adès 2013). If HMA therapy fails because of intolerable side effects or resistance and SCT is not feasible due to advanced age, frailty or comorbidities, there is no approved second-line therapy and patients have a median survival of less than six months (Steensma 2018).

Lower Risk MDS (LR-MDS) encompass IPSS-R low and intermediate-1. Some of those patients have no symptoms other than modest cytopenia, in which case they are monitored until symptoms appear. For other LR-MDS, treatment mainly aims at

ameliorating symptoms, for instance by treating anemia with erythropoiesis-stimulating agents (epoetin and darbepoetin) or luspatercept, which binds to TGF-β family proteins whose overexpression in MDS is responsible for insufficient erythropoiesis (Santini 2016; Steensma 2018; Fenaux et al. 2020). In addition, del(5q) MDS can be treated with lenalidomide (List et al. 2005).

The only somatic mutation that shows favorable prognosis in MDS is SF3B1, which has been recognized as its own subtype of MDS in the newest WHO classification from 2022 (Khoury et al. 2022; Zhang et al. 2022b). This is due to the strong influence the mutation has on pathophysiology, for instance by the accumulation of erythroblasts with iron-loaded mitochondria, so-called ring sideroblasts, in the bone marrow. The favorable prognosis seems to be restricted to LR-MDS, while in HR-MDS, there is no statistically significant effect on patient survival (Malcovati et al. 2020). This explains why earlier studies either found no prognostic value for SF3B1 mutations in MDS, or attributed it to falling into a favorable prognosis group (MDS-RS), which consists of up to 80% SF3B1 mutant MDS (Thol et al. 2012; Damm et al. 2012). Screening for recurrently mutated genes in the mononuclear cell fraction in patients revealed that the SF3B1 mutation can arise in HSC and be passed on to progeny. Homozygous mutation is embryonically lethal, and only heterozygous mutations are found in MDS with a VAF of ~40% (Mian et al. 2015; Malcovati et al. 2020). On a molecular scale, SF3B1 mutant blasts show enhanced proinflammatory signaling in comparison to non-SF3B1 (Pollyea et al. 2021). This is in parts due to differential splicing of IRAK4, which leads to stronger NF-κB signaling (Choudhary et al. 2022), which is a prime mediator of the NLRP3 inflammasome (Liu et al. 2017). A very recent study showed that SF3B1^{mut}-MDS leads to mis-splicing of COASY, a gene that encodes for coenzyme A synthase, which is required for efficient heme biosynthesis. The defect was rescued in primary *ex vivo* SF3B1^{mut} cells by supplementation with vitamin B5, highlighting how insights into molecular dysregulations in cancer cells can and will be used to ameliorate disease burden in cancer patients (Mian et al. 2023)

1.3 The cellular bone marrow niche

The concept of a stem cell niche was first proposed in 1978 by Schofield, who argued that stem cells should be seen in association with other cells that prevent maturation and

guarantee proliferation (Schofield 1978). Through pioneering work with mouse models, sophisticated imaging technologies and single-cell studies of the BM, it has become clear that HSC maintenance, proliferation, retention and quiescence are regulated by a network of cells, secreted factors and ligands, called the hematopoietic stem cell niche (Pinho and Frenette 2019). This BM niche is populated by a variety of stromal cells, immune cells, vasculature, and neurons that each influence HSC activity and retention, but also myeloid or lymphoid differentiation (Pinho and Frenette 2019).

1.3.1 Hematopoietic Stem Cells

For replenishment of blood, HSC must be tightly regulated to ensure constant supply of mature cell populations, i.e., HSC differentiation capacity, without exhaustion of stemness. This regulation occurs through extrinsic pathways, mediated for instance by soluble factors, but also through intrinsic mechanisms on both genetic and epigenetic scale. One example for epigenetic regulation is the repression of myeloid or lymphoid lineage-specific genes that occurs for instance through chromatin methylation (H3K9me1, H3K4me1, H3K79me2) or acetylation of histone 3 (Cedar and Bergman 2011). Oxygen supply also influences the metabolic activity of HSC: in an oxygen-rich environment, mitochondrial respiration is preferred, connected to high proliferation capacity and lineage output (Suda et al. 2011). Committed progenitors also adapt a mitochondrial respiration phenotype to provide the necessary energy for differentiation. Quiescent LT-HSC on the other hand prefer anaerobic or hypoxic conditions, which help them maintain their stemness (Papa et al. 2019). This explains why most of the LT-HSC locate near the endosteum, where poor vascularization leads to hypoxia (Guezguez et al. 2013; Ehninger and Trumpp 2011). This so-called endosteal niche differs in composition from the (peri)vascular niche (Figure 4).

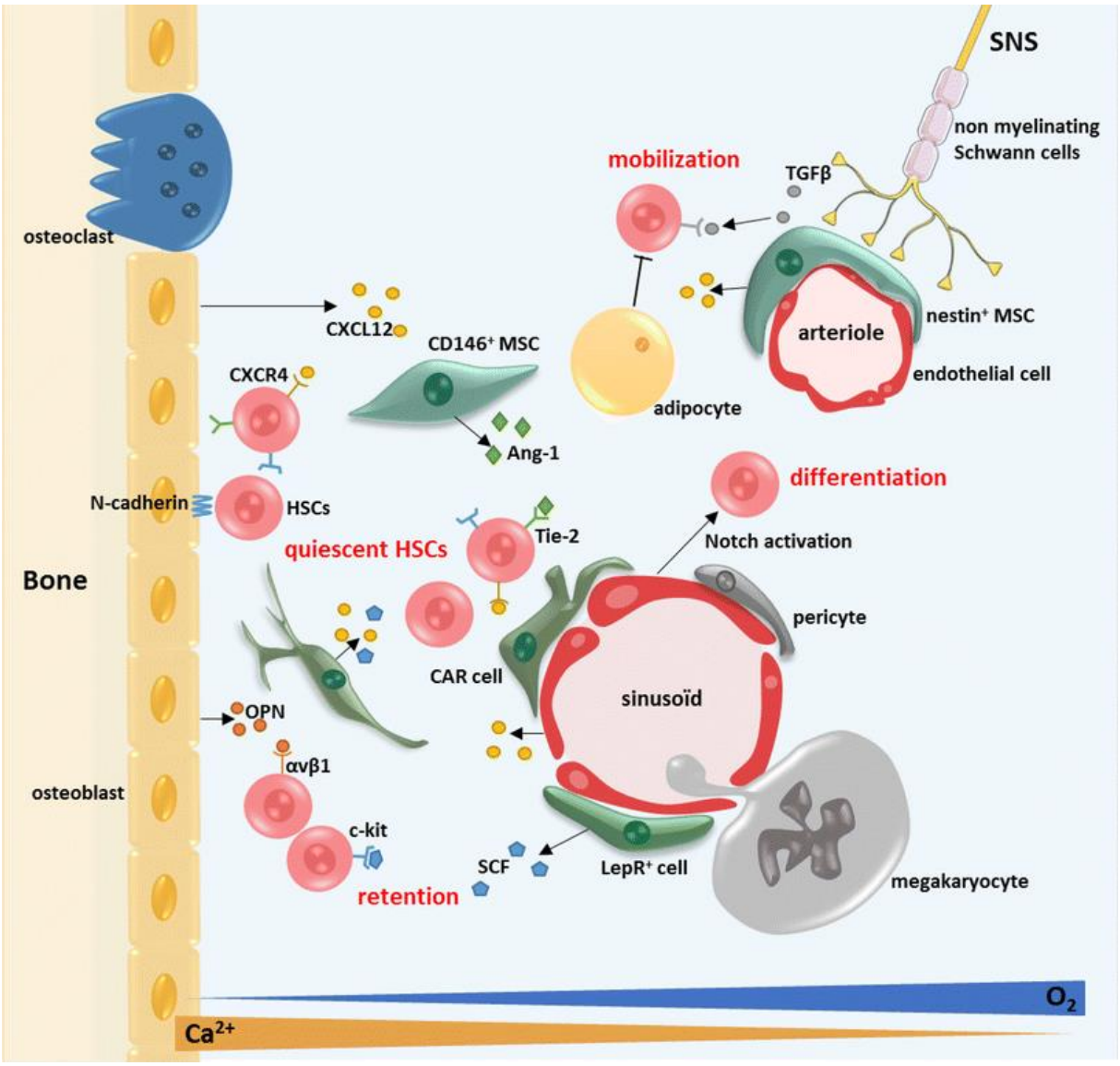

Figure 4: Schematic endosteal and perivascular niche with important regulatory signaling axes. In the hypoxic endosteal niche (left), HSC are kept quiescent through interplay with stromal cells and osteoblasts. In the perivascular niche (center/right), HSC are activated and mobilized through interplay with MSC and vasculature, which in turn are regulated by the Sympathetic Nervous System (SNS) (Goulard et al. 2018).

1.3.2 Mesenchymal stromal cells

Mesenchymal Stromal Cells (MSC) are a heterogenous stem cell population in the bone marrow whose primary function is the renewal of stromal populations, such as osteoblasts, chondrocytes, and adipocytes. MSC are found both in the endosteal niche (lining the bone surface), and the perivascular niche, where they intertwine with Endothelial Cells (EC) of the vasculature via adhesion to Vascular Cell Adhesion Molecule 1 (VCAM1), which is inducible by Tumor Necrosis Factor α (TNFα) and Interleukin 4 (IL-4) (Juneja et al. 1993; Aomatsu et al. 2014). They are defined mostly by expression of a

universal panel of cell surface markers (positive for CD73, CD90, CD105, negative for CD45, CD34, CD14, CD11b, CD79a and HLA-DR) and by their ability to adhere to plastic and the aforementioned trilineage potential *in vitro (Dominici et al. 2006)*. In the human bone marrow, other *bona fide* MSC markers are CD271, which define a stem-like population (Quirici et al. 2002), Leptin Receptor (LEPR), and CD146, restricted to a perivascular subset (Tormin et al. 2009; Matsuzaki et al. 2014). MSC are in an equilibrium between either adipogenic or osteochondrogenic differentiation, which is affected by a multitude of signals, including Extracellular Matrix (ECM) integrins, Wnt, Notch, BMP, Hedgehog and FGF pathways. The transcription factors PPARγ and C/EBP are master regulators that mediate adipogenic differentiation, while Runx2 and Osx facilitate osteochondrogenic lineage commitment (Woods and Guezguez 2021). This equilibrium can be disturbed during aging (see chapter 1.4.1) or dysregulated in myelodysplasia (chapter 1.4.3).

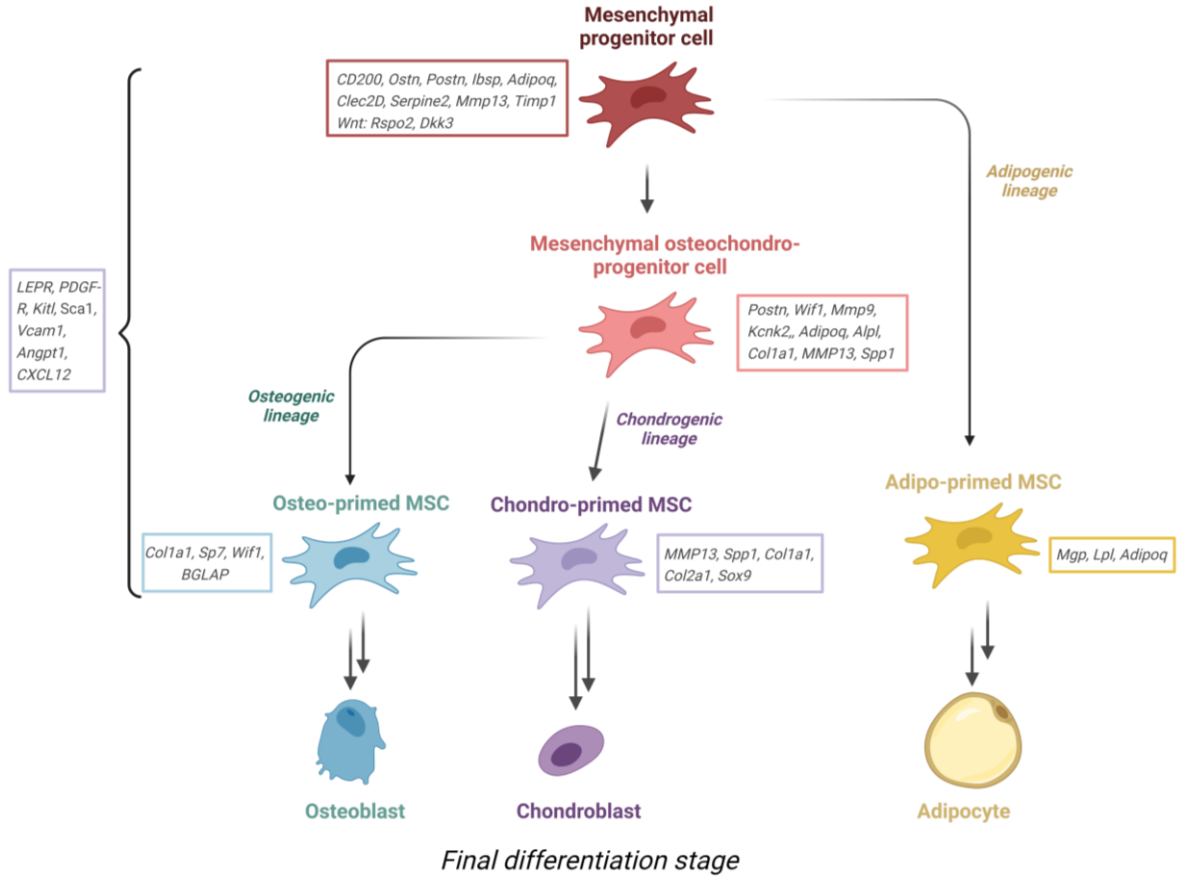

Figure 5: Mesenchymal stromal cells and their progeny are indispensable for bone marrow stroma replenishment. Mesenchymal progenitors give rise to either adipo-primed MSC or an osteochondro-progenitor, which in turn differentiates into chondro- or osteo-primed MSC. Those generate osteoblasts, chondroblasts and adipocytes. Boxed marker genes are derived from murine scRNA seq experiments and can be used to differentiate between populations (Woods and Guezguez 2021).

MSC are also vital for HSC regulation by producing soluble key factors. Along with endothelial cells and osteoblasts, MSC are the main secretors of the chemokine CXCL12 (also called Stroma-derived Factor 1, SDF-1), which binds to its receptor CXCR4 on HSPC, where it activates MAPK/ERK and PI3K/AKT pathways (Roversi et al. 2021; Singh et al. 2020), leading to modulation of HSC retention, quiescence and proliferation (Greenbaum et al. 2013; Nie et al. 2008; Tzeng et al. 2011). Stem Cell Factor (SCF), also known as KIT-ligand, supports HSC maintenance through binding to its receptor KIT on HSC and downstream activation of MAPK, PI3K and JAK/STAT signaling pathways (Reber et al. 2006). MSC were also shown to excrete a multitude of other regulatory factors for angiogenesis, immunomodulatory activity, anti-apoptotic activity, anti-oxidant and anti-microbial activity, for instance Vascular Endothelial Growth Factor (VEGF), Fibroblastic Growth Factor (FGF), Hepatocyte growth factor (HGF) as well as Angiopoietin-1 (Angpt1) and Transforming Growth Factor β (TGF-β) (González-González et al. 2020). Angpt1 and VEGF have long been reported to mobilize and stimulate HSC, highlighting the central role that MSC play in hematopoiesis (Hattori et al. 2001).

1.3.3 Osteoblasts

In the endosteal niche, HSC are in close contact with Osteoblasts (OB), which are derived from MSC via osteoprogenitors and are primarily responsible for synthesizing bone matrix proteins and minerals during bone formation (Woods and Guezguez 2021; Guezguez et al. 2013). Besides the hypoxia that distinguishes the vascular from the endosteal niche, osteoblasts, which comprise a unique and spatially localized cell population, are directly involved in maintenance and quiescence of HSC by releasing specific mediators. Osteopontin, an ECM factor mostly secreted by osteoblasts, can be cleaved by thrombin and attracts HSPC to the endosteum (Grassinger et al. 2009; Storan et al. 2015). Angpt1 leads to adherence of HSC and directly promotes quiescence (Arai et al. 2004). Other factors that contribute to HSC function are BMP4 (Goldman et al. 2009), but also the Notch and Wnt pathways, whose inhibition has been shown to have detrimental effects for self-renewal and quiescence (Lampreia et al. 2017; Fleming et al. 2008). In addition to regulating HSC activity, OB are also required for B-cell development by secreting VCAM-1, CXCL12 and IL-7 for pre-pro-B-cells and pro-B-cells (Zhu et al. 2007).

1.3.4 Adipocytes

The amount of adipocytes in the BM changes during lifetime, with almost no adipocytes present in young people to almost exclusively constituting the bone marrow in the elderly. An increase in Bone Marrow Adipose Tissue (BMAT) can also be observed after following a high-fat diet, where it has been shown to impair bone regeneration in mouse models (Ambrosi et al. 2017), as well as a result of anorexia, irradiation, caloric restriction and treatments with glucocorticoids (Devlin and Rosen 2015). One reason for proliferation in both fasting and a high-fat diet could be as a fine-tuning mechanism for energy that is needed in hematopoiesis; an expansion of BMAT reduces the amount of energy that would be used to sustain hematopoiesis (Turner et al. 2018). Loss of BMAT can be facilitated through exercise, cold exposure as well as treatment with metformin or Parathyroid Hormone (PTH) (Li et al. 2019).

This highlights the responsiveness and plasticity of BMAT for insults. Indeed, there seem to be two distinct populations of BMAT. Yellow marrow is constitutively and functionally linked to HSC quiescence, while regulated BMAT is responsive to hematopoietic demand and seems to play a role in HSC support. Both populations differ by localization, composition and levels of the transcription factors C/EBP-α and C/EBP-β (Li et al. 2019; Tratwal et al. 2021).

Due to the high fat content and subsequent low density, adipocytes are difficult to isolate, which explains why there are few studies done to functionally characterize adipocytes *ex vivo*. In the few studies that were done, BM adipocytes were shown to be able to support HSC cultures via for instance CXCL12 and SCF, but on a lower level than adipo-progenitors or MSC (Mattiucci et al. 2018). While $LEPR^{+}$ adipo-progenitors support proliferating HSC, adipocytes mainly favor HSC quiescence through secreted factors such as MCP-1, PAI-1, TGF-β or NRP1 (Tratwal et al. 2021; Harada et al. 2021; Ghode et al. 2017).

1.3.5 Endothelial Cells

Bones are highly vascularized tissues. Spatial imaging analysis of murine bone marrow show that the vascular network in long bones is separated between $CD31^{high}$ vessels near the metaphysis that are strictly organized in younger mammals and deteriorate with age (so-called type H vessels, referring to High expression of CD31), and type L vessels ("L" referring to Low expression of CD31) that are located towards the diaphysis (Chen et al.

2020). Type H vessels exert higher partial oxygen pressure than type L vessels, leading to distinct microenvironments with for instance lower amounts of reactive oxygen species in type L sinusoidal vessels (Chen et al. 2020) and comparably normal oxygen levels in the metaphysis in comparison to the hypoxic diaphysis (Sivaraj and Adams 2016). Endothelial cells, especially from sinusoidal vasculature, are in close contact with HSPC in the perivascular niche (Kiel et al. 2005). This close interaction is important for functional differentiation of HSPC, which was demonstrated with transgenic mouse models that lack EC-derived supportive factors, such as TPO, CXCL12, VCAM1, FGF4, and displayed impaired thrombopoiesis (Avecilla et al. 2004). Furthermore, pleiotrophin, secreted by EC, regulates HSC expansion and regeneration (Himburg et al. 2010; Himburg et al. 2014). Other studies highlighted the differences between arteriolar EC and sinusoidal EC, showing that SCF is secreted mainly by the former, while sinusoids express higher levels of CXCL12 and only small amounts of SCF (Xu et al. 2018; Ding et al. 2012).

In addition to enabling nutrient and metabolite transport from and to the bone and HSC support, vasculature in the bone marrow is responsive to inflammatory stress (Vandoorne et al. 2018), bone fracture (Bahney et al. 2015) and also affected during aging and diseases (Chen et al. 2020) with new vasculature forming in a process called angiogenesis. Mechanistically, angiogenesis requires partial degradation of the basal membrane of a pre-existing vessel, which is followed by migration of endothelial cells towards an angiogenic factor (sprouting). Pericytes, for instance MSC or CXCL12-Abundant Reticular (CAR) cells, are attracted to cover the vessel surface. In comparison to sprouting, splitting angiogenesis relies on division of intraluminal walls of pre-existing vessels into smaller ones (Aspriţoiu et al. 2021). The most important angiogenic factors that are involved in these processes are VEGF, which is secreted by EC and bone lineage cells and primarily promotes EC migration and proliferation (Abhinand et al. 2016), as well as Platelet-Derived Growth Factor (PDGF), secreted by ECs and pre-osteoclasts, which stimulates MSC and EC migration and proliferation via binding to PDGFR-β (Xie et al. 2014; Peng et al. 2020). Angiogenesis is coupled closely with osteogenesis through PDGF and VEGF signaling from type H vessels (Stucker et al. 2020), for instance through influencing MSC toward osteogenic differentiation (Grosso et al. 2017).

1.3.6 T lymphocytes

HSC are activated by inflammatory signaling, for instance through $CD8^+$ T cell-derived Interferon γ (IFNγ), leading to a reduction of self-renewal and repopulation, but an increase in proliferation potential (Leimkühler and Schneider 2019). This is a useful mechanism that couples inflammation, which can happen in diseases and as a result of injuries that could entail blood loss, to the reconstitution of the blood pool. Basal inflammatory signaling is always needed to sustain blood production. On the other side, aberrant inflammation leads to impaired self-renewal and imbalanced lineage output and can be a key contributor in the development of hematological malignancies (Pietras 2017).

One way to dampen inflammation in the bone marrow is through the presence and activity of $CD4^+$ $FoxP3^+$ regulatory T cells (Tregs), which are found to home to the BM niche via the CXCL12/CXCR4 axis (Zou et al. 2004). These BM-resident Tregs are also present in the more quiescent, endosteal niche as key regulators of HSC immune privilege against CD4 and CD8 T cells (Fujisaki et al. 2011) by expression and binding of co-inhibitory ligands such as TIGIT and CTLA-4 (Nicholls et al. 2021) on effector T cells, and through secreted adenosine, which results in decreased Reactive Oxygen Species (ROS) levels (Hirata et al. 2018). In addition, BM-resident Tregs are involved in MSC upkeep through IL-10, indirectly regulating HSC maintenance and quiescence (Camacho et al. 2020) and can regulate the levels of proinflammatory cytokines in the niche (Kotsianidis et al. 2009).

Although HSC have been thought to enjoy immune privilege by being shielded from immune cells, latest evidence suggests at least some immune surveillance of HSPC by CD4 T cells as a mechanism to eliminate neoantigen-expressing HSPC from the system (Hernández-Malmierca et al. 2022).

1.3.7 Innate immune cells

Besides lymphocytes, also innate immune cells are involved in HSC retention and support in the BM. In a conditional macrophage depletion mouse model, HSC egressed into the blood stream more easily as a result of lower levels of CXCL12, which in turn is controlled by oncostatin M (OSM) (Rasmussen et al. 2015; Chow et al. 2011). Similar findings in a

parallel study showed that downregulation of OSM by administration of G-CSF reduces CXCL12 levels, leading to HSC mobilization into the blood stream (Bisht et al. 2022).

Megakaryocytes (MK), which are mainly responsible for production of platelets, are mostly localized toward the quiescent endosteal niche (Tavassoli and Aoki 1989). Similar to macrophages, depletion of MK leads to loss of HSC retention and subsequent activation, which is due to the missing CXCL4-secretion by MKs (Bruns et al. 2014). In addition, MK-secreted Thrombin can cleave Osteopontin (OPN), leading to generation of thrombin-cleaved OPN, which binds and negatively regulates HSC differentiation and proliferation (Storan et al. 2015). One crucial MK-secreted factor is TGF-β, which maintains quiescence in HSC through TGF-β/SMAD signaling pathways (Zhao et al. 2014; Yamazaki et al. 2011) and can shift the myeloid-lymphoid HSPC ratio, favoring myelopoiesis over lymphopoiesis (Challen et al. 2010).

1.3.8 Neurons

One often overlooked stromal population that influences HSC activity in the BM are neurons. Innervation of the bone marrow was first described by Duverney in 1770 (Duverney 1770). Initially, the sensory and sympathetic fibers that were found were thought to act as pain sensing fibers that play a role in the vasomotor reflex (Kuntz and Richins 1945). Later, more systematic studies in monkeys, rabbits, rats and mice revealed complex networks that interact with the endothelial walls of the sinuses (Calvo 1968). With the emergence of transgenic mouse models and functional studies, it was found that sympathetic and sensory neurons are critical for HSC mobilization and maintenance. In a dual denervation study in an inducible mouse model, HSC were expanded significantly and showed a myeloid bias, both hallmarks of HSC aging (Gao et al. 2020; Lee et al. 2019). Ablation of sensory neurons alone also leads to a decrease in bone marrow cellularity and granulopoiesis (Broome and Miyan 2000). One common mechanism of HSC regulation through neurons is mediated by CXCL12 in a circadian manner. Photic cues, such as daylight, stimulate noradrenaline secretion by Sympathetic Neurons (SN) in the bone marrow, leading to binding to the β3-adrenergic receptor on stromal cells. This in turn leads to downregulation of Sp1, a transcription factor that regulates CXCL12 transcription (Méndez-Ferrer et al. 2008). The role of CXCL12 in HSC mobilization is highlighted in chapter 1.3.2. On the other hand, SN are also vital for G-CSF-mediated HSC egress from the bone marrow niche (Katayama et al. 2006) and mediate bone mass homeostasis by

osteoblast reduction and osteoclast formation, which influence HSC activity as described in chapter 1.3.3 (Kondo et al. 2005). In addition to SN-directed HSC regulation, $GFAP^+$ SN-ensheathing Schwann cells also promote HSC quiescence via the TGF-β/SMAD axis (Yamazaki et al. 2011).

In contrast to this indirect regulation of HSC activity, sensory neurons can act more directly: cGRP, a neuropeptide secreted by nociceptive nerves into the bone marrow, binds to its heterodimeric receptor, comprised of CALCRL and RAMP1. This leads to a downstream activation of the $G\alpha_s$-adenylyl cyclase–cAMP signaling pathway, resulting in HSC mobilization into the blood. Surprisingly, this effect can by simulated by a capsaicin-containing diet in mice, suggesting an influence of the diet on HSC activity (Gao et al. 2020; Tikhonova and Aifantis 2021). In addition, sensory ablation was shown to impact on MSC differentiation in mice, promoting adipogenesis and reducing bone mass (Hu et al. 2020), which offers another path to influence niche constitution.

All these regulatory axes influence hematopoiesis and illustrate the complexity that goes into maintaining HSC function throughout the lifetime. Besides these axes, there is also bidirectional crosstalk between stromal populations, which is beyond the scope of this thesis. An overview of discussed factors involved in the HSC niche is given in Figure 6.

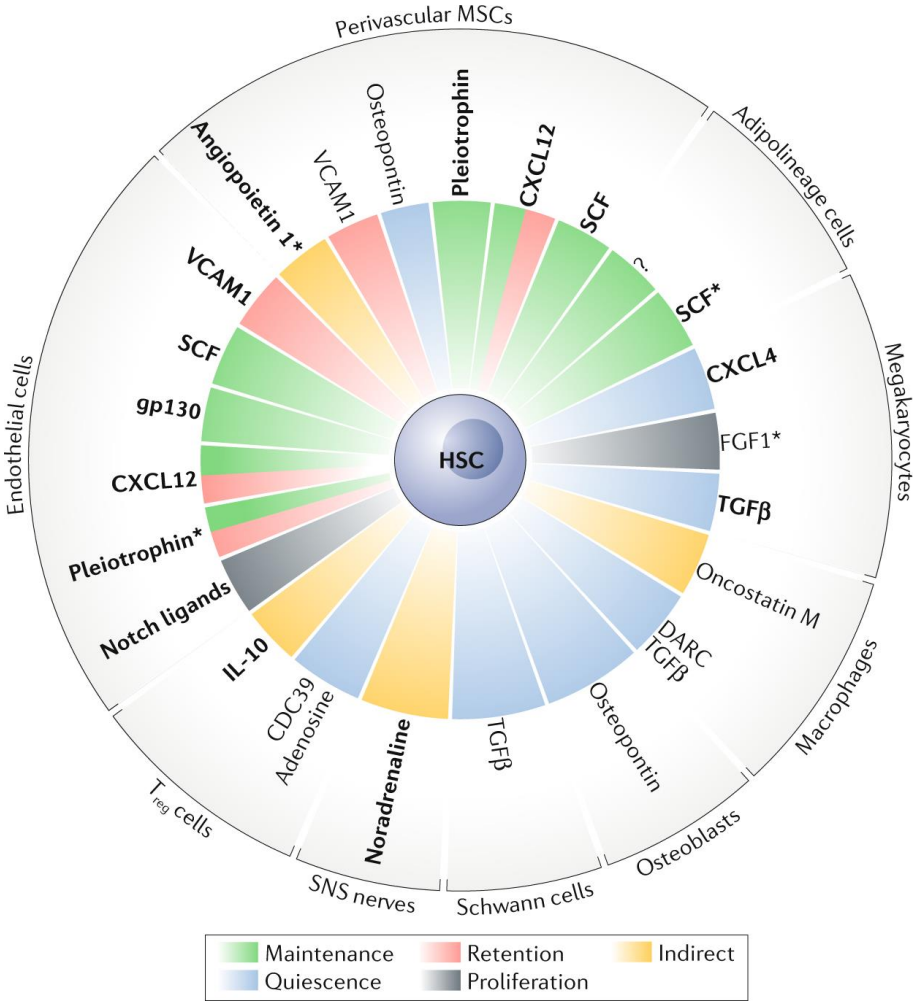

Figure 6: Cellular and molecular constituents of the HSC niche (Pinho and Frenette 2019). Molecules with an asterisk are involved in bone marrow regeneration after ablation. Question marks indicate factors that have not been determined, but where cellular interplay has been shown to be important. Bold printed molecules are supported by functional data from cell-specific genetic experiments.

1.4 Niche changes during aging, clonal hematopoiesis, and neoplasia

1.4.1 The aging niche

Both CHIP and MDS are considered diseases of the elderly, since most affected people are above 65 years old (Bick et al. 2020; Ma 2012). One hallmark of aging, which is defined as the time-dependent functional decline of organisms, is the accumulation of somatic mutations, which also explains the prevalence of CHIP and MDS in the elderly – it is simply more likely that stem cells acquire mutations the longer an individual lives. The functional decline of HSPC, one hallmark of aging, can be attenuated or aggravated by surrounding tissue and the microenvironment (López-Otín et al. 2013). This begs the question: how

does the bone marrow change with age, and how do aging HSPC impact the architecture of the BM microenvironment?

One very prominent change is the expansion of adipocytes, starting from the femur head and moving toward the diaphysis as aging progresses. This is a consequence of a shift in MSC differentiation output, favoring adipogenesis over osteogenesis (Woods and Guezguez 2021), accompanied by a decrease in secreted CXCL12, IGF1, Angpt1 and SCF (Bousounis et al. 2021). Changes in MSC abundancy are still a matter of debate due to contradictory findings. There are reports that show that MSC do not expand during aging (Aguilar-Navarro et al. 2020; Meza-León et al. 2021), as well as observations about an increase in specific subsets of MSC (Maryanovich et al. 2018; Frisch et al. 2019; Singh et al. 2019). The expanded BMAT contributes to cellular senescence of MSC through Senescence-Associated Secretory Phenotype (SASP) factors like IL-1α, IL-1β, NF-κB, and TGF-β, further impeding osteoblastogenesis (Aaron et al. 2022; Mitchell et al. 2023). In consequence, the number of osteoblasts and osteoprogenitors are decreased (Almeida et al. 2007; Maryanovich et al. 2018) and endosteal niches are less frequent in aged bone marrow while non-vascular niches expand (Ho et al. 2019).

The expansion of MSC with lower capability to maintain HSC longevity has also been attributed to a loss of sympathetic innervation during aging which diminishes their supportive adrenergic signaling (Maryanovich et al. 2018; Chartier et al. 2018). This is accompanied by a loss of arterioles and increased HSC numbers (Kusumbe et al. 2016; Maryanovich et al. 2018). In contrast to this, the total vasculature, including sinusoids, was shown to be expanded upon aging (Maryanovich et al. 2018) although the absolute number of endothelial cells determined by flow cytometry remained unchanged (Gomariz et al. 2018; Kusumbe et al. 2014; Poulos et al. 2017), which can be explained by poor recovery of aged and pre-senescent ECs in flow cytometry experiments (Mitchell et al. 2023). These vessels displayed increased leakiness and a decrease in secretion of CXCL12 and SCF (Poulos et al. 2017). There are also changes in the myeloid and lymphoid lineage: MKs have been shown to be expanded in aged mice, which is accompanied by enhanced secretion of TGF-β (Hilpert et al. 2014; Maryanovich et al. 2018). On the other hand, $CD4^+$ and $CD8^+$ T cell-frequency in the bone marrow is not altered, but the composition of the CD8 pool changes, where highly activated $CD8^+$ $CD28^-$ are expanded to the expense of naïve CD8 cells, due to an aging-related increase in IL-6 and IL-15. These cells are also

upregulated in inflammation-related disorders and numerous cancers and have recently been described as a subset of regulatory T cells (Chen et al. 2018).

1.4.1.1 Inflammaging of the BM niche

The described changes in bone marrow composition are accompanied (and partially caused) by an increase in inflammatory signaling termed "inflammaging" which is another hallmark of aging (Bousounis et al. 2021). Systemic levels of circulating inflammatory cytokines (e.g. IL-6, TNFα, IL-1RA, CRP, IL-18) are upregulated in healthy elderly people, also in the bone marrow (Hasegawa et al. 2000; Bousounis et al. 2021; Ferrucci et al. 2005; Baylis et al. 2013). These inflammatory cytokines in turn prime HSC towards myeloid differentiation via the NF-κB pathway, leading to more mature myeloid cells (Bousounis et al. 2021). Since the myeloid progeny is implicated in proinflammatory signaling as well – for instance through TNFα – this mechanism presents a self-amplifying loop which further alters HSC functions (Yamashita and Passegué 2019). In addition, with the age-related expansion of proinflammatory BMAT and perisinusoidal MSC, the stroma contributes to the "inflammaging" phenotype (Aaron et al. 2022). Targeting this age-related inflammation can lead to reconstitution of some of the aging HSC phenotypes: inhibition of IL-1 signaling with anakinra, a synthetic IL-1 receptor antagonist, in an inflammation mouse model led to an increase in LMPP, which are usually downregulated during aging. This was accompanied by a functional reconstitution of HSC with increased lymphoid output and erythrocyte production (Mitchell et al. 2023).

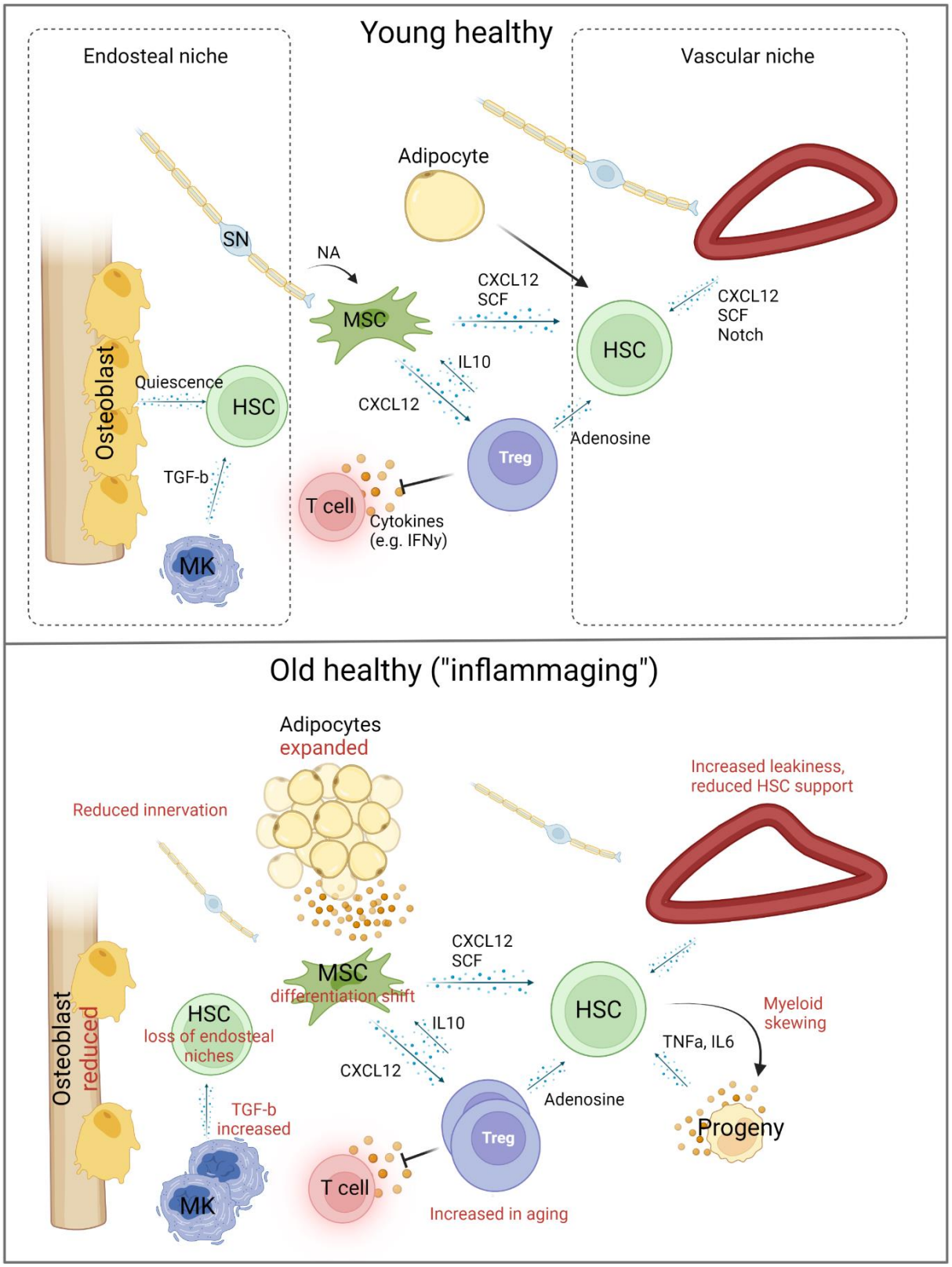

Figure 7: Niche changes in old vs. young bone marrow with schematic crosstalk between niche cells. NA: Noradrenaline. Created with Biorender.com.

1.4.2 Inflammatory signaling by CHIP progeny (niche changes in CHIP)

Since CHIP is an age-related phenomenon, the BM niche changes are similar to aged controls. However, progeny of mutated HSC has been implicated in additional inflammatory signaling both on a systemic and a local bone marrow level. For instance, individuals with CHIP displayed higher serum levels of IL-6, IL-8, TNFα, IL-1β and IL-18 (Jaiswal et al. 2017; Bick et al. 2020; Cook et al. 2019), with mutation-specific inflammatory signatures linking $TET2^{mut}$ to increased IL-1β and $JAK2/SF3B1^{mut}$ to increased circulating IL-18.

In relation to the bone marrow, $DNMT3A^{mut}$ CHIP has been clinically linked to osteoporosis in humans: $DNMT3A^{mut}$ myeloid cells enhanced osteoclastogenesis via macrophage-derived IL-20 in a $DNMT3A^{R882H/+}$ mouse model, leading to enhanced bone resorption and progressive bone loss (Kim et al. 2021). The vascular niche could also be target of niche-mediated remodeling: TET2-deficient myeloid cells have been shown to promote angiogenesis through secretion of S100A8/A9 in a lung cancer model (Nguyen et al. 2021). These effects are in addition to the inflammatory milieu found in the aged HCS niche and it has been shown that this environment confers a selective advantage for mutated HSC: $DNMT3A^{mut}$ HSPC show increased self-renewal in inflammatory fatty bone marrow in comparison with wildtype DNMT3A HSPC (Zioni et al. 2022). TNFα-mediated inflammation during aging also favors expansion of $DNMT3A^{R882H}$ and $TET2^{mut}$ HSPC (Abegunde et al. 2018; Liao et al. 2022; SanMiguel et al. 2020), showing a looping mechanism where mutated clones increase systemic and local inflammation, which in turn leads to expansion of the mutant clones.

1.4.3 Niche changes in MDS

The bone marrow microenvironment in MDS has been of interest for researchers for decades. Stromal alterations and abnormal localization of immature precursors, with HSPC residing in the BM interstitium instead of endosteal niche, was already seen as a histopathological hallmark of MDS in the 1980s (Mangi et al. 1991; Tricot et al. 1984; Dührsen and Hossfeld 1996), and with good reason:

Besides the main hypothesis of HSC-specific mutations that lead to development of MDS, the niche-initiated MDS development hypothesis gained some ground supported by findings that inducible deletion of Dicer1 in mesenchymal osteoprogenitors in a mouse

model led to development of MDS (Raaijmakers et al. 2010). This shows a possible mechanism that acts in addition to HSC-dependent disease progression, where a defect in the stroma leads to altered signaling towards HSC and contributes to the generation of genetic lesions. A lot of effort has been put into characterization of the myelodysplastic niche, among all discussed niche populations above, particular focus was set on MSC.

MSC are expanded in MDS, especially in HR-MDS (Johnson et al. 2014), and show reduced osteogenic and altered adipogenic differentiation potential, accompanied by higher levels of senescence and reduced proliferation rates (Geyh et al. 2013; Choi et al. 2020; Weickert et al. 2021). In addition, their secretome is altered, especially SCF, VEGF, Angpt1 and inflammatory cytokines like IL-1β, IL-6 and TNFα as well as chemokines like CXCL12 and CCL3 (Tosato et al. 2021). This leads to a reduced capacity to support normal hematopoiesis *in vivo*, which further favors the expansion of MDS blasts (Tosato et al. 2021). MSC-derived HSC support can however be restored, for instance through treatment with hypomethylating agents or luspatercept (Tosato et al. 2021; Wobus et al. 2021), revealing a potential new window in the clinic by targeting the HSC-stroma axis to restore physiological HSC regulation. Considering their anatomical distribution in the BM, an open question remains whether the expanded MSC are innervated and still under neuronal control; in fact, no research was done so far on possible neuronal changes in MDS. However, there are some observations from myeloproliferative neoplasms and acute myeloid leukemia showing sympathetic neuropathy in the bone marrow is involved in disease progression, which could be the result of increased local inflammation (Arranz et al. 2014; Hanoun et al. 2014).

The changes in lymphoid lineage and functional immune cells in MDS are somewhat understudied, however, studies in MDS found both a decrease in LR- and HR-MDS in $CD8^+$ T cells and their IFNγ secretion (Tao et al. 2016) as well as an increase in cytotoxic $CD8^+$ T cells (Kook et al. 2001). The latter could be a subset of Tregs that decreases $CD4^+$ T cell activation via IL-10 and surface expression of PD-L1, since they lack expression of granzyme B or perforin (Chen et al. 2018; Liu et al. 2015). This subset of Tregs is maintained and expanded by MSC, adding another layer of possible stromal dysregulation in immunosuppressive HR-MDS. The lack of deep immunophenotyping studies of the BM immune microenvironment is surprising, given the fact that T cells in MDS patients can be derived from a malignant clone and thus might exhibit functional differences (Vercauteren et al. 2012).

Tregs on the other hand receive increasing attention as critical regulators of HSC function and were shown to be diminished and functionally impaired in LR-MDS, mainly due to downregulation of CXCR4, leading to impaired BM homing (Kotsianidis et al. 2009). CXCR4 can be downregulated by G-CSF or mediated by inflammatory cytokines like TNFα, IL-1β, and IFNγ (Zou et al. 2004; Busillo and Benovic 2007), which are elevated in MDS BM. In HR-MDS on the other hand, $CD4^{+}$ $CD25^{high}$ $FoxP3^{+}$ Tregs are expanded in the peripheral blood and in the bone marrow in comparison to LR-MDS, which shows that immune suppression is more pronounced in HR-MDS. In LR-MDS patients, higher frequencies of BM Tregs were associated with worse disease progression (Giovazzino et al. 2019), highlighting the necessity for sterile inflammation and T cell-mediated HSPC pool surveillance to halt disease progression.

The increased inflammatory milieu in MDS is accompanied by elevated levels of angiogenic factors, such as VEGF, Ang-1, FGF and HGF both in serum and in the bone marrow (Brunner et al. 2002; Alexandrakis et al. 2005). Inflammation, for instance induced by LPS, results in a drastic (reversible) expansion of vasculature (Vandoorne et al. 2018), while VEGF controls leakage of sinusoids (Thurston 2002). This explains why the vascular density is increased in MDS, accompanied by increased leakage. VEGF is secreted by MDS blasts and can lead to an expansion of blasts through autocrine signaling (Bellamy et al. 2001), which is a possible reason why higher vessel density is associated with worse prognosis (Pruneri et al. 1999; Kim et al. 2016). The importance of this axis is reflected in the use of inhibitors of angiogenesis like bevacizumab (an anti-VEGF antibody), lenalidomide or arsenic trioxide in clinical trials (Aguayo et al. 2011). Of note, endothelial cells in MDS have been reported to exhibit the same chromosomal aberrations as the MDS clones, posing the question of how different these cells are in respect to HSC supportive capacities (Della Porta et al. 2008). A recent publication by Xing and colleagues showed reduced HSC support capacity in HR-MDS EC and reduced angiogenic potential in both LR- and HR-MDS, manifested in elevated ROS levels, increased apoptosis rates and decreased colony-forming unit plating efficiency of HSCs. In addition, co-culture with these EC led to increased differentiation of T cells towards Th17 in LR-MDS versus Th2 and Tregs in HR-MDS (Xing et al. 2022), showing an additional crosstalk of altered stromal cells with niche cells. The described niche changes are illustrated in Figure 8.

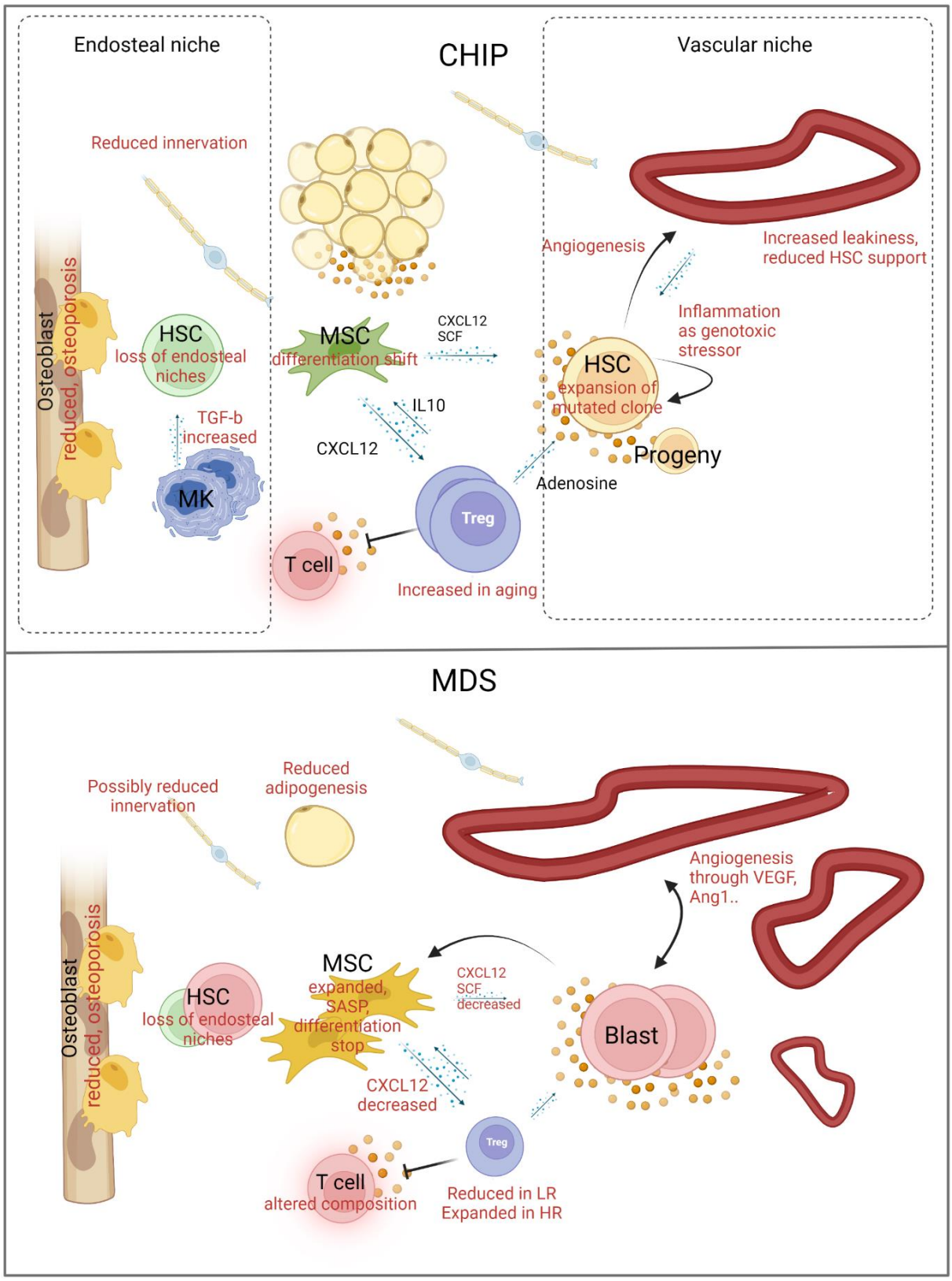

Figure 8: Niche changes in CHIP and MDS in comparison to healthy old BM with schematic crosstalk between niche cells. Created with Biorender.com.

1.5 New tools to study the complexity of the BM niche

During the last five years, increases in computational power, growing expertise in the analysis of omics data and, most of all, better affordability of kits and reagents led to a sharp surge in studies employing powerful new methods to study the complexity of the BM niche.

Single-cell transcriptomics of murine bone marrow was used to shed light on the cellular heterogeneity in BM cells, focusing especially on inferring cell-cell interactions via expression of receptor-ligand pairs in the niche (Tikhonova et al. 2019; Baccin et al. 2020; Baryawno et al. 2019). Another study united both transcriptional and epigenetic cues by combination of scRNA seq and single-cell ATAC sequencing, which allows assessment of chromatin accessibility. Combination of these techniques allowed the identification of distinct HSC and MPP populations and showed an early extensive epigenetic, but not transcriptional priming toward lineage commitment in human developmental hematopoiesis (Ranzoni et al. 2021).

In a pathologic context, scRNA seq was used to assess the influence of knockout (KO) of the CHIP mutations TET2 and DNMT3A on hematopoiesis in mouse models, showing that $TET2^{KO}$ led to myelomonocytic skewing in HSPC priming, while $DNMT3A^{KO}$ resulted in impaired erythropoiesis by affecting DNA-binding motifs of cell fate transcription factors (Izzo et al. 2020).

Recent advances in the development of antibodies that are tagged with RNA probes or elemental metal tags allowed the emergence of spatial transcriptomics and imaging mass cytometry, respectively. Combining spatial transcriptomics with scRNA seq allowed to identify and determine the localization of mesenchymal and CAR-cell subsets with distinct transcriptional profiles in the BM niche (Baccin et al. 2020). Other researchers classified novel regulators of HSC maintenance in stromal populations that were close to developing HSC in the embryonic developmental niche (Crosse et al. 2020). Imaging mass cytometry, allowing simultaneous detection of up to 40 markers, was used in different studies to analyze the spatial architecture of bone marrow in healthy people and MDS or AML patients (Oetjen et al. 2019; Oetjen et al. 2020). As of now, high cost of these multiplexed imaging approaches prevents broad studies on bigger patient cohorts, but this hurdle will likely fall in the near future, allowing further biological insight into the bone marrow architecture in a multitude of hematologic malignancies.

2 Objective

The aim of this thesis is the characterization of the cellular composition and the functional HSC support of the BM niche. Specifically, the stromal composition of the niche and changes in frequency and localization of main regulatory BM niche populations as outlined in the introduction will be assessed using multiplexed immunofluorescence imaging of human bone marrow FFPE samples. Changes in functionality and emergence of new subsets of stromal cells and immune cells will be analyzed using scRNA seq. Based on the results, functional models of interplay in the malignant niche will be used to gain insight in potential niche remodeling.

3 Material and Methods

3.1 Material

Table 2: List of chemicals and reagents that were used in the experiments.

Product	Catalog number	Company	Application
Acetone	67-67-1	Sigma Aldrich	Fixation of cells
ACK lysis buffer	A1049201	Thermo Fisher	Lysis of blood cells
aMEM	BE12-169F	Lonza	Cell culture
Bovine Serum Albumin (BSA)	90604-29-8	Roth	scRNA-seq
CellCover	800-250	Anacyte	Fixation of cells
Dibenzyl Ether (DBE)	103-50-4	Sigma Aldrich	iDisco+ clearing
Dichloromethane (DCM)	75-09-2	Sigma Aldrich	iDisco+ clearing
DMEM	61965026	Thermo Fisher	Cell culture
Dimethyl sulfoxide (DMSO)	67-68-5	Sigma Aldrich	Cell culture
DNAse	11243004	Th. Geyer	Sorting
Donkey serum	S2170-500	VWR	IF stainings
Ethylenediaminetetraacetic Acid (EDTA)	E5134	Sigma	IF stainings
Ethanol	64-17-5	Roth	DNA, RNA isolation
Fetal Bovine Serum (FBS)	16140071	Gibco	Cell culture
Glycin	56-40-6	Roth	iDisco+ clearing
GM-CSF	167300-03-B	Tebu Bio (Peprotech)	Cell culture
Human Platelet lysate (hPlt)	SCM152	Sigma Aldrich	Cell culture
Hoechst 33342	H1399	Invitrogen	IF stainings
Hydrogen peroxide (H_2O_2)	7722-84-1	Sigma Aldrich	iDisco+ clearing
Methanol	67-56-1	Roth	Fixation of cells
Mounting medium containing DAPI	ab104139	Abcam	IF stainings
Osteosoft	101728	VWR	Tissue preparation
Paraformaldehyde	30525-89-4	Sigma Aldrich	Tissue preparation
PBS	P3813	Roth	Buffers
Penicillin/Streptomycin (P/S)	15140122	Thermo Fisher	Cell culture
RPMI 1640	11530586	Gibco	Cell culture
Sodium azide (NaN_3)	S2002	Sigma Aldrich	Tissue preparation
Trilogy	920P	Cell Marque	IF stainings
Triton X-100	9002-93-1	Roth	IF stainings
Trueblack	23007	Biotium	IF stainings
Trueview	SP-8400	Vector Laboratories	IF stainings
TrypLE	12604013	Gibco	Cell culture
Tween 20	9005-64-5	Roth	IF stainings
Vectashield mounting medium	101098-042	Vector laboratories	IF stainings
Xylene	1330-20-7	Th. Geyer	IF stainings
Zinc formalin fixative	Z2902-3	Sigma	Tissue fixation

Table 3: List of consumables and kits.

Product	Model	Catalog number	Company
10x scRNA seq kit	Chromium Next GEM Single Cell 3' Kit v3.1	1000269	10x Genomics
96-well plate	Black clear F-bottom	655079	Greiner Bio One
Cell culture flask	CytoOne, Suspension cells, 75 cm^2	CC7672-4175	Starlab
	CytoOne, Adherent cells, 75 cm^2	CC7682-4875	Starlab
	CytoOne, Adherent cells, 225 cm^2	CC7682-4225	Starlab
	Adherent cells, FN1-coated, 75 cm^2	356242	Corning
Cell culture plates	Cellstar, 96-well, 24-well, 12-well, 6-well	655180	Greiner
	Spheroid, 96-well	4520	Corning
Conical centrifuge tubes	Falcon 15 ml	352096	Corning
	Falcon 50 ml	352070	
Cryovials	Cryogenic vials, external thread	430659	Corning
FACS tubes with cell strainer	Falcon 5 ml with cap	352058	Neolab
	Falcon 5 ml with filter cap	352235	
Gloves	Starguard comfort	SG-C-M	StarLab
Graduated pipettes	5 ml	606180	Greiner
	10 ml	607180	
	25 ml	760180	
	50 ml	768180	
Microtubes	1.7 ml	MCT-175-C	Corning
	0.6 ml	E1405-0610	StarLab
	1.7 ml Lo-bind	022431021	Eppendorf
Magnetic bead columns	LS plus columns	130-042-401	Miltenyi
Pipette filter tips	TipOne filter tip 10 µl	S1121-2710-C	Starlab
	TipOne filter tip 20 µl	S1120-1710-C	
	TipOne filter tip 200 µl	S1120-8710-C	
	TipOne filter tip 1000 µl	S1126-7710-C	
Pipette tips	TipOne 10 µl	S1111-3700-C	Starlab
	TipOne 200 µl	S1113-1700-C	
	TipOne 1000 µl	S1111-6700-C	
Pipetting reservoir	25 ml	04395-24	Argos Technologies
Cytokine assay	Procarta Plex 16-plex assay	PPX-16	Thermo Fisher
Serological aspirating pipettes	2 ml	710183	Greiner
Strainer	40 µm	352340	Neolab
	Easystrainer 70 µm	542070	Greiner
Syringe	10mL Syringes	sc-358907	Santa Cruz
Syringe needles	21G needles	613-4970	VWR
Weighing pan	89*89*25 mm	1-1125	NeoLab

Table 4: List of buffers and media and their composition.

Buffer	Composition	Application
Thawing buffer	FBS + 100 µg/ml DNAse	scRNA seq
Resuspension buffer	DMEM + 10% FBS + 100 ug/ml DNAse	scRNA seq
FACS buffer	PBS + 2% FCS	scRNA seq
Sorting buffer	PBS + 5% BSA	scRNA seq
Washing buffer	PBS + 1% donkey serum + 0.04% Tween 20	IF stainings
Permeabilization buffer	PBS + 0.2% Triton X-100	IF stainings
Blocking buffer	PBS + 5% donkey serum	IF stainings
Antibody incubation buffer	PBS + 0.25% Triton X-100 + 1% donkey serum	IF stainings
Permeabilization buffer	PBS-Triton X (0.5%) (PTx0.5)	Tissue clearing
Washing buffer	PBS + (0.5%) Tween 20 (PTwH0.5)	Tissue clearing
Blocking buffer A	78.6% PTx0.5, 1.4% glycine, 20% DMSO	Tissue clearing
Blocking buffer B	84% PTx0.5, 6% donkey serum, 10% DMSO	Tissue clearing
Antibody incubation buffer	92% PTwH0.5, 3% donkey serum, 5% DMSO	Tissue clearing

Table 5: List of primary antibodies used for Immunofluorescence (IF) stainings.

Antibody	Host	Reactivity	Concentration	Supplier	Catalog number
BCAM	Goat	Mouse	1:50	R&D systems	AF2899
CD105	Goat	Mouse, human	1:200	R&D systems	AF1320
CD271	Rabbit	Human	1:100	Abcam	Ab52987
CD3	Mouse	Human	1:100	LIFE Technologies	MA5-12577
CD3	Rabbit	Human, mouse	1:100	Dako	A0452
CD31	Goat	Mouse	1:200	R&D systems	AF3628
CD34	Sheep	Human	1:50	R&D systems	AF7227
CD34	Mouse	Human	1:50	Dako	M716529-2
CD8	Rat	Mouse	1:100	Thermo Fisher	MA5-16761
cGRP	Mouse	Human, mouse	1:100	Abcam	ab81887
CXCL12	Mouse	Human, mouse	1:50	R&D systems	MAB350
Endomucin	Rat	Mouse	1:100	Santa Cruz	Sc-65495
FoxP3	Rat	Mouse	1:100	Thermo Fisher	14-5773-82
FoxP3	Rat	Human	1:100	Thermo Fisher	14-4776-82
GFAP	Chicken	Human, mouse	1:100	Abcam	Ab4674
Lamin B1	Rat	Human	1:100	Sigma Aldrich	HS-404-017
LEPR	Goat	Mouse	1:100	Biotechne	AF497
OSM	Mouse	Human	1:100	Santa Cruz	sc-390253
PDGFRa	Goat	Mouse	1:100	R&D systems	AF1062
PDGFRb	Rabbit	Human, mouse	1:100	Cell Signaling Technology	3169
SCF-A647	Rabbit	Human, mouse	1:100	Biozol	BSS-BS-0545R-A647
Sca1	Rabbit	Mouse	1:100	Abcam	ab51317
SPARC	Goat	Human	1:100	Biotechne	AF941
Tyrosine Hydroxylase	Rabbit	Human, mouse	1:100	Merck	AB152
UEA1 FITC	-	Human	1:250	Biozol	VEC-FL-1061-2
UEA1 Dylight 649	-	Human	1:250	Biozol	VEC-DL-1068

Table 6: Secondary antibodies used for immunofluorescence stainings.

Antibody	Host	Reactivity	Concentration	Supplier	Catalog number
FluoTag-X2 Atto 488	Camelid	Rabbit	1:500	Biozol	NAT-N3202-AT488
AlexaFluor 488	Donkey	Mouse	1:500	Thermo Fisher	A21202
AlexaFluor 568	Donkey	Mouse	1:500	Thermo Fisher	A10037
AlexaFluor 647	Donkey	Mouse	1:500	Thermo Fisher	A32787
AlexaFluor 488	Donkey	Rabbit	1:500	Thermo Fisher	A32790
AlexaFluor 568	Donkey	Rabbit	1:500	Thermo Fisher	A10042
AlexaFluor 647	Donkey	Rabbit	1:500	Thermo Fisher	A31573
AlexaFluor 568	Donkey	Goat	1:500	Thermo Fisher	A11057
AlexaFluor 647	Donkey	Goat	1:500	Thermo Fisher	A21447
AlexaFluor 568	Donkey	Sheep	1:500	Thermo Fisher	A21099
AlexaFluor 568	Donkey	Rat	1:500	Thermo Fisher	A78946
AlexaFluor 647	Donkey	Rat	1:500	Thermo Fisher	A48272

Table 7: List of FACS antibodies used for cell sorting of human bone marrow aspirate.

Antibody	Fluorophore	Clone	Host species	Isotype	Company	Dilution
CD14	PE	HCD14	Mouse	IgG1	Biolegend	1:400
CD235a	PE	GA-R2 (HIR2)	Mouse	IgG2b	BD Biosciences	1:100
CD271	Vio-B515	REA844	Human	IgG1	Milteniy	1:50
CD3	BV650	UCHT1	Mouse	IgG1	BD Biosciences	1:400
CD31	AF647	WM59	Mouse	IgG1	BD Biosciences	1:100
CD34	PE-Vio770	AC136	Mouse	IgG2a	Milteniy	1:30
CD38	AF700	HIT2	Mouse	IgG1	BD Biosciences	1:30
CD45	BV711	HI30	Mouse	IgG1	BD Biosciences	1:300
CD71	PE	OKT9	Mouse	IgG1	Invitrogen	1:100
Fixable viability dye	eF780	-	-	-	Invitrogen	1:1000

Table 8: Microscopes used in the experiments.

Instrument	Manufacturer	Lasers/filter cubes	Objectives	Application
EVOS M5000	Thermo Fisher	Filters: DAPI, GFP, TxRed, Cy5, Cy7	4x air objective, NA 0.13 10x air objective, NA 0.3 20x air objective, NA 0.4 40x air objective, NA 0.95	ROI imaging (non-confocal)
Opera Phenix High-Content Screening System	Perkin Elmer	Lasers: 405, 488, 568, 647	4x air objective, 20x water objective, 40x water objective	High-throughput imaging (confocal)
UltraMicroscope Blaze	Miltenyi	Lasers: 488, 561, 640	4x oil objective, NA 0.35 20x oil objective, NA 0.53	3D microscopy

Table 9: Instrument and general equipment used.

Instrument	Manufacturer	Model
Automated cell counter	Invitrogen	Countess II Fl
Cell sorter	BD	FACS Aria
Centrifuge	Heraeus	Megafuge 1.0R
Centrifuge	Eppendorf	5415D
Centrifuge	Heraeus	Biofuge fresco
Chromium Controller	10x Genomics	Chromium Controller & Next GEM Accessory Kit
Fluorometer	Thermo Fisher Scientific	Qubit4
Freezer (-20 °C)	Liebherr	Premium NoFrost
Freezer (-80 °C)	Thermo Fisher Scientific	Forma 900 Series
Freezing container	Corning	CoolCell LX
Fume hood	Köttermann	2-453 GAND
Heating block	Starlab	Dry bath system
Incubator (cell culture)	Thermo Scientific	HeraCell 150
Inverted microscope	Zeiss	Primovert
Laminar flow hood	Heraeus	HSP18
Luminex instrument	Luminex	Magpix
Magnetic separator	Miltenyi	MidiMACS separator
Magnetic stirrer	Starlab	N2400-3010
Microplate reader	BMG Labtech Thermo Fisher Scientific	Fluostar Omega Varioskan LUX
Microvolume UV-Vis spectrophotometer	Thermo Fisher Scientific	Nanodrop
Microwave	Sharp	R-26ST-A
Mini centrifuge	Sunlab	SU1550
Mini vortex mixer	Sunlab	SU1900
Orbital shaker and incubator (benchtop)	Ohaus	SHRK04DG
pH meter	Mettler Toledo	FiveEasy
Pipettor	Integra	PipetBoy2
Precision balance	Kern	EW620-3NM
Refrigerator (4 °C)	Liebherr	Economy
Rocking shaker	IKA	Rocker 2D digital
Sequencing system	Illumina	NextSeq 2000
Tube roller	Starlab	N2400-7010
Waterbath	Memmert Grant	WNB14 SUB Aqua Pro

Table 10: List of software used for analysis.

Software	Version	Application
Bitplane Imaris	9.2	3D image analysis and visualization
FIJI	1.53a	Image analysis and processing
FlowJo	10.8.1	Flow data analysis
GeoDa	1.20.0.8	Clustering and dot-plots
GraphPad PRISM	9.5.0	Data analysis and visualization
Microsoft Office Excel	Excel 2016	Data analysis and processing
Microsoft Office Powerpoint	Powerpoint 2016	Graphic creation
Microsoft Office Word	Word 2016	Text processing
Perkin Elmer Harmony	4.8	Image analysis
Shiny App	V0.29	Visualization, annotation of scRNA seq data
String Database	V12	Functional enrichment analysis, protein-protein association networks
WebGestalt	2019	Gene set enrichment analysis

Table 11: Cell lines used for co-culture experiments.

Cell line	Medium	Origin	Supplier
hTERT-MSC	DMEM + 7% human platelet lysate + 1% P/S	Aspirate from healthy male donor, immortalized	Michelle Churchman (St. Jude's Hospital, Memphis)
MDS-L	RPMI + 10% FBS +1% P/S + 40 ng/ml GM-CSF	52-year-old male MDS patient	Wolfgang Seifarth (University Clinic Mannheim)
OCI-AML3	DMEM + 10% FCS + 1% P/S	57-year-old male AML patient	Martino Gabra (University of Toronto)

3.2 Methods

3.2.1 Processing of bone marrow trephine biopsates

Bone marrow trephine biopsates were obtained from willing donors enrolled in the BoHemE (**Bo**ne and **He**matology in the **E**lderly) study headed by Prof. Dr. Uwe Platzbecker (NCT02867085). Samples were obtained from the iliac crest from healthy donors, CHIP donors and MDS patients.

Table 12: Overview over the sample donors, including age, sex, eventual treatment, and the HSC mutation Variant Allele Frequency (VAF) found at the time of sample collection. If multiple mutations are present in one gene, all VAFs are listed, separated by slashes.

Patient ID	Classification	Age	Sex	Treatments	Mutation VAF	Used in
19/0062	CHIP	64	f	-	SF3B1 2.6%	IF
19/0299	CHIP	84	f	-	TET2 3.2/5%	IF
19/0318	CHIP	80	m	-	TET2 2.1/3.3%, PPM1D 1.1%	IF
19/0305	CHIP	72	f	-	DNMT3A 6.5%	IF
19/0377	CHIP	63	f	-	TET2 2.5%, DNMT3A 3.2%, BCOR 1.2%, ZRSR2 31%	scRNA seq, IF
19/0423	CHIP	69	m	-	DNMT3A 12%, IDH2 7.4%	scRNA seq, IF
19/0438	CHIP	79	f	-	TET2 2,2%	IF
19/0439	CHIP	84	m	-	TET2 3%, KRAS 22%	scRNA seq, IF
20/0161	CHIP	79	f	-	SRP72 3.16%	IF
19/0069	Control	69	f	-	-	IF
19/0084	Control	62	f	Irradiated	-	IF
19/0039	Control	62	m	Irradiated	-	IF
19/0103	Control	63	f	-	-	IF
19/0130	Control	68	f	-	-	IF
19/0152	Control	79	f	-	-	IF
19/0122	Control	65	f	-	-	IF
19/0163	Control	75	f	-	-	IF
19/0209	Control	76	f	-	DNMT3A 1.4%	IF
19/0213	Control	68	f	-	-	scRNA seq, IF
19/0254	Control	76	m	-	TET2 1.7%	IF
19/0281	Control	64	m	-	-	IF
19/0310	Control	67	f	-	-	IF
19/0302	Control	77	f	-	-	IF
19/0309	Control	77	f	Irradiated	-	IF
19/0317	Control	79	f	-	-	IF
19/0355	Control	75	f	-	TET2 1.1%, DNMT3A 1.6%	IF
19/0027	Control	75	f	Irradiated	-	IF
19/0383	Control	71	m	Irradiated	-	IF
19/0392	Control	60	f	-	-	IF

19/0254	Control	76	m	-	TET2 1.7%	IF
19/0514	Control	67	f	-	-	IF
20/0011	Control	63	f	-	-	scRNA seq, IF
20/0158	Control	72	f	-	-	IF
20/0169	Control	66	m	-	-	IF
20/0153	Control	70	m	-	-	IF
20/0185	Control	76	f	-	DNMT3A 1.94%	IF
20/0219	Control	79	f	-	DNMT3A 1.42%	IF
20/0184	Control	66	f	-		IF
17/0566	MDS	70	f	Azacytidine	TET2 30/20/7.6%, DNMT3A 28%	IF
17/0730	MDS	71	m	Luspatercept, erythropoetin + G-CSF, chelation	SF3B1 82%	IF
17/0731	MDS	76	m	-	SF3B1 36%, TET2 16%, DNMT3A 32%	scRNA seq
17/0751	MDS	79	f	Erythropoetin + Growth factors	TET2 35%, MPL 56%	IF
17/0771	MDS	72	f	Luspatercept	ASXL1 23%, TP53 7%, KIT 12%, SETBP1 6/3%, STAT3 2.6%	IF
17/0757	MDS	66	m	-	No mutation detectable	IF
17/0803	MDS	73	f	Luspatercept, chelation	SF3B1 45%, TET2 30/23%	scRNA seq
18/0218	MDS	89	m	EPO + G-CSF	SF3B1 21/6/6/2.1%, DNMT3A 44%	IF
18/0248	MDS	67	f	Azacytidine	TET2 1.9%	IF
18/0369	MDS	77	f	Luspatercept, chelation	SF3B1 46%	IF
18/0388	MDS	83	m	Luspatercept	SF3B1 32%, ASXL1 1.6%, DNMT3A 30/1.5%	IF
18/0471	MDS	75	f	Luspatercept	SF3B1 24%	IF
18/0871	MDS	78	m	Azacytidine	SF3B1 43%, TET2 43%, RUNX1 43%, BCORL1 83%, NRAS 24/7.5/1.12/1.05%, KRAS 1.05%, PPM1D 1.05%	IF
18/0899	MDS	62	m	Luspatercept	SF3B1 33%, DNMT3A 29%	scRNA seq
19/0024	MDS	79	m	-	TET2 87%	IF
19/0189	MDS	66	m	Allo-SCT	DNMT3A 1.5%	IF
17/1028	MDS	69	m	-	DNMT3A 1.12%, BCOR 4.67%	IF
20/0075	MDS	62	f	-	SRSF2 27.9%, ASXL1 39.8%, ETNK1 1.7%, CBL 13.4%, ZRSR2 36%, SETBP1 40.7%	IF
17/0708	MDS	76	m	-	SRSF2 27%, TET2 41/35%, ZRSR2 72%	scRNA seq
17/0803	MDS	73	f	Luspatercept, chelation	SF3B1 45%, TET2 30/23%	scRNA seq

Iliac crest or femur biopsies were fixated in 4% PFA solution and transferred to 50% ethanol solution after 24 h to avoid overfixation and artifacts. These samples were collected and processed together after up to 6 months. Decalcification, embedding, cutting, and mounting of tissue on charged slides was done by the biobank of the University Medical Center in Mainz.

For mouse experiments, murine femurs from young and old control as well as DNMT3A^{R878H} were obtained from Logan Schwartz (Trowbridge lab, Jackson laboratories). The DNMT3A mutation was induced in young animals (9 weeks) by intraperitoneal injection of 15 mg/kg polyinosinic-polycytidylic acid (polyI:C) for five consecutive days. 4 months later, mice were sacrificed. Femurs were fixated in 4% PFA at 4 °C overnight and shipped in PBS + 0.3% NaN_3. After decalcification, bones were embedded in paraffin, cut, and mounted on charged slides for subsequent stainings. Mice of 16–86 weeks were taken for stainings, the corresponding age in human was estimated according to the supplier's recommendations (Jackson Laboratory). Mice up to 30 weeks were considered "young." Mice from 68 weeks and older were considered "old."

Table 13: Overview over the mouse samples used in the staining experiments.

Sample	Sex	Genotype	Age (in weeks)	Group	Corresponding age in humans
B6-1	f	C57bl6	68	Old control	Mid-50s
B6-2	f	C57bl6	68	Old control	Mid-50s
B6-3	f	C57bl6	68	Old control	Mid-50s
Contr1	f	MxCre-Control	26	Young control	Early 30s
Contr2	f	MxCre-Control	26	Young control	Early 30s
Contr3	f	MxCre-Control	26	Young control	Early 30s
D3A1	f	MxCre-DNMT3A	26	DNMT3A mutated	Early 30s
D3A2	f	MxCre- DNMT3A	26	DNMT3A mutated	Early 30s
D3A3	f	MxCre- DNMT3A	26	DNMT3A mutated	Early 30s

3.2.2 Immunofluorescence staining on bone marrow samples

For better adherence of tissue to the charged glass slides, the samples were baked at 37 °C overnight. Deparaffinization, rehydration and Heat-Induced Epitope Retrieval (HIER) were done using Trilogy 3-in-1 reagent in a pressure cooker at 105 °C, 1.4 bar for 10 min.

HIER is a method used to revert the effect of paraformaldehyde fixation in samples. Paraformaldehyde can crosslink proteins, masking the antigen binding sites. This leads to weaker binding of antibodies, resulting in weaker signals (Ezaki 2000). Slides were permeabilized with PBS + 0.2% Triton-X for 10 min, then blocked for 30 min with 5% donkey serum PBS-T. Antibodies were titrated in tests and used at optimal dilutions in 1% donkey serum PBS-Triton X (0.25%) overnight at 4 °C or for 1 h at RT, secondary antibodies were applied for 2 h at RT at a 1:500 concentration.

Tissues display autofluorescence, resulting from e.g. lipofuscin or heme proteins. This masks specific staining, making it necessary to use quenching reagents. Different techniques were tested to reduce bone marrow autofluorescence (Figure 46). For this thesis, slides were incubated for 3 min at RT with 100 µl Trueview (Vector Labs) and washed with PBS for 5 min afterwards. A drop of mounting medium containing DAPI was added to each slide, and they were sealed with a coverslip.

Bone marrow slides were imaged using an Opera Phenix high-content screening system (PerkinElmer) at 40x magnification for human samples and 20x for murine samples unless stated otherwise. Laser power was set to 100% for 200 ms, the channel sequence was changed to minimize the overlap between adjacent channels (DAPI with A488, A568 with A647). No-stain as well as secondary antibody-only controls were used to rule out unspecific staining. For Giemsa images, slides were imaged using an EVOS M5000 microscope.

3.2.2.1 Image analysis of bone marrow slide data

For 2D analysis of immunofluorescence bone marrow images, PerkinElmer Harmony High-Content Analysis Software was used. Image analysis pipelines for every experiment can be found in the annex (Figure 47 to Figure 54). Giemsa images for cellularity measurements were processed using FIJIs integrated trainable Weka segmentation plugin (Figure 50). Dot plots and density-based clustering were done using GeoDa software, based on the DBScan* algorithm. Clusters were defined as a minimum of 5 points, minimum cluster size of 5 and a distance threshold of 100 µm. These cluster values were determined experimentally; the distance threshold was set on the basis of paracrine signaling affecting cells most effectively in a 100 µm distance (Francis and Palsson 1997; Handly et al. 2015).

3.2.3 Tissue clearing of mouse femurs and trephine cores

Human trephine cores and murine femurs were processed according to the iDisco+ protocol (Jin et al. 2019). Samples were fixated overnight in zinc formaline fixative at 4 °C and washed with PBS afterwards. For storage and transport, samples were kept in PBS + 0.1% NaN_3 for up to 4 weeks.

To decalcify the bones, the femurs were incubated in Osteosoft solution for 2 days. The bones were washed in deionized H_2O for 2x 1 h and dehydrated in 20%, 40%, 60%, 80% and 100% MeOH for 90 min each, then incubated in 100% MeOH overnight. Incubation in 66% DCM/33% MeOH followed for 2 h and then, after a medium change ,overnight. After washing for 2x 3 h in 100% MeOH, samples were decolorized in 5% H_2O_2 in MeOH overnight at 4 °C. After rehydration in 80%, 60%, 40%, 20% MeOH and deionized H_2O for 90 min each, the bones were transferred to PTx0.5 and permeabilized for 2x 1 h and then overnight at 37 °C and finally for 48 h in permeabilization solution (Table 4) at 37 °C. Incubation in blocking solution to minimize unspecific binding was done for 48 h at 37 °C. Antibodies were diluted 1:500 in staining solution (Table 4) and samples were incubated for 7 days in total at 37 °C, with daily addition of a dose of 1:500 antibody over four days to a total end concentration of 1:100.

After a wash for 4 days in PTwH0.5 at 37 °C, samples were transferred to secondary antibody staining solution with 1:500 secondary antibody and were incubated for 7 days at 37 °C with a daily booster of 1:500 AB for four days to a final concentration of 1:100. After washing for 4 days with daily medium change in PTwH0.5 at 37 °C, samples were dehydrated with 20%, 40%, 60%, 80% and 100% MeOH and finally transferred to 66% DCM/33% MeOH for 2x 2 h and after medium change overnight. Refractive index was then adjusted by incubating in 100% DCM for 2x 3 h and 100% DBE for 2x 3 h; samples were stored in DBE for light sheet imaging.

3.2.3.1 Light sheet imaging

Cleared bones were imaged using an UltraMicrocope Blaze (Milentyi Biotec; in DBE) using a 4x objective and 1.66x zoom. Step size for stacks was 3 µm, laser power adjusted for

each independent experiment to allow optimal signal strength while maintaining comparability between samples of one experiment.

3.2.3.2 Light sheet imaging data analysis

Image data was analyzed and visualized using Bitplane Imaris 9.8.0. For vessel detection, a surface was generated using the "Add new surface" option with a voxel size filter to filter out $CD31^+$ blood cells and small artifacts. This surface was used as a template for a masked binary channel to prevent loss of lower intensity signal. The "Add new filaments" feature was employed using the "Threshold" (loops) option to reconstruct blood vessels on this masked channel. Vessel diameter and volume of all detected vessels was taken as readout parameter to compare the vasculature.

3.2.4 In vitro co-culture experiments for secretome analysis

For co-culture secretome analysis, 200.000 hTERT-MSC were seeded in aMEM + 7% hPLt in a 6 well-plate. Using normal FBS led to high background signal in the secretome analysis. After 48 h, the wells were washed five times with PBS and twice with aMEM without platelet lysate. MDS-L cells were washed twice with PBS and once with aMEM, then added in fresh medium to the corresponding wells. Co-cultures with ratios of 1:0, 10:1, 1:1, 1:10, 0:1 were cultured for 24 h. Afterwards, the conditioned medium was collected, centrifuged at 300 *g* for 5 min, then at 10.000 *g* for 5 min to remove cellular debris. The samples were stored at -20 °C and processed within a week. Quality control, mass spectrometry and softcluster generation was kindly done by Gereon Poschmann (AG Stühler, MPL Düsseldorf). Data analysis was done using Microsoft Excel, pathway visualization with String-db.org and volcano plots with GraphPad Prism.

3.2.5 Luminex cytokine analysis

10 000 hTERT-MSC were seeded in 100 µl 7% hPLt aMEM in a 96-well spheroid culturing plate. After 3 days, spheroids formed and 50 µl medium were removed. 1000 MDS-L or OCI-AML3 cells were added to the spheroids in 50 µl fresh culture medium (Table 4). After 48 and 96 h, 50 µl supernatant were taken from each well, same conditions were pooled

and centrifuged at 300 *g* for 5 min to pellet residual cells. Supernatant was transferred to a fresh tube and centrifuged at 10 000 *g* for 5 min to remove cellular debris.

For cytokine analysis, a custom-made human cytokine assay kit from Thermo Fisher was purchased. Standards were prepared and the procedure was done as indicated in the manual with technical duplicates for each sample. In addition to the generated mono- and co-culture samples, media controls were included to see if cytokines from platelet lysate or FBS skew the results. The Luminex assay did not show any cytokines in the media controls besides GM-CSF which was added to the MDS-L cultures (data not shown). Measured cytokine concentrations were plotted and heatmaps were created using GraphPad Prism.

3.2.6 Processing of human bone marrow aspirates for flow cytometry and FACS

Human bone marrow aspirates were also obtained from the BoHemE cohort (Platzbecker, University Medical Clinic Leipzig). Samples with over 100 million cells from donors of similar age and sex were selected for sequencing. Each vial was thawed in a water bath, then immediately transferred to a 50 ml tube, and suspended in 1 ml thawing buffer to prevent clumping of extracellular DNA. Whenever clumping occurred, samples were left in DNAse-containing buffer and gently resuspended until clumps dissolved. 3 ml resuspension buffer was added; the samples were then centrifuged at 300 *g* for 5 min. The supernatant was discarded, the pellet was resuspended in 5 ml ACK lysis buffer and incubated for 7 min at RT. 25 ml of PBS were added, and the tube was centrifuged at 300 *g* for 5 min. The supernatant was aspirated, the sample was resuspended in 2 ml FACS buffer and filtered through a 70 µl cell strainer. The cells were stained using a fixable viability dye for 15 min at RT in the dark. After washing with FACS buffer and centrifugation at 300 *g* for 5 min, the pellet was resuspended in 1 ml CellCover for fixation (7 min, RT). The cells were centrifuged for 5 min at 300 *g* and stained in antibody staining solution at 4°C in the dark. Before sorting, cells were washed with FACS buffer again, centrifuged for 5 min at 300 *g*, resuspended in CellCover and filtered through a 40 µm filter. Sorting was done on a FACS Aria with a 130 µm nozzle with a maximum flow rate of 5000 evts/s and sorted into sorting buffer in BSA-coated LoBind tubes according to the sorting strategy.

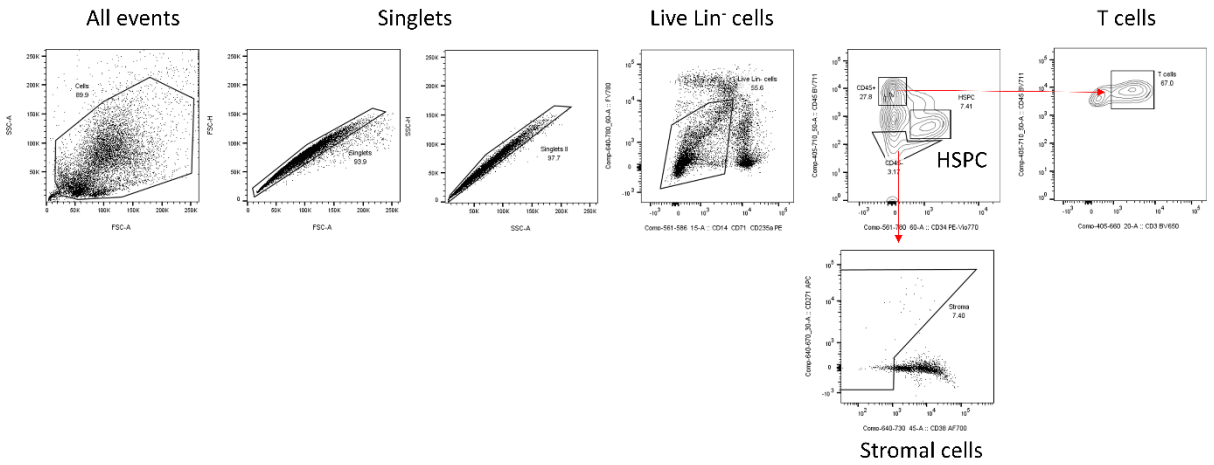

Figure 9: Sorting strategy for the human BM aspirates. T-cells were defined by Lin$^-$ CD45^{high} CD3$^+$, HSPC by Lin$^-$, CD45^{mid}, CD34$^+$ and stromal cells as Lin-, CD34$^-$, CD45^{low}, CD38$^-$.

The sorted populations were used in the 10x single cell RNA-sequencing protocol and sequenced on an Illumina NextSeq 2000. For sequencing, T-cells and HSPC were pooled together and put into one lane on the 10x chip in the Chromium controller, while stromal cells were put in another lane. All following steps were done according to the 10x scRNA seq protocol. Samples from different conditions (control, CHIP, MDS) were processed each experimental day to minimize batch effects. FACS data was visualized and analyzed using FlowJo software.

3.2.7 scRNA seq data analysis

Sequencing, data quality assessment and data processing was kindly done at EMBL Heidelberg by GeneCore and Maksim Kholmatov, respectively. Cluster annotation was done using previously validated datasets: Celltypist, Monaco and Blueprint immune cell atlases were used for curated annotation of immune cells (Domínguez Conde et al. 2022; Monaco et al. 2019; Qian et al. 2020), Tabula Sapiens, HCA BM atlas and other datasets for HSPC and stroma cells (Ennis et al. 2022; Jones et al. 2022; Mende et al. 2020; Woods and Guezguez 2021). For unidentified datasets, differentially expressed genes (DEG) for each cluster were analyzed and cell identities accordingly assigned. Differential gene expression from clusters and subclusters in comparison to other donors and between conditions were used for subsequent analysis. A web-based Shiny app generated in R was used for visualization of scRNA seq data.

3.2.8 Gene set enrichment analysis

Analysis of DEG was done using gene set enrichment analysis with WebGestalt, a web-based gene set analysis toolkit. Briefly, lists of DEG with corresponding log_2-fold change were uploaded to WebGestalt. GSEA analysis with Wikipathway as functional database was selected, with a minimum number of 3 genes per category, maximum number of 2000 per category, significance level top 10, 1000 permutations and p=1. A background gene list does not have to be provided, as it is derived from not significantly upregulated genes in the same list.

3.2.9 Statistical testing

For statistical testing, the following rationale was followed: Human bone marrow trephine cores are very heterogeneous in composition (depending on donor, sampling technique, age, sex, treatments, sampling site), which leads to the assumption that experiments on these samples generate non-normally distributed data. For this reason, for experiments with one readout parameter and more than two groups, the Mann-Whitney *U* test was employed and Kruskal-Wallis test with Dunn's multiple comparisons for samples with multiple readout parameters and multiple groups. Mouse samples are biologically more homogenous, which is why one-way ANOVA with Tukey's multiple comparisons was used for singular and two-way ANOVA with Šidák's multiple comparisons for multiple readout parameters and more than two groups. If only two groups were compared, Welch's t-test was employed. P values are plotted as asterisks and have the following significances:

Table 14: Symbols used for statistical significance and their corresponding p-values.

Symbol	Meaning
ns	$P > 0.05$
*	$P \leq 0.05$
**	$P \leq 0.01$
***	$P \leq 0.001$
****	$P \leq 0.0001$

4 Results

4.1 Characterization of the human BM HSC niche

The bone marrow trephine samples collected in the BoHemE study, encompassing control (non-disease), CHIP and MDS biopsies (Table 12), were first characterized in terms of donor age, sex, and Bone Marrow Cellularity (BMC) to guarantee comparability between the conditions.

4.1.1 Case-cohort sampling scheme, stratified by age, sex and cellularity

There is an overrepresentation of female donors in the control and CHIP group since the recruited patients are undergoing hip or knee replacement surgery, which are more frequent in women (Figure 10A, B). For this patient biopsy cohort, no strong correlation of patient age with overall BMC was detectable (Figure 10C). MDS samples have a higher mean BMC compared to control and CHIP samples, which is due to the lower number of adipocytes as observed in the Giemsa stainings (Figure 10D, E). In addition, trabecular bone structure was not as frequently observed in MDS samples.

A

Sample	Number of samples	Median age	Mean cellularity
Control	31	70	0.19
CHIP	9	79	0.11
MDS	16	72	1.66

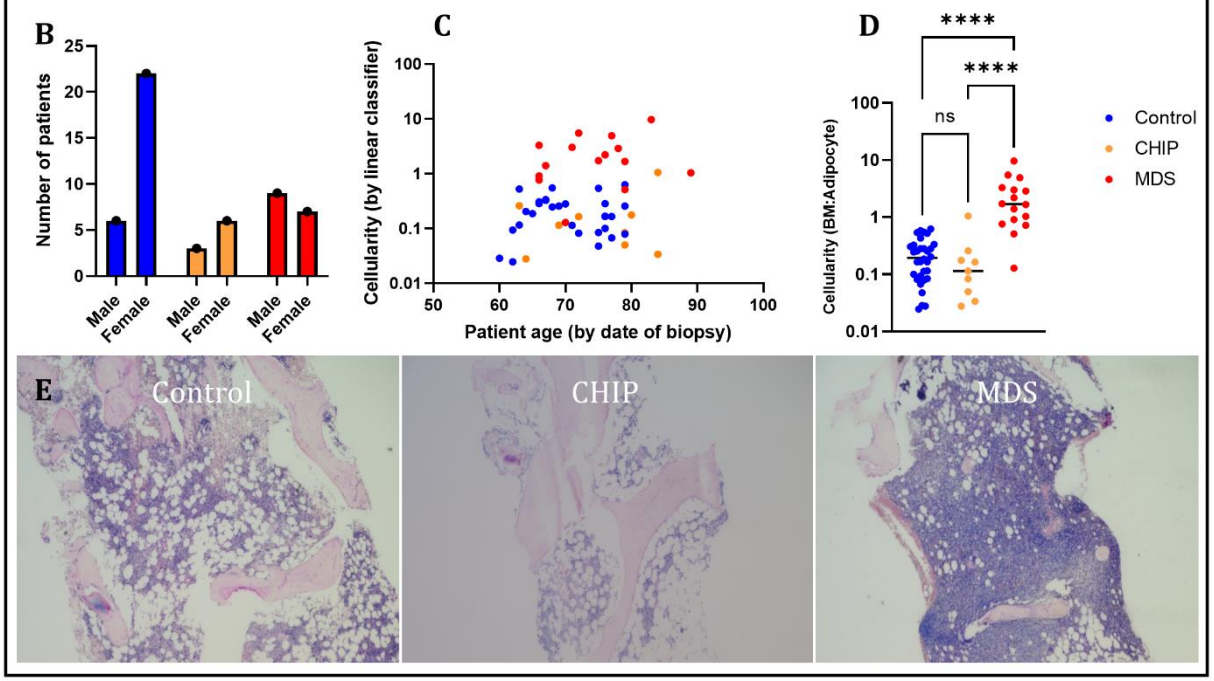

Figure 10: Characterization of sample cohort used for imaging experiments in human bone marrow hip trephine cores. ***A*** *Number of samples, median age and mean cellularity determined by linear classifier.* ***B*** *Number of donors by sex.* ***C*** *BMC as function of donor age.* ***D*** *Cellularity per sample determined by linear classifier. Kruskal-Wallis test was employed to test for statistical significance.* ***E*** *Representative Giemsa stainings of patient samples.*

4.1.2 Vasculature in the human bone marrow niche

For a complete characterization of the HSC niche in BM samples and due to the importance of vasculature in supporting HSC functions (as discussed in chapter 1.3.5), the relative frequency of sinusoidal and arteriolar vasculature was analyzed using immunostaining for CD105 (endoglin), a specific marker for sinusoidal vasculature in human (Fomin et al. 2013), and UEA-1, respectively. UEA-1 is a bright vasculature marker and leads to more consistent results than CD31 or CD34 staining, as seen in Figure 55 (annex).

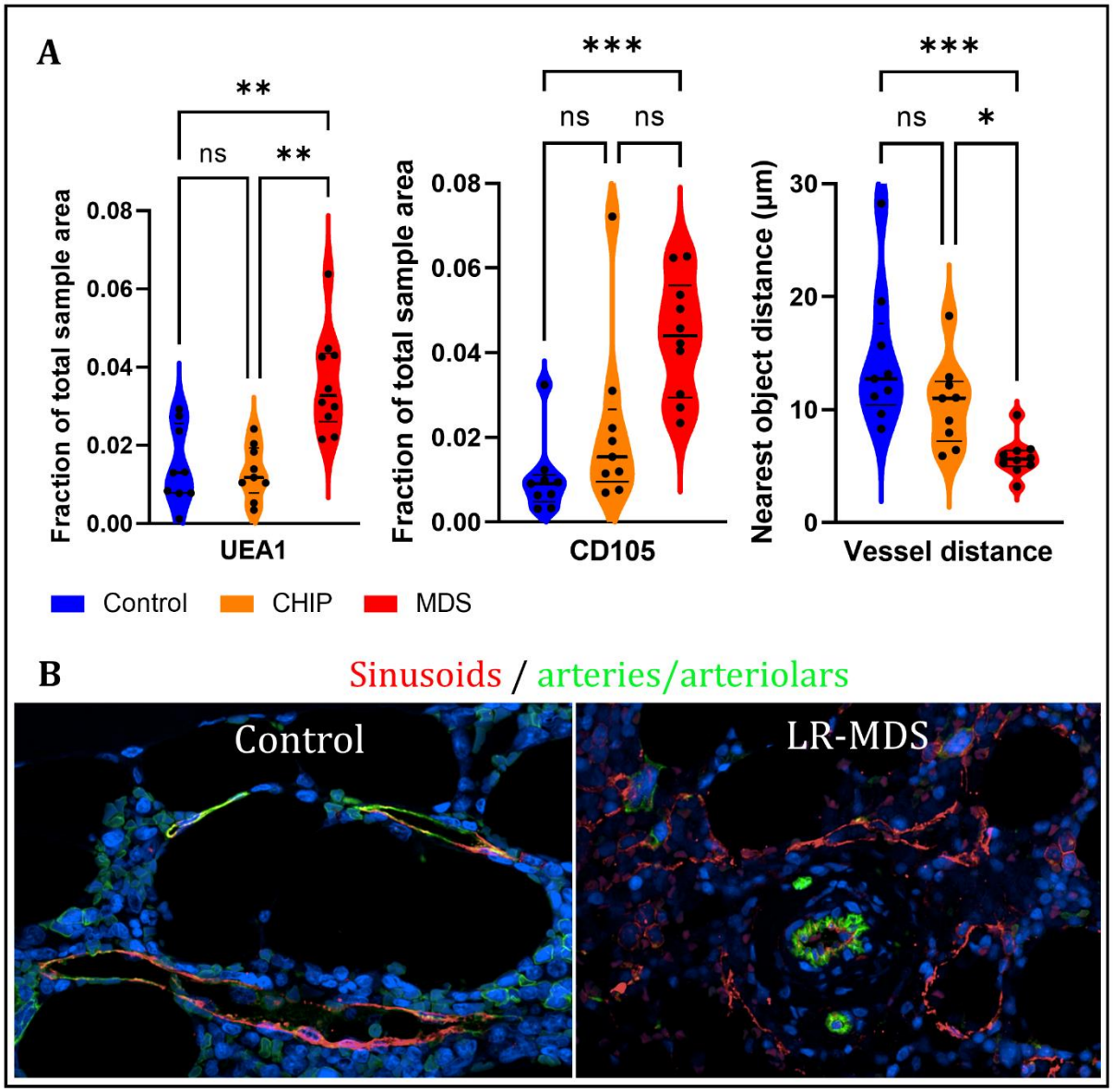

Figure 11: Vasculature analysis of human BM trephines. ***A*** *Fraction of total vessel surface (UEA-1) and sinusoids (CD105) as well as mean distance of vessels (N = 9–10). Kruskal-Wallis test was employed to test for statistical significance.* ***B*** *Representative images of sinusoids and total vasculature in control and MDS tissue. Brightness and contrast were adjusted for better visibility.*

The total vasculature area of MDS samples was increased in comparison to control and CHIP biopsies (Figure 11A). In addition, the sinusoidal $CD105^+$ vessel surface was extensively remodeled with an expansion of sinusoidal vessels in MDS in comparison with control, while CHIP samples showed a tendency towards increased sinusoid surface area. As a result of the increased vascular density in MDS samples, the mean distance between sinusoidal and arteriolar $CD105^-$ $UEA1^+$ vessels was decreased from 10–15 µm in control and CHIP to circa 5 µm in MDS. In addition, sinusoids in MDS samples showed disorganized, leaky vasculature and microvasculature (Figure 11B).

4.1.3 MSC in human BM biopsies

In addition to the vasculature, another major component of the BM niche are MSC, which were characterized by immunostaining for CD271, a marker that is expressed on the MSC population with the highest multipotency, differentiation- and reconstitution potential (Quirici et al. 2002). In addition, the functionality of vasculature and MSC to support HSC via CXCL12 as described in chapter 1.3.2 was evaluated by co-staining of CD105 and CD271 with CXCL12.

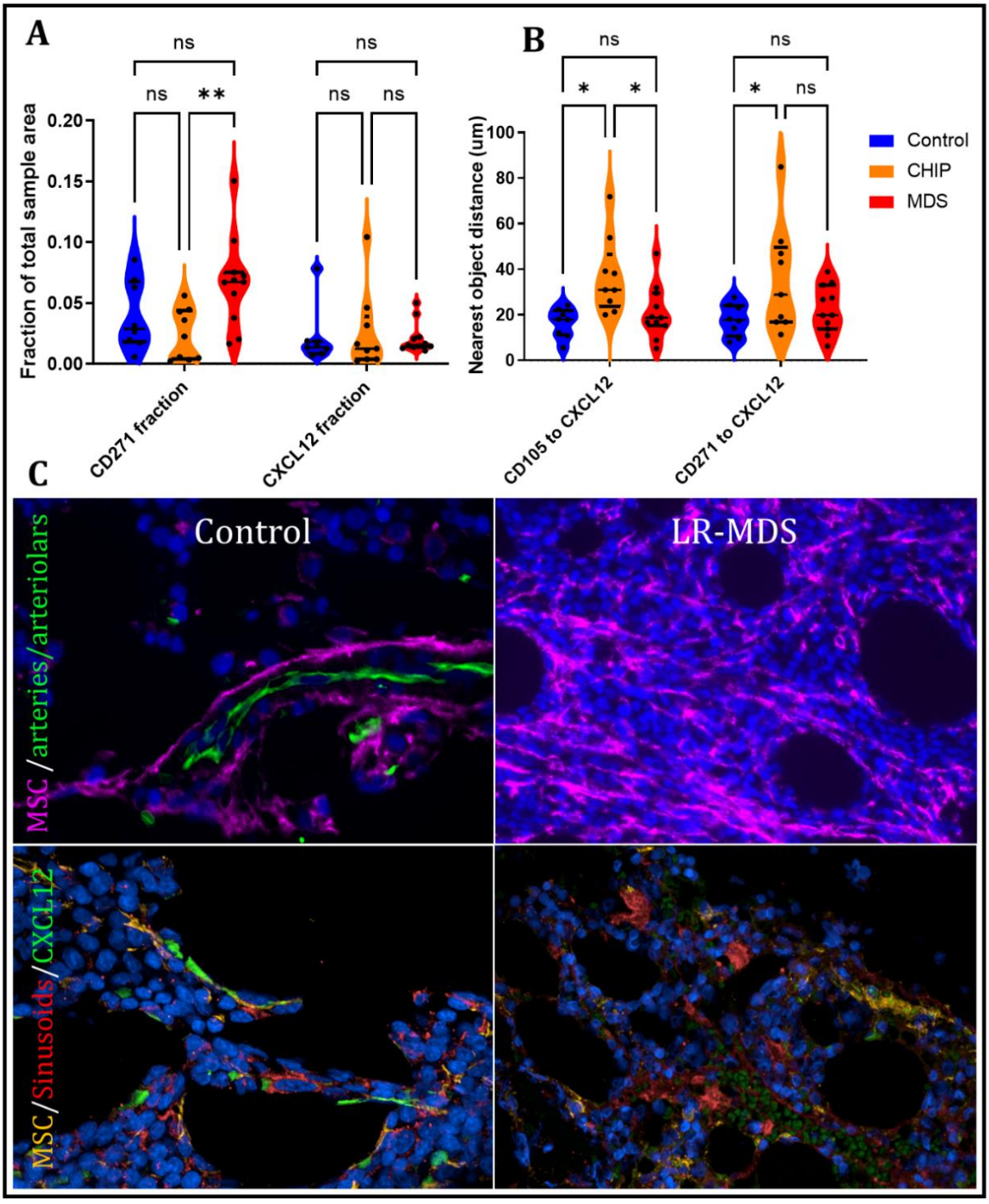

Figure 12: Stroma analysis in human BM. ***A*** *Fraction of total MSC surface (CD271) and CXCL12 surface as well as* ***B*** *mean distance of vessels and MSC to CXCL12 (N = 9–11). Kruskal-Wallis test was employed to test for statistical significance.* ***C*** *Representative images of MSC, sinusoids, arteriolars and arteries as well as CXCL12 in control and MDS tissue. Brightness and contrast were adjusted for better visibility.*

In most MDS samples, MSC were expanded in comparison to control and CHIP samples, apart from a few samples where no expansion was detectable. The overall tissue surface expressing CXCL12 was proportionally similar in the different conditions despite the expansion of sinusoids and MSC (Figure 12A). Despite that, ROI images showed fewer MSC

and sinusoidal cells with high expression of CXCL12 in MDS (Figure 12C, bottom panel). Interestingly, the distance of detected CXCL12 to sinusoids and MSC was higher in CHIP samples in comparison to controls (Figure 12B). Expanded MSC in MDS were not restricted to perivascular and periosteal localization (as for control and CHIP) but were heterogeneously distributed throughout the bone marrow, displaying a mesh-like phenotype (Figure 12C, upper row).

4.1.4 HSPC frequency in human BM samples

For a complete characterization of the HSC BM niche, the frequency of HSPC, determined by surface expression of CD34, was assessed.

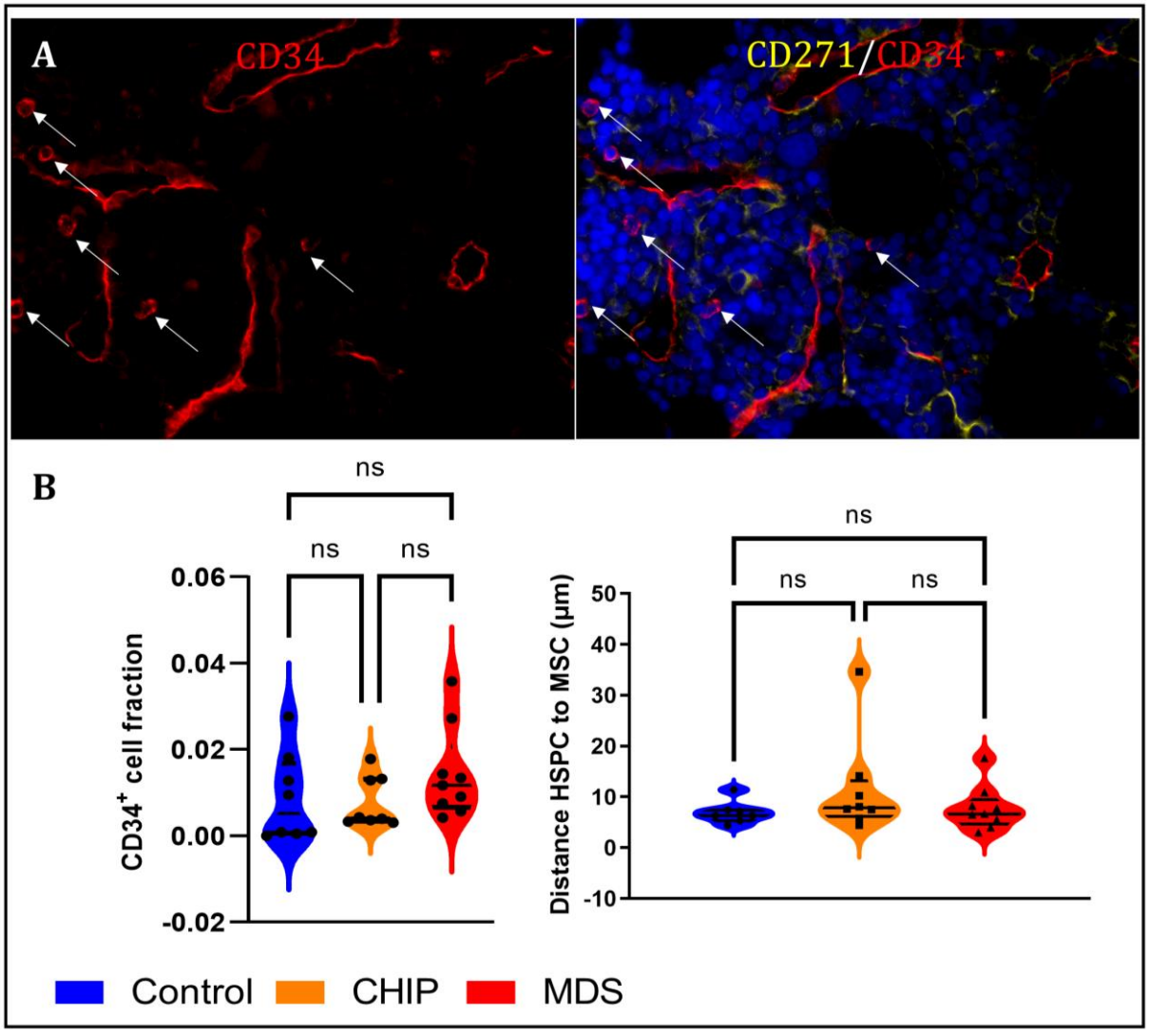

*Figure 13: HSPC analysis in human BM. **A** Example images of CD34+ HSPC in human BM. Vessel surface is also CD34+, which hinders automatic analysis. Brightness and contrast were adjusted for better visibility. **B** HSPC cell fraction and mean distance from HSPC to MSC (N = 9). Kruskal-Wallis test was employed to test for statistical significance.*

Tracking of HSPC in the bone marrow remained difficult due to the lack of specific markers. The most widely used one, CD34, is also found on vasculature, rendering automatic analysis challenging (Figure 13A), which is why manual analysis of ROI images was employed. Surprisingly, there was no apparent difference in the relative amount of HSPC in the bone marrow in either condition. The distance of HSPC to MSC was not visibly changed in any of the conditions, close proximity of both cell populations was found in all samples (Figure 13B).

4.1.5 Alterations in T lymphocytes in the human bone marrow niche

Given the dual role of T lymphocytes in HSC regulation (described in chapter 1.3.6), frequency of T cells (especially Treg) and their spatial distribution were studied, using CD3 as a general T cell marker and nuclear FoxP3 staining to identify Tregs.

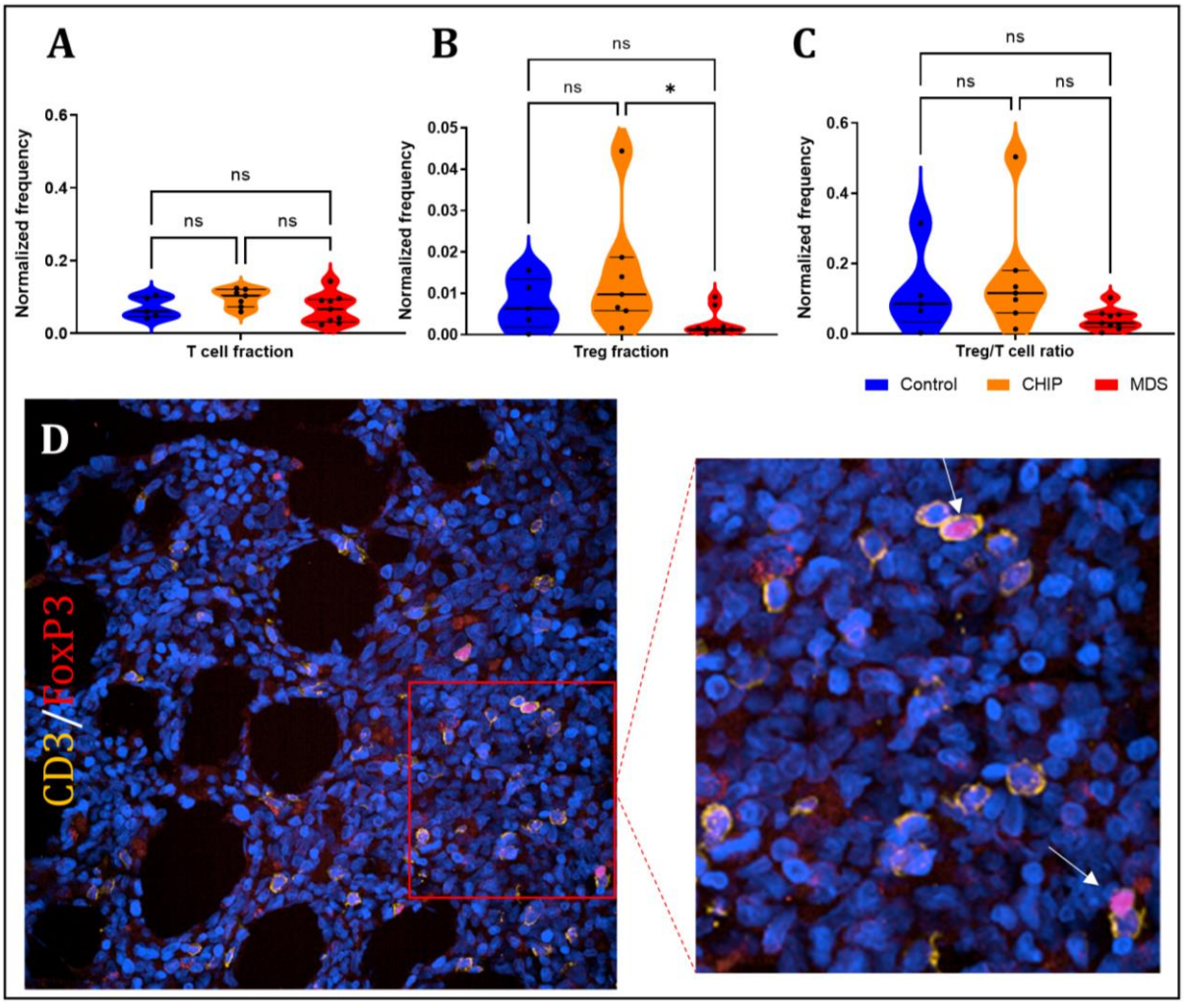

*Figure 14: T lymphocyte analysis in human BM. **A** T cell and Treg fraction as well as Treg to T cell ratio in human BM samples (N = 5–9). Kruskal-Wallis test was employed to test for statistical significance. **B** Representative images of T cells (CD3⁺) and Tregs (CD3⁺ FoxP3⁺) in human BM. Brightness and contrast were adjusted for better visibility.*

T cells in all samples were in the previously reported normal physiological range of 5–15% (Parmentier et al. 2020), and were often in close contact with Tregs (Figure 14A, D). Tregs were sparse in all conditions, but MDS samples showed a distinct reduction in Tregs in comparison to CHIP (Figure 14B). In addition, there was a trend towards decreased Treg/T cell ratios in MDS samples (Figure 14C), suggesting that Tregs constitute a smaller fraction of the total T cell pool in MDS. This effect is not statistically significant, but a trend became apparent. For better assessment of spatial distribution, individual T cells and Tregs were visualized as dot plots with their corresponding XY-coordinates and clusters of cells (>5 cells per cluster) were analyzed using the density-based clustering approach DB-scan.

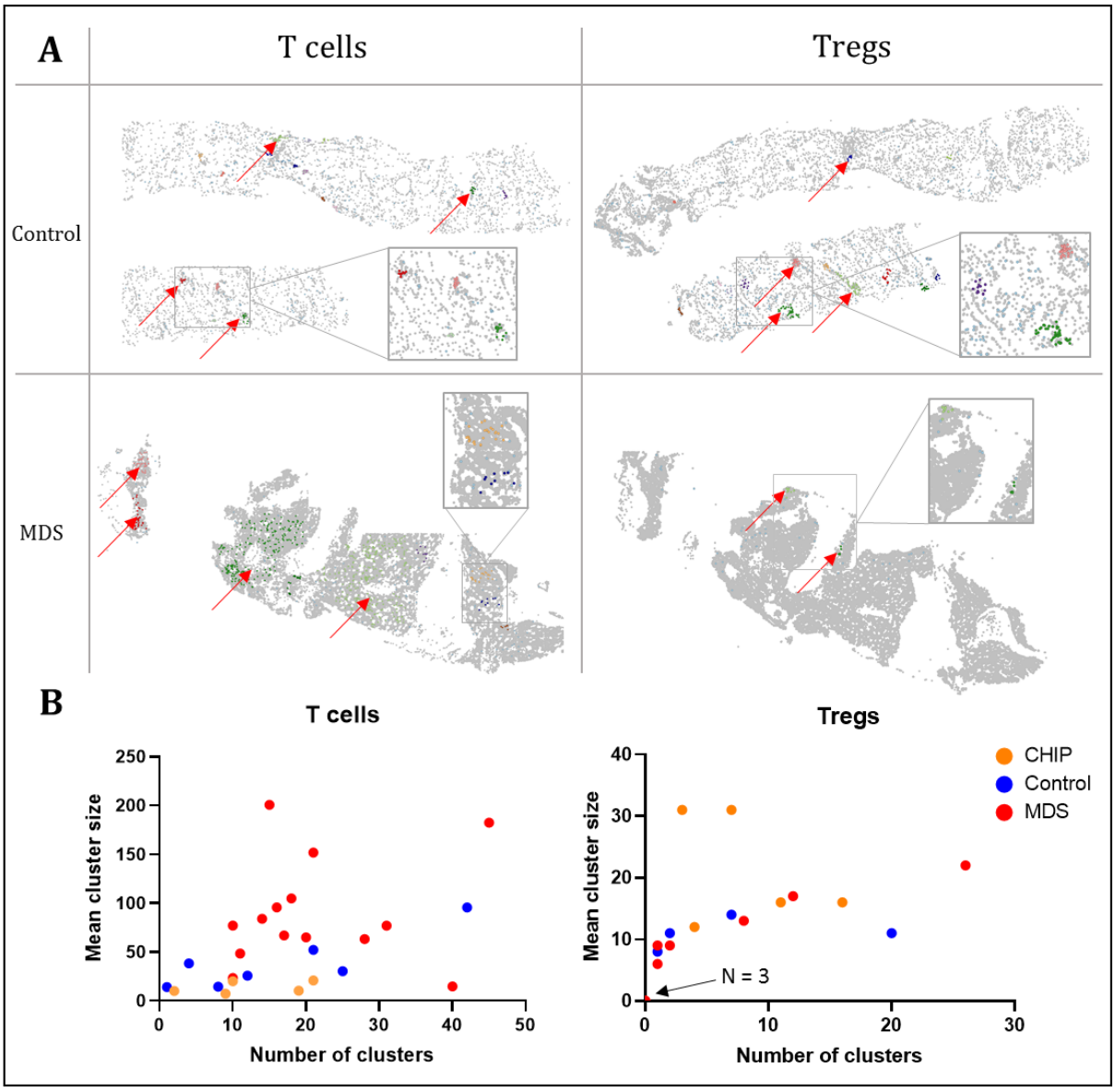

Figure 15: Spatial T cell distribution in the human BM. ***A*** *DB-Scan-generated clusters of T cells or Tregs (colored, against all nuclei in grey backdrop) for control and MDS samples.* ***B*** *Mean cluster size plotted against number of clusters for T cells and Tregs in all conditions. Clusters are defined as 5 or more cells in a 100 µm distance to each other.*

T cells formed big clusters in MDS, which is mostly a result of the higher cellularity, leading to densely packed bone marrow, while in control and CHIP tissues, fewer and smaller clusters could be observed (Figure 15B, left). Tregs on the other hand were nearly absent in MDS, with very few and small clusters forming, while more and bigger clusters formed in control and CHIP tissues (Figure 15B, right). Tregs are also in close contact with CXCL12-producing MSC in control samples, but not as close in MDS (Annex, Figure 56). These data indicate clear differences in Treg frequency and distribution in MDS.

4.2 SF3B1-mutated MDS samples display distinct marrow alterations

Considering the previous data on Tregs in MDS (Figure 15), four out of nine samples displayed bigger clustering patterns. A closer examination of the cytogenetic profile of the donors showed that they share the same mutation, SF3B1. As described in chapter 1.2, this mutation constitutes a distinct MDS subtype as of 2023 with favorable prognosis. Therefore, the data from MDS samples of performed experiments were retroactively stratified by SF3B1 and other mutations to examine possible subtype-specific stroma alterations.

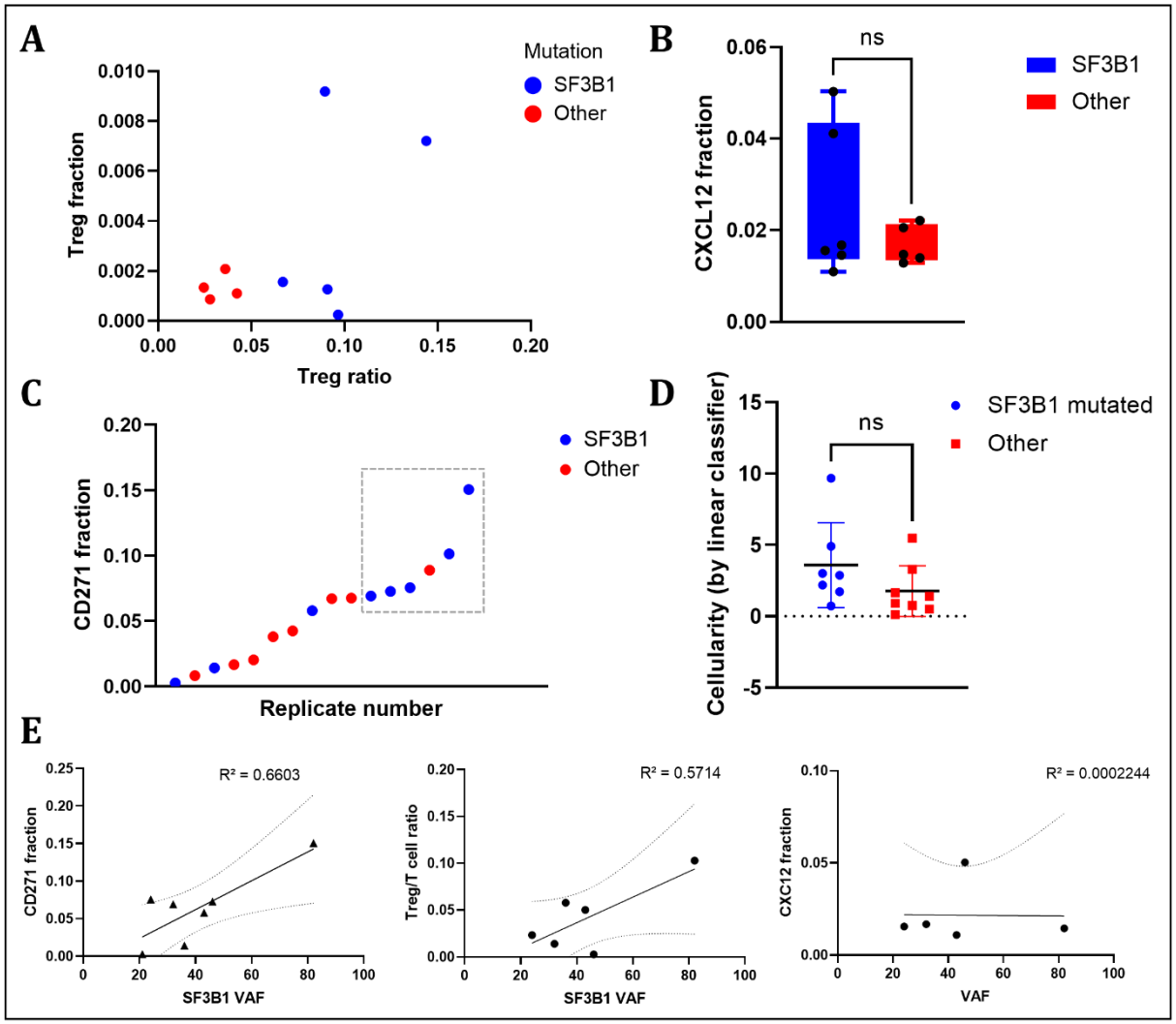

*Figure 16: SF3B1-mutated MDS show distinct bone marrow changes. Treg fraction and ratio (N= 4–5) (**A**), CXCL12 fraction (N = 4–5) (**B**), CD271 fraction (N = 8) (**C**) and cellularity (N = 7–8) (**D**) of MDS samples stratified by SF3B1 mutation. Mann-Whitney test was used to test for statistical significance. **E** SF3B1 VAF plotted against Treg/T cell ratio, CD271 fraction and CXCL12 fraction with linear regression and corresponding R^2 values.*

SF3B1^{mut} MDS showed a trend towards higher Treg ratios and -fractions in comparison to non-SF3B1^{mut} MDS (Figure 16A). While not being statistically significant, there was a

trend towards higher CXCL12 content for some SF3B1^{mut} samples (Figure 16B), higher MSC content and higher cellularity (Figure 16C, D). Higher SF3B1 VAF correlated with higher Treg/T cell ratios and CD271 frequencies, while higher VAFs did not show any correlation with CXCL12 signal (Figure 16E).

4.3 FACS experiments on bone marrow aspirate

To validate previous experimental findings of the BM architecture, a complimentary approach by flow cytometry-based quantification of cell populations in bone marrow aspirate was employed during subsequent sorting experiments on selected samples.

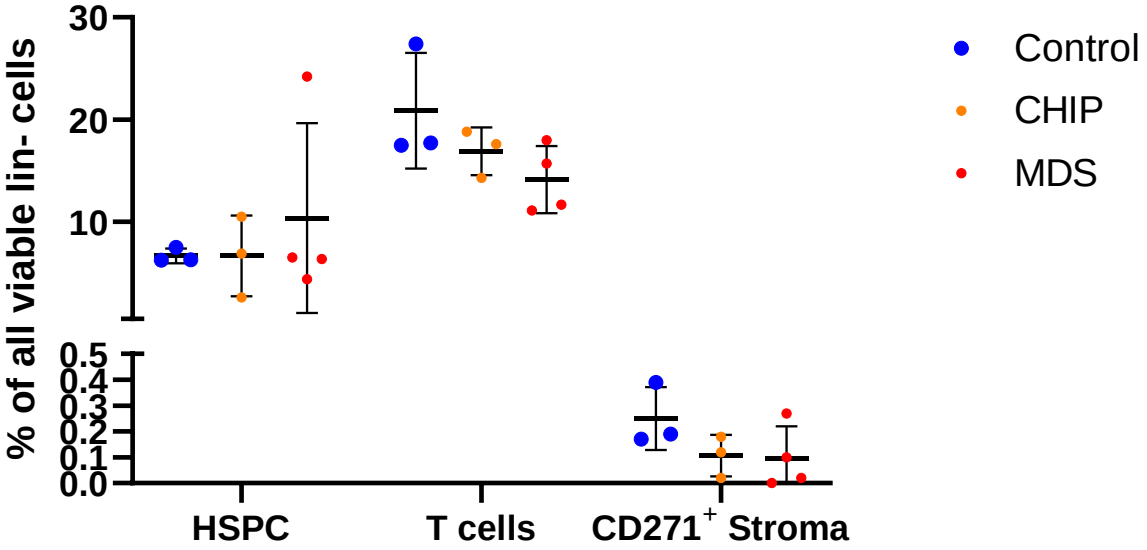

Figure 17: FACS data for bone marrow composition from human bone marrow aspirate used in scRNA-seq experiments. Sorting strategy can be found in chapter 3.2.6.

FACS analysis (Figure 17) did not show any alterations in HSPC and T cells between the different conditions, confirming the previous imaging data (Figure 13, Figure 14). However, in contrast to the expansion of MSC that was observed in MDS patients (Figure 12), FACS data show comparable percentages of MSC between the samples.

4.4 Characterization of DNMT3A^{R878H} mice

Considering the trend towards higher sinusoid content in imaging analysis of human CHIP samples where results were not statistically significant (Figure 11), one possible reason could be the low and inconsistent VAF sizes. To assess a possible clone-size dependent

effect more reliably, a high-VAF mouse model carrying the somatic mutation DNMT3A^{R878H}, which is the functional equivalent of the human DNMT3A^{R882H}, was characterized by immunostaining.

4.4.1 Bone marrow cellularity in DNMT3A^{R878H} mice

Giemsa stainings of femurs were used to assess BMC, followed by quantification using MarrowQuant, a machine learning-based plugin for QuPath designed specifically for measuring BMC (Tratwal et al. 2021).

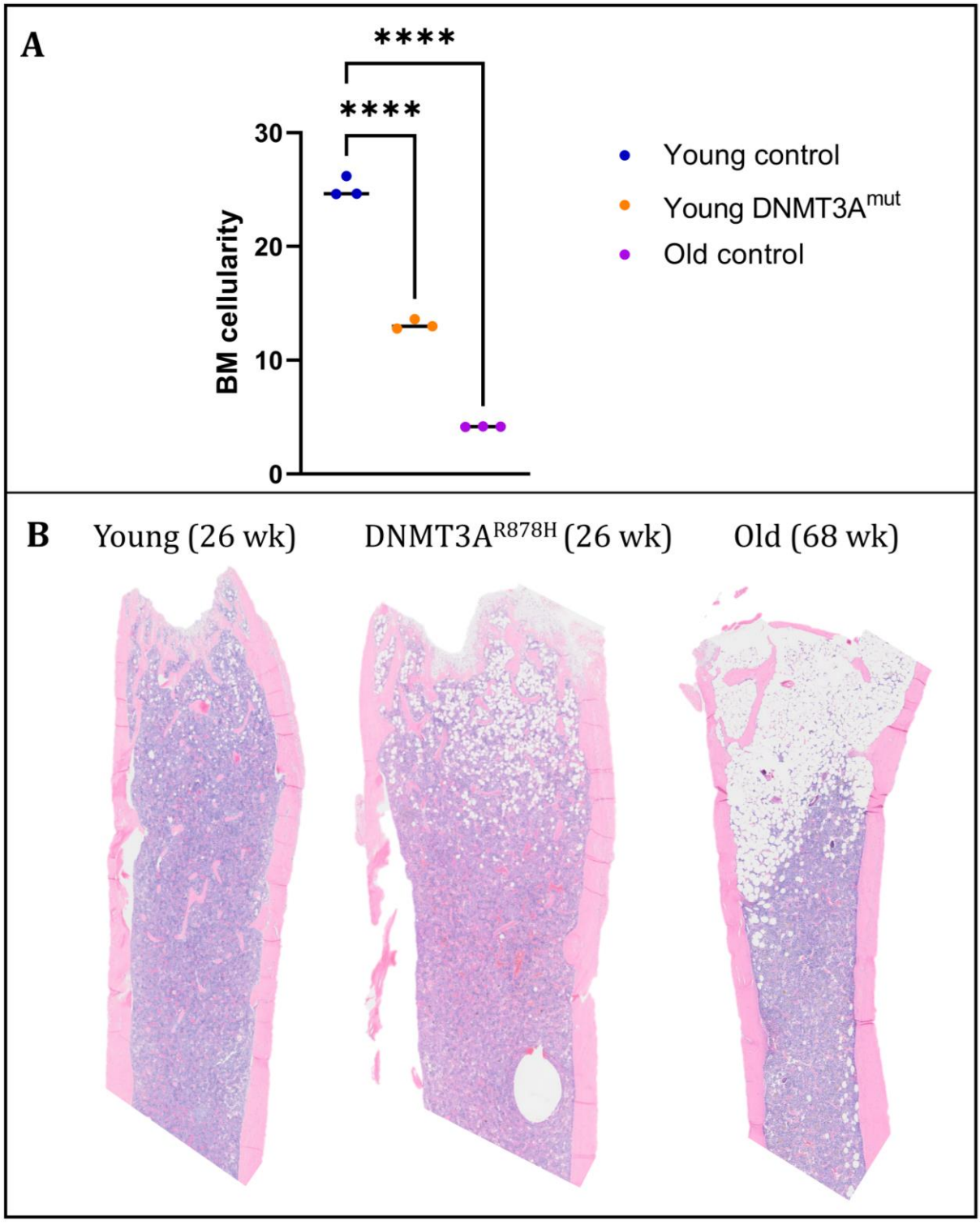

*Figure 18: **A** Bone marrow cellularity in murine DNMT3A^{R878H} femurs , determined by MarrowQuant (n = 3). One-way ANOVA with multiple comparisons was used to test for statistical significance. **B** Giemsa stainings of DNMT3A^{R878H}, young, and old control femur heads (wk = weeks).*

A first morphological analysis of Giemsa-stained femurs revealed that DNMT3A^{R878H} (abbreviated to DNMT3A^{mut}) showed an overall lower BM cellularity in comparison to young controls, while old controls had even lower cellularity than DNMT3A^{mut} mice

(Figure 18A). The Giemsa stainings showed an accumulation of adipocytes with accompanied reduction of red marrow in the femur head in DNMT3A^{mut}, with an expansion towards the diaphysis in aged mice (Figure 18B).

4.4.2 Vasculature in femurs of DNMT3A^{R878H} mice

Possible vasculature alterations in the high-VAF DNMT3A^{mut} model mice were determined using IF stainings in femurs of arteries (BCAM^{+}) and sinusoids (endomucin^{+}).

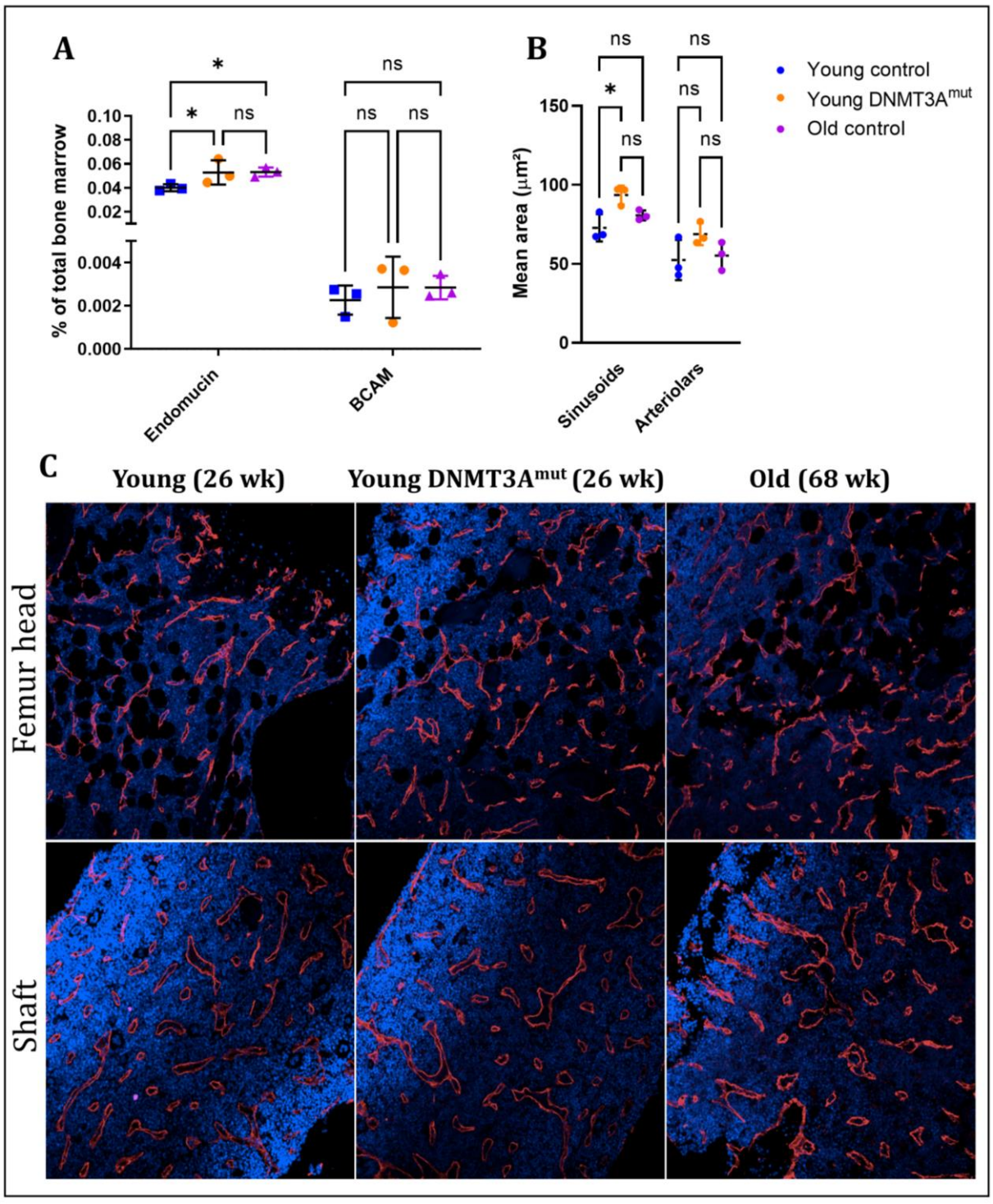

*Figure 19: Vasculature analysis of murine DNMT3A^{R882H} femurs. Sinusoidal (Endomucin) and arteriolar (BCAM) surface fraction (**A**) as well as mean vessel area (**B**). Two-way ANOVA with Šidák's multiple comparison test was employed to test for statistical significance (N = 3). **C** Representative images of femur head and shaft sinusoidal vessels (EMCN$^+$) in young control, young DNMT3A^{mut} and old control mice. Brightness and contrast were adjusted for better visibility.*

Sinusoidal endomucin$^+$ vessels were found to be expanded in DNMT3A mutant mice in comparison to young controls, but not in comparison to old controls while there were no differences in BCAM$^+$ arteriolar and arterial vasculature (Figure 19A). The sinusoidal expansion was accompanied by larger vessel sizes in mutant mice, particularly in the

femur head (Figure 19B, C). These observations confirm more robustly the previous tendencies toward higher sinusoid content in human CHIP BM biopsies.

4.4.3 Adipogenic and injury-responsive MSC subsets in DNMT3A^{878H} mice

Similarly to the investigation of the MSC content in human samples (chapter 4.1.3), the MSC compartment in DNMT3A^{mut} mice was also assessed in immunostainings, using PDGFRβ, a marker for a angiogenic and injury-responsive MSC subset with a fibroblastic behavior (MSC-Fibro) (Wang et al. 2018), and LEPR, an established marker for MSC with high CFU potential but primed toward adipogenic (MSC-Adipo) differentiation (Woods and Guezguez 2021).

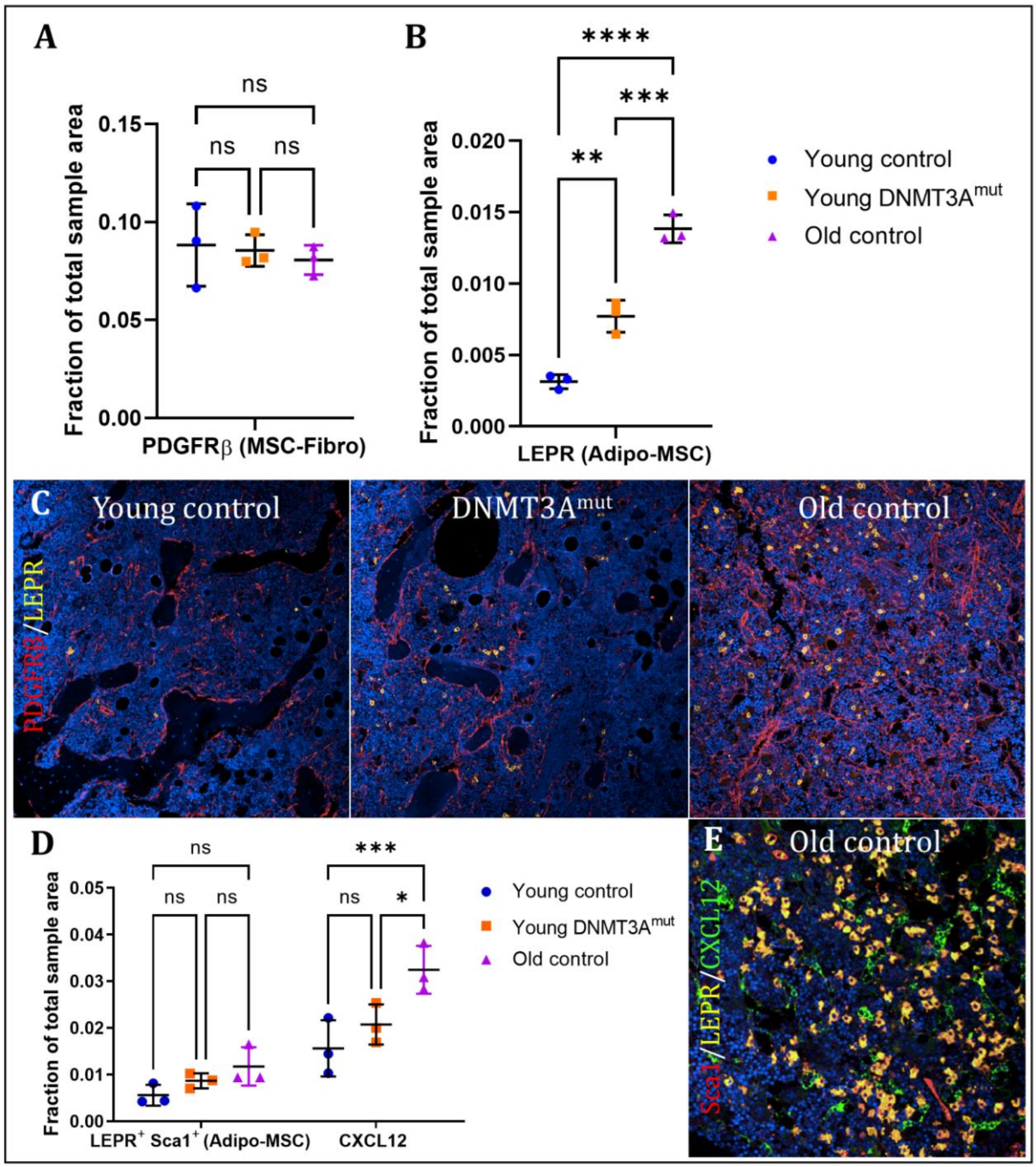

*Figure 20: **A** PDGFRβ and **B** LEPR^{high} area as fraction of the whole sample area in murine bones. **C** Example images for co-staining of LEPR and PDGFRβ. **D** LEPR^{high} Sca1^{+} fraction and CXC12 fraction in murine femurs. **E** Example images of triple positive perivascular cells in an old murine femur. Brightness and contrast were adjusted for better visibility.*

For the MSC-Fibro subset, no difference was found between young, DNMT3A^{mut}, and old samples in total PDGFRβ^{+} surface (Figure 20A). PDGFRβ^{+} positive cells were localized mostly perisinusoidal and endosteal. LEPR was also expressed on these cells, although there was a subpopulation of perivascular cells that showed high expression of LEPR (LEPR^{high}, Figure 20C). These LEPR^{high} cells were significantly increased in DNMT3A^{mut} with further expansion in aged mice (Figure 20B) and were localized towards the femoral

head, adjacent to expanding BMAT. Interestingly, recent reports showed a specific subpopulation of MSC (LEPR^{+} Sca1^{+}) with high clonogenic potential and an adipogenic differentiation bias to be upregulated upon irradiation, fracture and aging (Mo et al. 2021). Bearing in mind the previous results on CXCL12 stainings in human BM stroma (Figure 12), mouse bone sections were stained for Sca1, CXCL12 and LEPR. The expanded LEPR^{high} cells were mostly expressing Sca1 and were highly enriched in CXCL12. As a result, the overall levels of CXCL12 were significantly higher in young DNMT3A^{mut} and old control mice (Figure 20D, E). Taken together, high-VAF DNMT3A mutations impact the MSC repertoire, MSC subset expansion and their distribution across the BM.

4.4.4 T lymphocytes and Tregs in DNMT3A^{878H} mice

In order to get understanding of high-VAF effects on T lymphocyte repertoire (with an emphasis on the Treg subpopulation) and to mirror previous experiments in human samples (Figure 14), the same markers (CD3 for T cells and FoxP3 for Tregs) were used for IF stainings in DNMT3A^{mut} mice.

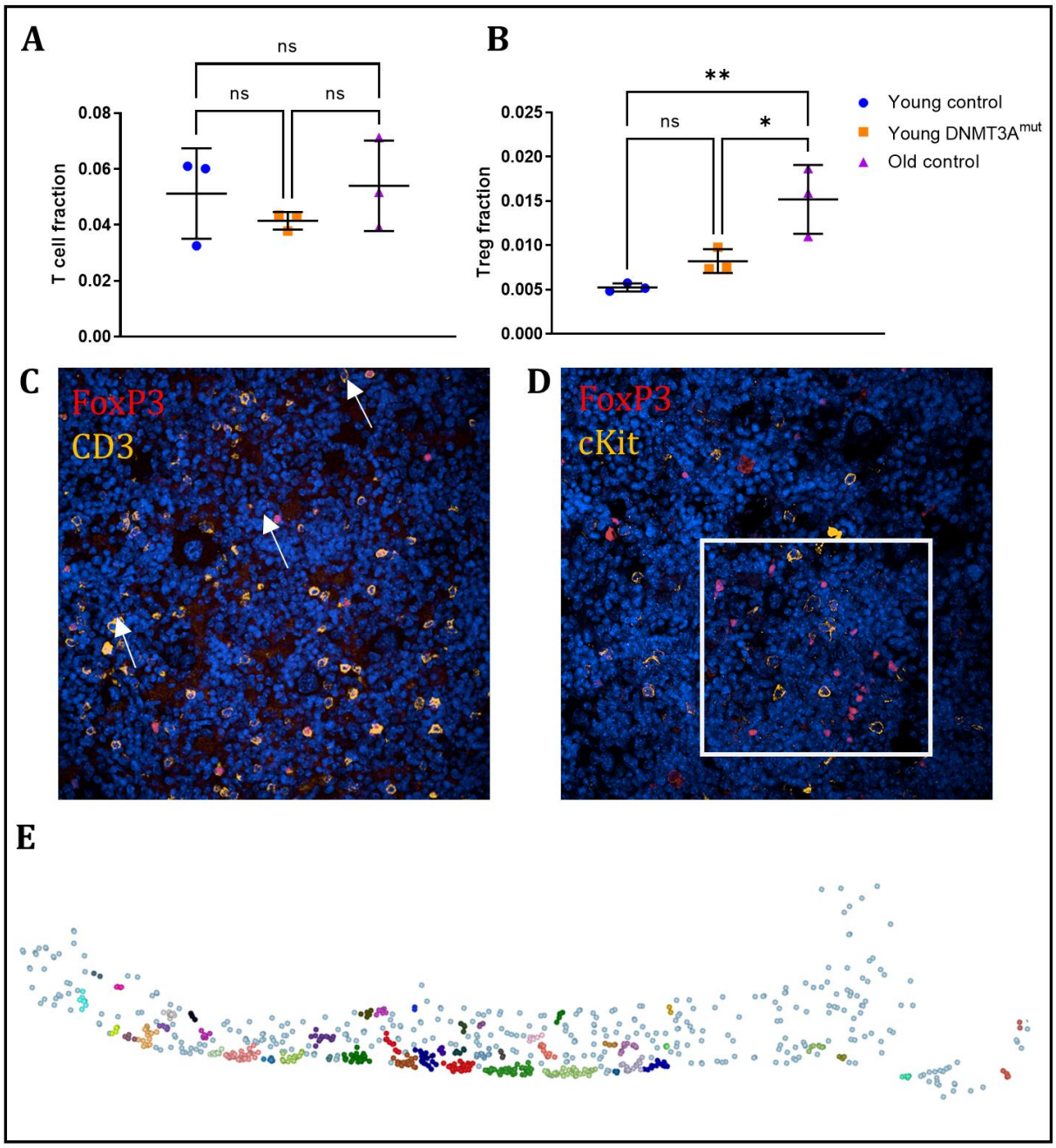

*Figure 21: T lymphocyte analysis in murine bones. T cell (**A**) and Treg (**B**) fraction of murine femurs. Ordinary one-way ANOVA with Tukey's multiple comparison test was employed to test for statistical significance (N = 3). **C** Example images of T cells (CD3⁺) and Tregs (CD3⁺ FoxP3⁺) in the murine bone marrow. Brightness and contrast were adjusted for better visibility. **D** Example image of cKit⁺ HSPC in close contact with FoxP3⁺ Tregs. **E** Example of clustered Tregs (colored) against T cell backdrop (light blue) in the murine bone marrow.*

These data indicate that T cells were less abundant in mouse bone marrow than in human (5% mean in comparison to 15%, based on previous reports by (Zhao et al. 2012). While the CD3⁺ T cell proportion was similar across all conditions (young, old and DNMT3A^{mut} mice), Treg frequency was elevated in old compared to mutant and young mice (Figure 21A, B). DNMT3A mutant mice also displayed a trend towards higher Treg content than controls, although the effect was not prominent enough to be statistically significant.

Strikingly, Tregs in all conditions clustered towards the endosteum (Figure 21E) and were often in direct contact to $CD3^+$ $FoxP3^-$ T cells (Figure 21C). Furthermore, Tregs were shown to form clusters with higher density of $cKit^+$ HSPC, potentially providing an immune-privileged milieu (Figure 21D).

4.4.5 Sympathetic innervation in DNMT3A^{878H} mice

To assess possible impact of CHIP clones on neuronal tissue in the BM, key populations were characterized by immunostaining. Tyrosine Hydroxylase (TH) is a marker for dopaminergic neurons, whose function in the BM is described in chapter 1.3.8. GFAP was used to stain glia cells which ensheathe the neurons to support their function. It is important to note that these stainings were not possible in human biopsies due to the scarcity of innervated arteries in the human BM samples but were instead done in murine femurs to analyze possible deterioration during aging and in DNMT3A mutation settings.

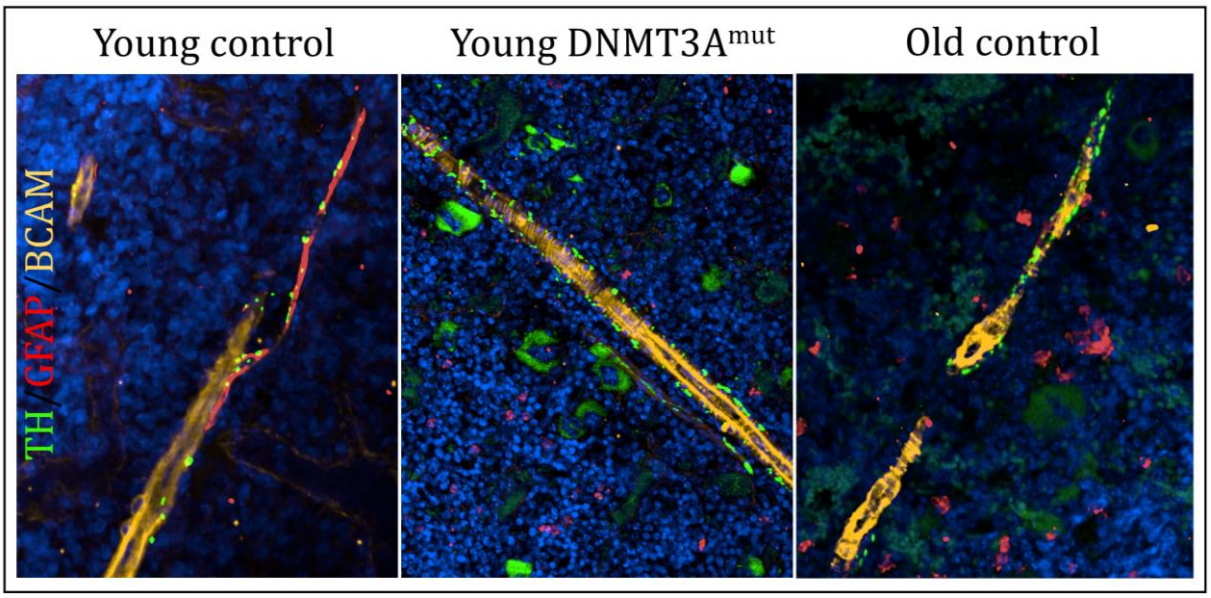

Figure 22: Neuron staining in murine femurs. Adrenergic neurons (TH^+), which are ensheathed by glial cells ($GFAP^+$), are wrapped around arteries ($BCAM^+$) (N = 3). Brightness and contrast were adjusted for better visibility.

ROI images were used for qualitative assessment which did not show differences in sympathetic innervation of blood vessels between the samples (Figure 22). A quantitative approach was not followed due to heterogeneity in artery distribution, which would skew the results. In conclusion, sympathetic innervation of young DNMT3A^{R878} and aged mice remained intact, but this question should be addressed again using quantitative approaches.

4.5 Megakaryocyte content

Seeing how MK are important for HSC maintenance in the endosteal niche (chapter 1.3.7), MK frequency and the spatial distribution in relation to sinusoidal vessels in DNMT3A^{mut} and aged mice was explored using CD41 as a specific MK marker.

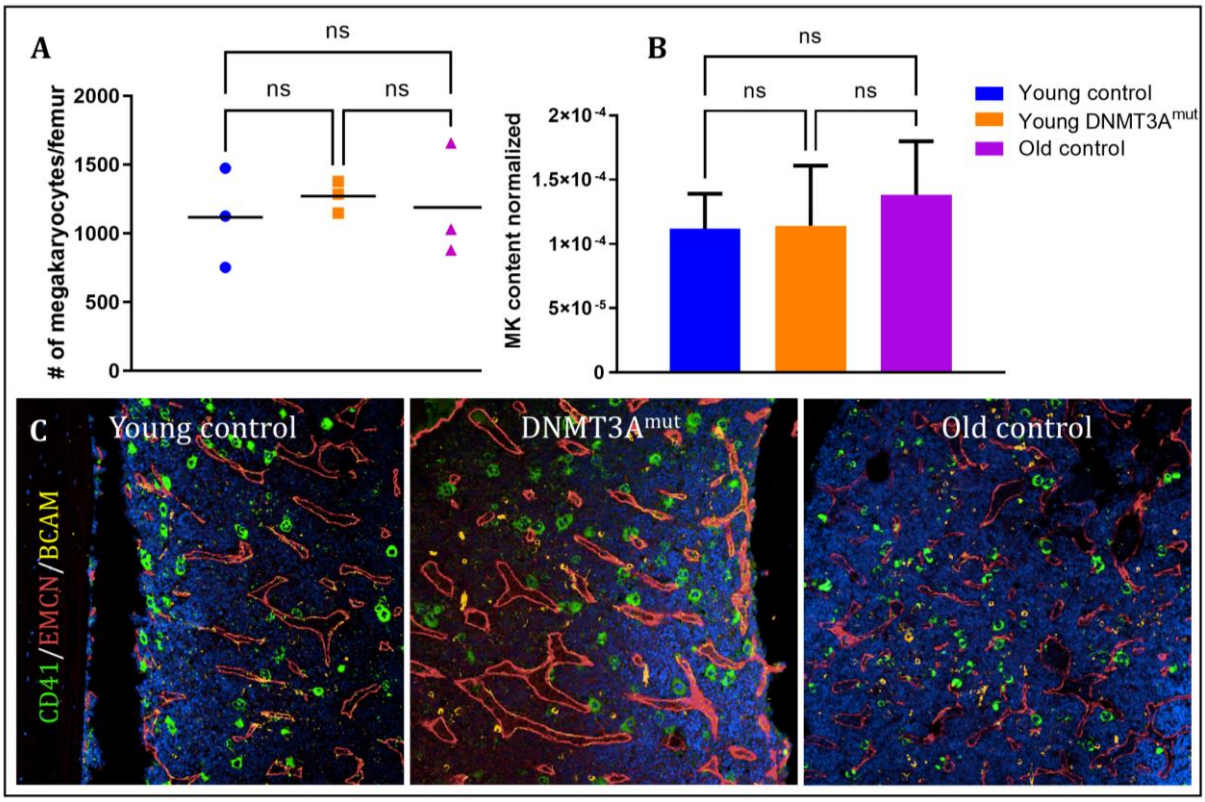

*Figure 23: Absolute number of megakaryocytes (**A**) and normalized MK frequency (**B**) per murine femur. **C** Representative images of megakaryocyte stainings in young, old, and DNMT3A^{mut} bone marrow. Ordinary one-way ANOVA with Tukey's multiple comparison test was employed to test for statistical significance. Brightness and contrast were adjusted for better visibility.*

There was no significant difference in MK abundancy between the samples (Figure 23A, B). However, qualitative ROI analysis suggested that in young femurs, more bone-lining megakaryocytes were present that were further apart from sinusoids, which is a distinctive feature of the endosteal niche (depicted in Figure 23C). In DNMT3A^{mut} and old samples, the vasculature was also extended towards the endosteum and there were fewer megakaryocytes directly lining the bone (Figure 23C). In brief, MK frequency was similar in all conditions, while cellular localization within the BM might be changed toward sinusoidal niches in aged and DNMT3A^{mut} mice.

4.6 Functional modelling of MSC-HSC interactions

Immunostainings of human BM FFPE tissue revealed striking differences in MSC and EC frequency in MDS. The expansion of MSC in MDS and the consequential remodeling of the bone marrow niche might indicate functionally altered interplay between MSC and MDS blasts. For a better understanding of these molecular alterations, an MDS-MSC co-culture model with changing ratios was set up, using established cell lines (MDS-L, a LR-MDS cell line and immortalized naïve hTERT-MSC).

4.6.1 Secretome analysis of MSC-MDS co-cultures

Based on the spatial distribution analysis, MSC and HSPC were not found to be always localized in direct contact (Figure 13). Therefore, an *in vitro* approach analyzing the secretome of an MDS-L/hTERT-MSC co-culture via mass spectrometry was used to assess cellular interplay.

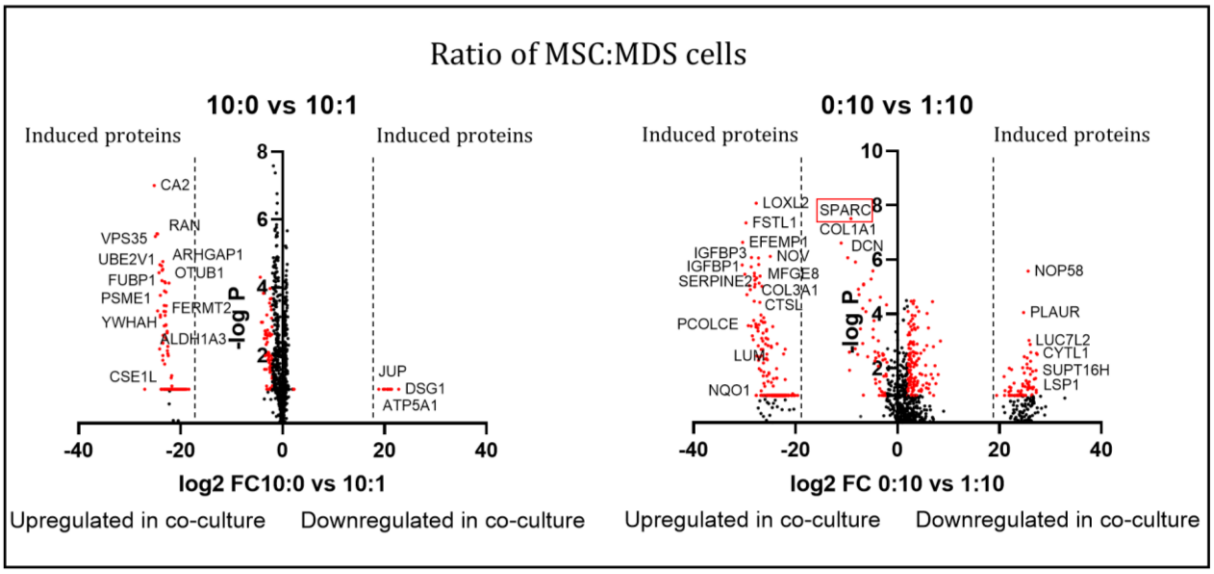

Figure 24: Volcano plot of detected proteins in co-culture to mono-culture conditions of hTERT-MSC and MDS-L cells. Red highlighted proteins are significantly upregulated (-logP>1, fold-change >2 or <-2). "Induced proteins" are present in one condition but not the other, for instance only in co-culture, but not in monoculture. For displaying these proteins, LFQ intensity in the missing condition was set to 1, which leads to these proteins being apparently strongly up- or downregulated.

The volcano plot of differentially secreted proteins in mono- versus co-culture shows a large number of proteins appearing upon adding MSC to MDS monoculture (Figure 24, right panel), but fewer in the opposite setting (left panel). To better analyze the origin of

the secreted proteins, a clustering analysis approach based on the protein signal in the different conditions was employed.

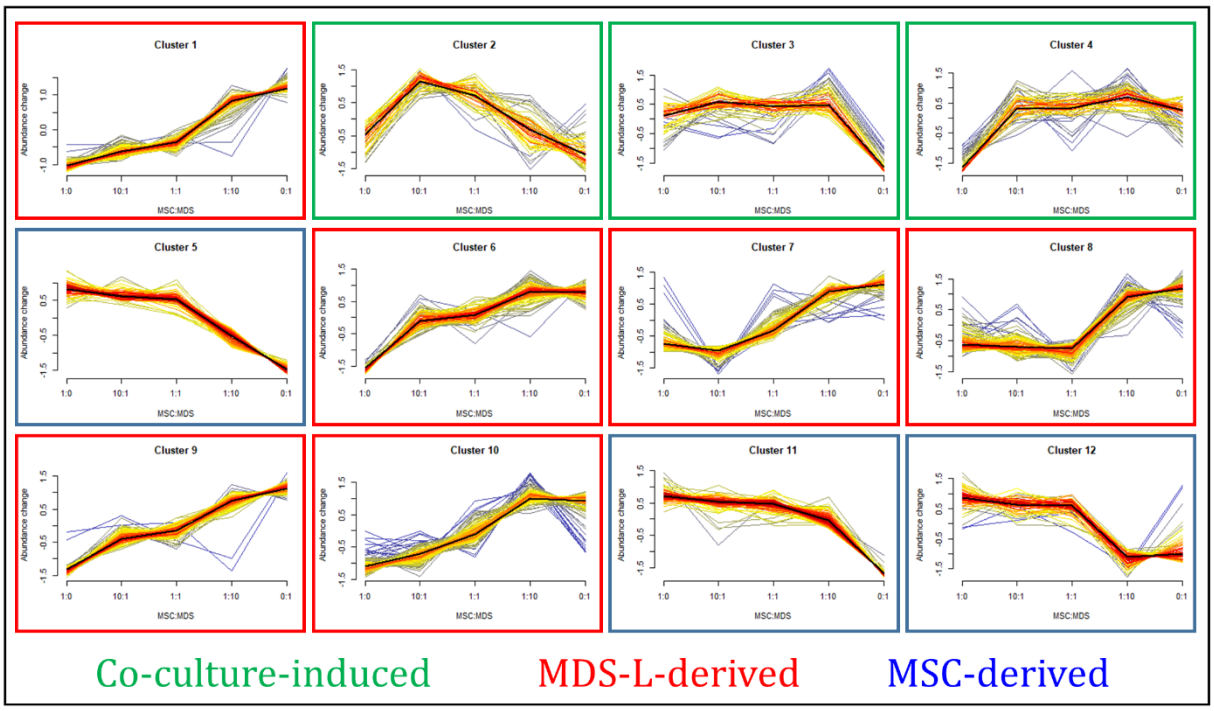

Figure 25: Softcluster analysis of secreted proteins from hTERT-MSC monoculture, co-culture with MDS-L in different ratios and MDS-L monoculture. For all conditions, 200,000 total cells were used. Clusters with the same outline color can be classified as coming from the same source, according to abundancy changes in the different conditions.

Secreted proteins were assigned to "softclusters", which are groups of proteins that change similarly between the different co-culture conditions. These softclusters were either proteins that were upregulated mostly in monoculture of either MDS blasts or MSC, or co-culture-induced proteins. Further grouping of these proteins and subsequent String analysis reveals the cellular processes at play (Figure 25).

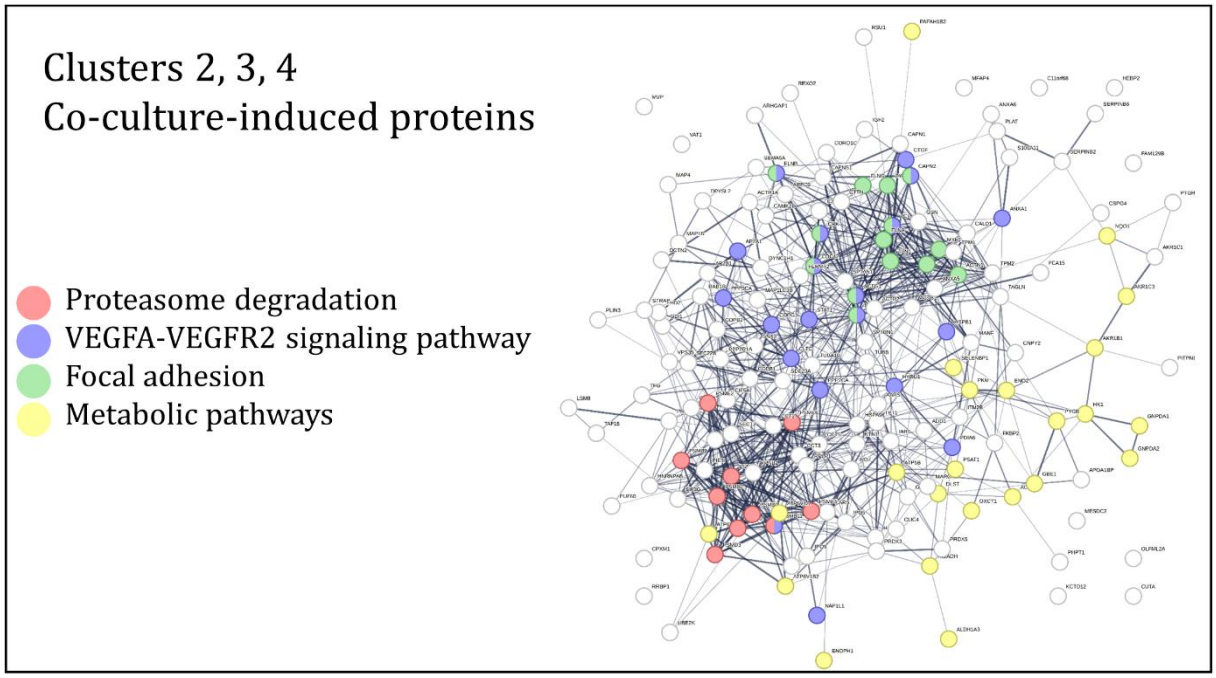

Figure 26: String analysis of significantly differentially secreted proteins in clusters 2, 3 and 4, which are induced or upregulated in co-culture only. Significance was tested using Student's t-test for mono-culture against co-culture expression (1:0 vs 1:1, p<0.05).

Co-culture-induced proteins found in clusters 2, 3 and 4 were mostly involved in proteasomal degradation, VEGF signaling pathways, focal adhesion, and different metabolic pathways like prostaglandin synthesis, aminoacid metabolism and glycogen synthesis or degradation pathways (Figure 26). These proteins were solely upregulated in co-culture and might be involved in or a result of a specific crosstalk between MDS blasts and MSC.

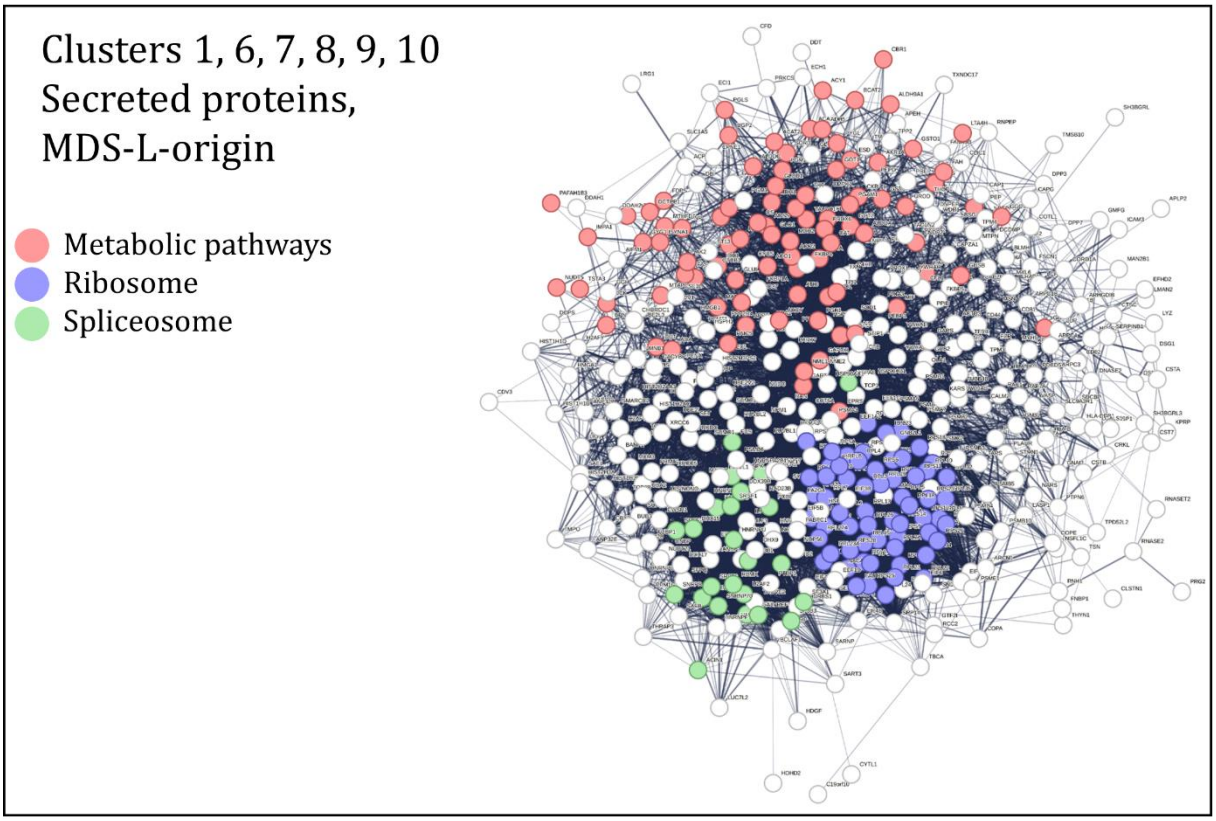

Figure 27: String-analysis of significantly differentially secreted proteins in clusters 1, 6, 7, 8, 9, 10, which are secreted by MDS-L cells. Significance was tested using Student's t-test for mono-culture against co-culture expression (1:0 vs 1:1, p<0.05).

Proteins that were primarily and constitutively secreted by MDS-L cells were related to metabolic pathways (glutathione metabolism, purine metabolism, glycolysis), ribosome related or involved in splicing as well as VEGF signaling pathways (Figure 27). Some of the ribosome-related proteins are also affected in Diamond-Blackfan anemia (Choesmel et al. 2007).

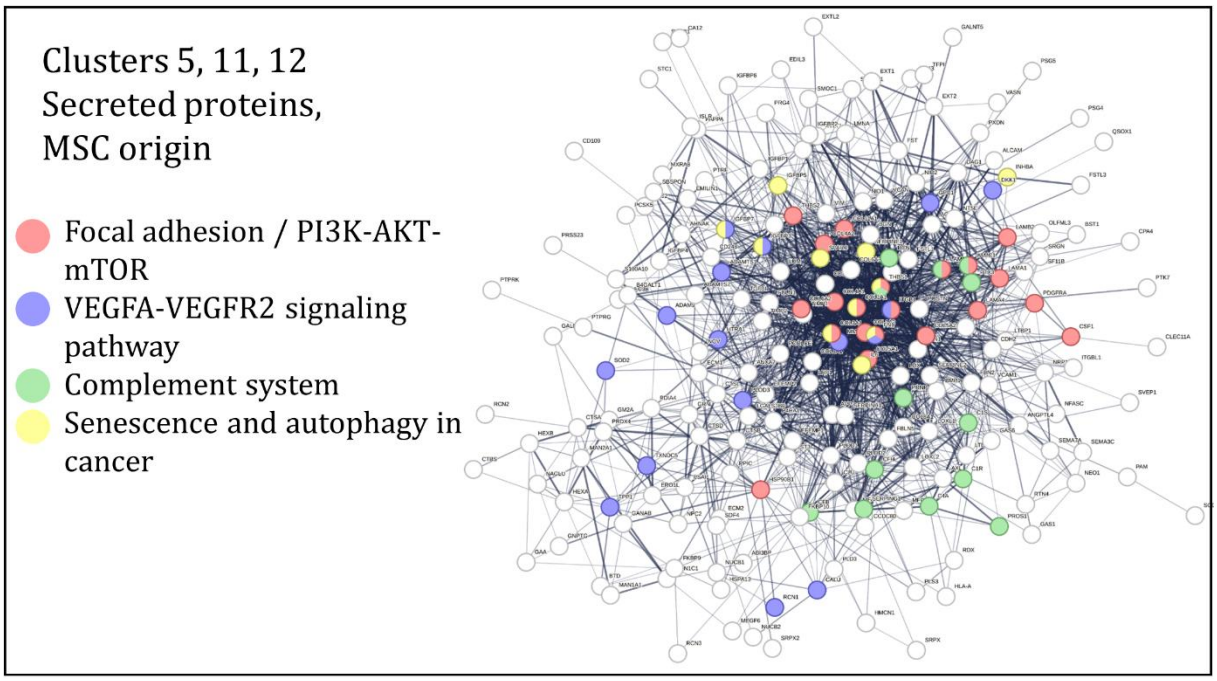

Figure 28: String-analysis of significantly differentially secreted proteins in clusters 5, 11, 12, which are secreted by hTERT-MSC cells. Significance was tested using Student's t-test for mono-culture against co-culture expression (1:0 vs 1:1, p<0.05).

hTERT-MSC secreted mostly proteins involved in focal adhesion, VEGF signaling pathway, senescence and autophagy-related pathways in cancer and the complement system. These proteins are constitutively secreted by MSC regardless of co-culture conditions (Figure 28).

4.6.2 Secreted factors in the human bone marrow niche

In co-culture experiments of MDS blasts with a cultured MSC cell line, Secreted Protein Acidic and Rich in Cysteine (SPARC) was strongly elevated in comparison to monoculture (Figure 24). SPARC is involved in cell adhesion, proliferation and angiogenesis and has been shown to be implicated in several hematological disorders, such as multiple myeloma, chronic myeloid leukemia and del5q MDS (Nian et al. 2022). Given the increase in vasculature of MDS samples in comparison to controls (Figure 11), levels of SPARC in the bone marrow were investigated.

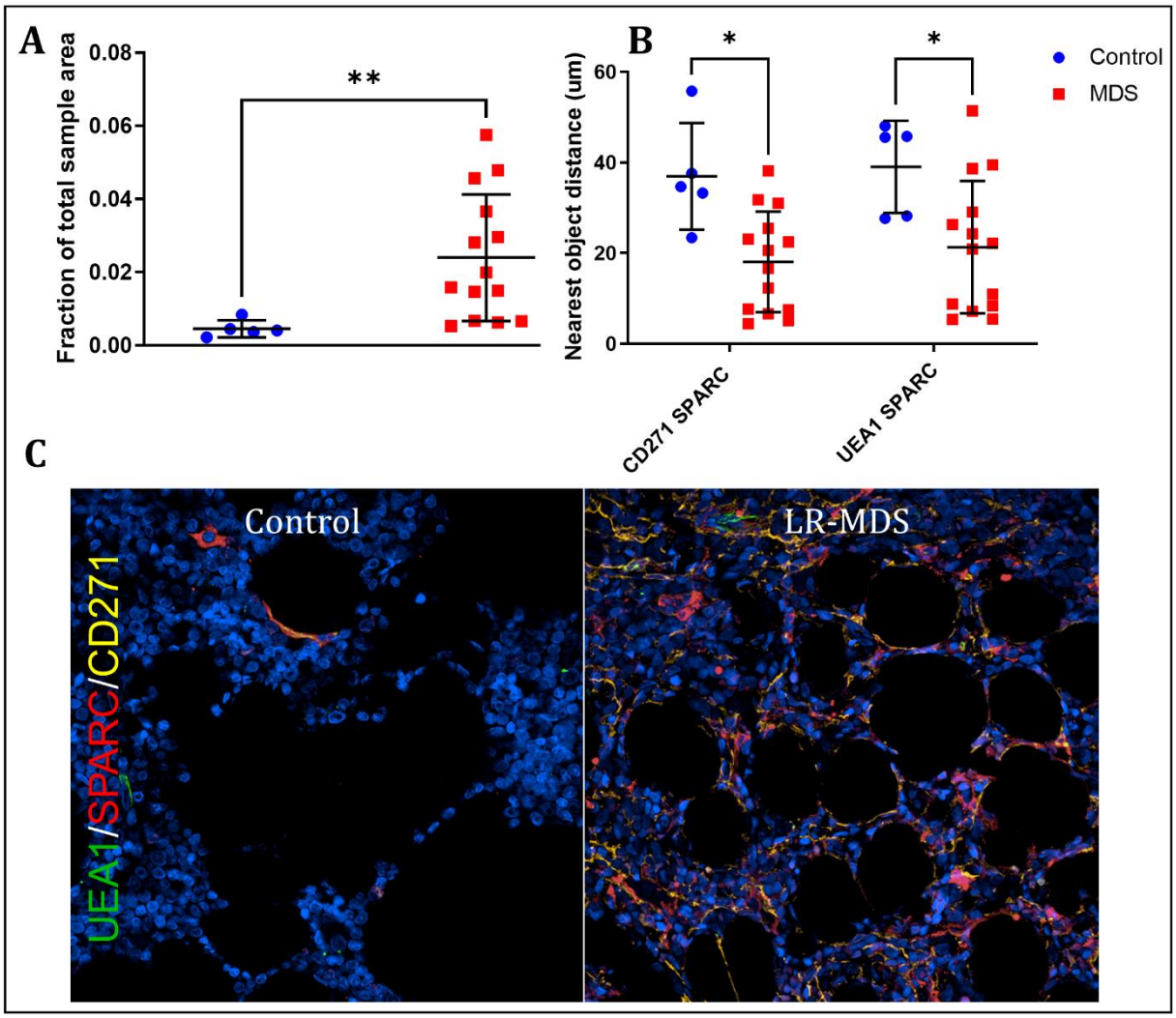

Figure 29: SPARC analysis in human BM samples. ***A*** *Fraction of SPARC+ surface in control and MDS tissue as well as nearest object distance from MSC (CD271,* ***B****) and vessels (UEA1, N = 5–14). Welch's t-test (A) and Two-way ANOVA with Tukey's multiple comparison test were employed to test for statistical significance.* ***C*** *Representative images of SPARC, MSC (CD271) and vessels (UEA1) in human BM. Brightness and contrast were adjusted for better visibility.*

In the BoHemE cohort, the SPARC⁺ fraction was strongly upregulated in MDS in comparison to control tissue (Figure 29A) and was more closely associated with MSC and vessels (Figure 29B, C).

Femurs from SPARC knockout mice were analyzed in respect to their vasculature content using 3D-rendering light sheet microscopy in order to understand the role of SPARC in endothelial development.

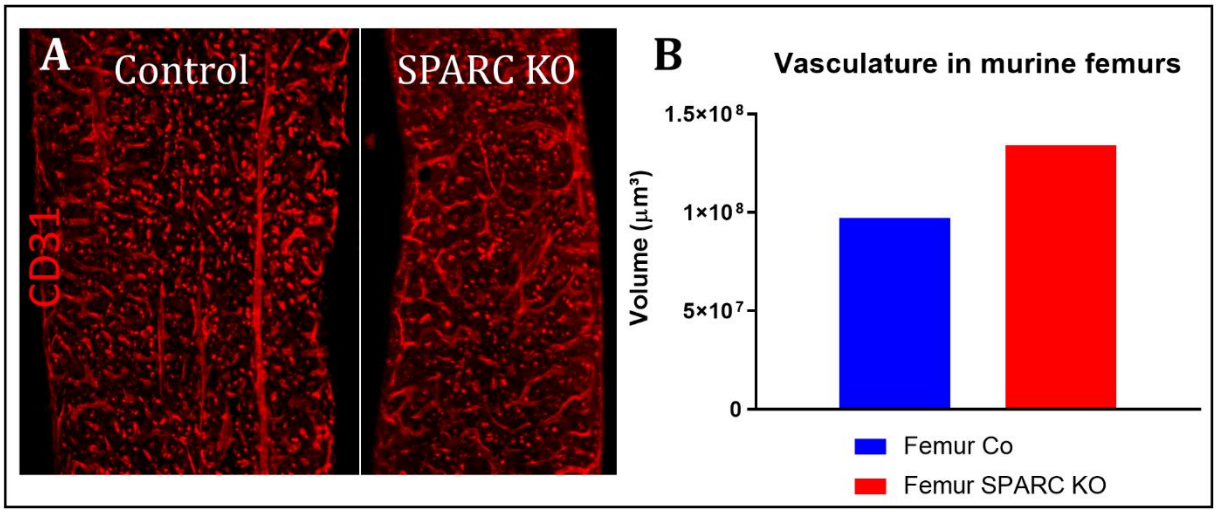

Figure 30: Effect of SPARC KO on murine femurs. ***A*** *Maximum projection over 15 µm of light sheet microscopy-generated data from murine BM (SPARC KO vs. control), stained with CD31. Brightness and contrast were adjusted for better visibility.* ***B*** *Total volume of vessels in control vs SPARC KO femur (N = 1.)*

Light sheet microscopy on one SPARC knockout femur suggest that the bone marrow vasculature might be expanded in comparison to a wild-type control (Figure 30B) and the vessel orientation might be changed from mostly small vessels next to big arteries to expanded sinusoids, while arteries are not as prominent (Figure 30A). In conclusion, SPARC is upregulated in co-culture settings and MDS bone marrow samples, and knockout mice show remodeled vasculature *in vivo*.

4.6.3 Cytokine profiling of co-culture supernatant

The same co-culture model described in chapter 4.6.1 was used in a Luminex assay, looking for differentially secreted cytokines in co-culture after 48 h and 96 h of culture.

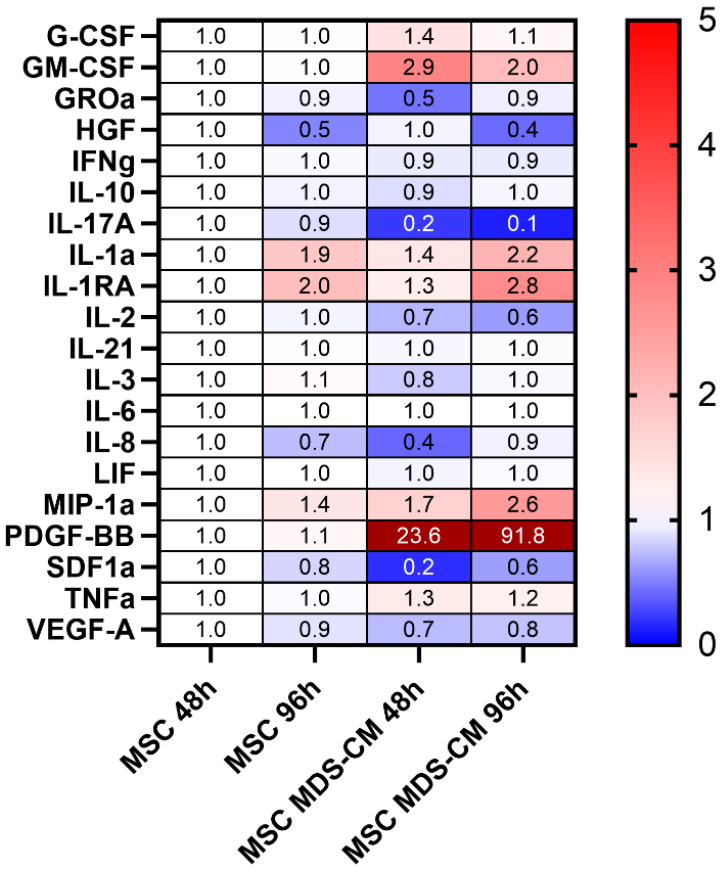

Figure 31: Cytokine profiling of the MSC-MDS-co-culture system. Heatmap of fold-change cytokine levels from MSC cell culture supernatant that were incubated with MDS-L-derived conditioned medium for 48–96 hours in comparison to standard culture (n=2). Numbers indicate fold-change in relation to MSC monoculture after 48 h. Absolute concentrations can be found in the annex (Figure 59–Figure 61). CM = Conditioned Medium.

In MSC, IL-1α and IL-1RA are 2-fold enriched after 96 h of culture, while HGF and IL-8 are reduced (Figure 31). VEGF-A is highly expressed in all conditions containing MSC. Co-culture of MDS and MSC showed a sharp increase in PDGF-BB and slight increases in GM-CSF as well as strong decreases in IL-17A and CXCL12 after 48 h, with the effects becoming stronger for PDGF-BB and IL-17A after 96 h. The CXCL12 and GM-CSF levels were closer to basal levels after 96 h, suggesting an initial response in co-culture with a kinetic course. Furthermore, IL-1RA and IL-1α as well as Macrophage Inflammatory Protein 1a (MIP-1a) are more upregulated after 96 h in co-culture than in monoculture, which could also show a time-dependent cytokine release, but more biological replicates are needed to validate the findings.

4.7 Single cell RNA sequencing of bone marrow aspirates

Following anatomical BM stroma characterization and functional modeling of diseased niche interplay, gene expression in patient BM aspirates from the BoHemE was analyzed to identify the profile of altered pathways, potential differentiation biases and subset expansion using a scRNA seq approach (10x genomics technology).

4.7.1 Gene cluster annotation heatmap

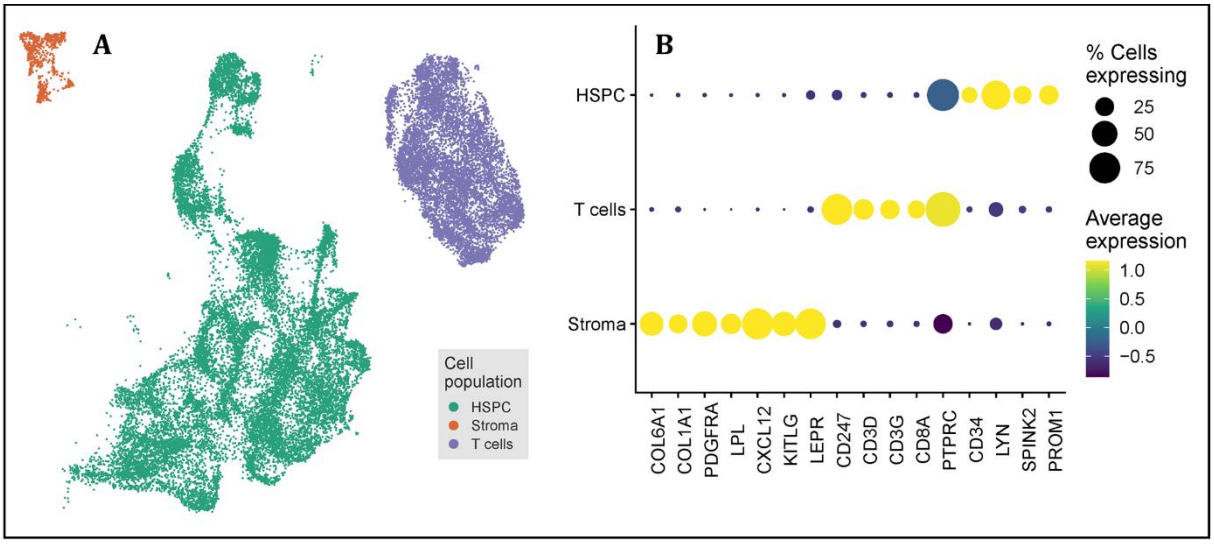

Figure 32: ScRNA seq cluster annotation. ***A*** *UMAP plots of all cells identified and annotated for scRNA seq.* ***B*** *Bubble plot for signature genes of HSPC, T cells and stroma.*

After cell sorting of HSPC, MSC and T cells, a total of 32,672 cells were sequenced, annotated and used for subsequent analysis (21,153 HSPC, 10,783 T cells and 736 stromal cells) with approximately 1,700 mean number of genes. Major cell populations clustered apart from each other in Uniform Manifold Approximation and Projection (UMAP) dimensional projections (Figure 32A), allowing a distinct identification with specific gene signatures (Figure 32B). MSC/Stroma was identified by expression of e.g. CXCL12 and LEPR, while T cells were positive for CD3D/G and CD247 and HSPC for CD34, underlining their use as markers in IF stainings. For downstream analysis, subclustering of each major population was performed, followed by differential gene expression analysis.

4.7.2 Subclustering on stroma cells and differential gene expression analysis

While the single cell mapping (UMAP plots) of the sorted samples provided a good overview over the total populations, the resolution of the dimensional clustering method

of the full dataset was not high enough to visualize subpopulations. For this reason, subclustering on only stromal cells was done while omitting gene expression of HSPC and T cells. This allowed further identification of six different MSC clusters (Figure 33A).

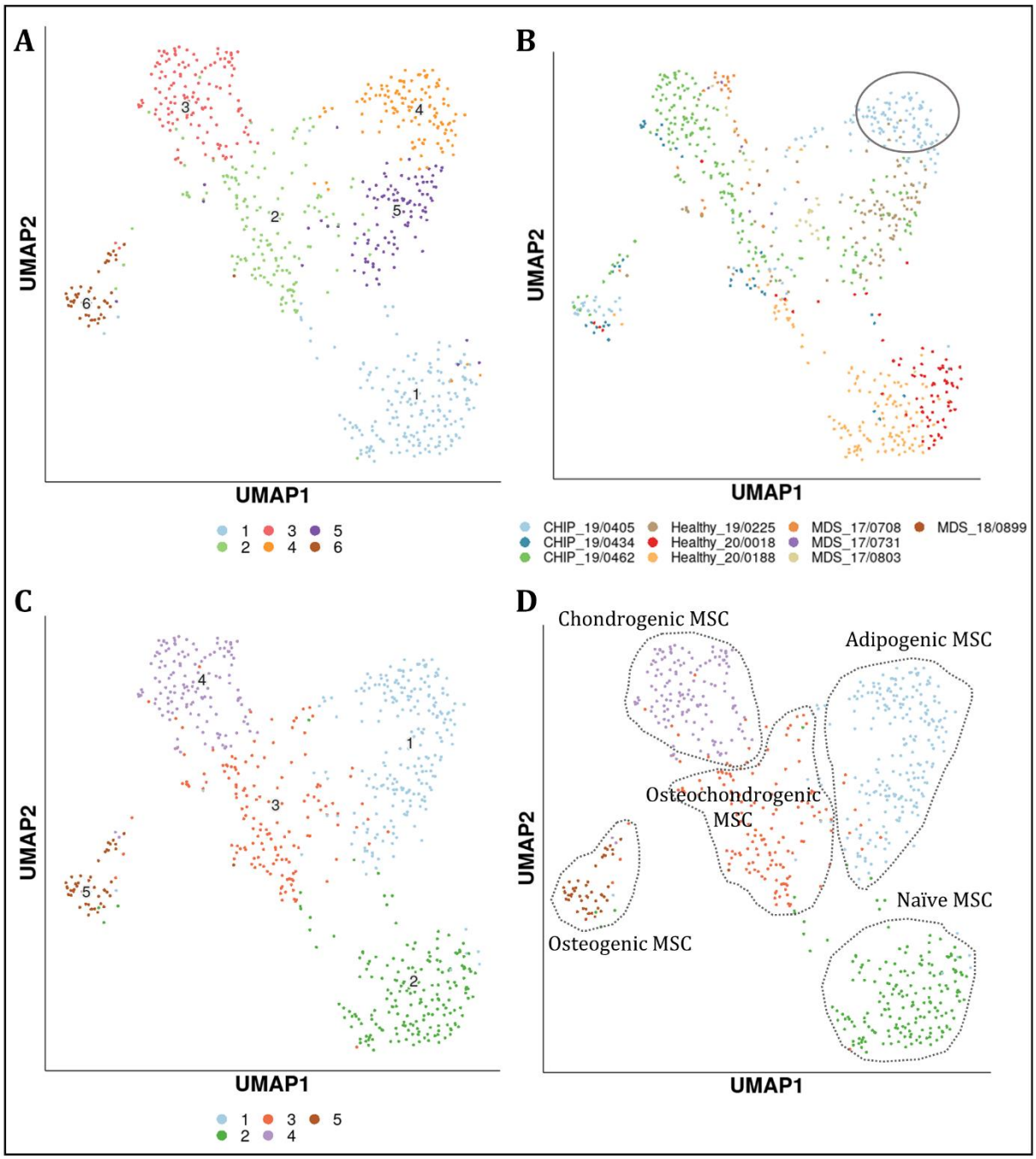

*Figure 33: **A** UMAP plot of stromal cells, identifying 6 distinct clusters. **B** UMAP plot with donor assignment of stromal cells. **C** UMAP plot of stromal cells with lower resolution, identifying five distinct clusters. **D** Annotation of clusters based on published marker genes and manually curated genes: Naïve (185 cells), osteochondrogenic (149 cells), osteogenic (47 cells), chondrogenic (137 cells) and adipogenic MSC (218 cells). A heatmap of the genes used for clustering can be found in the annex (Figure 62).*

Of note, all of the cells in cluster 4 came from one specific donor (Figure 33B) and shared most adipogenic signature genes with cluster 5, so both clusters were deemed similar and combined (Figure 33C). Gene signature mapping from recent scRNA seq studies on BM stroma, combined with highest differentially expressed genes in the respective clusters allowed identification of five populations: naïve multipotent, adipogenic-, osteochondrogenic-, osteogenic- and chondrogenic-primed MSC, which in line with the putative model for MSC differentiation (chapter 1.3.2).

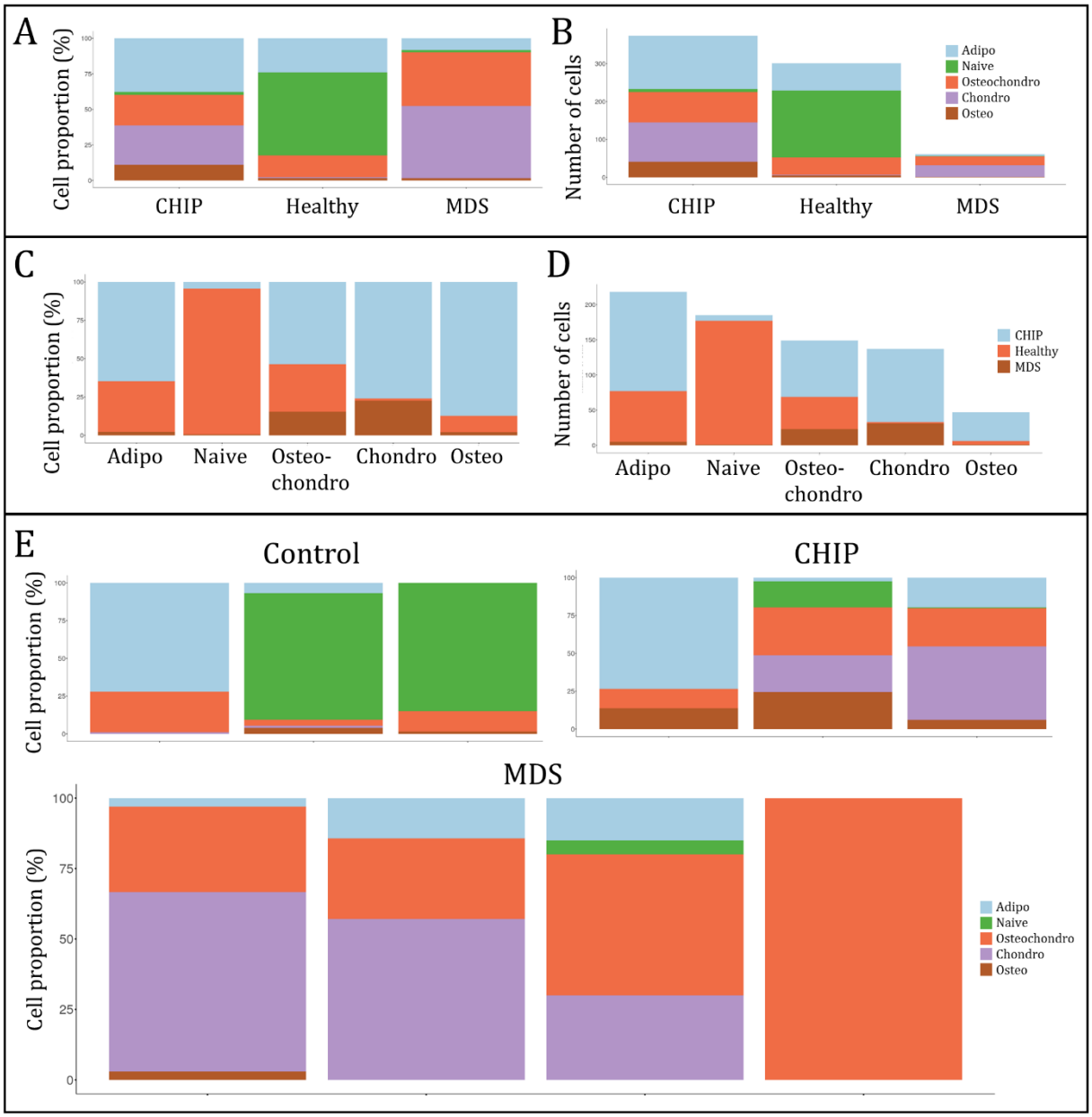

*Figure 34: Composition of stroma clusters. Relative (**A**) and absolute (**B**) stromal composition profile of CHIP, healthy and MDS samples. Relative (**C**) and absolute (**D**) composition of the different MSC clusters by condition. Individual donor stromal composition profile of control, CHIP and MDS samples (**E**).*

The composition profiles of MDS and CHIP stroma did share similarities, as both lacked naïve MSC, indicative of a possible lineage bias. Moreover, MDS samples showed only small amounts of adipogenic MSC in comparison to CHIP and control. It is noticeable that in all conditions, osteogenic MSC were very rare and in addition, control samples did not display chondrogenic MSC (Figure 34A). The total cell number was markedly lower in MDS samples, which impedes accurate comparison (Figure 34B). Concerning subcluster composition, it was noticeable that healthy MSC dominated the naïve cluster, but also populated the adipogenic and osteochondrogenic cluster, while CHIP MSC were almost exclusively found in the more committed clusters, especially in the osteogenic, osteochondrogenic and chondrogenic clusters (Figure 34C). MDS-MSC were mostly found in the chondro- and osteochondrogenic clusters, although contributing relatively few cells in total (Figure 34D). To assess if this was consistent in all donors or if it might be due to biological heterogeneity of the samples, the composition profiles of individual donors were compared (Figure 34E). The dominant naïve clusters were present in two of the three control samples, but not in two CHIP samples and only very small in the remaining CHIP donor. Three of the MDS donors were very similar in terms of composition, the fourth one was composed of only two osteochondrogenic cells and was thus omitted from discussion due to insufficient sample size.

Differentiation of MSC is regulated by different pathways as described in chapter 1.3.2, so possible differentiation biases in MDS and CHIP in comparison to control MSC could be due to altered gene expression. For this, differentially expressed genes between stromal cells from all conditions were compared using Gene Set Enrichment Analysis (GSEA).

4.7.2.1 Differential expression analysis of stromal cells between CHIP, MDS, and healthy

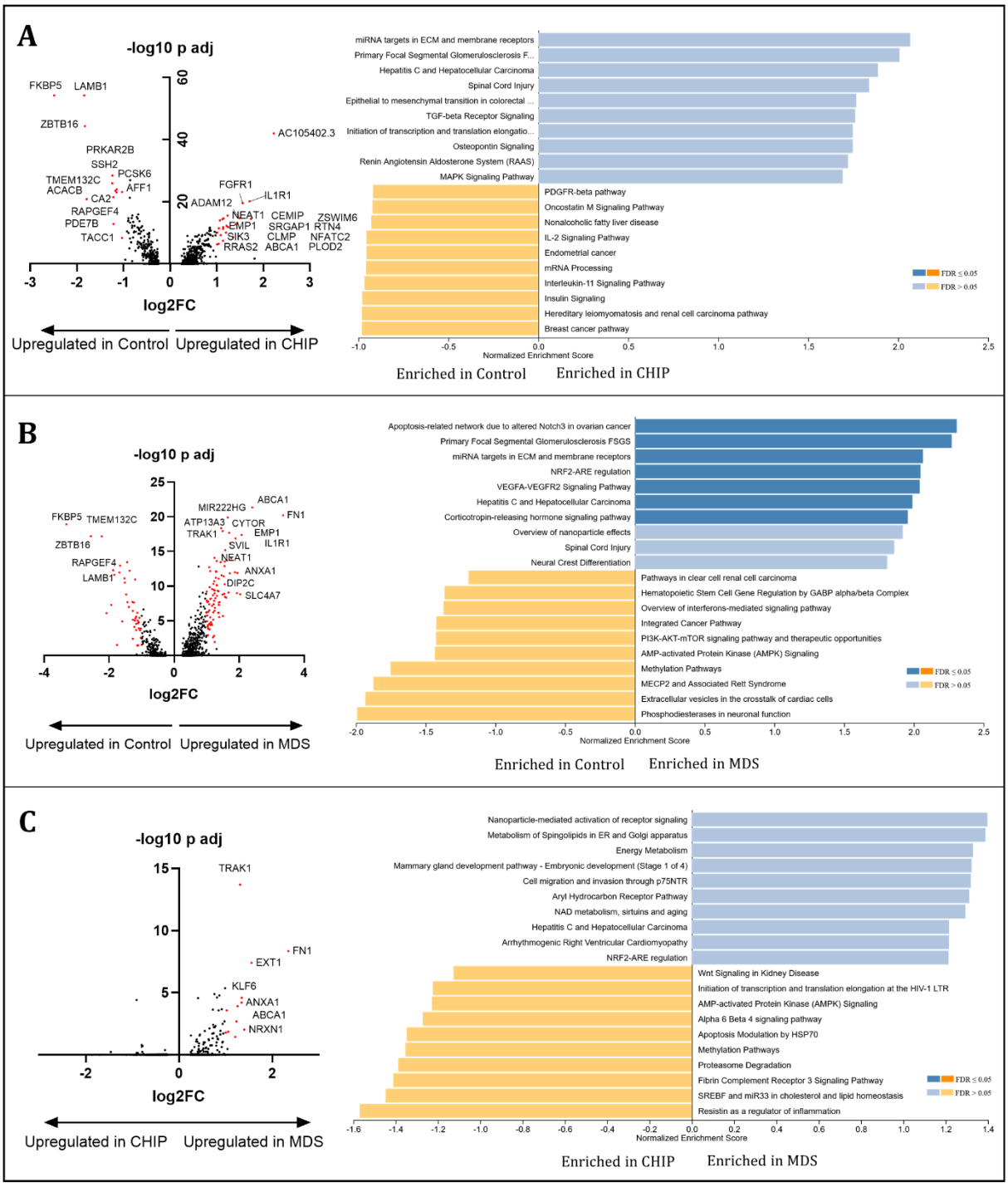

*Figure 35: Stroma analysis of differentially expressed genes. **A** Left: Volcano plot of differentially expressed genes (DEG) for stromal cells from CHIP and control donors. Significantly DEG (p<0.05, log2 fold-change>1 or <-1) are marked red, high p-value genes are annotated. Right: Gene set enrichment analysis of DEG using Wikipathway database. **B** Same plots for stroma from MDS and control or **C** MDS and CHIP donors.*

Comparing CHIP-derived MSC to controls, a total of 36 genes were significantly up- or downregulated (Figure 35A). Among the upregulated genes were genes involved in TGF-

β signaling, like IL-1R1, and ECM-related genes like ADAM12. No significantly enriched pathways were detected.

In MDS samples, 134 genes were significantly differentially expressed in comparison to controls (Figure 35B). FN1 was highly upregulated, which plays a central role in a multitude of cellular processes, for instance as part of the VEGFA-VEGFR2 signaling pathway, which was significantly enriched in MDS. Besides that, IL-1R1 was again highly expressed, and several ECM collagens like COL6A2, COL6A3, COL4A1 and COL4A2, suggesting possible differences in ECM composition which is in line with previous reports about dysregulated ECM in MDS (Bains et al. 2022).

Between MDS and CHIP, only 12 genes were significantly upregulated, and none downregulated, emphasizing a close proximity between these age-related conditions (Figure 35C). FN1 was again more highly expressed in MDS, in addition to TRAK1, a protein that is involved in endosomal-lysosomal transport, for instance of EGF-EGFR complexes (Webber et al. 2008). No pathway was significantly enriched. Keeping the strong HSC-supportive effect of MSC in mind, specific genes that are involved in HSC maintenance (Figure 6) were also investigated.

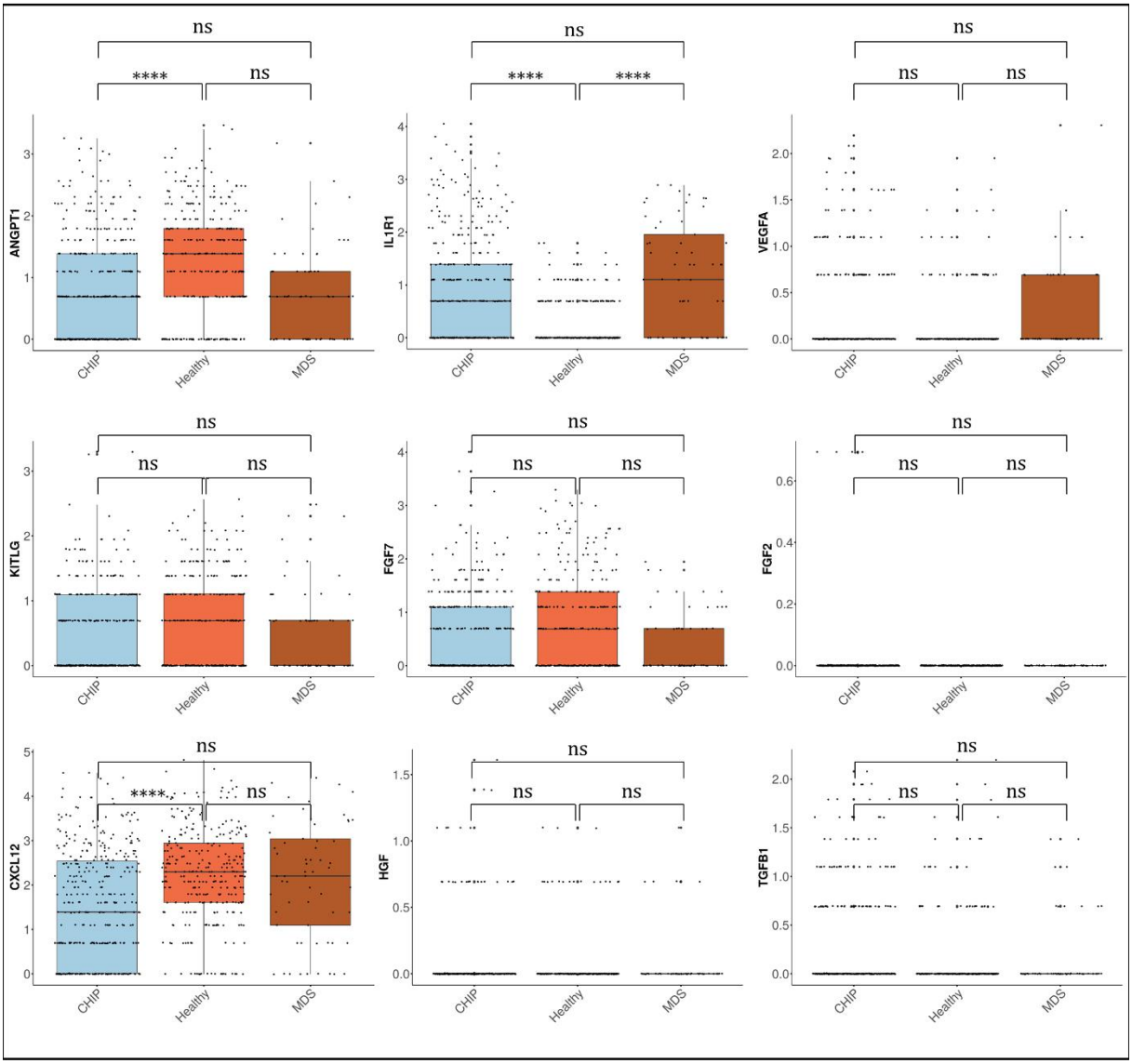

Figure 36: Box-and-whisker dot plots for selected HSC maintenance genes in stromal populations.

Because of the low number of MDS-MSC, results from this group were mostly not significant, with the exception of IL-1R1, which was induced in MDS in comparison to controls (Figure 36). No differences were found between MDS and CHIP. However, there was a noticeable decrease of Angpt1 and CXCL12, and an increase of IL-1R1 transcripts in CHIP MSC in comparison to controls.

The next open question was whether transcriptome differences between conditions were restricted to MSC subgroup composition and differential expression in the whole stroma, or also found in gene expression within the subclusters. Due to the low amount of MDS in the different clusters, subcluster analysis in comparison to MDS samples was not possible. For CHIP and control samples, clusters were populated too unevenly for comparative

DEG, since most control MSC were found in the naïve cluster while most CHIP MSC were of adipogenic nature.

4.7.3 Subclustering on T cells and differential gene expression analysis

To get insight into the dysregulation of the immune compartment in MDS and CHIP, 10,783 detected CD3⁺ T cells were clustered separately to reveal eight subclusters (Figure 37). Canonical T cell marker gene expression allowed annotation of these clusters (annex, Figure 63).

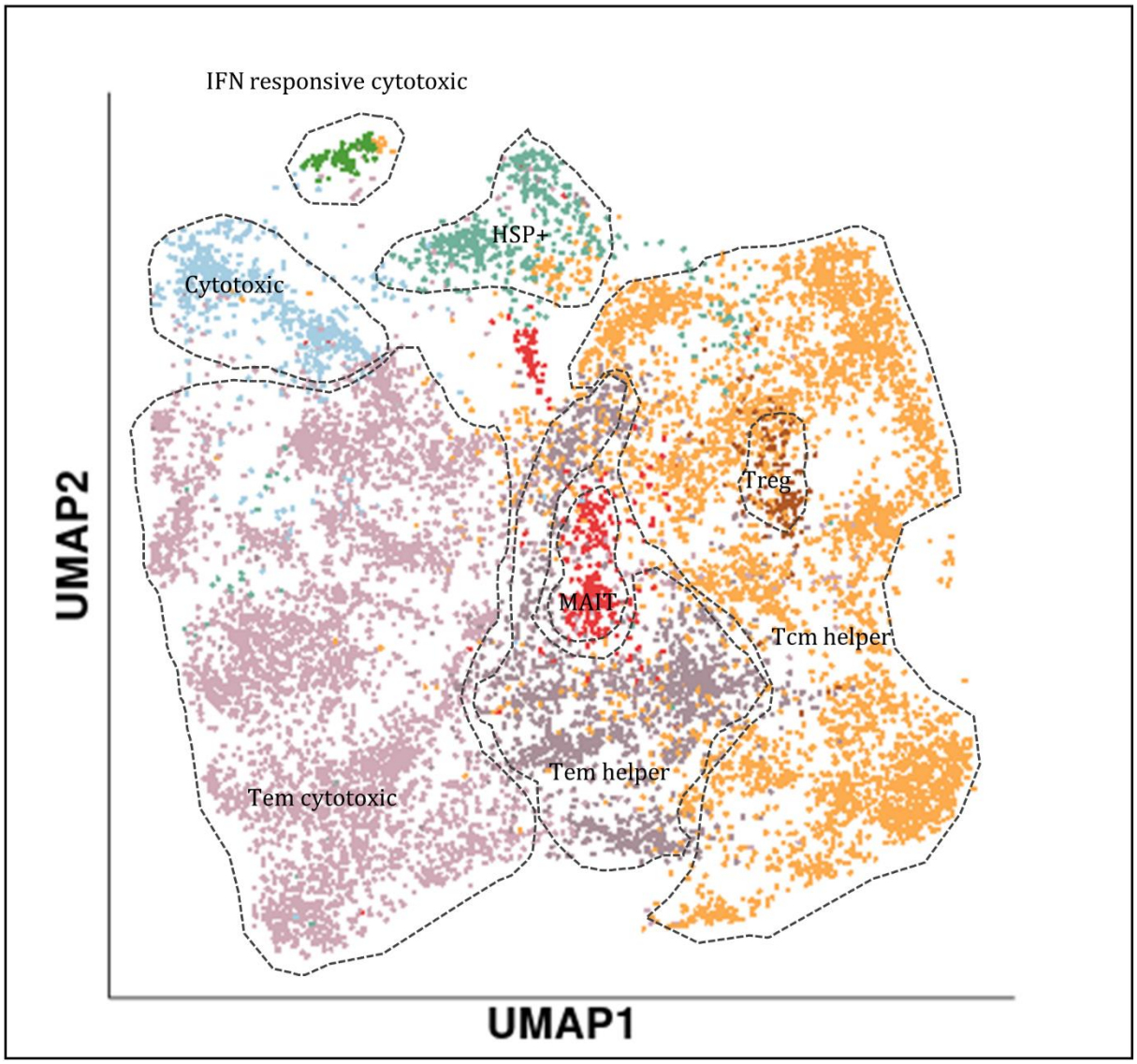

Figure 37: Subclustering on T cell with annotation of identified clusters. Tem: Effector memory T cell, Tcm: Central memory T cell, MAIT: Mucosal Associated Invariant T cell, HSP⁺: CD4/CD8 Heat-shock stimulated.

The two biggest populations that were found were effector memory T cells (Tem cytotoxic) and central memory T cells (Tcm helper), encompassing 3,901 and 3,840 of the 10,783 total annotated T cells. Besides these, 562 cytotoxic T cells, 446 heat shock protein-expressing T cells (HSP^+), 318 Mucosal Associated Invariant T cells (MAIT), 1,489 Tem helper cells as well as 139 Treg and 88 IFN responsive cytotoxic T cells were annotated (Figure 37).

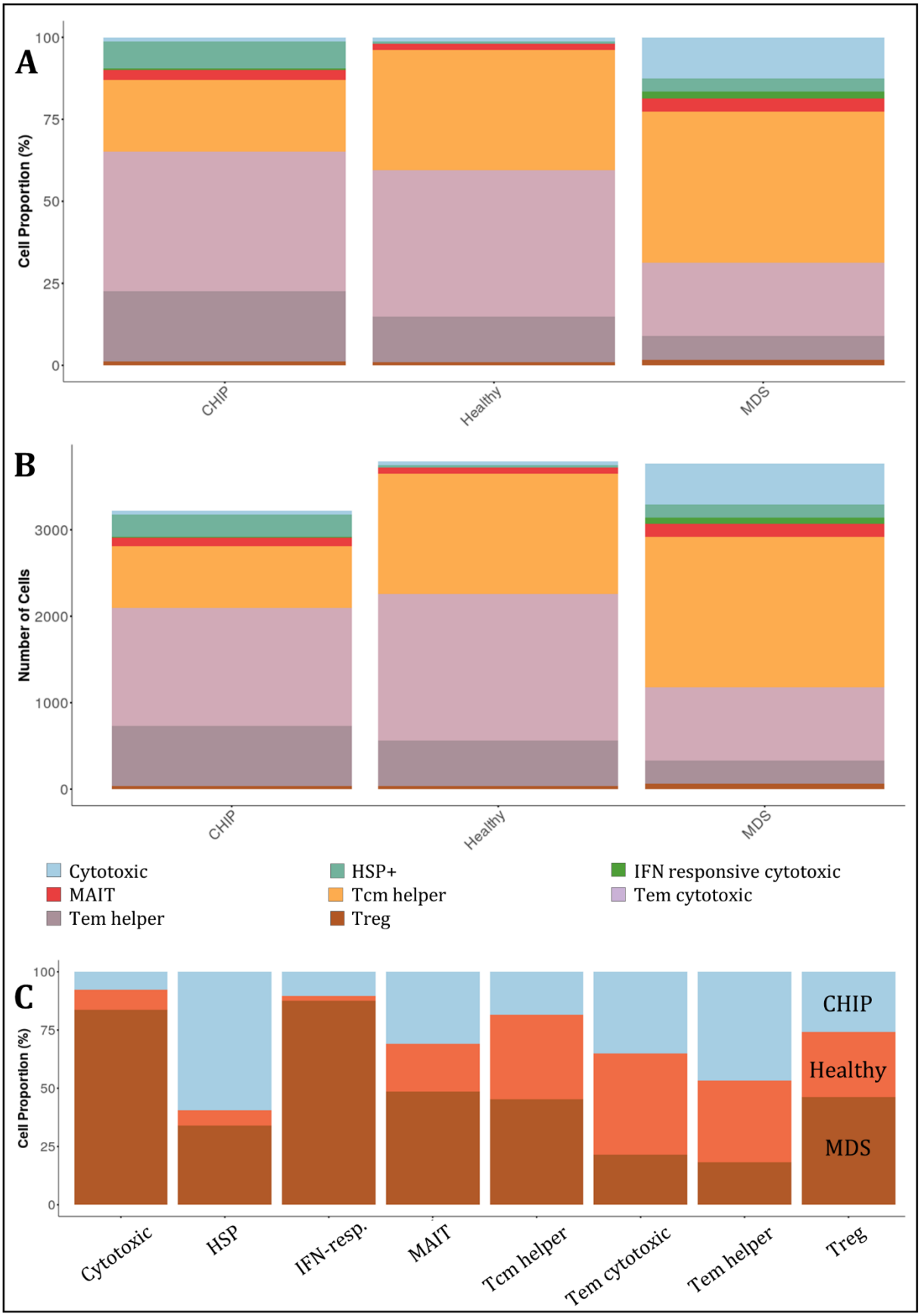

*Figure 38: T lymphocyte cluster composition. Relative (**A**) and absolute (**B**) T cell composition profile of CHIP, control and MDS samples. **C** Composition of T cell subcluster by condition.*

The cluster composition profiles of CHIP, control and MDS biopsies revealed heterogenous T cell population occurrence between the conditions based on their relative frequency (Figure 38A), while the overall cell numbers were comparable (Figure 38B). In control samples, an almost equal distribution of cytotoxic Tem and Tcm helper cells was found, with small percentages of Tem helper and all other subsets present. In CHIP, cytotoxic Tem were more frequent, while Tcm helper cells were almost halved. In addition, Tem helper, MAIT and HSP^+ CD4/CD8 T cells were expanded.

In MDS samples, a shift towards higher Tcm helper content and a drastic expansion of cytotoxic T cells was detected. In addition, HSP^+ and IFN responsive cytotoxic T cells were more prominent, while cytotoxic Tem cells and Tem helper cells were reduced. Meanwhile, Tregs were rare in all samples.

The composition of subclusters (Figure 38C) by condition also showed that MDS-T cells dominated MAIT, cytotoxic and IFN responsive cytotoxic clusters, CHIP samples the HSP^+ population, while Tem cytotoxic and Tem helper consisted mostly of CHIP and control samples.

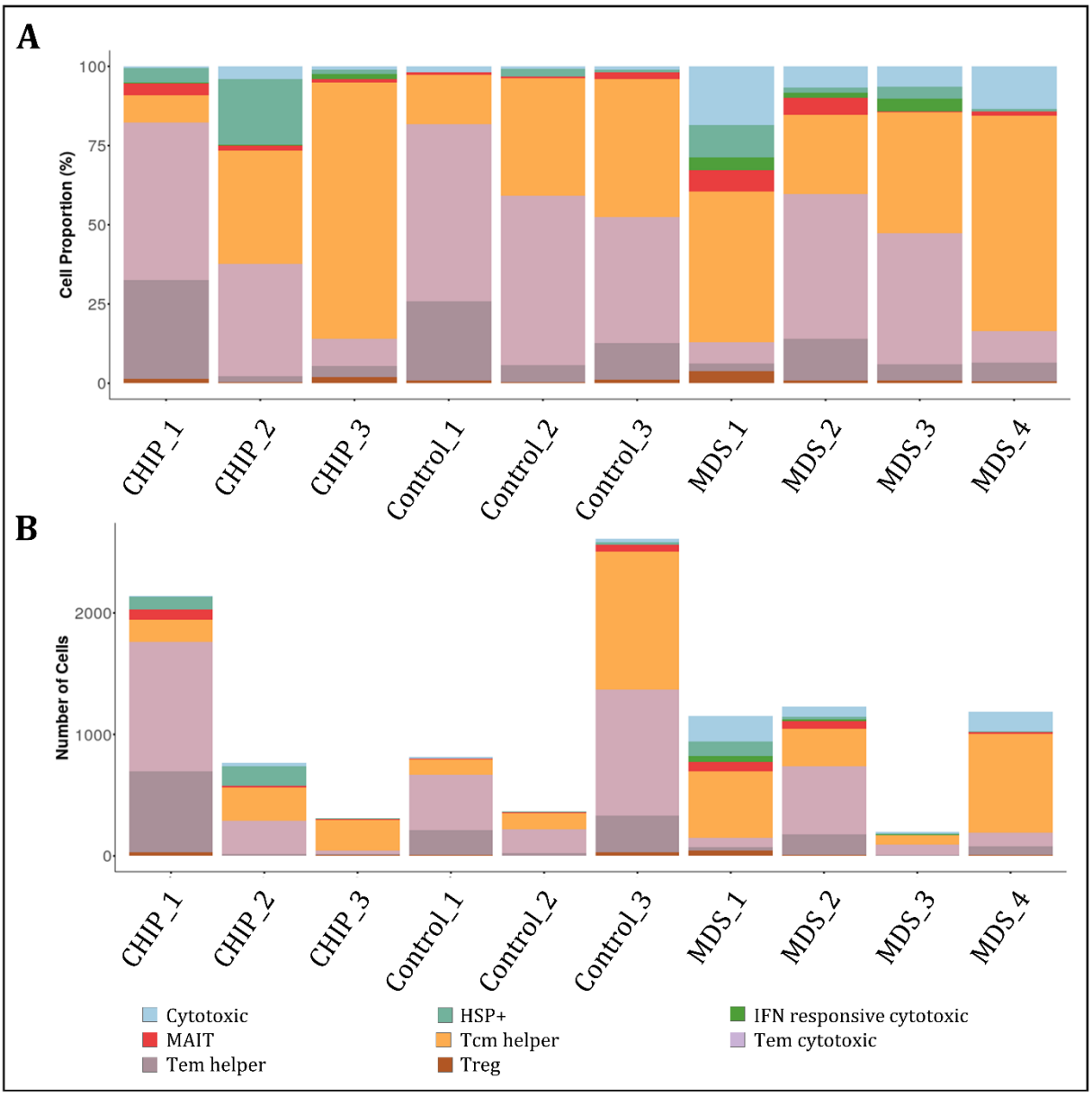

*Figure 39: Individual donor comparison for T cell subsets frequency (**A**) and absolute cell numbers (**B**).*

Inter-donor heterogeneity in cluster composition revealed which subgroups are consistently reduced or expanded between donors from one group (Figure 39A). Control samples were mostly alike, with the main differences being changes in what proportion of the sample consists of Tcm helper, Tem helper or Tem cytotoxic cells.

Two of three CHIP samples showed an expansion of HSP$^+$ CD4/CD8 T cells, while the remaining donor displayed a large proportion of Tcm helper cells.

In MDS, cytotoxic T cells were expanded in all donors, in addition to HSP$^+$ and IFN responsive cytotoxic T cells that were more frequent in two of four MDS patients. The

decrease in cytotoxic Tem cells was present in two of four samples. Two MDS and one CHIP donors exhibited a comparably higher proportion of MAIT cells.

The absolute numbers of T cells by donor show a good representation of all conditions, although one control, one CHIP, and one MDS sample contributed fewer than 500 cells (Figure 39B).

4.7.4 Differential gene expression of T cell subclusters

For all subclusters, sufficient cell numbers were present to do GSEA between conditions, revealing transcriptionally enriched or depleted pathways and allowing insight into molecular processes at play.

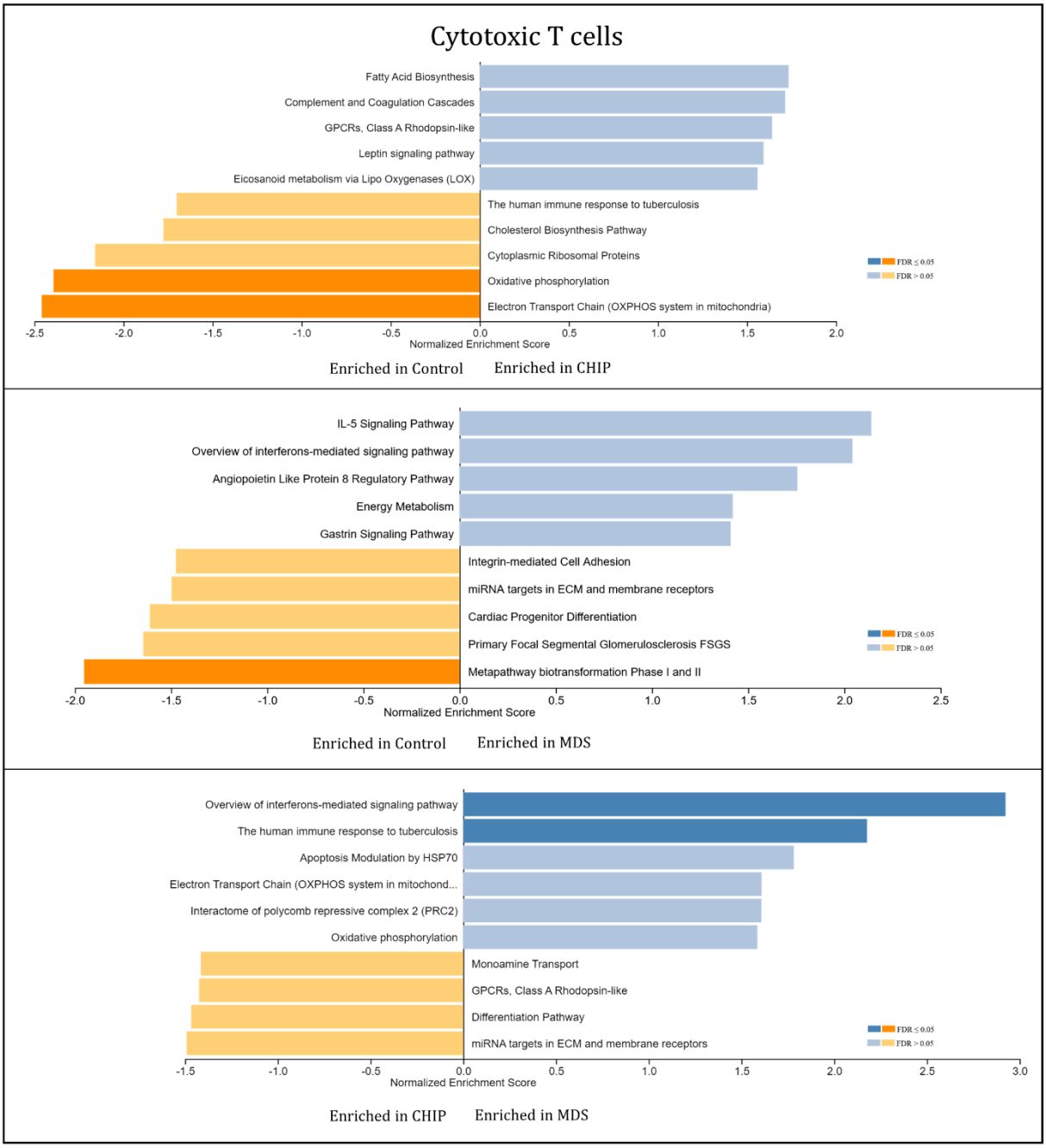

Figure 40: GSEA of cytotoxic T cells, comparing CHIP to control (top), MDS to control (middle) and MDS to CHIP (bottom) samples. Analysis was done using WebGestalt, for pathway enrichment the Wikipathways database was used and weighted in order to reduce multiple pathways that are related to the same set of genes.

Cytotoxic control cells displayed higher enrichment in oxidative phosphorylation pathways in comparison to CHIP donor-derived cells (Figure 40, top). In addition, control cells showed higher transcript levels of proteins that were involved in biotransformation pathways (middle). Comparing CHIP to MDS, interferon-mediated signaling pathways were more highly transcriptionally active in MDS (Figure 40, bottom).

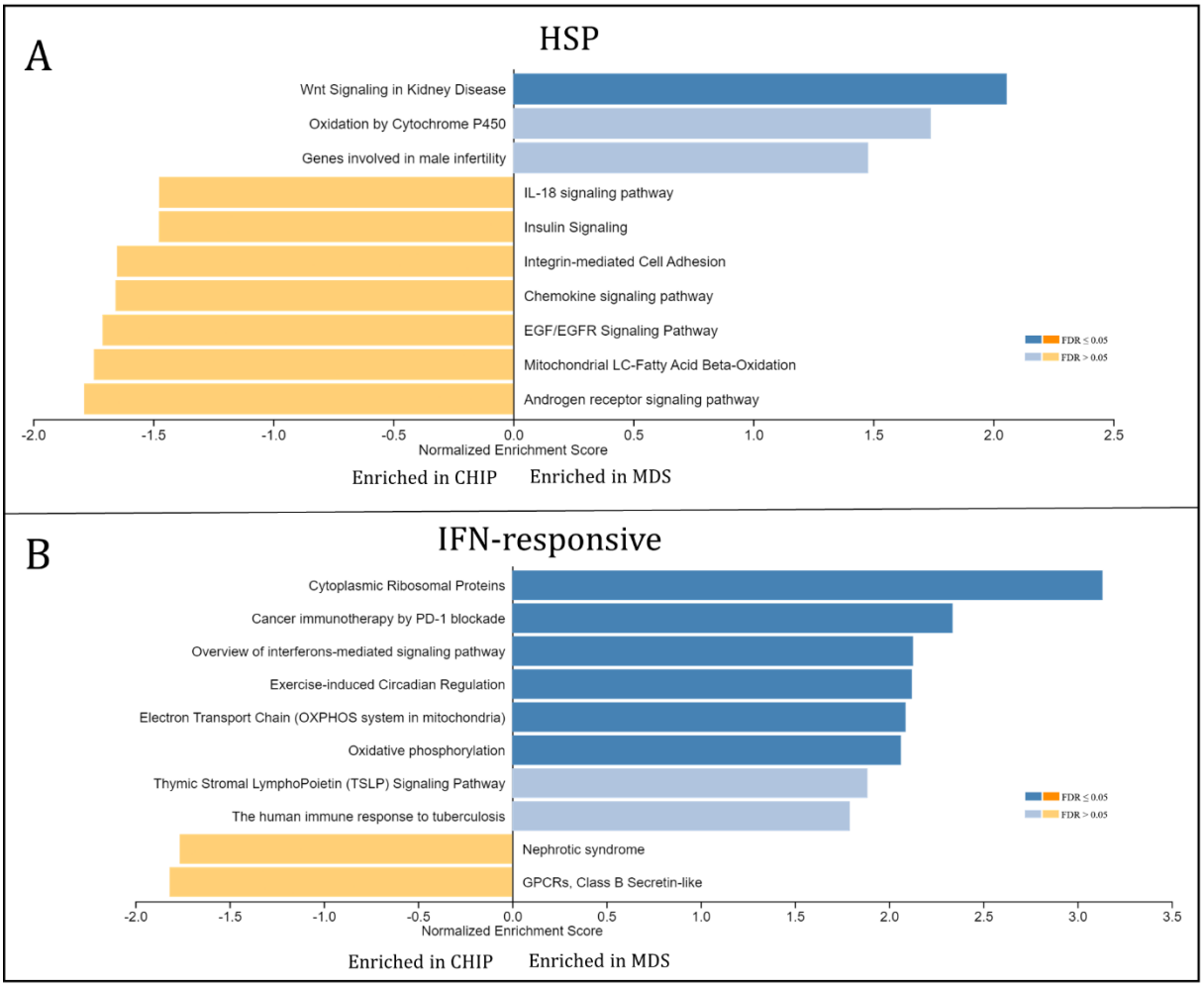

*Figure 41: GSEA of HSP⁺ T cells (**A**) and IFN-responsive cells (**B**), comparing MDS to CHIP cells. Analysis was done using WebGestalt, for pathway enrichment the Wikipathways database was used and weighted in order to reduce multiple pathways that are related to the same set of genes.*

HSP⁺ and IFN-responsive T cells consisted almost exclusively of CHIP and MDS-derived T cells, which is why no comparison to control cells could be made. In HSP⁺ MDS cells, Wnt pathway signaling was significantly enriched (Figure 41A). Interferon-responsive MDS T cells showed higher activity of ribosomal proteins, immunotherapy-related pathways, interferon signaling and oxidative phosphorylation pathways (Figure 41B).

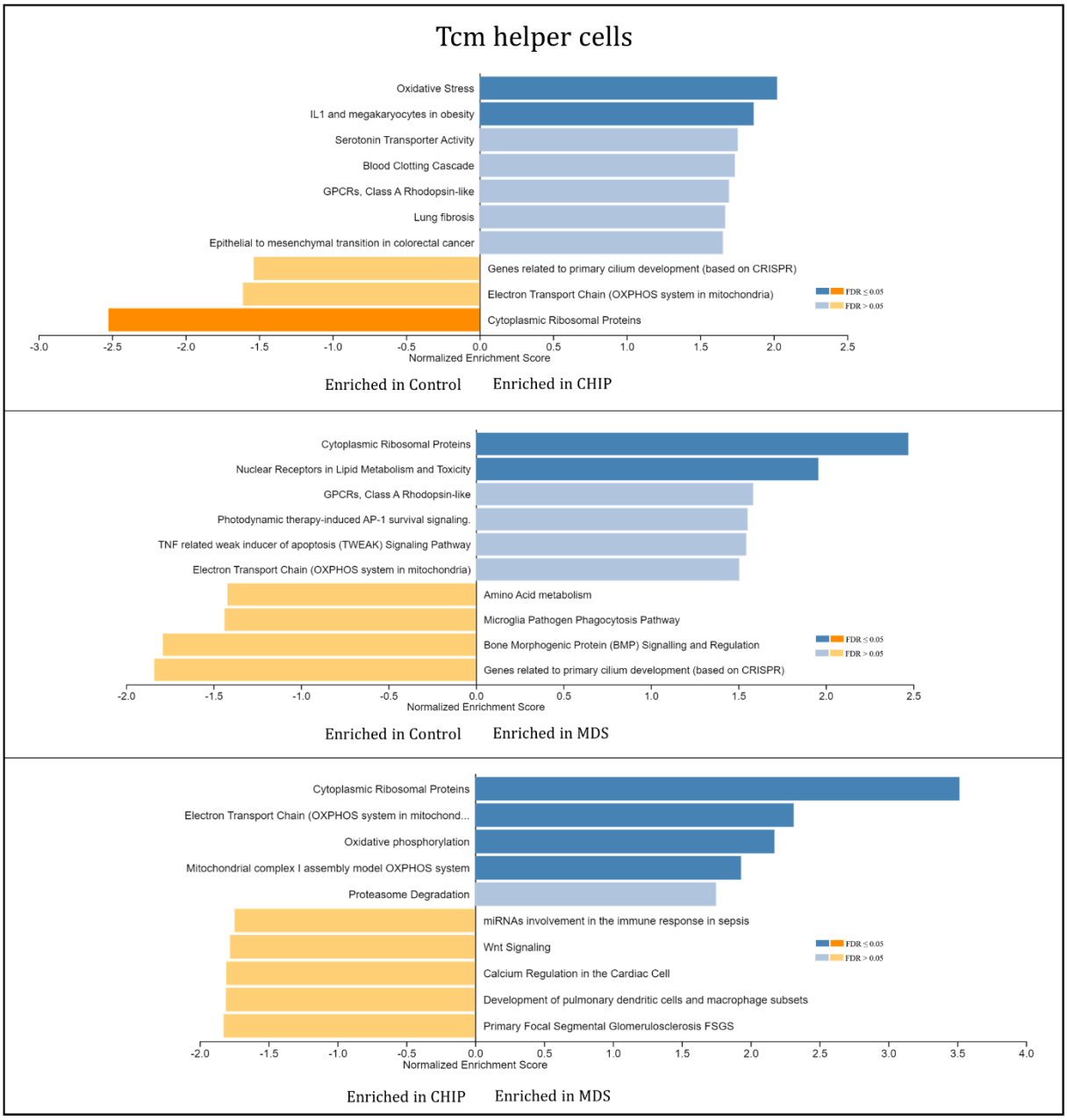

Figure 42: GSEA of Tcm helper cells, comparing CHIP to control (top), MDS to control (middle) and MDS to CHIP (bottom). Analysis was done using WebGestalt, for pathway enrichment the Wikipathways database was used and weighted in order to reduce multiple pathways that are related to the same set of genes.

In Tcm helper cells, IL-1 signaling and oxidative stress signatures were found at significantly higher levels than in control cells, while the latter showed higher transcripts of cytoplasmic ribosomal proteins (Figure 42, top). MDS Tcm helper cells showed even higher activity of those proteins in comparison to controls and were also enriched for nuclear receptors that are involved in lipid metabolism and toxicity (Figure 42, middle). Comparing MDS to CHIP, besides ribosomal proteins being upregulated in MDS, oxidative phosphorylation and proteasomal degradation pathways were highly enriched in MDS (Figure 42, bottom).

Figure 43: GSEA of MAIT cells, comparing CHIP to control (top), MDS to control (middle) and MDS to CHIP (bottom). Analysis was done using WebGestalt, for pathway enrichment the Wikipathways database was used and weighted in order to reduce multiple pathways that are related to the same set of genes.

Differences in gene expression of MAIT were only detected between CHIP and MDS, where MDS displayed higher transcripts of genes involved in cytoplasmic ribosomal proteins and interactors of the epigenetic PRC2 complex (Figure 43, bottom).

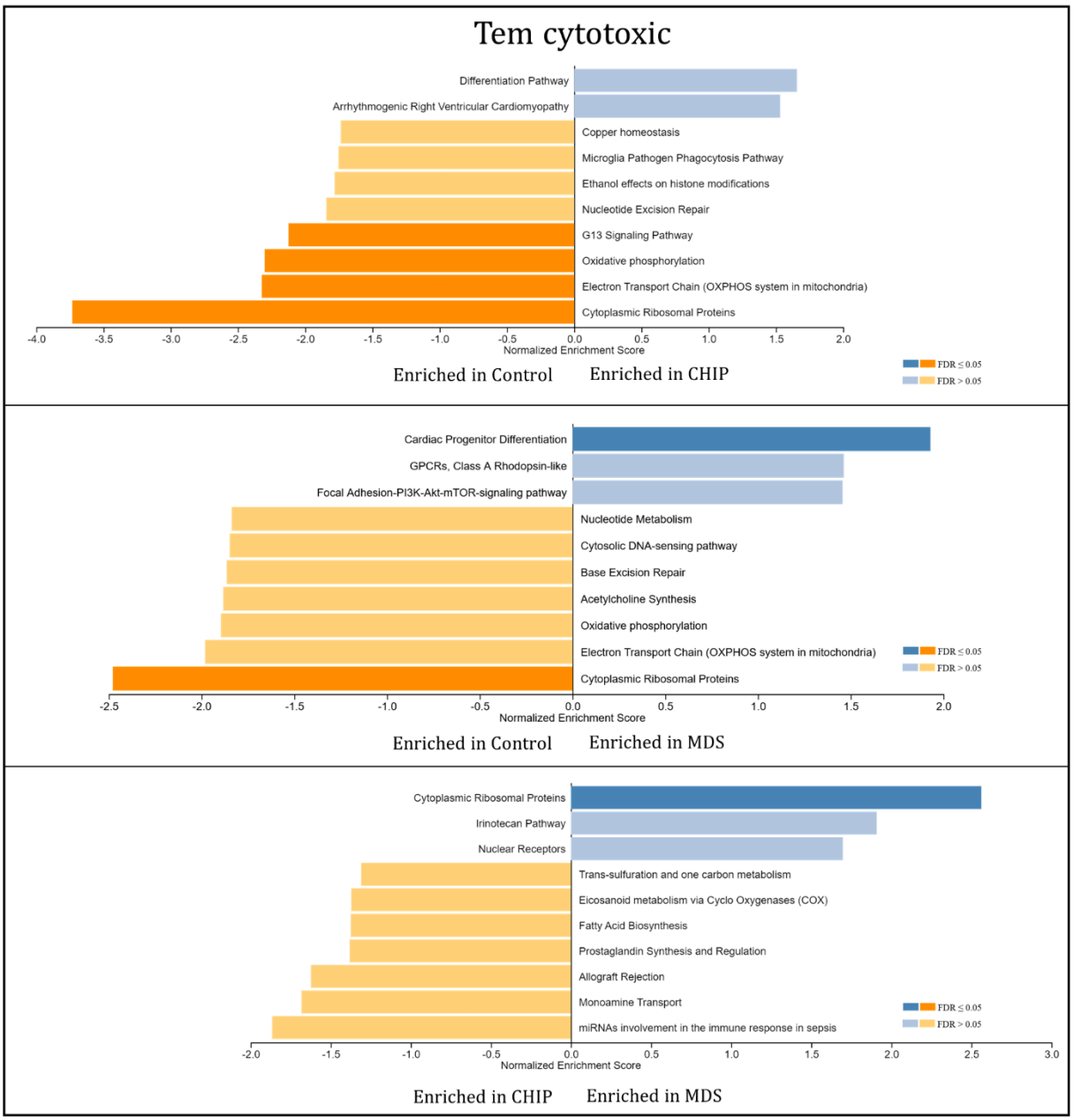

Figure 44: GSEA of Tem cytotoxic cells, comparing CHIP to control (top), MDS to control (middle) and MDS to CHIP (bottom). Analysis was done using WebGestalt, for pathway enrichment the Wikipathways database was used and weighted in order to reduce multiple pathways that are related to the same set of genes.

Cytotoxic Tem cells from control donors showed more oxidative phosphorylation genes, (La Fuente-Granada et al. 2019) as well as an activation of the G13 signaling pathway and cytoplasmic ribosomal proteins in comparison with CHIP (Figure 44, top). In comparison to MDS, control cells were enriched for cytoplasmic ribosomal protein transcripts (Figure 44, middle), while MDS were still exhibiting significant enrichment for ribosomal protein transcripts in comparison to CHIP (Figure 44, bottom). MDS Tem cytotoxic were also enriched in cardiac progenitor differentiation pathways in comparison to controls, which comprises Wnt genes and growth factor genes like IGF1 and FGF2.

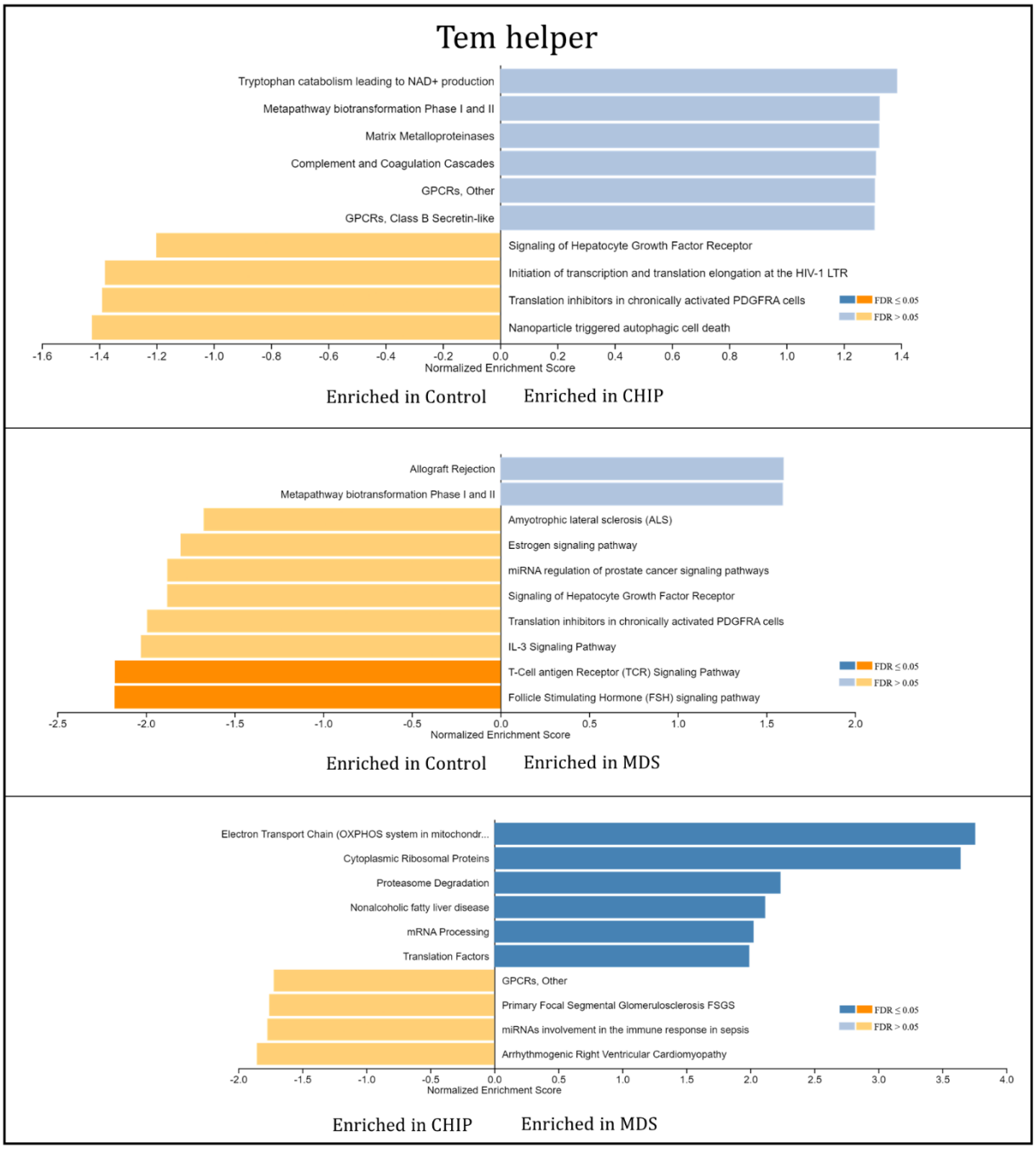

Figure 45: GSEA of Tem helper cells, comparing CHIP to control (top), MDS to control (middle) and MDS to CHIP (bottom). Analysis was done using WebGestalt, for pathway enrichment the Wikipathways database was used and weighted in order to reduce multiple pathways that are related to the same set of genes.

No significant differences were detected between control and CHIP-derived Tem helper cells (Figure 45, top). In contrast with MDS, control cells were enriched in T cell antigen receptor and follicle stimulating hormone signaling pathways (Figure 45, middle). Lastly, MDS T cells exhibited additional pathways related to oxidative phosphorylation, ribosomal proteins and proteasomal degradation, in addition to translation factors (Figure 45, bottom).

5 Discussion

The aim of this thesis was the characterization of the cellular BM niche in clonal hematopoiesis and MDS, with emphasis on possible stromal alterations that occur during malignant evolution. Bone marrow samples from donors enrolled in the BoHemE study, a prospective cohort of CHIP and MDS donors as well as controls, were analyzed by immunofluorescence imaging to understand anatomical and morphological alterations and by scRNA seq analysis to gain insight into transcriptional discrepancies. To unravel molecular alterations in niche interplay, co-culture systems of MSC and HSC were used while a high-VAF DNMT3A^{R878H} mouse model was used to model niche alterations in CHIP donors.

5.1 The human bone marrow niche undergoes a remodeling process in MDS

Bone marrow samples from MDS donors showed a complete remodeling of the bone marrow niche, with an emphasis on expanded sinusoidal vasculature (Figure 11) and a disorganized MSC network (Figure 12). The expansion of MSC could not be detected by FACS analysis (Figure 17), which can be explained by the sampling technique: for imaging experiments, bone marrow trephines were used, while BM aspirate was used for FACS analysis. This discrepancy can also be product of the site of extraction or cell isolation method. Stromal cells are embedded in the ECM and often need to be enzymatically digested for cell isolation, for instance with collagenase or dispase II (Wolock et al. 2019). This might also explain the slightly higher number of MSC in the aspirate of healthy donors, since the ECM is critically dysregulated and denser in MDS, making a thorough digestion even more necessary for cell isolation (Bains et al. 2022). In addition, the expanded MSC and EC were not displaying the same capacity to express CXCL12 as their healthy counterparts (Figure 12). All these changes are in line with an inflammatory bone marrow milieu, which has been shown to promote angiogenesis (Vandoorne et al. 2018), MSC expansion (Mitchell et al. 2023) and CXCL12 downregulation via induction of senescence in MSC (Balandrán et al. 2016; Gilbert et al. 2019). Increased bone marrow senescence has been reported on separate occasions (Shi et al. 2019; Civini et al. 2013) and was shown qualitatively in MDS samples by staining for β-galactosidase (annex, Figure 57), although the increased senescence signal was not restricted to a specific BM population such as MSC and seems to be a common BM milieu feature in MDS. Further

analysis of senescence in MSC will be instrumental to assess their role in inflammation and angiogenesis.

5.2 MDS- and CHIP-MSC diverge in cluster composition and differentiation potential

Stroma analysis from scRNA seq allowed identification of five different MSC subpopulations (Figure 33) that showed distinct molecular signatures for adipogenic, osteogenic, chondrogenic and osteochondrogenic progenitor states, in line with previous reports on MSC subsets based on lineage biases in murine BM-MSC (Wolock et al. 2019; Tikhonova et al. 2019) but also in human BM (Leimkühler et al. 2020). Although some biological heterogeneity among samples is expected considering different age, sex and mutation status of donors, MSC from control donors were mostly conferred to the naïve, multipotent cluster (Figure 34), marked by high expression of SPARCL1, FKBP5 and ZBTB16 (also known as ZNF145) which have also been considered markers for skeletal stem cells and freshly isolated $CD271^+$ BM cells with trilineage potential (Matthews et al. 2020; Kuçi et al. 2019). CHIP and MDS samples on the other hand, were mostly consisting of committed and lineage-primed MSC progenitors. Specifically, CHIP-MSC were evenly distributed across adipogenic, osteochondro- and chondrogenic clusters, while MDS-MSC were predominantly chondrogenic and osteochondrogenic, with essentially no other populations present. The low relative frequency of osteogenic-primed MSC in all conditions could be due to an inherent sample bias, since CHIP and control donors were recruited from hip and knee replacement surgeries, often suffering from osteoporosis or osteopenia. Indeed, CHIP and MDS have been described as risk factors for osteoporosis (Kim et al. 2021; Datzmann et al. 2018), with abnormal inflammatory signaling in CHIP progeny being linked to increased osteoclast-dependent bone degradation, thereby affecting MSC-driven osteo-regeneration. Studies in AML and MDS showed impaired osteogenic differentiation potential in primary patient-derived MSC, mediated by Extracellular Vesicles (EV) (Geyh et al. 2016; Hayashi et al. 2022). These EV contained miRNA, negative transcriptional factors, that target focal adhesion, MAPK signaling, TGF-β signaling pathway and axon guidance, all of which were also prevalent in MDS-derived stroma in the scRNA seq dataset (Figure 35).

Overall, the observed lineage commitment trajectory shift from the naïve MSC phenotype in the BM control samples to more differentiated ones in MDS and CHIP could be attributed to a niche-signaling mediated drive that pushes MSC toward activated states, i.e., more differentiated progenitor states. The adipogenic differentiation bias that was seen in two out of the three CHIP samples mimics the expanded $LEPR^{+}$ adipo-MSC observed in the $DNMT3A^{R878H}$ mouse model (Figure 20) and could indeed be a consequence of the CHIP mutation. This is reinforced by the decrease in BM cellularity of $DNMT3A^{R878H}$ mice due to an expansion of BMAT, which is derived from adipo-MSC. The naïve clusters were observed in only two of the three control samples, which could be within the window of biological cross-patient heterogeneity. More MSC samples of a wider range of clearly defined control, CHIP, and MDS donors should be tested to address this variance. For validation of the observed differentiation biases in CHIP and in MDS, prospective sorting and lineage differentiation studies should be performed on MSC using subset-specific surface markers, which have not been described so far. In addition to patient inter- and intra-heterogeneity, the current single cell MSC analysis has technical limitations, for instance the low cell number output from the processed samples, especially from MDS BM. Indeed, the data analysis demonstrated that most of the expected stromal cells (from the $CD45^{-}$ gate during sorting) from MDS were ultimately identified as erythroid progenitors and fell into the HSPC cluster in subsequent analysis, thereby reducing the number of *bona fide* stromal cells used for scRNA seq library construction. Consequently, to improve and refine the MSC subset characterization, a plate-based cell capture method of scRNA seq (SORT-seq) will be performed in future experiments on specifically sorted $CD271^{+}$ stromal cells instead of the shallower $CD45^{-}$ $lineage^{-}$ sorting strategy that was used in this thesis. The additional advantage of SORT-seq compared to 10x droplet-technology is the generation and analysis of a full-length transcriptome, allowing a better characterization of cell subtypes and better resolved cluster annotations (Muraro et al. 2016).

5.3 Single cell RNA sequencing reveals stromal alterations in CHIP and MDS

Most differences in gene expression of MSCs among the examined groups came from cells falling in different subclusters, which are differentiation-related genes. For instance, the highly downregulated FKBP5 and SPARCL1 in CHIP- and MDS-MSC are both marker genes of naïve MSC, which are present mostly in control BM (Figure 35). This is in line with

changes in HSC supportive factors, (Figure 36) where Angpt1 and CXCL12 are significantly downregulated in CHIP, since these factors are mostly expressed in the naïve cluster. The same trends are present in MDS-MSC: the upregulated ECM pathways (Figure 35B) encompass genes that are involved in osteochondrogenic differentiation like collagens, laminin, and fibronectin. At the same time, laminin isoforms have been shown to enhance homing, while fibronectin supports expansion of HSPC (Lee-Thedieck et al. 2022), highlighting that differentiation bias and HSC-supportive capacities of MSC are linked and should not be considered independent.

The significantly enriched Notch signaling-related pathways in MDS (Figure 35B), "Apoptosis-related network due to altered Notch3 in ovarian cancer" and "FSGS") reflect also changes in MSC differentiation, as the Notch pathway is involved in the adipogenic-osteogenic differentiation balance as depicted in chapter 1.3.2. The enriched NRF2-ARE pathway protects against oxidative stress, but has also been shown to be involved in osteogenic differentiation of MSC (Yoon et al. 2016). Besides that, activation of the VEGFA-VEGFR2 signaling pathway was observed, connecting to the findings of secretome analysis and cytokine profiling (Figure 26 and Figure 31) and showing upregulation of angiogenic processes which will be discussed in chapter 5.6.

For CHIP, ECM-related genes like ADAM12 were upregulated, which are linked to a proinflammatory and fibrosis-related subset of MSC that gets upregulated in response to TGF-β (Cipriani et al. 2016; Dulauroy et al. 2012). ADAM12$^+$ cells are found in the chondrogenic cluster, which is populated by CHIP and MDS cells (Figure 38) and could represent fibrotic-primed or activated MSC, thus reflecting physiological responses to BM inflammation. Previous scRNA seq studies on BM stroma found the same chondrogenic or fibroblastic MSC population and showed high expression of CD44 and IL-1R1 for this subset (Li et al. 2023; Stalmann et al. 2022). In the dataset of this thesis, CD44 and IL-1R1 were also found to be subset-specific marker genes for the chondrogenic cluster (annex, Figure 62) in CHIP and MDS samples. On a similar note, this subset is also induced in multiple myeloma and expresses high levels of cytokines (Jong et al. 2021; Stalmann et al. 2022). With this in mind, a functional characterization of CD44$^+$ IL-1R1$^+$ MSC should be conducted to confirm the inflammatory nature and decipher their possibly disruptive role in HSPC support and niche remodeling in CHIP and MDS.

5.4 Interplay of MDS blasts and MSC is linked to inflammatory processes

The reason for emergence of this chondrogenic MSC subset could be due to interplay with mutated HSPC or MDS blasts, as illustrated by the secretome analysis of an *in vitro* co-culture system of established MSC and MDS cell lines. Secretome analysis demonstrated that secreted proteins in the presented co-culture settings matched previously reported secreted proteins in primary MDS-derived MSC in comparison to healthy-derived MSC, such as LOLX2, SPARC, and IGFBP2 (Figure 26) (Medyouf et al. 2014). This supports the model of an MDS-MSC phenotype inducible by signaling from MDS blasts and demonstrates the validity of the *in vitro* system as a proxy for BM niche interplay. The secretome analysis displayed ratio-dependent protein secretion by both cell types, which could signify a dynamic signaling between MSC and MDS, depending on disease state along with MSC and MDS blast expansion.

Inversely, the secreted proteins from the MDS-L monoculture (Figure 27) were found to be involved in glycolysis and amino acid catabolism, which are typical cancer-associated metabolic processes, supporting prolonged neoplastic cell growth.

Pathway overrepresentation analysis in co-culture settings demonstrated enrichment of proteasomal degradation, VEGFA-VEGFR2 signaling, focal adhesion/PI3K-Akt signaling and several metabolic pathways (Figure 26). Focal adhesion and PI3K-Akt signaling pathways have been described to be dysregulated in MDS, resulting in survival advantages of cancer cells (Aanei et al. 2011; Wu et al. 2017), but also promoting proliferation and lowering adipogenic differentiation capacity of MSC (Chen et al. 2013). The proteasomal degradation pathways, and more specifically proteins involved in the 26S proteasome, were also enriched in co-culture conditions, and were shown to be secreted by MDS cells (Figure 27). The normal role of the 26S proteasome is protein homeostasis by degradation of ubiquitinylated proteins, but it is generally upregulated in AML and linked to worse overall survival (Lara et al. 2022). Mechanistically, the 26S proteasome is involved in regulating proinflammatory cellular responses by degradation of the transcription factor IκB, which usually binds and inhibits NF-κB, a downstream effector pathway of various inflammatory pathways, such as TNF-α or IL-1 (Karin and Delhase 2000; Hayden and Ghosh 2014; Liu et al. 2017). The secretion of this proteasomal complex might thus exert a protein degradation-dysregulating effect on surrounding cells, possibly resulting in inflammation-like consequences. Although this mode of action seems elusive and requires additional functional validation, the same mechanism of secreted 26S

proteasomal proteins was also found to play a role in remodeling the cytoskeletal network in erythrocytes by malaria parasites (Dekel et al. 2021), showing that molecular alterations via this mechanism are possible.

In addition to these pathways, a Luminex assay revealed the differential regulation of inflammatory cytokines in co-culture (Figure 31). IL-17a, a proinflammatory regulator cytokine that is usually secreted by Th17 T cells (for instance as a pathogen defense mechanism, but also as a mediator of CD8 T cell antitumor effects (Li et al. 2016)), was severely downregulated in co-culture. IL1-α and IL-1RA, known inflammatory stress cytokines (Volarevic et al. 2010), were both constitutively secreted by MSC, which shows their potent inherent immunomodulatory effect, and both were secreted at higher levels after addition of MDS-L. MIP-1α was also strongly increased in co-culture, a protein that is produced by a wide range of hematopoietic cells and leads to inflammation via induction of IL-1 and TNF-α signaling by monocytes (Nath et al. 2006).

Taken together, the data suggest that the immunomodulatory nature of MSC is changed toward an inflammatory stress state as a result of interplay with MDS cells, leading to differential secretion of pro- and anti-inflammatory cytokines. The precise effect on surrounding niche cells (including T cells) could not be addressed in this *in vitro* study but should be explored in the future in more sophisticated niche models. In addition, the chronic effect of co-culture might differ from effects after 48 or 96 h and should be matter of future research to assess temporal dynamics of cytokines and secreted factors in different conditions.

5.5 MSC-derived hematopoietic support factors are perturbed by MDS exposure

As discussed above, SPARC is increased in LR-MDS BM (Figure 29), but also highly secreted in the co-culture system (Figure 24). Besides its role in vasculature remodeling, SPARC can also regulate proliferation of HSC: transgenic knockout mice display accelerated turnover of HSC from activated to quiescent state (Lee-Thedieck et al. 2022), suggesting that SPARC overexpression as observed in Figure 29 might have negative impact on HSC quiescence. Concurrently, CXCL12 signals in IF experiments were not significantly lower in MDS than in controls (Figure 12) even though known main producers of CXCL12 such as EC and MSC were significantly expanded in these samples, which should result in higher CXCL12 signals (as seen in murine experiments, Figure 20).

Taking together these anatomical observations along with the *in vitro* reduction of CXCL12 produced by MSC-MDS-L co-cultures (Figure 31) and the transcriptional downregulation of Angpt1 in CHIP and MDS scRNA seq data (Figure 36), mounting evidence implies functional impairment of HSC-supportive capacities of MSC after exposure to inflammatory stimuli or MDS blasts. Interestingly, this deleterious phenotype was reverted in MDS-derived MSC in a recent study after treatment with luspatercept, a TGF-β pathway inhibitor, underscoring the importance of the TGF-β pathway in the dysregulation of MSC functionalities (Wobus et al. 2021). This pharmacological approach could be incorporated into primary MSC-MDS co-culture systems to verify if this TGF-β effect is universal or restricted to specific MDS subtypes.

5.6 Activation of angiogenic pathways as a result of MDS-MSC interplay

Regarding the expansion of sinusoids in MDS, secretome experiments revealed an inherent angiogenic potential of MSC by high expression of VEGF, aggravated by co-culture with MDS, which also resulted in strong secretion of PDGF, thus inducing angiogenesis via PDGF signaling pathways (Figure 35). PDGF signaling can also lead to expansion of MSC (Zhang et al. 2016), suggesting a possible mechanism for the observed MSC expansion in MDS and linking both cellular processes. Furthermore, the secretome findings of the *in vitro* co-culture model are also supported by the induction of the proangiogenic VEGF-VEGFR2 pathway in MDS-derived MSC at the transcriptomic level (scRNA-seq analysis) in comparison to controls (Figure 35). Overall, these obtained results are in line with previous reports of increased proangiogenic factors like VEGF in MDS (Legros et al. 2012), although their main source seemed to be MSC as seen in the Luminex assays, where no increase in VEGF-A secretion was detectable (Figure 31).

In addition, SPARC was found among the highest differentially secreted proteins in the co-culture (Figure 24), which is an important regulator of HSC quiescence but also angiogenesis as shown in a knock-out mouse model (Figure 30). The strong increase in $CD31^+$ vasculature in the femur after genetic deletion of SPARC implies that it functions mainly as anti-angiogenic, and this effect was substantiated by original studies on recombinant SPARC protein (Sage et al. 1984; Sage 1986). However, the effect of SPARC is highly context-dependent and strongly debated, with studies showing stimulatory as well as inhibitory effects on angiogenesis (reviewed in detail by Rivera et al. 2011). This

view is supported by a concomitant increase of SPARC in MDS bone marrow samples of the BoHemE cohort that showed higher sinusoidal content, preferentially secreted by MSC and EC (Figure 29).

Given the complex genetic heterogeneity of MDS, results from one established MDS cell line should be complemented by cytokine profiling and secretome analysis of primary patient-derived MDS blasts with patient-matched MSC to determine mutation- or subtype-specific similarities and differences.

5.7 T cell compartment composition shifts towards effector subsets in CHIP and MDS

T cell annotation for scRNA seq remains challenging, due to the low number of features or genes T cells express and their generally more quiescent nature (as shown in Figure 64, annex). This leads to UMAP projections lacking the clear demarcation of subsets compared to other more proliferative cell types. In this study, eight T cell subsets could confidently be identified containing a total of 10,783 cells. The cellular origin of the identified subsets is divided by their adaptive immunity nature: the $CD4^+$ subcluster (helper T cell), containing Tcm helper, Treg, Tem helper on one hand, and the $CD8^+$ subcluster (cytotoxic T cells), entailing Tem cytotoxic, effector cytotoxic and IFN-responsive cytotoxic T cells. Of note, Heat Shock Protein-positive T cells (HSP^+) and MAIT were found to be mixed CD4/CD8 populations, although MAIT consist primarily of $CD4^+$ and HSP^+ cells mostly of $CD8^+$ cells (Figure 38). It should be noted that surface marker expression was not prominent on mRNA expression levels (no consistent CD4/CD8 expression was found in this dataset), which is why some techniques (Ab-seq) employ additional steps of cell surface antibody-labeling with barcode DNA-antibodies for easier annotation (Shahi et al. 2017). While the T cell cluster did not feature prominent, clearly distinct clusters beside HSP, IFN-responsive cytotoxic and cytotoxic T cells, the canonical gene signature annotation approach (annex, Figure 63) led to reliable identification of important T cell subsets, which will be briefly outlined below.

5.8 T cell subset heterogeneity in the bone marrow niche

MAIT are a T cell subset that can get activated by inflammatory cytokines without additional priming by antigen binding and have proinflammatory and effector-like

functions, for instance by secretion of IL-18, IFN-γ, granzyme B and TNF (Napier et al. 2015; Hinks 2016). They are thought to function as a defense mechanism against viral infections but are also found in chronic inflammatory settings like autoimmune disorders and cancer. MAIT can play a pathogenic role by further aggravating inflammation and cytotoxicity (Toubal et al. 2019). Accumulating clinical evidence demonstrated that MAIT, usually located in the digestive system, circulate and re-locate to the BM or other hematopoietic tissues in chronic inflammatory diseases (Cho et al. 2014; Serriari et al. 2014; Magalhaes et al. 2015).

Effector memory T cells (Tem cytotoxic) are CD8 cells that recognized and reacted to a cognate antigen and persist in tissues as an immune reservoir for rapid reactivation in case of a recurrent stimulus (Di Rosa 2016).

Effector memory helper T cells (Tem helper) are a subset of $CD4^+$ T lymphocytes and mainly found in peripheral tissue where they control immediate and acute immune defense by secretion of cytokines like IFN-γ and LTα (Th1), IL-4, IL-5, IL-13 (Th2) or IL-17A/F and IL-6 (Th17) (Weaver et al. 2006). They differ from T central memory helper (Tcm helper) cells mostly by their trafficking pattern: While Tem localize in peripheral tissue, Tcm cells home to secondary lymphoid tissues like lymph nodes and spleen (Benichou et al. 2017).

Cytotoxic T cells on the other hand are a CD8 effector population that bind MHC-I and lyse target cells by secretion of cytotoxic factors such as TNF-α, IFN-γ, granzyme B or perforin. They are usually not highly present in the bone marrow but become more prominent for emergency hematopoiesis or for immune effector functions, for instance against viruses or cancer cells (Schürch et al. 2014). In LR-MDS, several studies showed a clonal expansion of cytotoxic T cells, corresponding to cancer cell lysis activity (Kook et al. 2001; Pülhorn et al. 2012). A special subset of these cells, IFN-responsive cytotoxic T cells, have been described in viral infections and in tumor context as bystander T cells that get activated by IFN-γ, and might display anti-tumor activity (Holay et al. 2022; Pauken et al. 2021). A clear biological function that separates this IFN subset from other cytotoxic T cells has however not been reported yet.

Regulatory T cells (Tregs) are a specialized subpopulation of T cells that act to suppress immune response, thereby maintaining immune homeostasis and self-tolerance. The function of Treg in the BM has been described in detail in chapter 1.3.6. Unfortunately,

only few Tregs could be retrieved and annotated in the scRNA seq experiment, rendering meaningful gene expression analysis between groups inconclusive.

HSP$^+$ T cells consist of both CD4 and CD8-derived cells and are linked to chronic inflammation, where they might act as T cell suppressors (Wang et al. 2021; van Eden et al. 2005). The expansion of this subset could again be a physiological response to an inflammatory BM milieu. Interestingly, this subset is often described as a stress-induced artifact, since upregulation of HSP proteins is often found under duress, thereby their exact biological function remains to be revealed (van der Leun et al. 2020).

5.9 Transcriptional differences in metabolic and functional pathways in MDS and CHIP T lymphocytes

In the scRNA seq dataset, total recovered T cells from MDS, CHIP and control donors were similarly represented, allowing a meaningful comparison of cluster composition. Inter-donor heterogeneity was noticeably high (Figure 39), but still, condition-specific trends were detectable without patient sample overrepresentation. Control samples consisted predominantly of Tcm helper and Tem cytotoxic cells, with almost equal proportions. In addition, Tem helper cells were present at approximately 5–10% of all T cells. This reinforces the view of the bone marrow as an immune reservoir for memory T cells (Zhao et al. 2012). CHIP samples additionally showed a higher proportion of HSP$^+$ in two out of three donors as well as in one MDS donor.

As described above, HSP$^+$ cells are often found in chronic inflammation, which is in accordance with the inflammatory BM signature seen in CHIP stromal cells (chapter 5.3). Since these cells were only sufficiently found in CHIP and MDS, a comparison to control cells was not possible. GSEA between CHIP and MDS-HSP$^+$ on the other hand revealed enrichment of Wnt-related pathways in MDS (Figure 41). High Wnt signaling is associated with enhanced proliferation capacities in effector T cells and is needed for terminal differentiation (Boudousquié et al. 2014; Ma et al. 2012). Upregulation of Wnt is also implicated in inflammatory priming of CD4$^+$ T cells and Treg, although the most highly expressed gene, WNT10B, has been shown to be a negative regulator of polarization toward inflammatory CD4 phenotypes in a genetic knockout model (Trischler et al. 2016). The difference in Wnt signaling could be a result of differential proliferation signaling between the conditions, but a connection to immune-regulatory functions of HSP should

be investigated, as well as a clear functional analysis of the HSP subset to determine its biological purposes.

MAIT were also strongly expanded in one of the three CHIP and two of the four MDS samples (Figure 39). Again, this subset is often found in chronic inflammation, further cementing the view of both CHIP and MDS BM as chronically inflamed. On the transcriptional level, only the comparison between MDS and CHIP MAIT was possible due to the low number of cells from control samples (66 for healthy, 98 for CHIP, 154 for MDS). Apparent differences were an enrichment of cytoplasmic ribosomal proteins in MDS, which could be linked to an increase of protein synthesis towards an activation state (Figure 43). This enrichment was found in almost all MDS subclusters in comparison to both control and CHIP and could thus be a common feature in MDS. An increase in cytoplasmic ribosomal proteins has been found in many cancers, including MDS (Kang et al. 2021; Rinker et al. 2016) as well as in the secretome analysis of MDS blasts in this study (Figure 27) and has been linked to altered ribosomal function of cancer cells. If this is indeed an MDS-inherent effect, MAIT and other T cells that display this signature could be product of lymphoid progeny of MDS blasts, which should be investigated more thoroughly. Furthermore, transcripts relating to the PRC2 complex were significantly enriched in MDS. This complex is related to epigenetic chromatin silencing via tri-methylation of histone 3 at lysine 27. In T cells, suppression of this complex leads to immunosuppression, showing its direct regulatory role in T cell activation (Dobenecker et al. 2018). Overall, these data demonstrate that MAIT appear to be in a more active state in MDS compared to CHIP and control cells.

MDS samples were also the most frequent contributors to cytotoxic and IFN-responsive cytotoxic clusters (Figure 38). GSEA analysis showed that CHIP cytotoxic T cells display lower levels of transcripts for oxidative phosphorylation pathways than control cells, suggesting a distinct metabolic switch that might again be related to an altered activity state (Figure 40). Activated T cells often exhibit higher rates of glycolysis and lowered oxidative phosphorylation capacity, while exhausted T cell are more quiescent for both pathways (Franco et al. 2020). It remains unclear how the transcriptional alteration in metabolic pathways translates to cellular metabolism rates, which could be elucidated by functional measurements using metabolic flux assays of isolated T cell subpopulations. In comparison to MDS, control cytotoxic T cells were enriched for biotransformation pathways of metabolites, including sulfotransferases, acetyltransferases as well as

cytochrome P450 family members. Altered capacities to transform exogenous chemicals has been reported as a result of interferon signaling, which would explain the observed expansion of effector subsets in MDS BM (Williams and Farrell 1986). Enrichment of interferon signaling was detected when comparing MDS with CHIP, and to a lesser extent, in MDS in comparison with control cells. This is characteristic of a strong chronic immune response and an enhanced activation state of cytotoxic T cell, as expected in LR-MDS (Welsh et al. 2012).

Similarly, IFN-responsive cytotoxic T cells were only detectable at sufficient levels in CHIP and MDS (Figure 41). Qualitatively, MDS cells again showed an upregulation of cytoplasmic ribosomal proteins and oxidative phosphorylation pathways, indicating a transcriptionally and energetically more active phenotype as discussed above. In addition, immune recognition-related genes were enriched, especially T cell surface glycoproteins and co-receptors of the T cell receptor (TCR), such as CD3D, CD3G and CD8, and downstream effector kinases of TCR signaling. This reinforces the image that MDS-derived cells are highly active and engaged in their effector function.

Although other T cell subpopulations were present in all conditions, transcriptional differences between the groups were still apparent. For Tem cytotoxic, the switch in CHIP cells to lowered oxidative phosphorylation and cytoplasmic ribosomal proteins in comparison to control cells was again a common feature of these cells (Figure 44). In addition, the G13 signaling pathway was lowered in CHIP. This pathway regulates cytoskeleton remodeling and focal adhesion, and disorganization of the actin cytoskeleton has been found to have detrimental effects on cytotoxic T cell activation potential through TCR signaling (Kumari et al. 2014). Again, functional validation of isolated cytotoxic Tem should be considered to elucidate possible defects. MDS Tem displayed enrichment for cardiac progenitor differentiation pathways. While not relevant in the bone marrow, the most highly upregulated gene, INHBA, is part of the activin and inhibin complexes that regulate IFN secretion in T cells (Petraglia et al. 1991). Genetic knockout leads to Treg expansion in a mouse model, which was found to be regulated by dendritic cells (La Fuente-Granada et al. 2019). Whether overexpression of this gene in other immune cells has regulatory effects on Treg homeostasis remains to be explored.

Tcm helper cells displayed an enrichment of oxidative stress and IL-1 signaling pathways in CHIP samples in comparison to controls, with IL-1β, IL-1R1, alarmin and CCR3 among the most significantly upregulated genes (Figure 42). IL-1 is a key inflammatory cytokine

that has recently been identified as a main driver of hematopoietic aging due to stromal niche inflammation (Mitchell et al. 2023). Furthermore, it is also important in proinflammatory priming and CD4 T cell differentiation toward Th17 and Th9 effector subsets (Ben-Sasson et al. 2009). Oxidative stress is induced as a result of ligation and stimulation of TCR (Jackson et al. 2004), and IL-1 signaling and oxidative stress pathways are interconnected (Harijith et al. 2014), explaining why both processes are present in these cells. In MDS Tcm helper cells, nuclear receptors in lipid metabolism and toxicity were found to be upregulated in comparison to controls, among them vitamin D receptor and CYP27B1. This latter gene has been used previously in cell culture models as a mark for activated T cells and supplies CD4 T cells with vitamin D, which is needed for differentiation toward Th2 and Treg (Kongsbak et al. 2014; Lochner et al. 2015). Rewiring of this pathway in MDS could again have an effect on naïve CD4 differentiation toward effector and Treg subsets, which coincidentally has been described in MDS previously (Solomou et al. 2008). Further assessment of possible differentiation changes in CD4 cells should be employed by flow cytometry for the samples used in these experiments.

Tem helper cells from CHIP and control donors displayed no significantly enriched pathways (Figure 45). Comparison of MDS against control cells on the other hand showed a downregulation of the TCR signaling pathway, which in parallel to the results from IFN-responsive T cells could represent an impeded function of memory cells to respond to antigen presentation by antigen-presenting cells. FSH pathways were also enriched, driven by strong downregulation of AREG in MDS. Cell-surface AREG enhances Treg function by binding to EGFR on Tregs (Zaiss et al. 2013), presenting another possible altered Treg support axis.

In summary, CHIP T cells showed a strong expansion of cells expanded in chronic inflammatory diseases like HSP^+ T cells and MAIT. Cytotoxic and Tem cytotoxic T cells showed a metabolic switch with lower oxidative phosphorylation pathways, while helper cells showed signatures of inflammation and upregulation of the IL-1 pathway, linking the T cell compartment to the inflammatory response seen in stromal cells.

T lymphocytes from MDS cells were skewed toward active cytotoxic populations to the expense of Tem helper and Tem cytotoxic cells. The expanded cells displayed enriched IFN response and changes in metabolism-related pathways. Helper T cell sub-populations showed several dysregulated pathways connected to Th/Treg differentiation and Treg regulation.

5.10 Tregs are reduced in MDS BM in imaging studies

While the overall T cell fraction of the bone marrow was unchanged, assessed in both histological immunostainings and FACS analysis, the amount of Tregs and the fraction in the total T cell pool was diminished in MDS, as seen in (Figure 14). These changes were not statistically significant for the Treg:T cell ratios and for the overall Treg content only in comparison to CHIP samples, which is due to the low number of replicates used in these experiments. This in turn was a direct consequence of the overall sample quality and red marrow content, where CHIP and control samples had low fraction of hematopoietic cells due to the heavily increased BMAT (Figure 10). The reduction of Treg frequency in LR-MDS could not be evaluated in scRNA seq experiments (Figure 17), where a very low number of total Treg was detected for all conditions with almost equal proportions. The overall Tregs:T cell fraction in scRNA seq was detected at around 1.4% for all conditions and significantly lower than in imaging experiments (Figure 14), where the mean Treg:T cell ratio was 3% in MDS to 8% in control and 11% in CHIP samples, which is more in accordance with previous literature reports (Niedźwiecki et al. 2018; Giovazzino et al. 2019). This could either signify that Tregs were underrepresented in the BM aspirate for scRNA seq studies, maybe due to sticking more closely to ECM-producing MSC as seen in Figure 56 (annex), or that they were recovered with lower success rates in the annotation process, perhaps due to low transcriptional activity due to their highly quiescent state.

The reduction in Tregs has however also been described in some case-cohort studies on LR-MDS, where it was inversely correlated cytotoxic T cell expansion (Giovazzino et al. 2019). A possible explanation for the reduction in Tregs could be linked to the downregulation of CXCL12 in stromal cells, and more explicitly in MSC as shown collectively in imaging, cytokine and scRNA seq analysis (Figure 12, Figure 31, Figure 36). Tregs are recruited to the bone marrow via binding of secreted CXCL12 to the CXCR4 receptor, which is expressed on their cell surface (Zou et al. 2004). CXCR4 expression has been shown to be regulated by secreted IL-1β, TGF-β and TNF-α (Gupta et al. 1998; Feil and Augustin 1998; Buckley et al. 2000), linking prolonged exposure to inflammatory signaling to a downregulation of Tregs. TNF-α was also found to be secreted from MDS-L blasts in culture (Figure 58, annex), while the upregulation of IL-1R on stromal cells in MDS in scRNA seq analysis (Figure 35) suggests this pathway to be dysregulated as well. In addition, IL-1 signaling was transcriptionally upregulated in Tcm helper cells, as seen in (Figure 42). Interestingly, Tregs are significantly upregulated in HR-MDS in comparison

to LR-MDS (Kordasti et al. 2007; Moon et al. 2011). These seemingly contradictory outcomes for MDS are explained by different immunophenotypes in the BM, as reviewed by Peng and colleagues: the LR-MDS bone marrow immune cell compartment is populated mostly by proinflammatory cells, which secrete cytokines that promote HSC apoptosis and result in immune activation, while HR-MDS bone marrow is populated by immunosuppressive cells that lead to tumor escape of malignant cells (Peng et al. 2022).

5.11 SF3B1-mutated MDS samples might show distinct niche alterations

Looking at subtype-specific stromal alterations, only SF3B1 was sufficiently represented in the BoHemE cohort to warrant further analysis. Given the impact the mutation has on conferring overall survival benefits in comparison to other mutations (as described in 1.2), it was hypothesized that this mutation leads to distinct alterations in the bone marrow that mitigate disease progression. Analysis of spatial imaging data suggested that the mutation does seem to have distinct effects on niche remodeling. SF3B1-mutated samples showed a trend towards higher MSC, Treg and CXCL12 content and higher cellularity (Figure 16). Since this analysis was retrospectively done, the sample cohort was too small to obtain statistically significant results; nevertheless, a trend towards an increase of the described populations was observed. In addition, a direct correlation between SF3B1 mutation VAF and an increase in MSC and Treg content was also found. This leads to the question of whether there are mutation-specific cellular processes that lead to differential alterations of the BM niche. Mutations in SF3B1 lead to aberrant RNA splicing, directly and indirectly resulting in altered gene expression and alternative splicing of hundreds of genes, which can lead to clonal expansion (Kesarwani et al. 2017). One effect of this is the hyperactivation of NF-κB pathways by downregulation of MAK3K7, resulting in increased inflammatory cytokines in patients (Lee et al. 2018; Smith et al. 2019), On the other hand, this mutation is often associated with low blast burden in the bone marrow (Huber et al. 2023) which could dampen the stronger inflammatory effect LR-MDS with higher blast percentages usually display and explain the maintained levels of Tregs. This would however, depending on the signaling axis that is involved, also decrease the vascular remodeling, which was not observed in this study. So far, no reports have been made on LR-MDS subtype-specific proinflammatory cytokine levels in the bone marrow, therefore this remains an open question.

5.12 High-VAF DNMT3A mutation leads to distinct niche changes in mice

In human imaging studies, no discernible niche remodeling effect was found for low-VAF CHIP besides a slight increase in CXCL12 distance towards vessels and MSC, a trend towards higher sinusoidal fraction and a slight trend towards higher Treg fractions in comparison to controls. Due to confounding variables like comorbidities, lifestyle and normal biological and patient inter-heterogeneity and taken together with the low VAF the donors displayed (Table 12), these effects remain inconclusive. For a better isolation of mutation-dependent effects, the high-VAF DNMT3A^{R878H} mouse model was used. Induction of the Cre-lox system with poly(I:C) at a young age leads to heterozygous expression of the mutant DNMT3A^{R878H} allele in HSC and is carried over to the progeny, leading to a VAF of around 50% (Loberg et al. 2019). While most CHIP carriers display low VAFs of below 10%, the mutated clone can expand further and VAFs of 10–20% are frequently seen with increased age (Midic et al. 2020). This model thus recapitulates isolated effects of the DNMT3A mutation in the bone marrow.

The DNMT3A^{R878H} mice displayed a decreased BMC, increased sinusoidal content and blood vessel size, along with a sharp accumulation of LEPR+ adipo-MSC and higher CXCL12 content that is found mostly located in the femoral head near BMAT. This was accompanied by a trend toward a larger Treg fraction. The latter observation was not statistically significant and shows the necessity of more biological replicates to confirm the findings.

The abnormal sinusoidal vasculature found in this study (Figure 19) can also be seen in proinflammatory milieux, where the vasculature reacts to the stimulus by proliferation of endothelial cells, forming new vessels or expanding already existing ones. This phenomenon might be due to an increase in emergency hematopoiesis, which leads to fast expansion of sinusoids as trafficking sites for activated HSPC (Vandoorne et al. 2018). It is also in line with the findings that arterioles were not observed to be altered, since they are not strongly involved in the mobilization of HSPC into the blood stream (Itkin et al. 2022). Interestingly, the sinusoids were expanded into the endosteal regions of the bone as well as the femoral head (Figure 23) and qualitatively, endosteal-lining MKs were less frequent in old and DNMT3A^{R878H} mice. This implies a shift towards less endosteal niches and more vascular niches, consequently leading to increased hematopoiesis and fewer quiescent LT-HSC. The question of altered MK localization should be studied more extensively, with the use of recently identified MK-subset specific markers like ARNTL,

MYLK4 and LSP1 that discriminate MK subsets associated with platelet production, HSC maintenance in the endosteal niche and immune regulation, respectively (Sun et al. 2021). In line with vasculature changes in inflammation, the expanded LEPR$^+$ Sca1$^+$ MSC subset that was found to be strongly expanded in DNMT3A^{R878H} mice (Figure 20) was reported to be induced by inflammation, injury or irradiation (Mitchell et al. 2023; Asada et al. 2017). These MSC have a higher clonogenic potential and adipocytic bias (Mo et al. 2021), which, taken together with the close proximity they display to BMAT, exemplifies their potential to give rise to adipocytes. Additionally, in response to irradiation, LEPR$^+$ MSC proliferate rapidly up to four weeks after original insult, after which the proliferation rate returns to pre-irradiation levels (Zhou et al. 2014). As described in chapter 1.3.4, LEPR$^+$ adipoprogenitors support hematopoiesis, while adipocytes favor HSC quiescence. One possible mechanism that explains the morphological changes in the BM of DNMT3A^{R878H} mice could be CHIP-induced acute inflammation, leading to an expansion of LEPR$^+$ Sca1$^+$ MSC, which promote and sustain emergency hematopoiesis, while this subset of MSC differentiates to mature adipocytes in chronic inflammation to maintain LT-HSC quiescence. This hypothesis could be tested by using *ex vivo* expansion of Sca1$^+$ MSC and subsequent adipogenic differentiation and subsequently assess their effect on HSC proliferation and CFU potential. Given the fact that Sca1 does not have a human ortholog, validation of this MSC subset in human scRNA seq data remains challenging.

The increase in Tregs in aged mice, and to a lesser extent in DNMT3A^{R878H} (Figure 21), differs from the slight downregulation of Tregs in human MDS samples. Despite that niche changes in both species are in line with inflammatory processes, it is unclear why Treg abundance behaves so differently. The role of Tregs is suppressing CD4 and CD8 T cell activation in the bone marrow, providing immune privilege to the niche (Fischer et al. 2019). Besides this canonical function, BM Tregs confer a direct HSC-supportive function, as described in chapter 1.3.6. However, the main signaling axis of CXCL12-CXCR4 that leads to trafficking of Tregs to the BM, is disrupted in MDS (for instance by downregulation of CXCL12, as discussed above), while CXCL12 content is elevated in DNMT3A^{R878H} mice (Figure 20) through the upregulation of insult-responsive LEPR$^+$ MSC. The main difference between the stromal response in CHIP and MDS could thus be the impact of mutant clones on MSC, which is supported by the changes seen in MDS-MSC in comparison to CHIP-MSC (chapter 5.2). The importance of the CXCL12-CXCR4 signaling axis should be tested more extensively, for instance by Crispr/Cas9 genetic deletion of

CXCL12 in MSC and assessing their impact on Treg homing to the bone marrow. On the other hand, the direct effect of Tregs on inflammation and HSC maintenance needs to be elucidated further to understand the effects of altered Treg ratios on bone marrow function. Using a mouse model in which the transcription factor that is necessary for Treg development (FoxP3) is deleted, would allow to characterize the effect of Tregs on the BM niche architecture and HSC differentiation biases (Chen et al. 2005).

Keeping in mind the regulative function of adrenergic innervation on MSC as described in chapter 1.3.8, qualitative staining of neurons wrapped around arteries were performed, which revealed no apparent differences between young, old, and young DNMT3A^{R878H} mice. A previous study by Maryanovich and colleagues reported a decrease in sympathetic innervation upon aging, marked by reduced expression of synaptophysin around arteries (Maryanovich et al. 2018). The approach of this study was to use z-stack projections of multiple ROI images from three biological replicates of old and young mice. This methodology could be biased by selection of ROI images and additionally by the amount of long, innervated arteries the samples display in that specific tissue slide. In the herein presented imaging experiments on murine femurs (Figure 22), artery distribution was very different in the biological and even technical replicates, depending on position in the femur. Mostly main arteries were innervated, which led to big deviations in frequency that rendered quantification of positive signal area inconclusive. This could be improved upon by switching to 3D light-sheet microscopy of cleared femurs, where the entire innervation of the femur is taken into account instead of one thin slide. Doing so might highlight possible denervation of the BM with aging, which could further skew MSC function.

Inflammation as a result of DNMT3A mutation has been shown in both mouse and human settings, as described in chapter 1.1.3. The exact source of increased cytokine levels are most likely myeloid lineage cells expanded as a result of the DNMT3A mutation, which favors myelopoiesis over lymphopoiesis (Loberg et al. 2019). Revealing the exact inflammatory mechanisms and the cellular sources at play for a possible therapeutic intervention could pave the way to alleviate age-related and, moreover, CHIP-related remodeling of the BM niche and possibly prevent age-related cytopenias and MDS emergence.

6 Conclusion

The global findings presented in this thesis demonstrated that the BM microenvironment in CHIP shows signs of additional chronic inflammation in addition to typical age-related inflammaging signs, thereby impacting stromal populations that regulate HSC activity. Within the BM, MSC develop an additional adipogenic bias, resulting in reduced cellularity, while sinusoids expand and disturb the more quiescent, endosteal niche. In terms of immune repertoire, Treg expand and accumulate in the endosteal niche to dampen these perturbations and maintain HSC quiescence. Strikingly, these effects are dependent on the VAF clone size.

The same changes are also apparent but exacerbated in MDS conditions, with drastic effects on the cellular morphology of sinusoids and MSC. Inflammatory and angiogenic signatures of niche cells, for instance IL-1, IFN and VEGF signaling pathways, accompanied by increased senescence in the bone marrow, result in transcription and differentiation changes in MSC and a depletion of immune regulatory T cells. As a result, the HSC-support capacity of MSC is dysregulated, transforming the BM niche into a dysfunctional state.

Along these findings, the connecting link, morphological and transcriptional changes of the BM niche in response to chronic inflammation, could be leveraged to intervene and prevent the emergence of MDS in CHIP carriers.

7 Outlook

This study shed light into stromal dysregulations in the context of clonal hematopoiesis and myelodysplasia. Some bottlenecks of the herein described methods were sample quality and availability, as well as the low VAF of CHIP donors. In order to gain more insight into stromal alterations in MDS, sort-seq on $CD271^{+}$ MSC will be employed to get comparable and enriched MSC proportion. This might pave the way to identify critical niche alterations in CHIP that could predict emergence of MDS and give a chance for clinical intervention, for instance by targeting dysregulated pathways in at-risk CHIP carriers.

The effect of dysregulated inflammatory signaling on stromal cells is evident in the changes that are found in imaging studies in MDS and high-VAF CHIP models. Human CHIP samples displayed a very low VAF, resulting in no observable changes. In order to confirm the findings from the $DNMT3A^{R878H}$ mouse model, high-VAF CHIP samples from human donors should be used for future studies, focusing on the recurrent $DNMT3A^{R882H}$ mutation. VAFs of over 10–15% should be included, and morphological niche changes as well as a wide panel of inflammation-related pathways should be characterized in comparison to age-matched controls.

In order to identify MDS-subtype specific stromal alterations, our group is working on a study on SF3B1-mutant LR-MDS, with the idea in mind to identify possible alterations in inflammatory signaling that could explain the trends found in imaging analysis, especially regarding Treg content. Additionally, the elusive nature of Tregs in the context of HSC and MSC regulation should be assessed, for instance by using knockout-mice that lack the Treg transcription factor FoxP3. This will allow to answer the question if these cells are mainly immune-suppressive, or if they also confer effects on HSC differentiation and MSC upkeep, and if depletion in LR-MDS exacerbates the dysregulation of the HSC niche.

The drawback of studies in knockout organisms is the transferability of results to human settings, but also the ethical issues that come with animal models, especially with high severity mouse CHIP/MDS models with chronic inflammation. One alternative of this could be developing the co-culture system of niche and MDS cells that was used for this thesis, as it displays some of the *in vivo* changes that are also found in primary cells from MDS donors. This has the additional benefit of integrating the complexity of variables like age, sex, genetic mutations, VAF and possible stroma mutations on niche interplay.

Finally, the sorted and sequenced HSPC from control, CHIP and MDS donors will be analyzed to get a full picture of possible dysregulations that are found in the HSC niche. CHIP mutation influence on differentiation capacities could be explored by identifying trajectories from CHIP mutant cells versus wild-type cells. In addition, HSPC subtype-specific markers will be isolated, verified and tested for imaging applications to close the gap between novel high resolution sequencing techniques and established cell surface markers that lack specificity, leading to more robust canonical markers and lineage-specific transcription factors.

8 Acknowledgement

During the four years I spent learning new techniques, planning and performing experiments, reading and discussing literature and writing this thesis, I was always surrounded by helpful, kind and supportive people that I would like to thank explicitly.

First, my gratitude goes out to Dr. Borhane Guezguez, who was willing to take on a student without strong background in any related field and, through his patience, kindness and support, imparted some of his knowledge on me and helped me develop the tools that I needed to quench my scientific curiosity. You always gave me the opportunity to go in a new direction, get additional training, meet new people that might help with a current problem. Thank you for that.

All members of the Guezguez group shaped a warm working environment that allowed me to be happy to go to work almost every day, and if some cold and rainy patches occurred, you were there with a cup of coffee to listen to my complaints. Angelique, you always presented a new and different perspective, often helping me see things in a new light. Eric, working with you instilled me (hopefully!) with some of your critical takes on research, but also with your desire to make science better and never settle with the most comfortable solution. Costy, your energy and passion for science was inspiring and motivated me immensely.

I also want to thank Professor Theobald and Professor Schneider as my supervisors for their support, comments, supervision and time they spent to get this project on the right track. On a similar note, our scientific collaborators Karin, Max and Judith from Heidelberg were always compassionate and shared their wealth of knowledge with us, immensely helping with the sequencing experiments.

This would not have been possible without the benevolence of all people that were part of the BoHemE study in Dresden and Leipzig: the clinicians and technicians that collected the biosamples, but most of all the people that freely gave parts of their body to help us, and to ultimately help others by gaining just a little more insight into clonal hematopoiesis and myelodysplasia. Also, a big thank you to all members of the biobank of the UMC Mainz whose expertise in tissue preparation and cutting of tissue slides helped me to always have another slide to stain. Similarly, the imaging core facility and especially Sandra, always happy to help with questions about imaging and image analysis, have my gratitude.

Acknowledgement

To my family and friends, who were often there for support, understanding and kind words, that kept me going: thank you. You anchored me whenever I needed it, and provided mental support or helpful distraction, whatever was more necessary. And to my siblings, for their physical and mental support during gym sessions. As Socrates so eloquently put it: “No pain, no gain”, and both pain and gain were had in the last few years.

Also again thank you to Borhane, Eric, Costy, and Kim for proofreading this thesis and providing me with new ideas and paths to follow, and frankly, more work. It is appreciated!

Last but most importantly, to my (soon-to-be) wife Melanie. You were always there for me and shared excitement, curiosity, frustration, and anger. I am always grateful for the constant love and understanding you show. Thank you.

9 Annex

9.1 Complementary material for the introduction

9.1.1 WHO classification of MDS (2016 and 2022)

Table 15: Overview over MDS subtypes according to 2016 WHO classification (Khoury et al. 2022; Zhang et al. 2022b; Ming Hong and Guangsheng He 2017).

MDS subtype	Dysplastic lineages	Cytopenias	Ring sideroblasts in erythroid elements of BM	Blasts	Cytogenetics
MDS-5q	1 –3	1–2	None or any	<1% in PB, <5% in BM, no Auer rods	Del(5q) alone or with 1 additional abnormality except -7 or del(7q)
MDS-SLD	1	1–2	<15% or <5% with SF3B1^{mut}	<1% in PB, <5% in BM, no Auer rods	Any, unless 5q-criteria are met
MDS-MLD	2–3	1–3	<15% or <5% with SF3B1^{mut}	<1% in PB, <5% in BM, no Auer rods	Any, unless 5q-criteria are met
MDS-RS-SLD	1	1–2	RS >15% or >5% with SF3B1^{mut}	<1% in PB, <5% in BM, no Auer rods	Any, unless 5q-criteria are met
MDS-RS-MLD	2–3	1–3	RS >15% or >5% with SF3B1^{mut}	<1% in PB, <5% in BM, no Auer rods	Any, unless 5q-criteria are met
MDS-EB1	0–3	1–3	None or any	2 – 4% in PB or 5 – 9% in BM, no Auer rods	Any
MDS-EB2	0–3	1–3	None or any	5 - 19% in PB or 10 – 19% in BM or Auer rods	Any
MDS-U with 1% blasts	1–3	1–3	None or any	1% in PB, <5% in BM, no Auer rods	Any
MDS-U with SLD and pancytopenia	1	3	None or any	<1% in PB, <5% in BM, no Auer rods	Any
MDS-U based on defining cytogenetic abnormality	0	1–3	<15%	<1% in PB, <5% in BM, no Auer rods	MDS-defining abnormality
Refractory cytopenia of childhood	1–3	1–3	None	<2% in PB, <5% in BM	Any

Table 16: 2022 WHO classification of MDS by percentage of blasts, cytogenetics, and mutations (Khoury et al. 2022).

MDS subtype	Blasts	Cytogenetics	Mutations
MDS-5q	<5% BM and <2% PB	5q deletion alone, or with 1 other abnormality other than monosomy 7 or 7q deletion	
MDS-SF3B1	<5% BM and <2% PB	Absence of 5q deletion, monosomy 7, or complex karyotype	SF3B1
MDS-biTP53	<20% BM and PB	Usually complex	Two or more TP53 mutations, or one mutation with evidence of TP53 copy number loss or copy neutral loss of heterozygosity
MDS-LB (low blast)	<5% BM and <2% PB		
MDS-h (hypoblastic)	<5% BM and <2% PB		
MDS-IB1 (increased blast)	5–9% BM or 2–4% PB		
MDS-IB2	10–19% BM or 5–19% BM PB or Auer rods		
MDS-f (with fibrosis)	5–19% BM, 2–19% PB		

9.1.2 IPSS-R criteria

The IPSS-R prognostic scoring system is a point-based system that evaluates cytogenetic, morphologic, and clinical parameters to stratify and predict the development of a MDS disorder. The following criteria are scored:

1. Percentage of blast cells in bone marrow
    a. Less than 5 = 0 points
    b. 5–10 = 0.5 points
    c. 11–20 = 1.5 points
    d. 20–30 = 2 points
2. Cytogenetics (chromosome changes)
    a. None, del(5q), del(20q) = 0 points
    b. Other abnormalities = 0.5 points
    c. Three or more abnormalities, abnormal chromosome 7 = 1 point
3. Number of cytopenias (anemia, neutropenia, or thrombocytopenia)
    a. 0 or 1 = 0 points
    b. 2 or 3 = 0.5 points

The risk groups are based on the total risk score:

1. 0 points = low
2. 0.5–1 point = Intermediate-1
3. 1.5–2 points = Intermediate-2
4. >2.5 = High

9.2 Complementary material for material and methods

9.2.1 Quenching of autofluorescence in human bone marrow samples

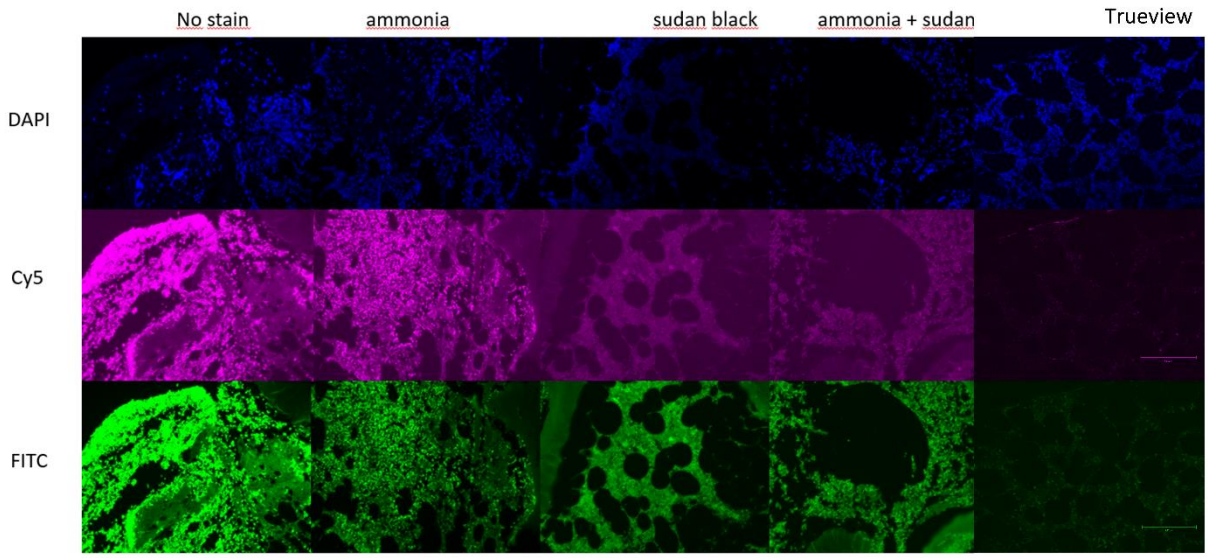

Figure 46: Quenching of autofluorescence in human FFPE bone marrow samples.

Bone marrow displays high Autofluorescence (AF), coming mainly from lipofuscin and erythrocytes, but also collagen and elastin as well as formalin fixation (Davis et al. 2014). There have been several different methods applied to reduce AF, including diazo dyes (Sudan black, Eriochrome T) and other chemical reagents (sodium borohydride, ammonia). In addition, commercial suppliers designed products that have been reported to work. We compared different quenching methods and found that Trueview (Vector Laboratories) and Trueblack (Hölzel Biotech, not shown) lead to a marked reduction of AF in all channels, especially in the GFP channel. Sudan black reduced AF in the Cy5 channel, but introduced AF in the far-red (Cy7, not shown). Sodium borohydride (not shown) and ammonia did not have any effect on tissue AF. For the scope of this thesis, Trueview was used for IF on FFPE tissue.

9.2.2 Quantification of HSPC in the bone marrow

Manual analysis was done to identify single HSPC and all total cells due to the unspecific staining of CD34 in the bone marrow. Besides HSPC, blood vessels are also positive for this marker, so cells adjacent to vasculature would be counted false-positive as HSPC.

For each sample, 10 ROI images were analyzed. Total cells and $CD34^+$ cells were counted as well as the distance between HSPC and the closest $CD271^+$ MSC using FIJI software.

9.2.3 Vasculature content analysis for human and murine samples

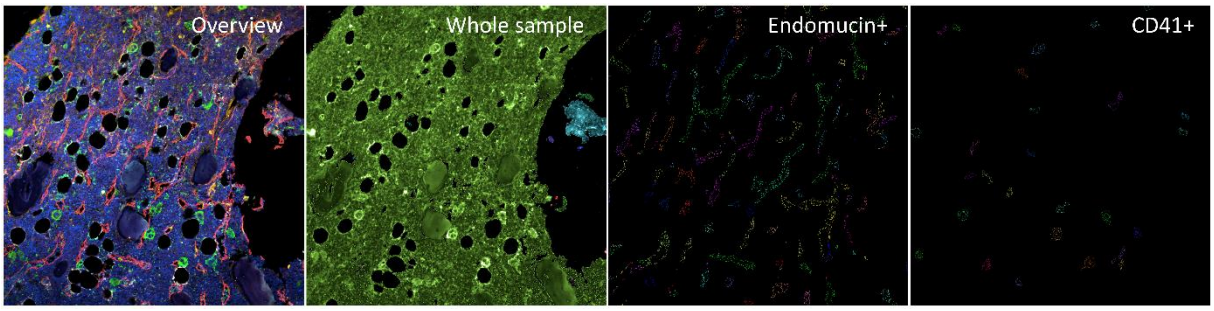

Figure 47: Analysis pipeline for vasculature quantification in human and murine BM samples.

Whole sample area was detected for normalization (absolute threshold on GFP-AF). $CD105^+$-area and $UEA1^+$-area were detected by common threshold (depending on background intensity, sample dependent) and measured. In addition, the distance between UEA1- and CD105-surfaces as well as overlap was measured. The same analysis was used for assessment of vasculature content in murine femurs, using endomucin as a marker for sinusoidal and BCAM for arteriolar vasculature.

9.2.4 SPARC signal co-stain with MSC and EC

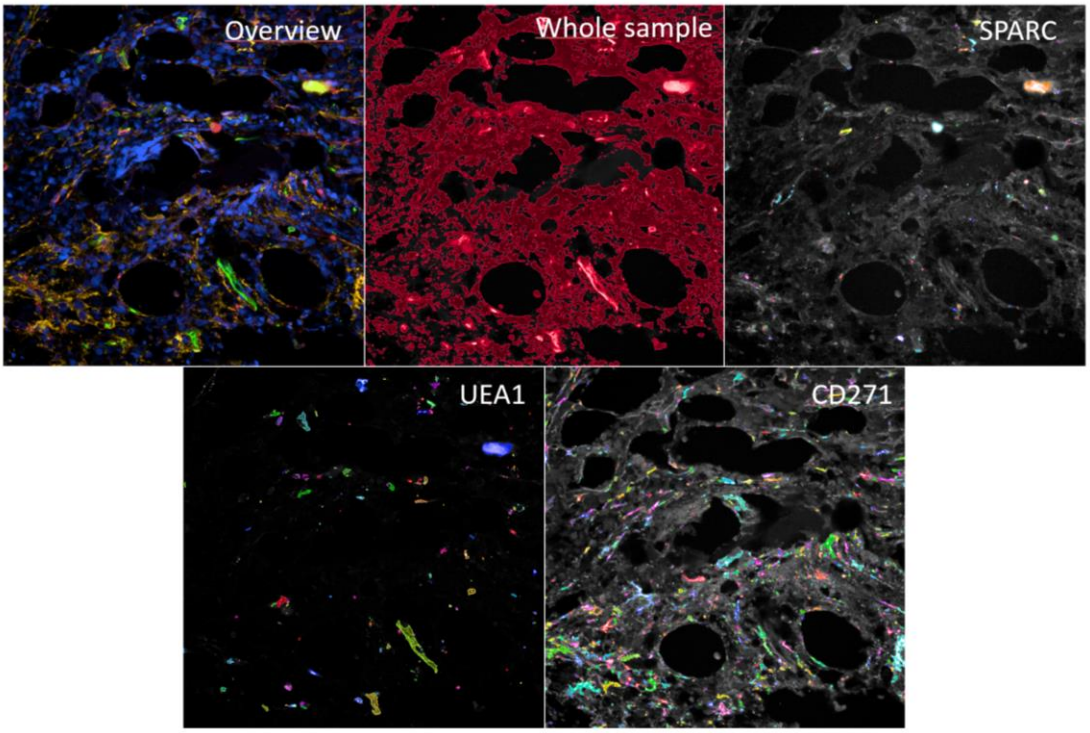

Figure 48: SPARC co-stain analysis in human BM samples.

Whole sample area was measured for normalization (absolute threshold on GFP-autofluorescence). $SPARC^+$-, $UEA1^+$- and $CD271^+$-area was detected by common threshold (depending on background intensity, sample dependent). Overlap and distance of $SPARC^+$ objects to $CD271^+$/$UEA1^+$-regions were measured.

9.2.5 T cell content in the bone marrow

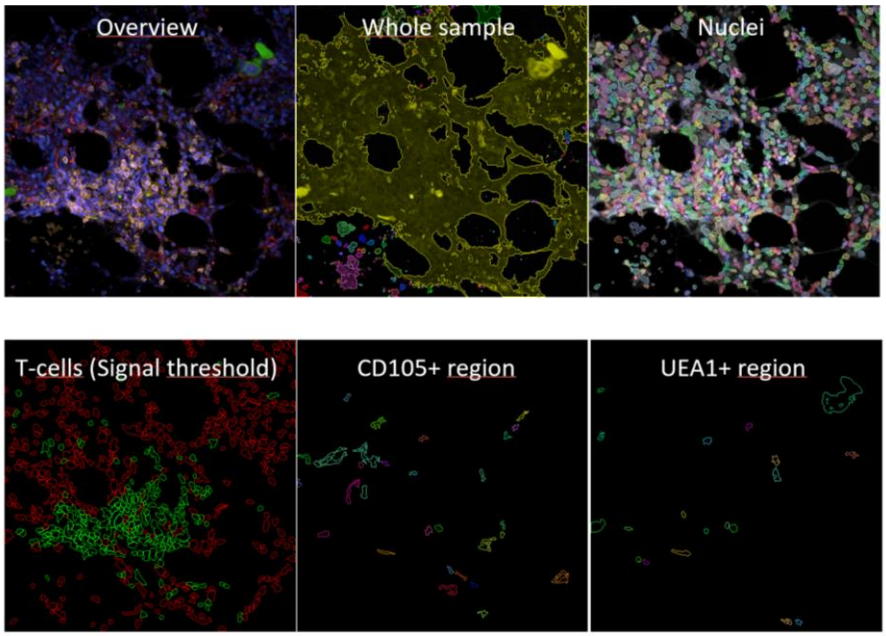

Figure 49: T cell analysis in human and murine BM samples.

Whole sample area was measured for normalization (absolute threshold on GFP-AF). Nuclei were detected using "Find nuclei" (method M). For erythrocyte-rich samples, an additional filter step was employed to prevent false-positives. CD3-signal was used to threshold for positive cells. The coordinates of all cells and the detected T-cells were calculated. The threshold was adjusted for each sample, since the signal intensities vary between samples. $CD105^{+}$ and $UEA1^{+}$ regions were detected using a common threshold and the distance to the T-cells were calculated.

9.2.6 Bone marrow cellularity from Giemsa images

For human samples, the FIJI software plugin Weka Segmentation was used to train a classifier which detects bone, marrow and adipocytes. For mouse femurs, Qupath software with the Marrowquant plugin was used. Bone surface is detected in green, marrow in blue, adipocytes in yellow and interstitial space in red (not used for analysis). Areas for each class were measured.

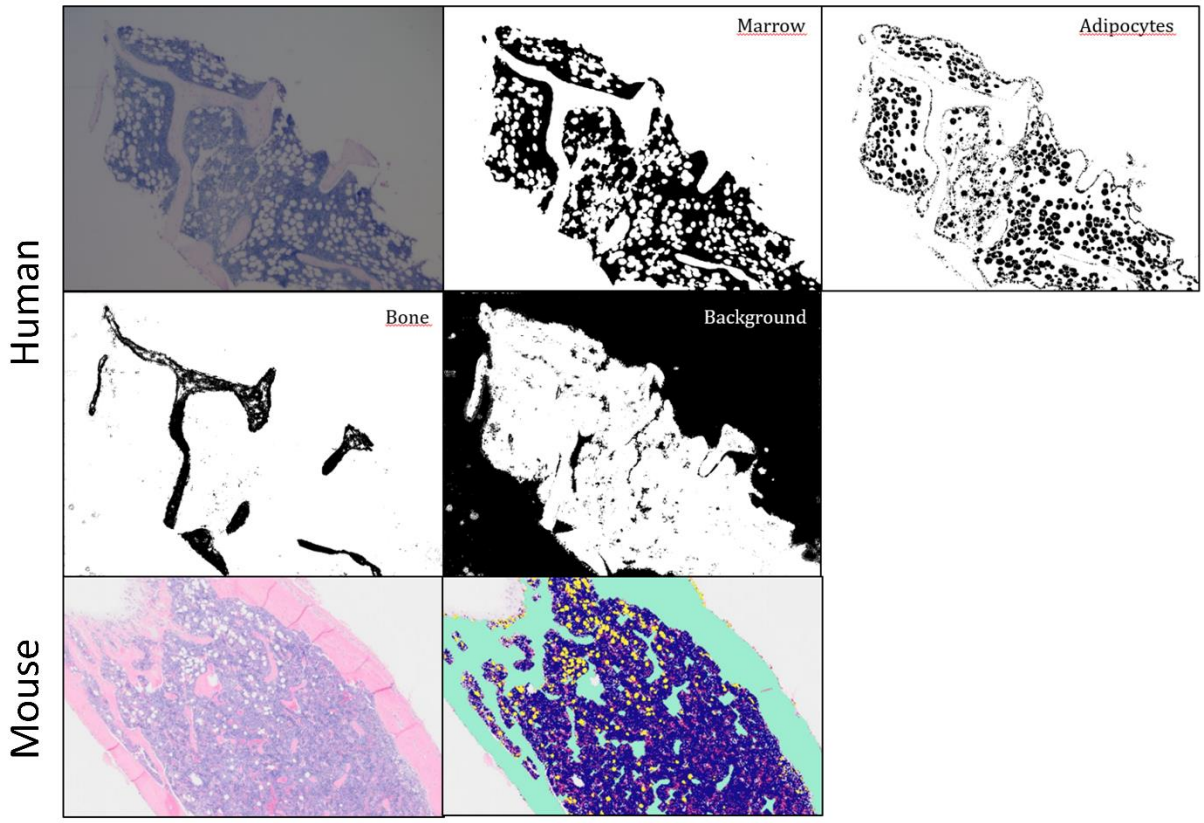

Figure 50: Analysis of Giemsa-stained BM slides for BMC using Weka segmentation (top) and Qupath Marrowquant (bottom).

9.2.7 CXCL12 signal in the bone marrow, co-stained with MSC and ECs

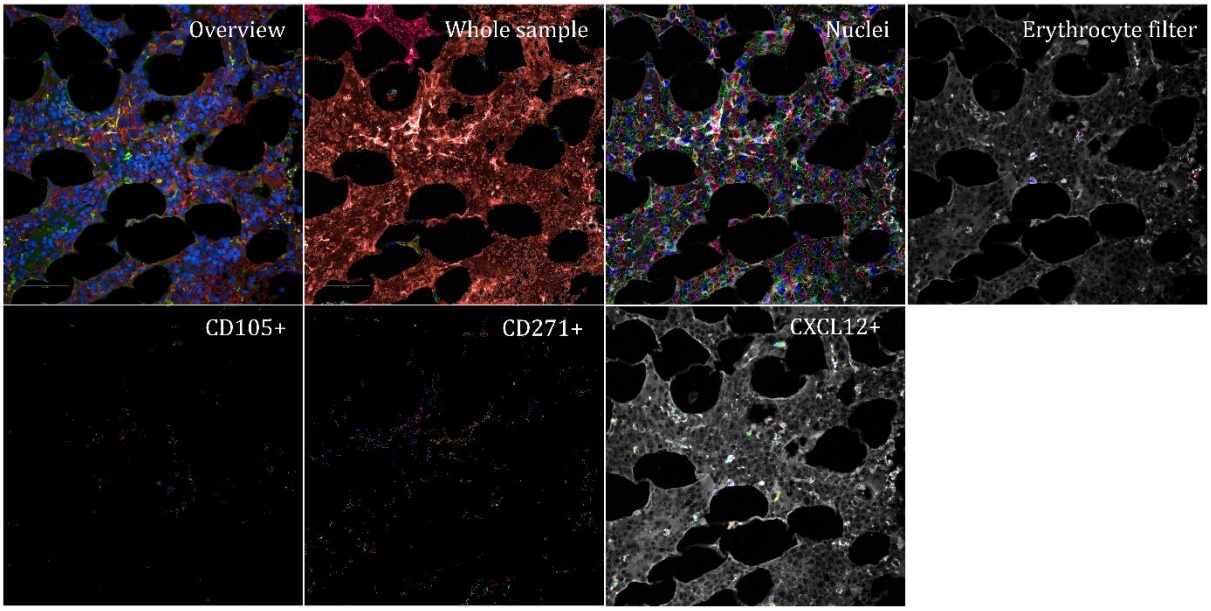

Figure 51: CXCL12 co-staining in the human BM.

For detection of CXCL12 production in sinusoidal vessels and MSC, the whole sample was detected using GFP AF. Nuclei were detected by "method M" for segmentation, erythrocytes were filtered out via high AF in the GFP channel. Thresholding in the TxRed, Cy5, and GFP channel yielded sinusoids, MSC, and CXCL12 populations, respectively. Overlap with erythrocytes was filtered out for all populations and distance and overlap of both cell populations with CXCL12 was measured.

9.2.8 Megakaryocyte analysis in murine bone

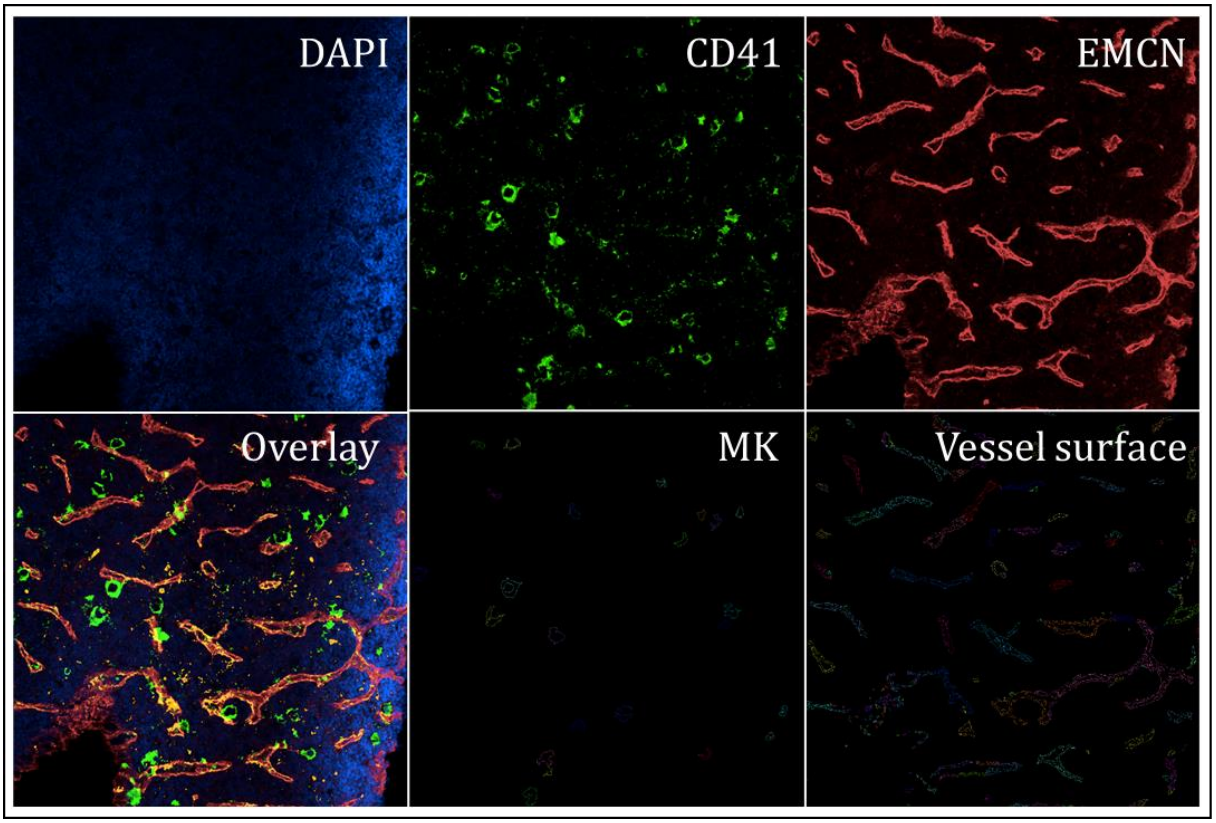

Figure 52: Megakaryocyte analysis in murine BM.

Whole samples surface was detected using GFP autofluorescence. Thresholding on the Cy5 and GFP channel yielded the vessels (endomucin$^+$) and CD41$^+$ surface, respectively. Filtering for size and roundness allowed identification of megakaryocytes in the CD41$^+$ population. A nuclei segmentation approach was not useful in this case, due to the size and multinuclearity of megakaryocytes.

9.2.9 Treg analysis in human and murine bone

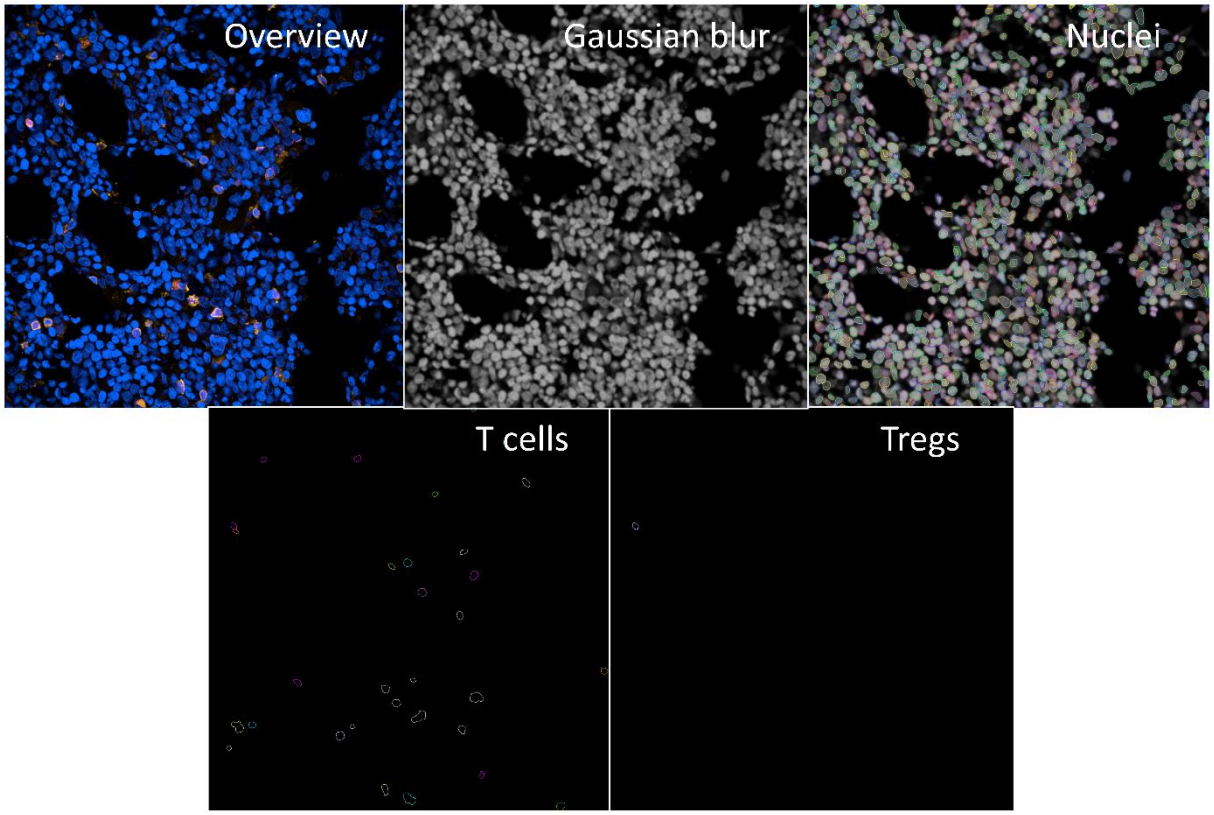

Figure 53: Treg analysis in human and murine BM.

Nuclei segmentation was done by applying a gaussian blur filter. This allowed detection of unevenly stained nuclei, which are often found in densely packed tissue like murine bone marrow. Nuclei segmentation (method M) was applied. Intensity of CD3 (TxRed) was used to identify T cells. Within the T cell population, nuclear FoxP3 intensity (Cy5 channel) was used to identify Treg cells. Thresholds were adjusted for each sample individually and uneven staining intensities across the samples were considered. Fields with artifacts and high background were excluded from the analysis.

9.2.10 MSC, CXCL12, Sca1 analysis in mouse femurs

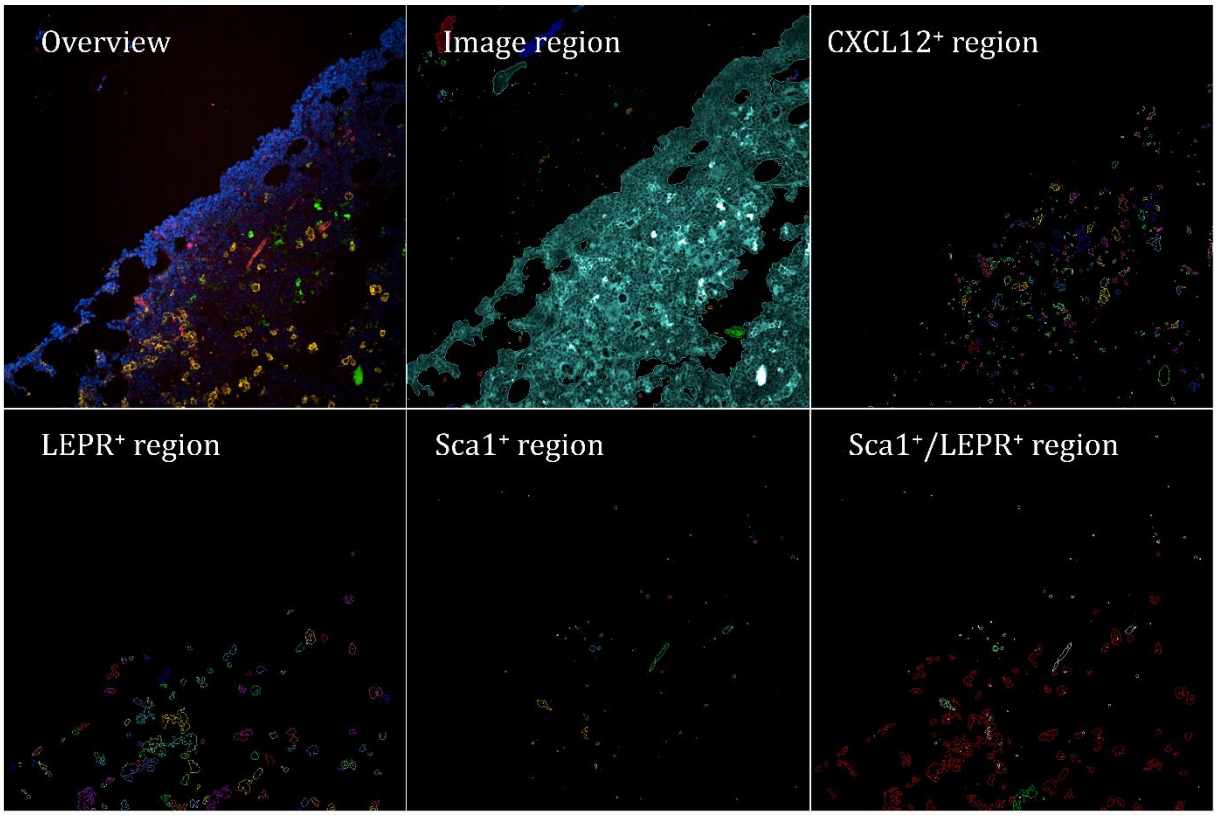

Figure 54: CXCL12 and MSC co-stain in murine BM.

Thresholding on GFP signal with a low threshold gave the image region. Subsequent thresholding on CXCL12, LEPR and Sca1 signal gave the respective positive regions. Overlapping Sca1 and LEPR surfaces were selected as double positive regions.

9.3 Complementary material for results

9.3.1 UEA-1 is a superior vessel marker to CD34 and CD31

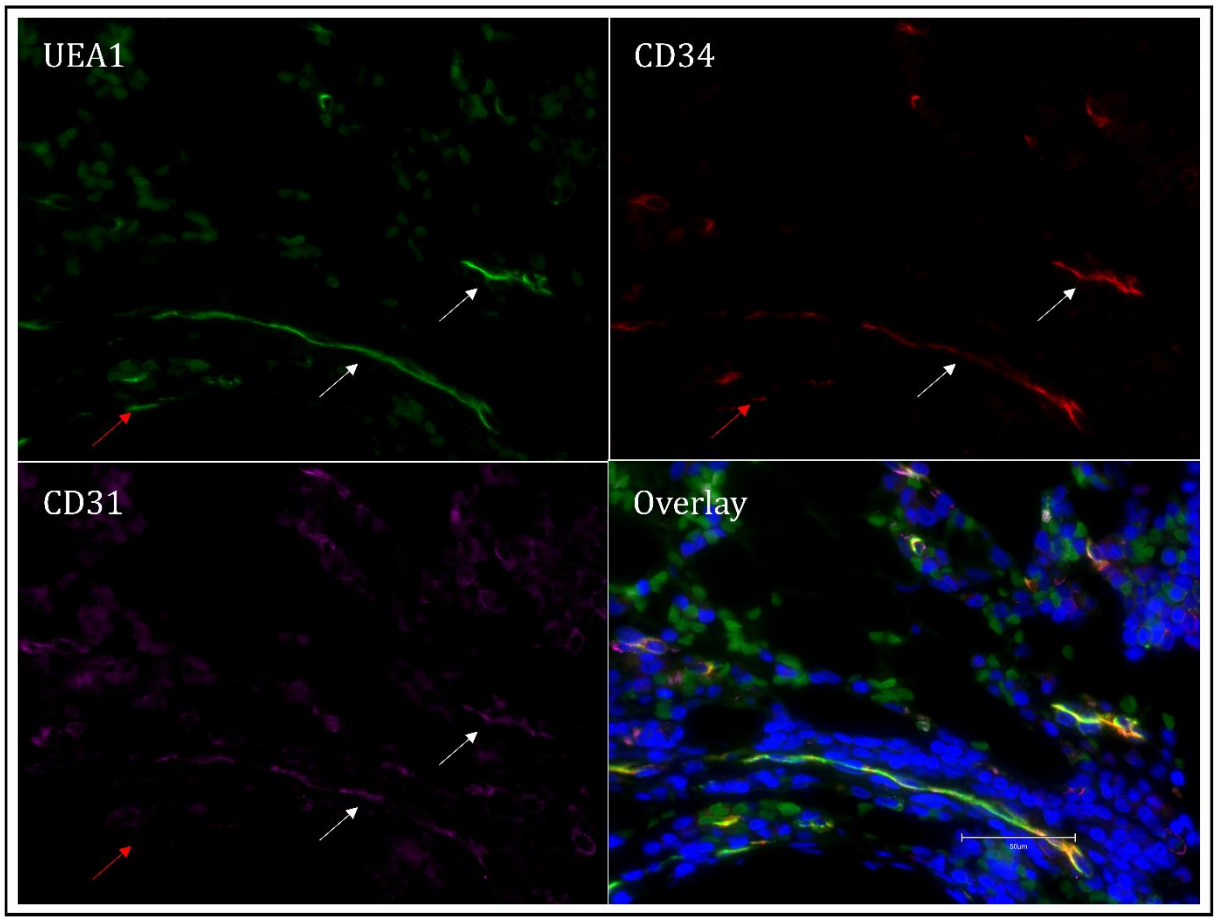

Figure 55: UEA-1 is a more reliable vessel marker in human BM. Brightness and contrast were enhanced to allow better visibility.

Co-staining of UEA-1, CD34 and CD31 in the bone marrow revealed mostly overlapping stainings, but UEA-1 staining identified whole vessels and was positive on all vessel populations (white arrows), while CD31 and CD34 were not always expressed by vasculature (indicated by red arrows).

9.3.2 Tregs are in close contact with CD271+ CXCL12-producing cells

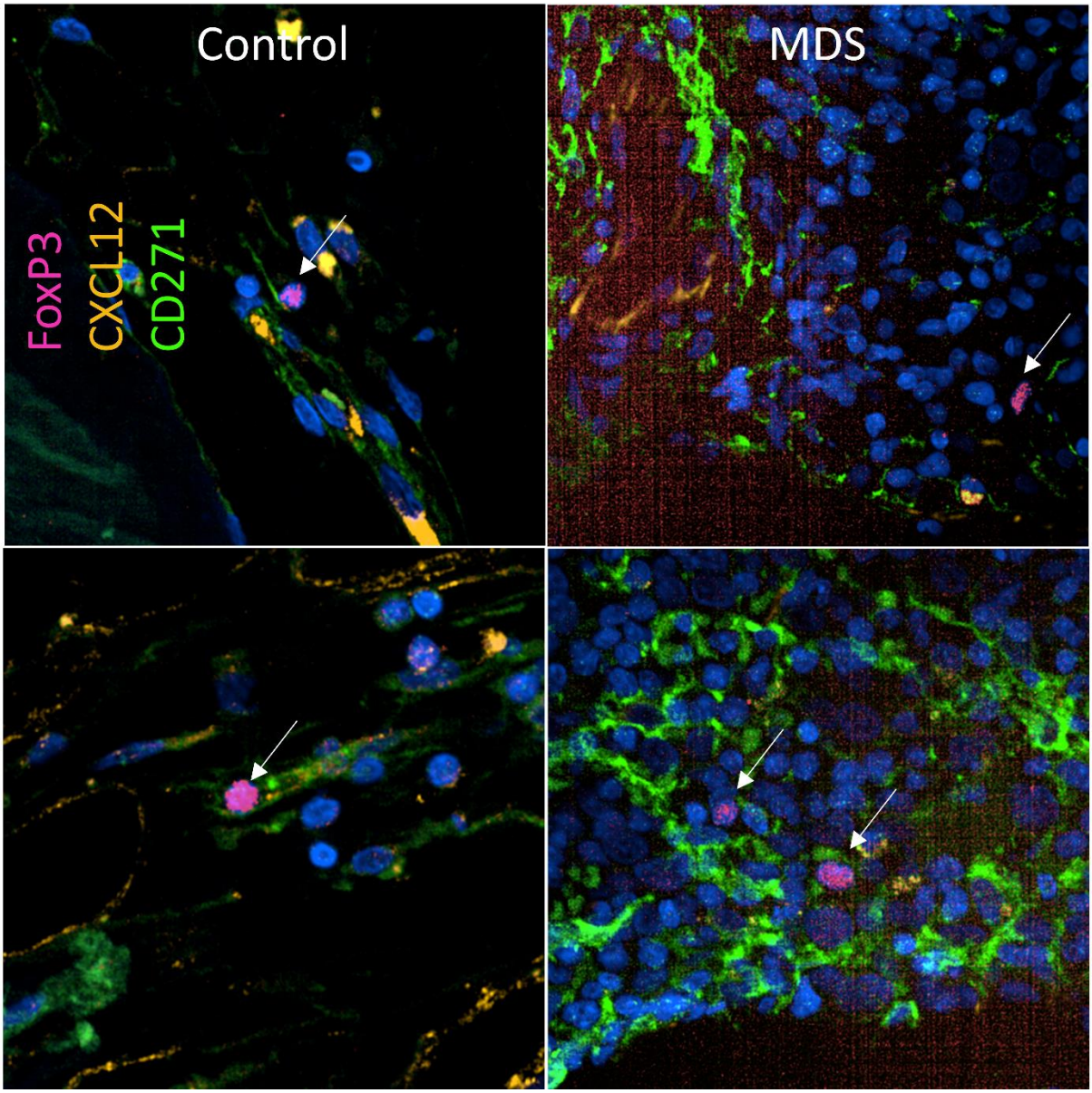

Figure 56: Staining in human bone marrow for Tregs (FoxP3), CXCL12 and MSC (CD271). Tregs are located in close contact with CXCL12-expressing MSC in control tissue, but further away in MDS, where MSC don't produce high levels of CXCL12. Brightness and contrast were enhanced to allow better visibility.

In control and CHIP tissue, Tregs were located close to MSC, which expressed CXCL12 (Figure 56, left). In the few Tregs that were detected in MDS (right), these cells were either not close to MSC or MSC were not expressing CXCL12 as highly as in control cells.

9.3.3 Senescence in human bone marrow MDS samples

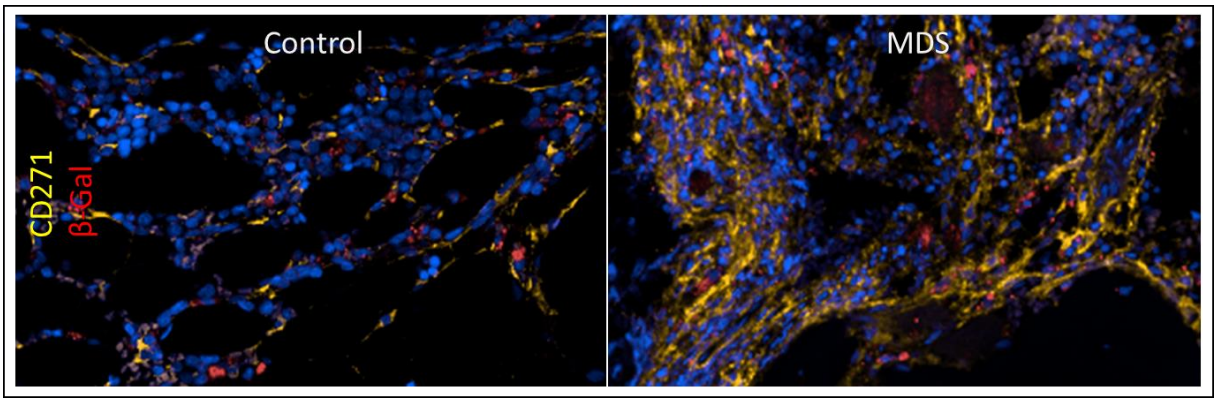

Figure 57: β-Galactosidase staining of human BM samples, co-stained with CD271 as a MSC marker. Brightness and contrast were enhanced to allow better visibility.

Human MDS bone marrow samples showed more β-Gal⁺ staining in MDS slides, as displayed in the example image above. There is also more overlap between CD271 and β-Gal in MDS, indicating senescent MSC in MDS.

9.3.4 Cytokine concentrations from Luminex assay

The absolute concentrations of cytokines in hTERT-MSC/MDS-L co-culture supernatant, determined by Luminex assay, are depicted below. Cytokines are divided by source of cytokines.

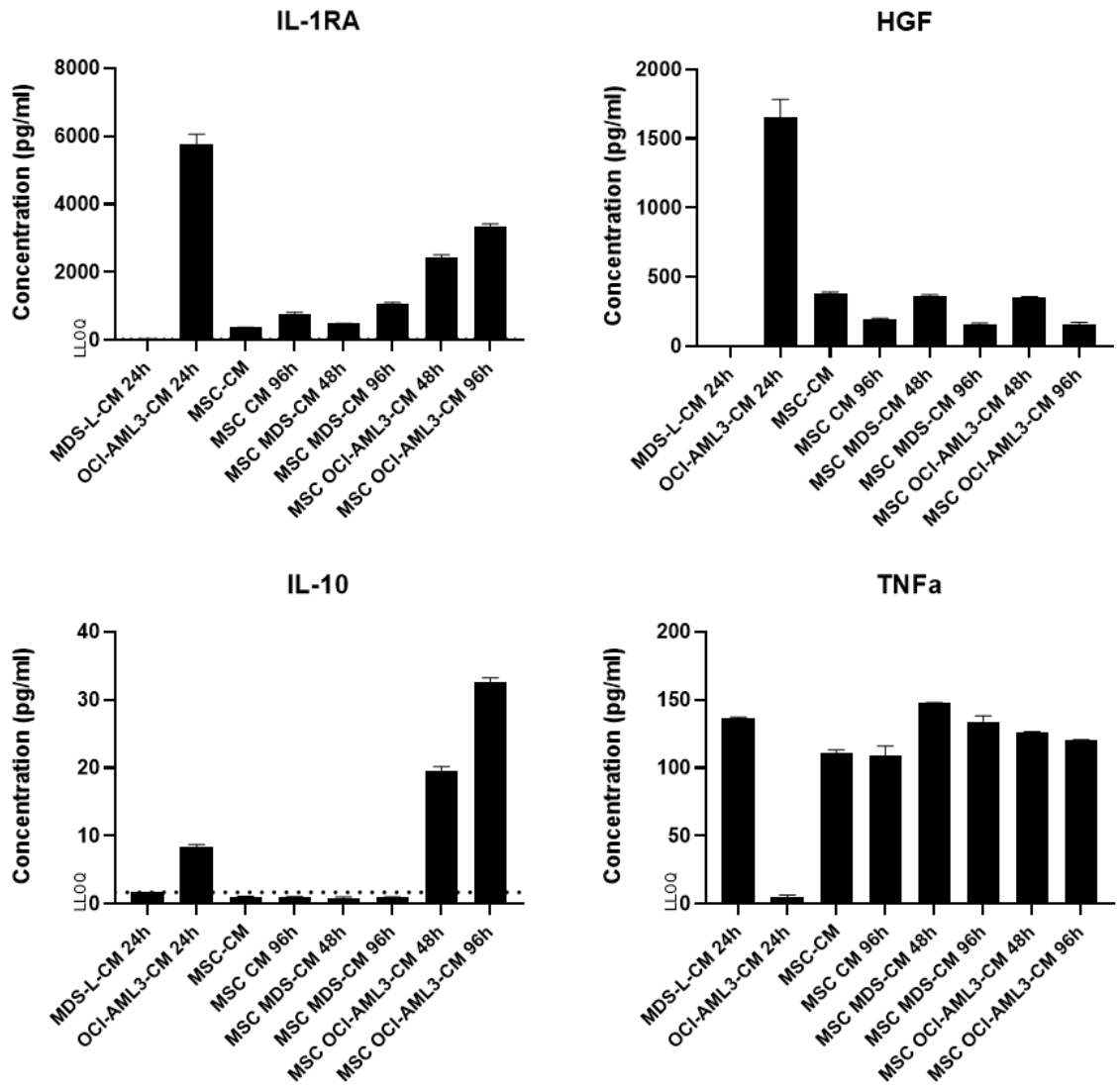

Figure 58: MDS-L/OCI-AML3-produced cytokines that were present mainly in the conditioned media of cultured MDS/AML cell lines.

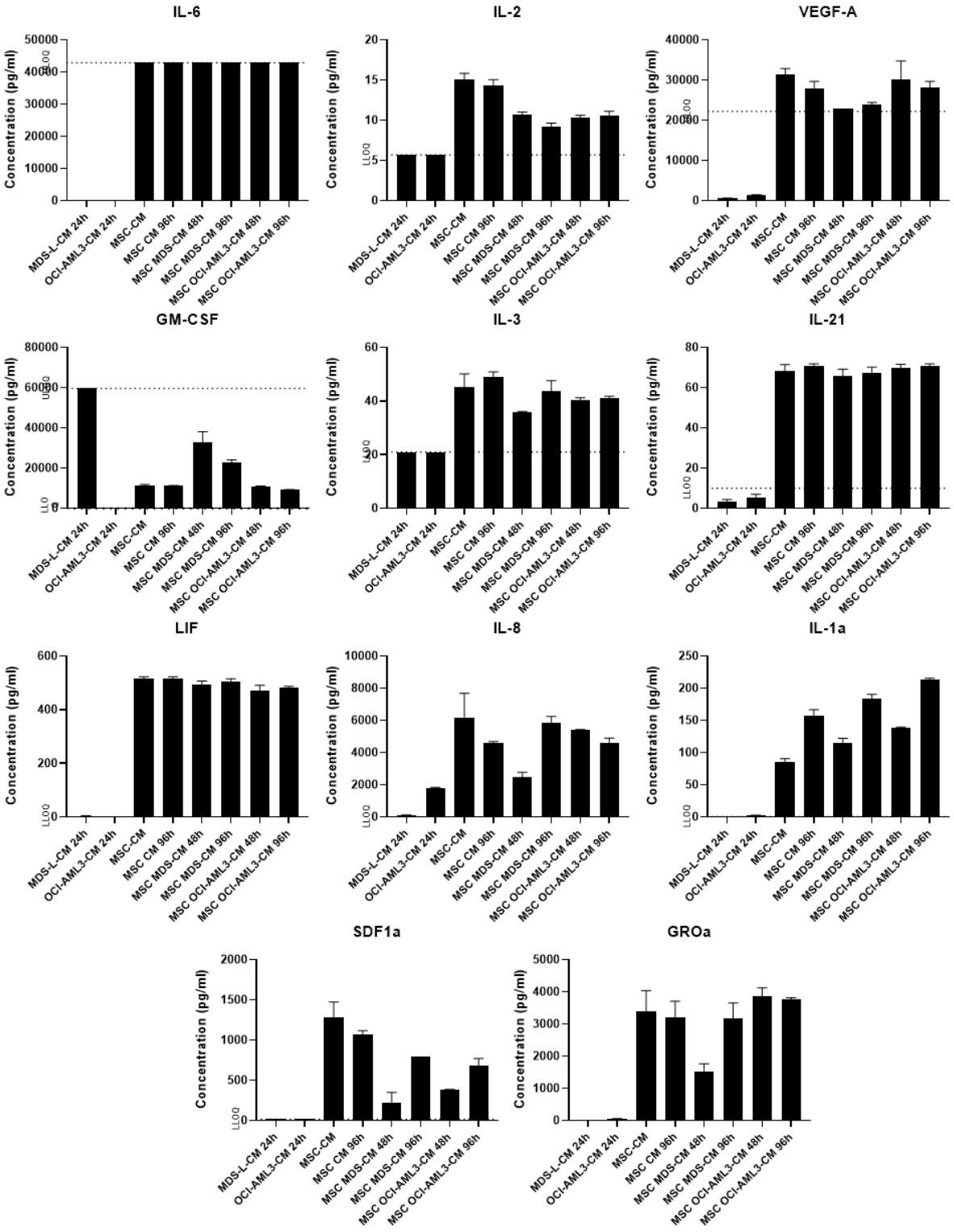

Figure 59: hTERT-MSC-derived cytokines that were present mostly in MSC monoculture.

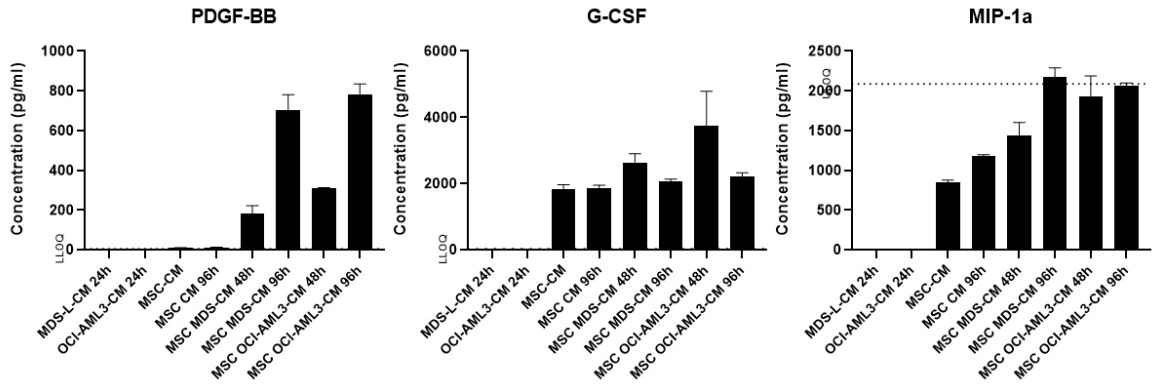

Figure 60: Co-culture-induced cytokines that were present in monoculture, but strongly induced in co-culture.

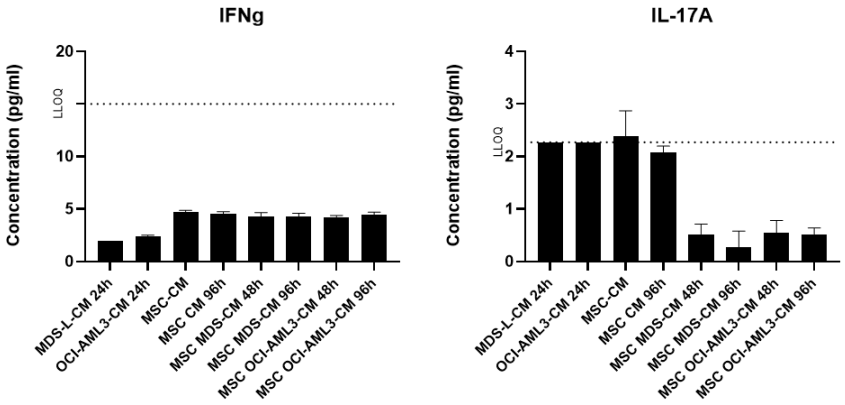

Figure 61: Cytokines where no difference in expression was noticed and signal was below lower detection threshold (extrapolation results in an estimation of the signal by the machine).

9.3.5 Signature gene heatmap for stromal subcluster annotation

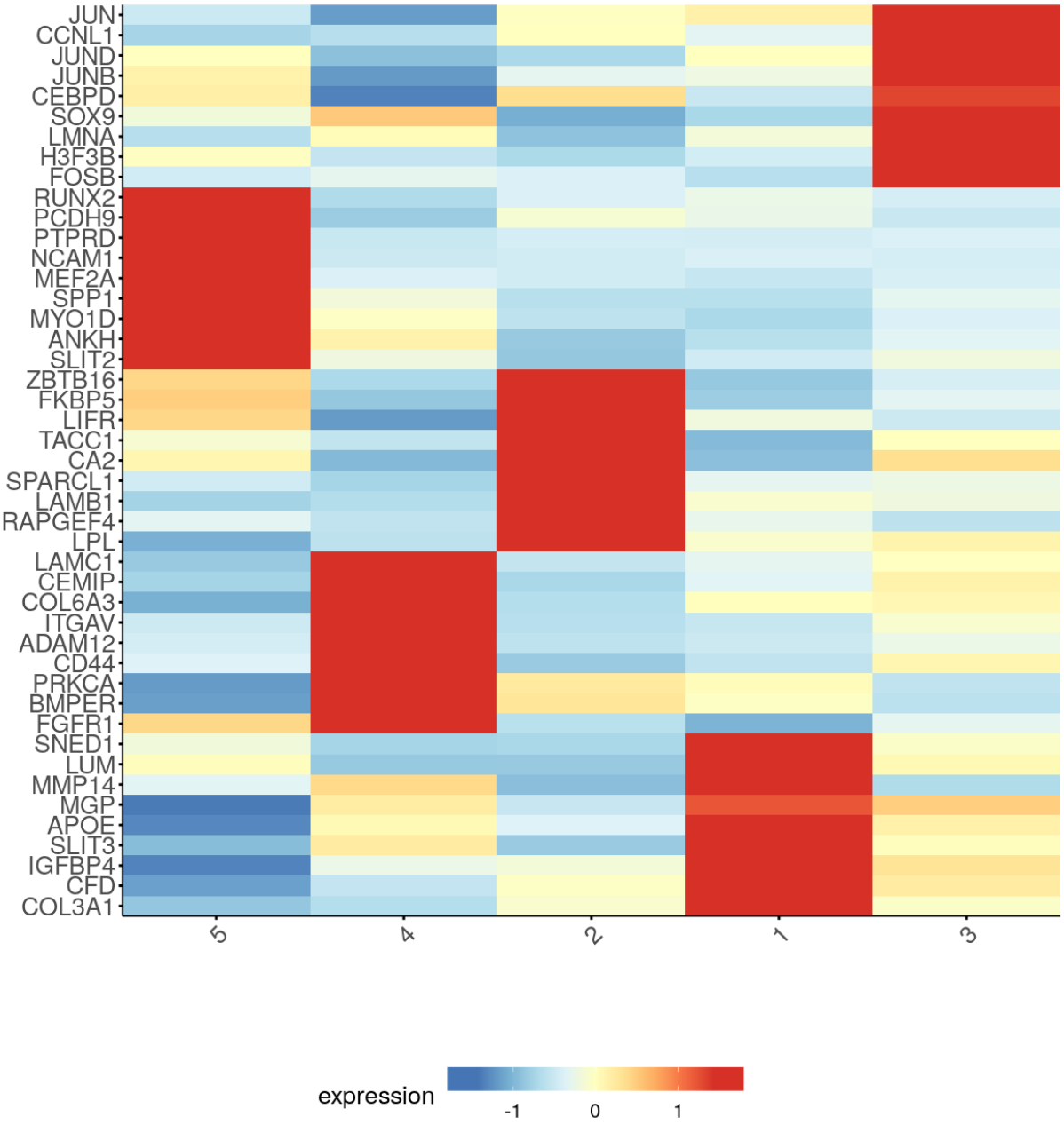

Figure 62: Heatmap of signature genes for stroma subclusters , curated from existing libraries as described in chapter 3.2.7 and highest expressed genes per cluster. Cluster 1 is adipogenic, cluster 2 naïve, cluster 3 osteochondrogenic, cluster 4 chondrogenic, cluster 5 osteogenic.

9.3.6 Heatmap for T cell marker genes

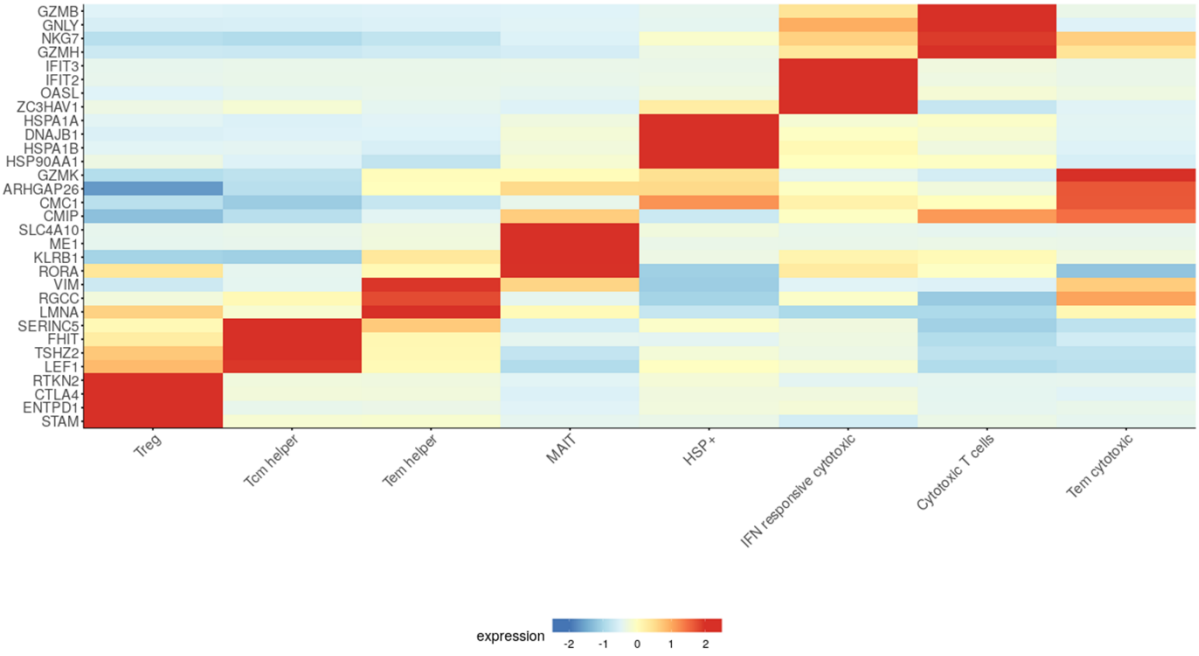

Figure 63: Heatmap for T cell cluster annotation marker genes, curated from existing libraries as described in chapter 3.2.7 and highest expressed genes per cluster.

9.3.7 T cells express fewer genes and are more quiescent than other populations

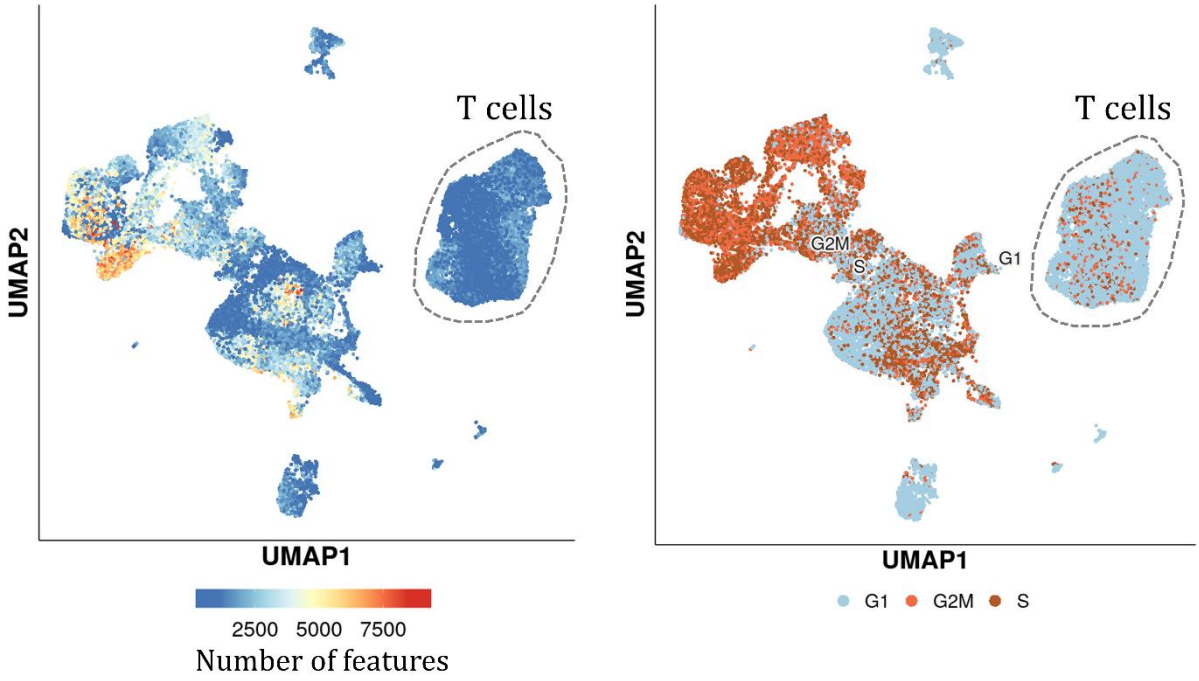

Figure 64: UMAP projection, showing number of features per cell (left) and cell cycle distribution (right).

T cells were difficult to annotate because of the lower number of genes (features) present and the high percentage of quiescent T cells that are in G0/G1 phase.

9.3.8 Volcano plots of T cell subpopulations

Volcano plots of log2-fold change expression against -log10 of the adjusted p value (-log10 p adj) for all T cell subclusters. The adjustment is used to correct for inflated p values that result from treating all cells as technical replicates. For MAIT and IFN-responsive cells, only CHIP and MDS had sufficient cells for direct comparison.

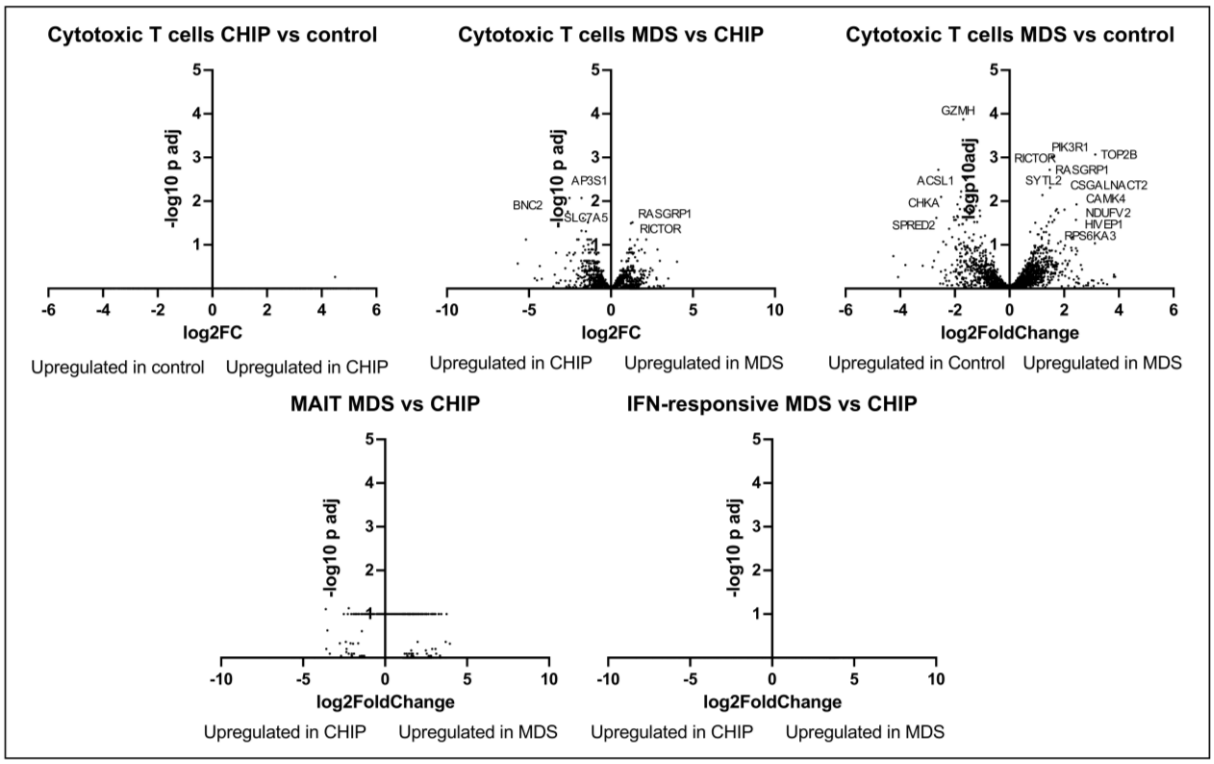

Figure 65: Volcano plot of DEG for cytotoxic T cells, MAIT and IFN-responsive T cells. Top significantly upregulated genes are annotated.

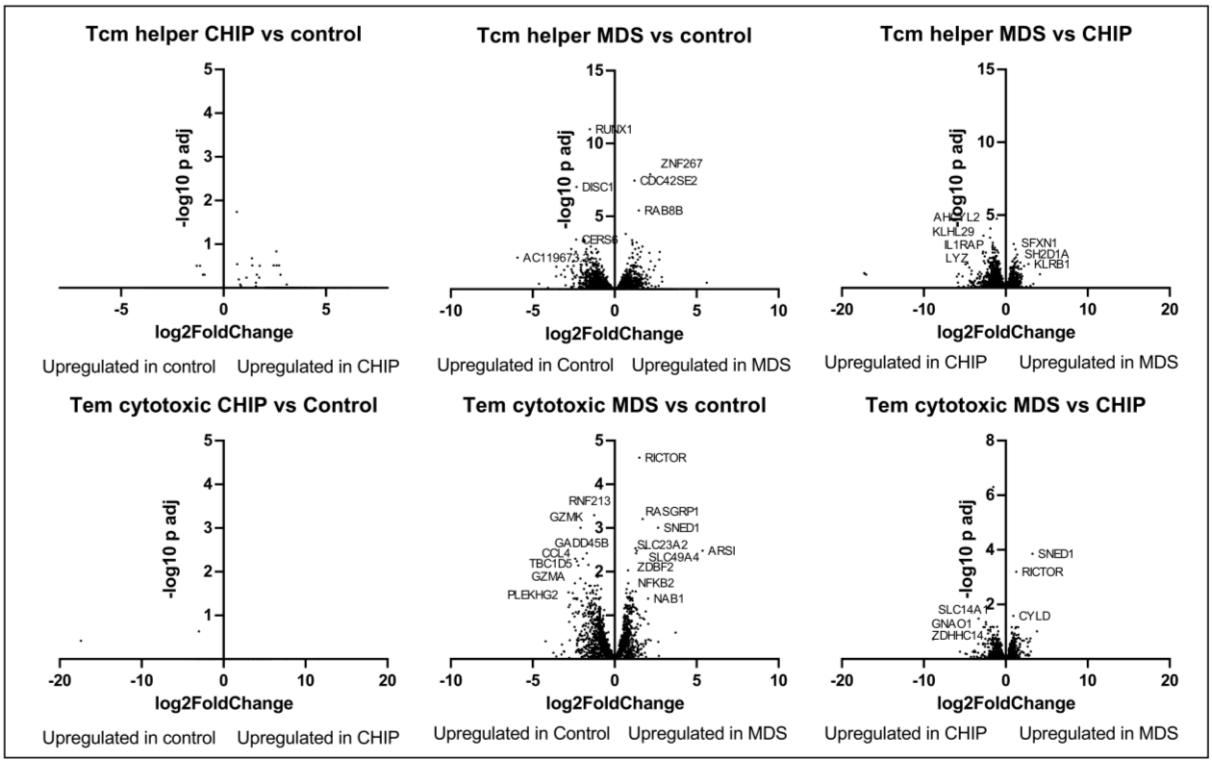

Figure 66: Volcano plot of DEG for Tcm helper cells and Tem cytotoxic cells. Top significantly upregulated genes are annotated.

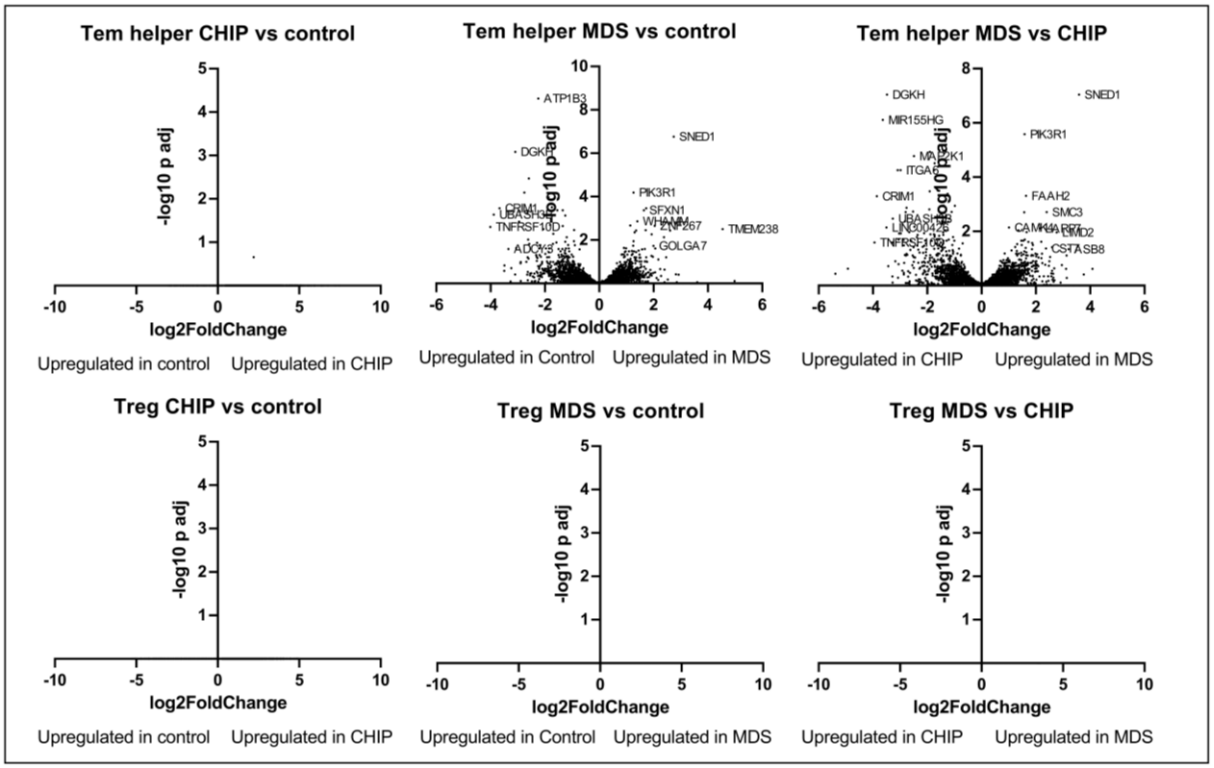

Figure 67: Volcano plot of DEG for Tem helper T cells and Treg. Top significantly upregulated genes are annotated.

List of figures

List of tables

Publication bibliography

Aanei, Carmen Mariana; Eloae, Florin Zugun; Flandrin-Gresta, Pascale; Tavernier, Emmanuelle; Carasevici, Eugen; Guyotat, Denis; Campos, Lydia (2011): Focal adhesion protein abnormalities in myelodysplastic mesenchymal stromal cells. In *Experimental cell research* 317 (18), pp. 2616–2629. DOI: 10.1016/j.yexcr.2011.08.007.

Aaron, Nicole; Costa, Samantha; Rosen, Clifford J.; Qiang, Li (2022): The Implications of Bone Marrow Adipose Tissue on Inflammaging. In *Frontiers in endocrinology* 13, p. 853765. DOI: 10.3389/fendo.2022.853765.

Abdel-Wahab, Omar; Adli, Mazhar; LaFave, Lindsay M.; Gao, Jie; Hricik, Todd; Shih, Alan H. et al. (2012): ASXL1 mutations promote myeloid transformation through loss of PRC2-mediated gene repression. In *Cancer cell* 22 (2), pp. 180–193. DOI: 10.1016/j.ccr.2012.06.032.

Abegunde, Samuel O.; Buckstein, Rena; Wells, Richard A.; Rauh, Michael J. (2018): An inflammatory environment containing TNFα favors Tet2-mutant clonal hematopoiesis. In *Experimental hematology* 59, pp. 60–65. DOI: 10.1016/j.exphem.2017.11.002.

Abhinand, Chandran S.; Raju, Rajesh; Soumya, Sasikumar J.; Arya, Prabha S.; Sudhakaran, Perumana R. (2016): VEGF-A/VEGFR2 signaling network in endothelial cells relevant to angiogenesis. In *Journal of cell communication and signaling* 10 (4), pp. 347–354. DOI: 10.1007/s12079-016-0352-8.

Adolfsson, J.; Borge, O. J.; Bryder, D.; Theilgaard-Mönch, K.; Astrand-Grundström, I.; Sitnicka, E. et al. (2001): Upregulation of Flt3 expression within the bone marrow Lin(-)Sca1(+)c-kit(+) stem cell compartment is accompanied by loss of self-renewal capacity. In *Immunity* 15 (4), pp. 659–669. DOI: 10.1016/s1074-7613(01)00220-5.

Aguayo, A.; Armillas-Canseco, F. M.; Martínez-Baños, D. (2011): Antiangiogenesis in myelodysplastic syndrome. In *Current cancer drug targets* 11 (9), pp. 1044–1052. DOI: 10.2174/156800911798073104.

Aguilar-Navarro, Alicia G.; Meza-León, Berenice; Gratzinger, Dita; Juárez-Aguilar, Fany G.; Chang, Qing; Ornatsky, Olga et al. (2020): Human Aging Alters the Spatial Organization between CD34+ Hematopoietic Cells and Adipocytes in Bone Marrow. In *Stem Cell Reports* 15 (2), pp. 317–325. DOI: 10.1016/j.stemcr.2020.06.011.

Alexandrakis, M. G.; Passam, F. H.; Pappa, C. A.; Damilakis, J.; Tsirakis, G.; Kandidaki, E. et al. (2005): Serum evaluation of angiogenic cytokine basic fibroblast growth factor, hepatocyte growth factor and TNF-alpha in patients with myelodysplastic syndromes: correlation with bone marrow microvascular density. In *International journal of immunopathology and pharmacology* 18 (2), pp. 287–295. DOI: 10.1177/039463200501800211.

Almeida, Maria; Han, Li; Martin-Millan, Marta; Plotkin, Lilian I.; Stewart, Scott A.; Roberson, Paula K. et al. (2007): Skeletal involution by age-associated oxidative stress and its acceleration by loss of sex steroids. In *The Journal of biological chemistry* 282 (37), pp. 27285–27297. DOI: 10.1074/jbc.M702810200.

Ambrosi, Thomas H.; Scialdone, Antonio; Graja, Antonia; Gohlke, Sabrina; Jank, Anne-Marie; Bocian, Carla et al. (2017): Adipocyte Accumulation in the Bone Marrow during Obesity and Aging Impairs Stem Cell-Based Hematopoietic and Bone Regeneration. In *Cell stem cell* 20 (6), 771-784.e6. DOI: 10.1016/j.stem.2017.02.009.

Aomatsu, Emiko; Chosa, Naoyuki; Nishihira, Soko; Sugiyama, Yoshiki; Miura, Hiroyuki; Ishisaki, Akira (2014): Cell-cell adhesion through N-cadherin enhances VCAM-1 expression via PDGFRβ in a ligand-independent manner in mesenchymal stem cells. In *International journal of molecular medicine* 33 (3), pp. 565–572. DOI: 10.3892/ijmm.2013.1607.

Arai, Fumio; Hirao, Atsushi; Ohmura, Masako; Sato, Hidetaka; Matsuoka, Sahoko; Takubo, Keiyo et al. (2004): Tie2/angiopoietin-1 signaling regulates hematopoietic stem cell quiescence in the bone marrow niche. In *Cell* 118 (2), pp. 149–161. DOI: 10.1016/j.cell.2004.07.004.

Arranz, Lorena; Sánchez-Aguilera, Abel; Martín-Pérez, Daniel; Isern, Joan; Langa, Xavier; Tzankov, Alexandar et al. (2014): Neuropathy of haematopoietic stem cell niche is essential for myeloproliferative neoplasms. In *Nature* 512 (7512), pp. 78–81. DOI: 10.1038/nature13383.

Asada, Noboru; Takeishi, Shoichiro; Frenette, Paul S. (2017): Complexity of bone marrow hematopoietic stem cell niche. In *International journal of hematology* 106 (1), pp. 45–54. DOI: 10.1007/s12185-017-2262-9.

Aspriţoiu, Veronica Mădălina; Stoica, Ileana; Bleotu, Coralia; Diaconu, Carmen Cristina (2021): Epigenetic Regulation of Angiogenesis in Development and Tumors Progression: Potential Implications for Cancer Treatment. In *Frontiers in cell and developmental biology* 9, p. 689962. DOI: 10.3389/fcell.2021.689962.

Avecilla, Scott T.; Hattori, Koichi; Heissig, Beate; Tejada, Rafael; Liao, Fang; Shido, Koji et al. (2004): Chemokine-mediated interaction of hematopoietic progenitors with the bone marrow vascular niche is required for thrombopoiesis. In *Nature medicine* 10 (1), pp. 64–71. DOI: 10.1038/nm973.

Baccin, Chiara; Al-Sabah, Jude; Velten, Lars; Helbling, Patrick M.; Grünschläger, Florian; Hernández-Malmierca, Pablo et al. (2020): Combined single-cell and spatial transcriptomics reveal the molecular, cellular and spatial bone marrow niche organization. In *Nature cell biology* 22 (1), pp. 38–48. DOI: 10.1038/s41556-019-0439-6.

Bahney, Chelsea S.; Hu, Diane P.; Miclau, Theodore; Marcucio, Ralph S. (2015): The multifaceted role of the vasculature in endochondral fracture repair. In *Frontiers in endocrinology* 6, p. 4. DOI: 10.3389/fendo.2015.00004.

Bains, Amanpreet Kaur; Behrens Wu, Lena; Rivière, Jennifer; Rother, Sandra; Magno, Valentina; Friedrichs, Jens et al. (2022): Bone marrow mesenchymal stromal cell-derived extracellular matrix displays altered glycosaminoglycan structure and impaired functionality in Myelodysplastic Syndromes. In *Frontiers in oncology* 12, p. 961473. DOI: 10.3389/fonc.2022.961473.

Balandrán, Juan Carlos; Purizaca, Jessica; Enciso, Jennifer; Dozal, David; Sandoval, Antonio; Jiménez-Hernández, Elva et al. (2016): Pro-inflammatory-Related Loss of CXCL12 Niche Promotes Acute Lymphoblastic Leukemic Progression at the Expense of Normal Lymphopoiesis. In *Frontiers in immunology* 7, p. 666. DOI: 10.3389/fimmu.2016.00666.

Baryawno, Ninib; Przybylski, Dariusz; Kowalczyk, Monika S.; Kfoury, Youmna; Severe, Nicolas; Gustafsson, Karin et al. (2019): A Cellular Taxonomy of the Bone Marrow Stroma in Homeostasis and Leukemia. In *Cell* 177 (7), 1915-1932.e16. DOI: 10.1016/j.cell.2019.04.040.

Baylis, Daniel; Bartlett, David B.; Patel, Harnish P.; Roberts, Helen C. (2013): Understanding how we age: insights into inflammaging. In *Longevity & healthspan* 2 (1), p. 8. DOI: 10.1186/2046-2395-2-8.

Bejar, Rafael (2013): Prognostic models in myelodysplastic syndromes. In *Hematology: the American Society of Hematology Education Program* 2013, pp. 504–510. DOI: 10.1182/asheducation-2013.1.504.

Bellamy, W. T.; Richter, L.; Sirjani, D.; Roxas, C.; Glinsmann-Gibson, B.; Frutiger, Y. et al. (2001): Vascular endothelial cell growth factor is an autocrine promoter of abnormal localized immature myeloid precursors and leukemia progenitor formation in myelodysplastic syndromes. In *Blood* 97 (5), pp. 1427–1434. DOI: 10.1182/blood.v97.5.1427.

Benichou, Gilles; Gonzalez, Bruno; Marino, Jose; Ayasoufi, Katayoun; Valujskikh, Anna (2017): Role of Memory T Cells in Allograft Rejection and Tolerance. In *Frontiers in immunology* 8, p. 170. DOI: 10.3389/fimmu.2017.00170.

Ben-Sasson, Shlomo Z.; Hu-Li, Jane; Quiel, Juan; Cauchetaux, Stephane; Ratner, Maya; Shapira, Ilana et al. (2009): IL-1 acts directly on CD4 T cells to enhance their antigen-driven expansion and differentiation. In *Proceedings of the National Academy of Sciences of the United States of America* 106 (17), pp. 7119–7124. DOI: 10.1073/pnas.0902745106.

Bick, Alexander G.; Weinstock, Joshua S.; Nandakumar, Satish K.; Fulco, Charles P.; Bao, Erik L.; Zekavat, Seyedeh M. et al. (2020): Inherited causes of clonal haematopoiesis in 97,691 whole genomes. In *Nature* 586 (7831), pp. 763–768. DOI: 10.1038/s41586-020-2819-2.

Bisht, Kavita; McGirr, Crystal; Lee, Seo-Youn; Tseng, Hsu-Wen; Fleming, Whitney; Alexander, Kylie A. et al. (2022): Oncostatin M regulates hematopoietic stem cell (HSC) niches in the bone marrow to restrict HSC mobilization. In *Leukemia* 36 (2), pp. 333–347. DOI: 10.1038/s41375-021-01413-z.

Boiko, Julie R.; Borghesi, Lisa (2012): Hematopoiesis sculpted by pathogens: Toll-like receptors and inflammatory mediators directly activate stem cells. In *Cytokine* 57 (1), pp. 1–8. DOI: 10.1016/j.cyto.2011.10.005.

Bolton, Kelly L.; Zehir, Ahmet; Ptashkin, Ryan N.; Patel, Minal; Gupta, Dipti; Sidlow, Robert et al. (2020): The Clinical Management of Clonal Hematopoiesis: Creation of a Clonal Hematopoiesis Clinic. In *Hematology/oncology clinics of North America* 34 (2), pp. 357–367. DOI: 10.1016/j.hoc.2019.11.006.

Boudousquié, Caroline; Danilo, Maxime; Pousse, Laurène; Jeevan-Raj, Beena; Angelov, Georgi S.; Chennupati, Vijaykumar et al. (2014): Differences in the transduction of canonical Wnt signals demarcate effector and memory CD8 T cells with distinct recall proliferation capacity. In *Journal of immunology (Baltimore, Md.: 1950)* 193 (6), pp. 2784–2791. DOI: 10.4049/jimmunol.1400465.

Bousounis, Pavlos; Bergo, Veronica; Trompouki, Eirini (2021): Inflammation, Aging and Hematopoiesis: A Complex Relationship. In *Cells* 10 (6). DOI: 10.3390/cells10061386.

Broome, C. S.; Miyan, J. A. (2000): Neuropeptide control of bone marrow neutrophil production. A key axis for neuroimmunomodulation. In *Annals of the New York Academy of Sciences* 917, pp. 424–434. DOI: 10.1111/j.1749-6632.2000.tb05407.x.

Brunner, B.; Gunsilius, E.; Schumacher, P.; Zwierzina, H.; Gastl, G.; Stauder, R. (2002): Blood levels of angiogenin and vascular endothelial growth factor are elevated in myelodysplastic syndromes and in acute myeloid leukemia. In *Journal of hematotherapy & stem cell research* 11 (1), pp. 119–125. DOI: 10.1089/152581602753448586.

Bruns, Ingmar; Lucas, Daniel; Pinho, Sandra; Ahmed, Jalal; Lambert, Michele P.; Kunisaki, Yuya et al. (2014): Megakaryocytes regulate hematopoietic stem cell quiescence through CXCL4 secretion. In *Nature medicine* 20 (11), pp. 1315–1320. DOI: 10.1038/nm.3707.

Buckley, C. D.; Amft, N.; Bradfield, P. F.; Pilling, D.; Ross, E.; Arenzana-Seisdedos, F. et al. (2000): Persistent induction of the chemokine receptor CXCR4 by TGF-beta 1 on synovial T cells contributes to their accumulation within the rheumatoid synovium. In *Journal of immunology (Baltimore, Md.:1950)* 165 (6), pp. 3423–3429. DOI: 10.4049/jimmunol.165.6.3423.

Busillo, John M.; Benovic, Jeffrey L. (2007): Regulation of CXCR4 signaling. In *Biochimica et biophysica acta* 1768 (4), pp. 952–963. DOI: 10.1016/j.bbamem.2006.11.002.

Calvo, W. (1968): The innervation of the bone marrow in laboratory animals. In *The American journal of anatomy* 123 (2), pp. 315–328. DOI: 10.1002/aja.1001230206.

Camacho, Virginia; Matkins, Victoria R.; Patel, Sweta B.; Lever, Jeremie M.; Yang, Zhengqin; Ying, Li et al. (2020): Bone marrow Tregs mediate stromal cell function and support hematopoiesis via IL-10. In *JCI insight* 5 (22). DOI: 10.1172/jci.insight.135681.

Catlin, Sandra N.; Busque, Lambert; Gale, Rosemary E.; Guttorp, Peter; Abkowitz, Janis L. (2011): The replication rate of human hematopoietic stem cells in vivo. In *Blood* 117 (17), pp. 4460–4466. DOI: 10.1182/blood-2010-08-303537.

Cedar, Howard; Bergman, Yehudit (2011): Epigenetics of haematopoietic cell development. In *Nature reviews. Immunology* 11 (7), pp. 478–488. DOI: 10.1038/nri2991.

Challen, Grant A.; Boles, Nathan C.; Chambers, Stuart M.; Goodell, Margaret A. (2010): Distinct hematopoietic stem cell subtypes are differentially regulated by TGF-beta1. In *Cell stem cell* 6 (3), pp. 265–278. DOI: 10.1016/j.stem.2010.02.002.

Chartier, Stephane R.; Mitchell, Stefanie A. T.; Majuta, Lisa A.; Mantyh, Patrick W. (2018): The Changing Sensory and Sympathetic Innervation of the Young, Adult and Aging Mouse Femur. In *Neuroscience* 387, pp. 178–190. DOI: 10.1016/j.neuroscience.2018.01.047.

Chen, Edwin; Mullally, Ann (2014): How does JAK2V617F contribute to the pathogenesis of myeloproliferative neoplasms? In *Hematology: the American Society of Hematology Education Program* 2014 (1), pp. 268–276. DOI: 10.1182/asheducation-2014.1.268.

Chen, Jiezhong; Crawford, Ross; Chen, Chen; Xiao, Yin (2013): The key regulatory roles of the PI3K/Akt signaling pathway in the functionalities of mesenchymal stem cells and applications in tissue regeneration. In *Tissue engineering. Part B, Reviews* 19 (6), pp. 516–528. DOI: 10.1089/ten.teb.2012.0672.

Chen, Junyu; Hendriks, Michelle; Chatzis, Alexandros; Ramasamy, Saravana K.; Kusumbe, Anjali P. (2020): Bone Vasculature and Bone Marrow Vascular Niches in Health and Disease. In *Journal of bone and mineral research : the official journal of the American Society for Bone and Mineral Research* 35 (11), pp. 2103–2120. DOI: 10.1002/jbmr.4171.

Chen, Sisi; Wang, Qiang; Yu, Hao; Capitano, Maegan L.; Vemula, Sasidhar; Nabinger, Sarah C. et al. (2019): Mutant p53 drives clonal hematopoiesis through modulating epigenetic pathway. In *Nature communications* 10 (1), p. 5649. DOI: 10.1038/s41467-019-13542-2.

Chen, Xiaoyong; Liu, Qiuli; Xiang, Andy Peng (2018): CD8+CD28- T cells: not only age-related cells but a subset of regulatory T cells. In *Cellular & molecular immunology* 15 (8), pp. 734–736. DOI: 10.1038/cmi.2017.153.

Chen, Zhibin; Herman, Ann E.; Matos, Michael; Mathis, Diane; Benoist, Christophe (2005): Where CD4+CD25+ T reg cells impinge on autoimmune diabetes. In *The Journal of experimental medicine* 202 (10), pp. 1387–1397. DOI: 10.1084/jem.20051409.

Cheng, Hui; Zheng, Zhaofeng; Cheng, Tao (2020): New paradigms on hematopoietic stem cell differentiation. In *Protein & cell* 11 (1), pp. 34–44. DOI: 10.1007/s13238-019-0633-0.

Cho, Young-Nan; Kee, Seung-Jung; Kim, Tae-Jong; Jin, Hye Mi; Kim, Moon-Ju; Jung, Hyun-Ju et al. (2014): Mucosal-associated invariant T cell deficiency in systemic lupus erythematosus. In *Journal of immunology (Baltimore, Md. : 1950)* 193 (8), pp. 3891–3901. DOI: 10.4049/jimmunol.1302701.

Choesmel, Valérie; Bacqueville, Daniel; Rouquette, Jacques; Noaillac-Depeyre, Jacqueline; Fribourg, Sébastien; Crétien, Aurore et al. (2007): Impaired ribosome biogenesis in Diamond-Blackfan anemia. In *Blood* 109 (3), pp. 1275–1283. DOI: 10.1182/blood-2006-07-038372.

Choi, Hayoung; Kim, Yonggoo; Kang, Dain; Kwon, Ahlm; Kim, Jiyeon; Min Kim, Jung et al. (2020): Common and different alterations of bone marrow mesenchymal stromal cells in myelodysplastic syndrome and multiple myeloma. In *Cell proliferation* 53 (5), e12819. DOI: 10.1111/cpr.12819.

Choudhary, Gaurav S.; Pellagatti, Andrea; Agianian, Bogos; Smith, Molly A.; Bhagat, Tushar D.; Gordon-Mitchell, Shanisha et al. (2022): Activation of targetable inflammatory immune signaling is seen in myelodysplastic syndromes with SF3B1 mutations. In *eLife* 11. DOI: 10.7554/eLife.78136.

Chow, Andrew; Lucas, Daniel; Hidalgo, Andrés; Méndez-Ferrer, Simón; Hashimoto, Daigo; Scheiermann, Christoph et al. (2011): Bone marrow CD169+ macrophages promote the retention of hematopoietic stem and progenitor cells in the mesenchymal stem cell niche. In *The Journal of experimental medicine* 208 (2), pp. 261–271. DOI: 10.1084/jem.20101688.

Cipriani, Paola; Di Benedetto, Paola; Ruscitti, Piero; Liakouli, Vasiliki; Berardicurti, Onorina; Carubbi, Francesco et al. (2016): Perivascular Cells in Diffuse Cutaneous Systemic Sclerosis Overexpress Activated ADAM12 and Are Involved in Myofibroblast Transdifferentiation and Development of Fibrosis. In *The Journal of rheumatology* 43 (7), pp. 1340–1349. DOI: 10.3899/jrheum.150996.

Civini, Sara; Jin, Ping; Ren, Jiaqiang; Sabatino, Marianna; Castiello, Luciano; Jin, Jianjian et al. (2013): Leukemia cells induce changes in human bone marrow stromal cells. In *Journal of translational medicine* 11, p. 298. DOI: 10.1186/1479-5876-11-298.

Cook, Elina K.; Izukawa, Terumi; Young, Sherylan; Rosen, Gili; Jamali, Mina; Zhang, Liying et al. (2019): Comorbid and inflammatory characteristics of genetic subtypes of clonal hematopoiesis. In *Blood advances* 3 (16), pp. 2482–2486. DOI: 10.1182/bloodadvances.2018024729.

Crosse, Edie I.; Gordon-Keylock, Sabrina; Rybtsov, Stanislav; Binagui-Casas, Anahi; Felchle, Hannah; Nnadi, Nneka C. et al. (2020): Multi-layered Spatial Transcriptomics Identify Secretory Factors Promoting Human Hematopoietic Stem Cell Development. In *Cell stem cell* 27 (5), 822-839.e8. DOI: 10.1016/j.stem.2020.08.004.

Damm, Frederik; Kosmider, Olivier; Gelsi-Boyer, Véronique; Renneville, Aline; Carbuccia, Nadine; Hidalgo-Curtis, Claire et al. (2012): Mutations affecting mRNA splicing define distinct clinical phenotypes and correlate with patient outcome in myelodysplastic syndromes. In *Blood* 119 (14), pp. 3211–3218. DOI: 10.1182/blood-2011-12-400994.

Darman, Rachel B.; Seiler, Michael; Agrawal, Anant A.; Lim, Kian H.; Peng, Shouyong; Aird, Daniel et al. (2015): Cancer-Associated SF3B1 Hotspot Mutations Induce Cryptic 3' Splice Site Selection through Use of a Different Branch Point. In *Cell reports* 13 (5), pp. 1033–1045. DOI: 10.1016/j.celrep.2015.09.053.

Datzmann, Thomas; Trautmann, Freya; Tesch, Falko; Mies, Anna; Hofbauer, Lorenz C.; Platzbecker, Uwe; Schmitt, Jochen (2018): Associations of myeloid hematological diseases of the elderly with osteoporosis: A longitudinal analysis of routine health care data. In *Leukemia research* 69, pp. 81–86. DOI: 10.1016/j.leukres.2018.04.010.

Davis, A. Sally; Richter, Anke; Becker, Steven; Moyer, Jenna E.; Sandouk, Aline; Skinner, Jeff; Taubenberger, Jeffery K. (2014): Characterizing and Diminishing Autofluorescence in Formalin-fixed Paraffin-embedded Human Respiratory Tissue. In *The journal of histochemistry and cytochemistry : official journal of the Histochemistry Society* 62 (6), pp. 405–423. DOI: 10.1369/0022155414531549.

Dekel, Elya; Yaffe, Dana; Rosenhek-Goldian, Irit; Ben-Nissan, Gili; Ofir-Birin, Yifat; Morandi, Mattia I. et al. (2021): 20S proteasomes secreted by the malaria parasite promote its growth. In *Nature communications* 12 (1), p. 1172. DOI: 10.1038/s41467-021-21344-8.

Della Porta, M. G.; Malcovati, L.; Rigolin, G. M.; Rosti, V.; Bonetti, E.; Travaglino, E. et al. (2008): Immunophenotypic, cytogenetic and functional characterization of circulating endothelial cells in myelodysplastic syndromes. In *Leukemia* 22 (3), pp. 530–537. DOI: 10.1038/sj.leu.2405069.

Devlin, Maureen J.; Rosen, Clifford J. (2015): The bone-fat interface: basic and clinical implications of marrow adiposity. In *The lancet. Diabetes & endocrinology* 3 (2), pp. 141–147. DOI: 10.1016/S2213-8587(14)70007-5.

Di Rosa, Francesca (2016): Maintenance of memory T cells in the bone marrow: survival or homeostatic proliferation? In *Nat Rev Immunol* 16 (4), p. 271. DOI: 10.1038/nri.2016.31.

Ding, Lei; Saunders, Thomas L.; Enikolopov, Grigori; Morrison, Sean J. (2012): Endothelial and perivascular cells maintain haematopoietic stem cells. In *Nature* 481 (7382), pp. 457–462. DOI: 10.1038/nature10783.

Dobenecker, Marc-Werner; Park, Joon Seok; Marcello, Jonas; McCabe, Michael T.; Gregory, Richard; Knight, Steven D. et al. (2018): Signaling function of PRC2 is essential for TCR-driven T cell responses. In *The Journal of experimental medicine* 215 (4), pp. 1101–1113. DOI: 10.1084/jem.20170084.

Domínguez Conde, C.; Xu, C.; Jarvis, L. B.; Rainbow, D. B.; Wells, S. B.; Gomes, T. et al. (2022): Cross-tissue immune cell analysis reveals tissue-specific features in humans. In *Science (New York, N.Y.)* 376 (6594), eabl5197. DOI: 10.1126/science.abl5197.

Dominici, M.; Le Blanc, K.; Mueller, I.; Slaper-Cortenbach, I.; Marini, Fc; Krause, Ds et al. (2006): Minimal criteria for defining multipotent mesenchymal stromal cells. The International Society for Cellular Therapy position statement. In *Cytotherapy* 8 (4), pp. 315–317. DOI: 10.1080/14653240600855905.

Dührsen; Hossfeld (1996): Stromal abnormalities in neoplastic bone marrow diseases. In *Annals of Hematology* (73), pp. 53–70.

Dulauroy, Sophie; Di Carlo, Selene E.; Langa, Francina; Eberl, Gérard; Peduto, Lucie (2012): Lineage tracing and genetic ablation of ADAM12(+) perivascular cells identify a major source of profibrotic cells during acute tissue injury. In *Nature medicine* 18 (8), pp. 1262–1270. DOI: 10.1038/nm.2848.

Duverney (1770): Sur la structure intime et le sentiment de la moelle des os: Pierre Mortier (8).

Ehninger, Armin; Trumpp, Andreas (2011): The bone marrow stem cell niche grows up: mesenchymal stem cells and macrophages move in. In *The Journal of experimental medicine* 208 (3), pp. 421–428. DOI: 10.1084/jem.20110132.

Elias, H. K.; Schinke, C.; Bhattacharyya, S.; Will, B.; Verma, A.; Steidl, U. (2014): Stem cell origin of myelodysplastic syndromes. In *Oncogene* 33 (44), pp. 5139–5150. DOI: 10.1038/onc.2013.520.

Emperle, Max; Rajavelu, Arumugam; Kunert, Stefan; Arimondo, Paola B.; Reinhardt, Richard; Jurkowska, Renata Z.; Jeltsch, Albert (2018): The DNMT3A R882H mutant displays altered flanking sequence preferences. In *Nucleic acids research* 46 (6), pp. 3130–3139. DOI: 10.1093/nar/gky168.

Ennis, Sarah; Conforte, Alessandra; O'Reilly, Eimear; Cichocka, Tatiana; Pal Dhami, Sukhraj; Nicholson, Pamela et al. (2022): Single-cell characterisation of the hematopoietic bone marrow interactome in health and disease (79).

Ezaki, T. (2000): Antigen retrieval on formaldehyde-fixed paraffin sections: its potential drawbacks and optimization for double immunostaining. In *Micron (Oxford, England : 1993)* 31 (6), pp. 639–649. DOI: 10.1016/s0968-4328(99)00064-5.

Feil, C.; Augustin, H. G. (1998): Endothelial cells differentially express functional CXC-chemokine receptor-4 (CXCR-4/fusin) under the control of autocrine activity and exogenous cytokines. In *Biochemical and biophysical research communications* 247 (1), pp. 38–45. DOI: 10.1006/bbrc.1998.8499.

Fenaux, Pierre; Adès, Lionel (2013): How we treat lower-risk myelodysplastic syndromes. In *Blood* 121 (21), pp. 4280–4286. DOI: 10.1182/blood-2013-02-453068.

Fenaux, Pierre; Platzbecker, Uwe; Mufti, Ghulam J.; Garcia-Manero, Guillermo; Buckstein, Rena; Santini, Valeria et al. (2020): Luspatercept in Patients with Lower-Risk Myelodysplastic Syndromes. In *The New England journal of medicine* 382 (2), pp. 140–151. DOI: 10.1056/NEJMoa1908892.

Ferrone, Christina K.; Blydt-Hansen, Mackenzie; Rauh, Michael J. (2020): Age-Associated TET2 Mutations: Common Drivers of Myeloid Dysfunction, Cancer and Cardiovascular Disease. In *IJMS* 21 (2), p. 626. DOI: 10.3390/ijms21020626.

Ferrucci, Luigi; Corsi, Annamaria; Lauretani, Fulvio; Bandinelli, Stefania; Bartali, Benedetta; Taub, Dennis D. et al. (2005): The origins of age-related proinflammatory state. In *Blood* 105 (6), pp. 2294–2299. DOI: 10.1182/blood-2004-07-2599.

Fischer, Luise; Herkner, Caroline; Kitte, Reni; Dohnke, Sebastian; Riewaldt, Julia; Kretschmer, Karsten; Garbe, Annette I. (2019): Foxp3+ Regulatory T Cells in Bone and Hematopoietic Homeostasis. In *Frontiers in endocrinology* 10, p. 578. DOI: 10.3389/fendo.2019.00578.

Fleming, Heather E.; Janzen, Viktor; Lo Celso, Cristina; Guo, Jun; Leahy, Kathleen M.; Kronenberg, Henry M.; Scadden, David T. (2008): Wnt signaling in the niche enforces hematopoietic stem cell quiescence and is necessary to preserve self-renewal in vivo. In *Cell stem cell* 2 (3), pp. 274–283. DOI: 10.1016/j.stem.2008.01.003.

Fomin, Marina E.; Zhou, Yanchen; Beyer, Ashley I.; Publicover, Jean; Baron, Jody L.; Muench, Marcus O. (2013): Production of factor VIII by human liver sinusoidal endothelial cells transplanted in immunodeficient uPA mice. In *PloS one* 8 (10), e77255. DOI: 10.1371/journal.pone.0077255.

Francis, K.; Palsson, B. O. (1997): Effective intercellular communication distances are determined by the relative time constants for cyto/chemokine secretion and diffusion. In *Proceedings of the National Academy of Sciences of the United States of America* 94 (23), pp. 12258–12262. DOI: 10.1073/pnas.94.23.12258.

Franco, Fabien; Jaccard, Alison; Romero, Pedro; Yu, Yi-Ru; Ho, Ping-Chih (2020): Metabolic and epigenetic regulation of T-cell exhaustion. In *Nature metabolism* 2 (10), pp. 1001–1012. DOI: 10.1038/s42255-020-00280-9.

Friedrich, Chloé; Kosmider, Olivier (2022): The Mesenchymal Niche in Myelodysplastic Syndromes. In *Diagnostics (Basel, Switzerland)* 12 (7). DOI: 10.3390/diagnostics12071639.

Frisch, Benjamin J.; Hoffman, Corey M.; Latchney, Sarah E.; LaMere, Mark W.; Myers, Jason; Ashton, John et al. (2019): Aged marrow macrophages expand platelet-biased hematopoietic stem cells via Interleukin1B. In *JCI insight* 5 (10). DOI: 10.1172/jci.insight.124213.

Fujisaki, Joji; Wu, Juwell; Carlson, Alicia L.; Silberstein, Lev; Putheti, Prabhakar; Larocca, Rafael et al. (2011): In vivo imaging of Treg cells providing immune privilege to the haematopoietic stem-cell niche. In *Nature* 474 (7350), pp. 216–219. DOI: 10.1038/nature10160.

Gao, Xin; Zhang, Dachuan; Xu, Chunliang; Li, Huihui; Caron, Kathleen M.; Frenette, Paul S. (2020): Nociceptive nerves regulate haematopoietic stem cell mobilization. In *Nature*. DOI: 10.1038/s41586-020-03057-y.

Genovese, Giulio; Kähler, Anna K.; Handsaker, Robert E.; Lindberg, Johan; Rose, Samuel A.; Bakhoum, Samuel F. et al. (2014): Clonal hematopoiesis and blood-cancer risk inferred from blood DNA sequence. In *The New England journal of medicine* 371 (26), pp. 2477–2487. DOI: 10.1056/NEJMoa1409405.

Geyh, S.; Oz, S.; Cadeddu, R-P; Fröbel, J.; Brückner, B.; Kündgen, A. et al. (2013): Insufficient stromal support in MDS results from molecular and functional deficits of mesenchymal stromal cells. In *Leukemia* 27 (9), pp. 1841–1851. DOI: 10.1038/leu.2013.193.

Geyh, S.; Rodríguez-Paredes, M.; Jäger, P.; Khandanpour, C.; Cadeddu, R-P; Gutekunst, J. et al. (2016): Functional inhibition of mesenchymal stromal cells in acute myeloid leukemia. In *Leukemia* 30 (3), pp. 683–691. DOI: 10.1038/leu.2015.325.

Ghode, Suprita S.; Bajaj, Manmohan S.; Kulkarni, Rohan S.; Limaye, Lalita S.; Shouche, Yogesh S.; Kale, Vaijayanti P. (2017): Neuropilin-1 Is an Important Niche Component

and Exerts Context-Dependent Effects on Hematopoietic Stem Cells. In *Stem cells and development* 26 (1), pp. 35–48. DOI: 10.1089/scd.2016.0096.

Gilbert, William; Bragg, Robert; Elmansi, Ahmed M.; McGee-Lawrence, Meghan E.; Isales, Carlos M.; Hamrick, Mark W. et al. (2019): Stromal cell-derived factor-1 (CXCL12) and its role in bone and muscle biology. In *Cytokine* 123, p. 154783. DOI: 10.1016/j.cyto.2019.154783.

Giovazzino, Angela; Leone, Stefania; Rubino, Valentina; Palatucci, Anna Teresa; Cerciello, Giuseppe; Alfinito, Fiorella et al. (2019): Reduced regulatory T cells (Treg) in bone marrow preferentially associate with the expansion of cytotoxic T lymphocytes in low risk MDS patients. In *British journal of haematology* 185 (2), pp. 357–360. DOI: 10.1111/bjh.15496.

Goldman, Devorah C.; Bailey, Alexis S.; Pfaffle, Dana L.; Al Masri, Azzah; Christian, Jan L.; Fleming, William H. (2009): BMP4 regulates the hematopoietic stem cell niche. In *Blood* 114 (20), pp. 4393–4401. DOI: 10.1182/blood-2009-02-206433.

Gomariz, Alvaro; Helbling, Patrick M.; Isringhausen, Stephan; Suessbier, Ute; Becker, Anton; Boss, Andreas et al. (2018): Quantitative spatial analysis of haematopoiesis-regulating stromal cells in the bone marrow microenvironment by 3D microscopy. In *Nature communications* 9 (1), p. 2532. DOI: 10.1038/s41467-018-04770-z.

Gondek, Lukasz P.; DeZern, Amy E. (2020): Assessing clonal haematopoiesis: clinical burdens and benefits of diagnosing myelodysplastic syndrome precursor states. In *The Lancet. Haematology* 7 (1), e73-e81. DOI: 10.1016/S2352-3026(19)30211-X.

González-González, Alberto; García-Sánchez, Daniel; Dotta, Monica; Rodríguez-Rey, José C.; Pérez-Campo, Flor M. (2020): Mesenchymal stem cells secretome: The cornerstone of cell-free regenerative medicine. In *World journal of stem cells* 12 (12), pp. 1529–1552. DOI: 10.4252/wjsc.v12.i12.1529.

Goulard, Marie; Dosquet, Christine; Bonnet, Dominique (2018): Role of the microenvironment in myeloid malignancies. In *Cellular and molecular life sciences : CMLS* 75 (8), pp. 1377–1391. DOI: 10.1007/s00018-017-2725-4.

Grassinger, Jochen; Haylock, David N.; Storan, Melonie J.; Haines, Gemma O.; Williams, Brenda; Whitty, Genevieve A. et al. (2009): Thrombin-cleaved osteopontin regulates hemopoietic stem and progenitor cell functions through interactions with alpha9beta1 and alpha4beta1 integrins. In *Blood* 114 (1), pp. 49–59. DOI: 10.1182/blood-2009-01-197988.

Greenbaum, Adam; Hsu, Yen-Michael S.; Day, Ryan B.; Schuettpelz, Laura G.; Christopher, Matthew J.; Borgerding, Joshua N. et al. (2013): CXCL12 in early mesenchymal progenitors is required for haematopoietic stem-cell maintenance. In *Nature* 495 (7440), pp. 227–230. DOI: 10.1038/nature11926.

Grosso, Andrea; Burger, Maximilian G.; Lunger, Alexander; Schaefer, Dirk J.; Banfi, Andrea; Di Maggio, Nunzia (2017): It Takes Two to Tango: Coupling of Angiogenesis and Osteogenesis for Bone Regeneration. In *Frontiers in bioengineering and biotechnology* 5, p. 68. DOI: 10.3389/fbioe.2017.00068.

Guezguez, Borhane; Campbell, Clinton J. V.; Boyd, Allison L.; Karanu, Francis; Casado, Fanny L.; Di Cresce, Christine et al. (2013): Regional localization within the bone marrow influences the functional capacity of human HSCs. In *Cell stem cell* 13 (2), pp. 175–189. DOI: 10.1016/j.stem.2013.06.015.

Gupta, S. K.; Lysko, P. G.; Pillarisetti, K.; Ohlstein, E.; Stadel, J. M. (1998): Chemokine receptors in human endothelial cells. Functional expression of CXCR4 and its transcriptional regulation by inflammatory cytokines. In *The Journal of biological chemistry* 273 (7), pp. 4282–4287. DOI: 10.1074/jbc.273.7.4282.

Guryanova, Olga A.; Shank, Kaitlyn; Spitzer, Barbara; Luciani, Luisa; Koche, Richard P.; Garrett-Bakelman, Francine E. et al. (2016): DNMT3A mutations promote anthracycline resistance in acute myeloid leukemia via impaired nucleosome remodeling. In *Nature medicine* 22 (12), pp. 1488–1495. DOI: 10.1038/nm.4210.

Haas, Simon; Trumpp, Andreas; Milsom, Michael D. (2018): Causes and Consequences of Hematopoietic Stem Cell Heterogeneity. In *Cell stem cell* 22 (5), pp. 627–638. DOI: 10.1016/j.stem.2018.04.003.

Handly, L. Naomi; Pilko, Anna; Wollman, Roy (2015): Paracrine communication maximizes cellular response fidelity in wound signaling. In *eLife* 4, e09652. DOI: 10.7554/eLife.09652.

Hanoun, Maher; Zhang, Dachuan; Mizoguchi, Toshihide; Pinho, Sandra; Pierce, Halley; Kunisaki, Yuya et al. (2014): Acute myelogenous leukemia-induced sympathetic neuropathy promotes malignancy in an altered hematopoietic stem cell niche. In *Cell stem cell* 15 (3), pp. 365–375. DOI: 10.1016/j.stem.2014.06.020.

Harada, Kaito; Yahata, Takashi; Onizuka, Makoto; Ibrahim, Abd Aziz; Kikkawa, Eri; Miyata, Toshio; Ando, Kiyoshi (2021): Plasminogen activator inhibitor type-1 is a negative regulator of hematopoietic regeneration in the adipocyte-rich bone marrow microenvironment. In *Biochemical and biophysical research communications* 557, pp. 180–186. DOI: 10.1016/j.bbrc.2021.04.017.

Harijith, Anantha; Ebenezer, David L.; Natarajan, Viswanathan (2014): Reactive oxygen species at the crossroads of inflammasome and inflammation. In *Frontiers in physiology* 5, p. 352. DOI: 10.3389/fphys.2014.00352.

Hasegawa, Y.; Sawada, M.; Ozaki, N.; Inagaki, T.; Suzumura, A. (2000): Increased soluble tumor necrosis factor receptor levels in the serum of elderly people. In *Gerontology* 46 (4), pp. 185–188. DOI: 10.1159/000022157.

Hattori, K.; Dias, S.; Heissig, B.; Hackett, N. R.; Lyden, D.; Tateno, M. et al. (2001): Vascular endothelial growth factor and angiopoietin-1 stimulate postnatal hematopoiesis by recruitment of vasculogenic and hematopoietic stem cells. In *The Journal of experimental medicine* 193 (9), pp. 1005–1014. DOI: 10.1084/jem.193.9.1005.

Hayashi, Yasutaka; Kawabata, Kimihito C.; Tanaka, Yosuke; Uehara, Yasufumi; Mabuchi, Yo; Murakami, Koichi et al. (2022): MDS cells impair osteolineage differentiation of MSCs via extracellular vesicles to suppress normal hematopoiesis. In *Cell reports* 39 (6), p. 110805. DOI: 10.1016/j.celrep.2022.110805.

Hayden, Matthew S.; Ghosh, Sankar (2014): Regulation of NF-κB by TNF family cytokines. In *Seminars in immunology* 26 (3), pp. 253–266. DOI: 10.1016/j.smim.2014.05.004.

Hecker, Judith S.; Hartmann, Luise; Rivière, Jennifer; Buck, Michèle C.; van der Garde, Mark; Rothenberg-Thurley, Maja et al. (2021): CHIP and hips: clonal hematopoiesis is common in patients undergoing hip arthroplasty and is associated with autoimmune disease. In *Blood* 138 (18), pp. 1727–1732. DOI: 10.1182/blood.2020010163.

Hernández-Malmierca, Pablo; Vonficht, Dominik; Schnell, Alexandra; Uckelmann, Hannah J.; Bollhagen, Alina; Mahmoud, Mohamed A. A. et al. (2022): Antigen presentation

safeguards the integrity of the hematopoietic stem cell pool. In *Cell stem cell* 29 (5), 760-775.e10. DOI: 10.1016/j.stem.2022.04.007.

Hilpert, Morgane; Legrand, Céline; Bluteau, Dominique; Balayn, Natalie; Betems, Aline; Bluteau, Olivier et al. (2014): p19 INK4d controls hematopoietic stem cells in a cell-autonomous manner during genotoxic stress and through the microenvironment during aging. In *Stem Cell Reports* 3 (6), pp. 1085–1102. DOI: 10.1016/j.stemcr.2014.10.005.

Himburg, Heather A.; Muramoto, Garrett G.; Daher, Pamela; Meadows, Sarah K.; Russell, J. Lauren; Doan, Phuong et al. (2010): Pleiotrophin regulates the expansion and regeneration of hematopoietic stem cells. In *Nature medicine* 16 (4), pp. 475–482. DOI: 10.1038/nm.2119.

Himburg, Heather A.; Yan, Xiao; Doan, Phuong L.; Quarmyne, Mamle; Micewicz, Eva; McBride, William et al. (2014): Pleiotrophin mediates hematopoietic regeneration via activation of RAS. In *The Journal of clinical investigation* 124 (11), pp. 4753–4758. DOI: 10.1172/JCI76838.

Hinks, Timothy S. C. (2016): Mucosal-associated invariant T cells in autoimmunity, immune-mediated diseases and airways disease. In *Immunology* 148 (1), pp. 1–12. DOI: 10.1111/imm.12582.

Hirata, Yuichi; Furuhashi, Kazuhiro; Ishii, Hiroshi; Li, Hao Wei; Pinho, Sandra; Ding, Lei et al. (2018): CD150high Bone Marrow Tregs Maintain Hematopoietic Stem Cell Quiescence and Immune Privilege via Adenosine. In *Cell stem cell* 22 (3), 445-453.e5. DOI: 10.1016/j.stem.2018.01.017.

Ho, Ya-Hsuan; Del Toro, Raquel; Rivera-Torres, José; Rak, Justyna; Korn, Claudia; García-García, Andrés et al. (2019): Remodeling of Bone Marrow Hematopoietic Stem Cell Niches Promotes Myeloid Cell Expansion during Premature or Physiological Aging. In *Cell stem cell* 25 (3), 407-418.e6. DOI: 10.1016/j.stem.2019.06.007.

Holay, Namit; Kennedy, Barry E.; Murphy, J. Patrick; Konda, Prathyusha; Giacomantonio, Michael; Brauer-Chapin, Tatjana et al. (2022): After virus exposure, early bystander naïve CD8 T cell activation relies on NAD+ salvage metabolism. In *Frontiers in immunology* 13, p. 1047661. DOI: 10.3389/fimmu.2022.1047661.

Hsu, Joanne I.; Dayaram, Tajhal; Tovy, Ayala; Braekeleer, Etienne de; Jeong, Mira; Wang, Feng et al. (2018): PPM1D Mutations Drive Clonal Hematopoiesis in Response to Cytotoxic Chemotherapy. In *Cell stem cell* 23 (5), 700-713.e6. DOI: 10.1016/j.stem.2018.10.004.

Hu, Bo; Lv, Xiao; Chen, Hao; Xue, Peng; Gao, Bo; Wang, Xiao et al. (2020): Sensory nerves regulate mesenchymal stromal cell lineage commitment by tuning sympathetic tones. In *The Journal of clinical investigation* 130 (7), pp. 3483–3498. DOI: 10.1172/JCI131554.

Huber, Sandra; Haferlach, Torsten; Meggendorfer, Manja; Hutter, Stephan; Hoermann, Gregor; Summerer, Isolde et al. (2023): Mutations in spliceosome genes in myelodysplastic neoplasms and their association to ring sideroblasts. In *Leukemia* 37 (2), pp. 500–502. DOI: 10.1038/s41375-022-01783-y.

Inoue, Daichi; Kitaura, Jiro; Togami, Katsuhiro; Nishimura, Koutarou; Enomoto, Yutaka; Uchida, Tomoyuki et al. (2013): Myelodysplastic syndromes are induced by histone methylation–altering ASXL1 mutations. In *The Journal of clinical investigation* 123 (11), pp. 4627–4640. DOI: 10.1172/JCI70739.

Itkin, Tomer; Duarte, Delfim; Passaro, Diana (2022): Editorial: The Dynamic Interface Between Vascular Blood Vessels to Blood Forming Hematopoietic Stem Cells in Health and Disease. In *Frontiers in cell and developmental biology* 10, p. 870129. DOI: 10.3389/fcell.2022.870129.

Izzo, Franco; Lee, Stanley C.; Poran, Asaf; Chaligne, Ronan; Gaiti, Federico; Gross, Baptiste et al. (2020): DNA methylation disruption reshapes the hematopoietic differentiation landscape. In *Nature genetics* 52 (4), pp. 378–387. DOI: 10.1038/s41588-020-0595-4.

Jackson, Sharon H.; Devadas, Satish; Kwon, Jaeyul; Pinto, Ligia A.; Williams, Mark S. (2004): T cells express a phagocyte-type NADPH oxidase that is activated after T cell receptor stimulation. In *Nature immunology* 5 (8), pp. 818–827. DOI: 10.1038/ni1096.

Jackson Laboratory: Life Span as a Biomarker. Available online at https://www.jax.org/research-and-faculty/research-labs/the-harrison-lab/gerontology/life-span-as-a-biomarker, checked on 8/1/2022.

Jaiswal, Siddhartha; Natarajan, Pradeep; Silver, Alexander J.; Gibson, Christopher J.; Bick, Alexander G.; Shvartz, Eugenia et al. (2017): Clonal Hematopoiesis and Risk of Atherosclerotic Cardiovascular Disease. In *The New England journal of medicine* 377 (2), pp. 111–121. DOI: 10.1056/NEJMoa1701719.

Jin, Michelle; Nguyen, Joseph D.; Weber, Sophia J.; Mejias-Aponte, Carlos A.; Madangopal, Rajtarun; Golden, Sam A. (2019): SMART: An open source extension of WholeBrain for iDISCO+ LSFM intact mouse brain registration and segmentation.

Johnson, Ryan C.; Kurzer, Jason H.; Greenberg, Peter L.; Gratzinger, Dita (2014): Mesenchymal stromal cell density is increased in higher grade myelodysplastic syndromes and independently predicts survival. In *Am J Clin Pathol* 142 (6), pp. 795–802. DOI: 10.1309/AJCP71OPHKOTLSUG.

Jones, Robert C.; Karkanias, Jim; Krasnow, Mark A.; Pisco, Angela Oliveira; Quake, Stephen R.; Salzman, Julia et al. (2022): The Tabula Sapiens: A multiple-organ, single-cell transcriptomic atlas of humans. In *Science (New York, N.Y.)* 376 (6594), eabl4896. DOI: 10.1126/science.abl4896.

Jong, Madelon M. E. de; Kellermayer, Zoltán; Papazian, Natalie; Tahri, Sabrin; Hofste Op Bruinink, Davine; Hoogenboezem, Remco et al. (2021): The multiple myeloma microenvironment is defined by an inflammatory stromal cell landscape. In *Nature immunology* 22 (6), pp. 769–780. DOI: 10.1038/s41590-021-00931-3.

Juneja, H. S.; Schmalsteig, F. C.; Lee, S.; Chen, J. (1993): Vascular cell adhesion molecule-1 and VLA-4 are obligatory adhesion proteins in the heterotypic adherence between human leukemia/lymphoma cells and marrow stromal cells. In *Experimental hematology* 21 (3), pp. 444–450.

Kang, Jian; Brajanovski, Natalie; Chan, Keefe T.; Xuan, Jiachen; Pearson, Richard B.; Sanij, Elaine (2021): Ribosomal proteins and human diseases: molecular mechanisms and targeted therapy. In *Signal transduction and targeted therapy* 6 (1), p. 323. DOI: 10.1038/s41392-021-00728-8.

Karin, M.; Delhase, M. (2000): The I kappa B kinase (IKK) and NF-kappa B: key elements of proinflammatory signalling. In *Seminars in immunology* 12 (1), pp. 85–98. DOI: 10.1006/smim.2000.0210.

Katayama, Yoshio; Battista, Michela; Kao, Wei-Ming; Hidalgo, Andrés; Peired, Anna J.; Thomas, Steven A.; Frenette, Paul S. (2006): Signals from the sympathetic nervous

system regulate hematopoietic stem cell egress from bone marrow. In *Cell* 124 (2), pp. 407–421. DOI: 10.1016/j.cell.2005.10.041.

Kesarwani, A. K.; Ramirez, O.; Gupta, A. K.; Yang, X.; Murthy, T.; Minella, A. C.; Pillai, M. M. (2017): Cancer-associated SF3B1 mutants recognize otherwise inaccessible cryptic 3' splice sites within RNA secondary structures. In *Oncogene* 36 (8), pp. 1123–1133. DOI: 10.1038/onc.2016.279.

Khoury, Joseph D.; Solary, Eric; Abla, Oussama; Akkari, Yassmine; Alaggio, Rita; Apperley, Jane F. et al. (2022): The 5th edition of the World Health Organization Classification of Haematolymphoid Tumours: Myeloid and Histiocytic/Dendritic Neoplasms. In *Leukemia* 36 (7), pp. 1703–1719. DOI: 10.1038/s41375-022-01613-1.

Kiel, Mark J.; Yilmaz, Omer H.; Iwashita, Toshihide; Yilmaz, Osman H.; Terhorst, Cox; Morrison, Sean J. (2005): SLAM family receptors distinguish hematopoietic stem and progenitor cells and reveal endothelial niches for stem cells. In *Cell* 121 (7), pp. 1109–1121. DOI: 10.1016/j.cell.2005.05.026.

Kim, Chan Kyu; Han, Dong Hoon; Ji, Young Seok; Lee, Min Sung; Min, Chang Wook; Park, Seong Kyu et al. (2016): Biomarkers of angiogenesis as prognostic factors in myelodysplastic syndrome patients treated with hypomethylating agents. In *Leukemia research* 50, pp. 21–28. DOI: 10.1016/j.leukres.2016.08.012.

Kim, Peter Geon; Niroula, Abhishek; Shkolnik, Veronica; McConkey, Marie; Lin, Amy E.; Słabicki, Mikołaj et al. (2021): Dnmt3a-mutated clonal hematopoiesis promotes osteoporosis. In *The Journal of experimental medicine* 218 (12). DOI: 10.1084/jem.20211872.

Kondo, Hisataka; Nifuji, Akira; Takeda, Shu; Ezura, Yoichi; Rittling, Susan R.; Denhardt, David T. et al. (2005): Unloading induces osteoblastic cell suppression and osteoclastic cell activation to lead to bone loss via sympathetic nervous system. In *The Journal of biological chemistry* 280 (34), pp. 30192–30200. DOI: 10.1074/jbc.M504179200.

Kongsbak, Martin; Essen, Marina Rode von; Levring, Trine Bøegh; Schjerling, Peter; Woetmann, Anders; Ødum, Niels et al. (2014): Vitamin D-binding protein controls T cell responses to vitamin D. In *BMC immunology* 15, p. 35. DOI: 10.1186/s12865-014-0035-2.

Kook, H.; Zeng, W.; Guibin, C.; Kirby, M.; Young, N. S.; Maciejewski, J. P. (2001): Increased cytotoxic T cells with effector phenotype in aplastic anemia and myelodysplasia. In *Experimental hematology* 29 (11), pp. 1270–1277. DOI: 10.1016/s0301-472x(01)00736-6.

Kordasti, Shahram Y.; Ingram, Wendy; Hayden, Janet; Darling, David; Barber, Linda; Afzali, Behdad et al. (2007): CD4+CD25high Foxp3+ regulatory T cells in myelodysplastic syndrome (MDS). In *Blood* 110 (3), pp. 847–850. DOI: 10.1182/blood-2007-01-067546.

Kotsianidis, I.; Bouchliou, I.; Nakou, E.; Spanoudakis, E.; Margaritis, D.; Christophoridou, A. V. et al. (2009): Kinetics, function and bone marrow trafficking of CD4+CD25+FOXP3+ regulatory T cells in myelodysplastic syndromes (MDS). In *Leukemia* 23 (3), pp. 510–518. DOI: 10.1038/leu.2008.333.

Kuçi, Selim; Kuçi, Zyrafete; Schäfer, Richard; Spohn, Gabriele; Winter, Stefan; Schwab, Matthias et al. (2019): Molecular signature of human bone marrow-derived mesenchymal stromal cell subsets. In *Scientific reports* 9 (1), p. 1774. DOI: 10.1038/s41598-019-38517-7.

Kumari, Sudha; Curado, Silvia; Mayya, Viveka; Dustin, Michael L. (2014): T cell antigen receptor activation and actin cytoskeleton remodeling. In *Biochimica et biophysica acta* 1838 (2), pp. 546–556. DOI: 10.1016/j.bbamem.2013.05.004.

Kuntz, A.; Richins, C. (1945): Innervation of the bone marrow. In *The Journal of Comparative Neurology* 83 (3), pp. 213–222.

Kusumbe, Anjali P.; Ramasamy, Saravana K.; Adams, Ralf H. (2014): Coupling of angiogenesis and osteogenesis by a specific vessel subtype in bone. In *Nature* 507 (7492), pp. 323–328. DOI: 10.1038/nature13145.

Kusumbe, Anjali P.; Ramasamy, Saravana K.; Itkin, Tomer; Mäe, Maarja Andaloussi; Langen, Urs H.; Betsholtz, Christer et al. (2016): Age-dependent modulation of vascular niches for haematopoietic stem cells. In *Nature* 532 (7599), pp. 380–384. DOI: 10.1038/nature17638.

La Fuente-Granada, Marisol de; Olguín-Alor, Roxana; Ortega-Francisco, Sandra; Bonifaz, Laura C.; Soldevila, Gloria (2019): Inhibins regulate peripheral regulatory T cell induction through modulation of dendritic cell function. In *FEBS open bio* 9 (1), pp. 137–147. DOI: 10.1002/2211-5463.12555.

Lampreia, Fabio Pereira; Carmelo, Joana Gonçalves; Anjos-Afonso, Fernando (2017): Notch Signaling in the Regulation of Hematopoietic Stem Cell. In *Current Stem Cell Reports* 3 (3), pp. 202–209. DOI: 10.1007/s40778-017-0090-8.

Lara, Joshua J.; Bencomo-Alvarez, Alfonso E.; Gonzalez, Mayra A.; Olivas, Idaly M.; Young, James E.; Lopez, Jose L. et al. (2022): 19S Proteasome Subunits as Oncogenes and Prognostic Biomarkers in FLT3-Mutated Acute Myeloid Leukemia (AML). In *International journal of molecular sciences* 23 (23). DOI: 10.3390/ijms232314586.

Lee, Jungwoon; Yoon, Suk Ran; Choi, Inpyo; Jung, Haiyoung (2019): Causes and Mechanisms of Hematopoietic Stem Cell Aging. In *International journal of molecular sciences* 20 (6). DOI: 10.3390/ijms20061272.

Lee, Stanley Chun-Wei; North, Khrystyna; Kim, Eunhee; Jang, Eunjung; Obeng, Esther; Lu, Sydney X. et al. (2018): Synthetic Lethal and Convergent Biological Effects of Cancer-Associated Spliceosomal Gene Mutations. In *Cancer cell* 34 (2), 225-241.e8. DOI: 10.1016/j.ccell.2018.07.003.

Lee-Thedieck, Cornelia; Schertl, Peter; Klein, Gerd (2022): The extracellular matrix of hematopoietic stem cell niches. In *Advanced drug delivery reviews* 181, p. 114069. DOI: 10.1016/j.addr.2021.114069.

Legros, Laurence; Slama, Bohrane; Karsenti, Jean-Michel; Vey, Norbert; Natarajan-Amé, Shanti; Watel, Eric et al. (2012): Treatment of myelodysplastic syndromes with excess of blasts by bevacizumab is well tolerated and is associated with a decrease of VEGF plasma level. In *Annals of Hematology* 91 (1), pp. 39–46. DOI: 10.1007/s00277-011-1242-z.

Leimkühler, Nils B.; Gleitz, Hélène F. E.; Ronghui, Li; Snoeren, Inge A. M.; Fuchs, Stijn N. R.; Nagai, James S. et al. (2020): Heterogeneous bone-marrow stromal progenitors drive myelofibrosis via a druggable alarmin axis. In *Cell stem cell*. DOI: 10.1016/j.stem.2020.11.004.

Leimkühler, Nils B.; Schneider, Rebekka K. (2019): Inflammatory bone marrow microenvironment. In *Hematology: the American Society of Hematology Education Program* 2019 (1), pp. 294–302. DOI: 10.1182/hematology.2019000045.

Li, Hongzhe; Bräunig, Sandro; Dhapolar, Parashar; Karlsson, Göran; Lang, Stefan; Scheding, Stefan (2023): Identification of phenotypically, functionally, and anatomically distinct stromal niche populations in human bone marrow based on single-cell RNA sequencing. In *eLife* 12. DOI: 10.7554/eLife.81656.

Li, Jing; Yue, Lanzhu; Wang, Huaquan; Liu, Chunyan; Liu, Hui; Tao, Jinglian et al. (2016): Th17 Cells Exhibit Antitumor Effects in MDS Possibly through Augmenting Functions of CD8+ T Cells. In *Journal of immunology research* 2016, p. 9404705. DOI: 10.1155/2016/9404705.

Li, Yujue; Meng, Yang; Yu, Xijie (2019): The Unique Metabolic Characteristics of Bone Marrow Adipose Tissue. In *Frontiers in endocrinology* 10, p. 69. DOI: 10.3389/fendo.2019.00069.

Liao, Min; Chen, Ruiqing; Yang, Yang; He, Hanqing; Xu, Liqian; Jiang, Yuxuan et al. (2022): Aging-elevated inflammation promotes DNMT3A R878H-driven clonal hematopoiesis. In *Acta pharmaceutica Sinica. B* 12 (2), pp. 678–691. DOI: 10.1016/j.apsb.2021.09.015.

Libby, Peter; Sidlow, Robert; Lin, Amy E.; Gupta, Dipti; Jones, Lee W.; Moslehi, Javid et al. (2019): Clonal Hematopoiesis: Crossroads of Aging, Cardiovascular Disease, and Cancer: JACC Review Topic of the Week. In *Journal of the American College of Cardiology* 74 (4), pp. 567–577. DOI: 10.1016/j.jacc.2019.06.007.

List, Alan; Kurtin, Sandy; Roe, Denise J.; Buresh, Andrew; Mahadevan, Daruka; Fuchs, Deborah et al. (2005): Efficacy of lenalidomide in myelodysplastic syndromes. In *The New England journal of medicine* 352 (6), pp. 549–557. DOI: 10.1056/NEJMoa041668.

Liu, Qiuli; Zheng, Haiqing; Chen, Xiaoyong; Peng, Yanwen; Huang, Weijun; Li, Xiaobo et al. (2015): Human mesenchymal stromal cells enhance the immunomodulatory function of CD8(+)CD28(-) regulatory T cells. In *Cellular & molecular immunology* 12 (6), pp. 708–718. DOI: 10.1038/cmi.2014.118.

Liu, Ting; Zhang, Lingyun; Joo, Donghyun; Sun, Shao-Cong (2017): NF-κB signaling in inflammation. In *Signal transduction and targeted therapy* 2, 17023-. DOI: 10.1038/sigtrans.2017.23.

Loberg, Matthew A.; Bell, Rebecca K.; Goodwin, Leslie O.; Eudy, Elizabeth; Miles, Linde A.; SanMiguel, Jennifer M. et al. (2019): Sequentially inducible mouse models reveal that Npm1 mutation causes malignant transformation of Dnmt3a-mutant clonal hematopoiesis. In *Leukemia* 33 (7), pp. 1635–1649. DOI: 10.1038/s41375-018-0368-6.

Lochner, Matthias; Berod, Luciana; Sparwasser, Tim (2015): Fatty acid metabolism in the regulation of T cell function. In *Trends in immunology* 36 (2), pp. 81–91. DOI: 10.1016/j.it.2014.12.005.

Longo, Dan L. (2008): Bone Marrow in Aging: Changes? Yes; Clinical Malfunction? Not So Clear. In *Blood* 112 (11), sci-1-sci-1. DOI: 10.1182/blood.V112.11.sci-1.sci-1.

López-Otín, Carlos; Blasco, Maria A.; Partridge, Linda; Serrano, Manuel; Kroemer, Guido (2013): The hallmarks of aging. In *Cell* 153 (6), pp. 1194–1217. DOI: 10.1016/j.cell.2013.05.039.

Ma, Jian; Wang, Ruiqing; Fang, Xianfeng; Sun, Zuoming (2012): β-catenin/TCF-1 pathway in T cell development and differentiation. In *Journal of neuroimmune pharmacology : the official journal of the Society on NeuroImmune Pharmacology* 7 (4), pp. 750–762. DOI: 10.1007/s11481-012-9367-y.

Ma, Xiaomei (2012): Epidemiology of myelodysplastic syndromes. In *The American journal of medicine* 125 (7 Suppl), S2-5. DOI: 10.1016/j.amjmed.2012.04.014.

Macaulay, Iain C.; Svensson, Valentine; Labalette, Charlotte; Ferreira, Lauren; Hamey, Fiona; Voet, Thierry et al. (2016): Single-Cell RNA-Sequencing Reveals a Continuous Spectrum of Differentiation in Hematopoietic Cells. In *Cell reports* 14 (4), pp. 966–977. DOI: 10.1016/j.celrep.2015.12.082.

Magalhaes, Isabelle; Pingris, Karine; Poitou, Christine; Bessoles, Stéphanie; Venteclef, Nicolas; Kiaf, Badr et al. (2015): Mucosal-associated invariant T cell alterations in obese and type 2 diabetic patients. In *The Journal of clinical investigation* 125 (4), pp. 1752–1762. DOI: 10.1172/JCI78941.

Malcovati, Luca; Stevenson, Kristen; Papaemmanuil, Elli; Neuberg, Donna; Bejar, Rafael; Boultwood, Jacqueline et al. (2020): SF3B1-mutant MDS as a distinct disease subtype: a proposal from the International Working Group for the Prognosis of MDS. In *Blood* 136 (2), pp. 157–170. DOI: 10.1182/blood.2020004850.

Mangi, M. H.; Salisbury, J. R.; Mufti, G. J. (1991): Abnormal localization of immature precursors (ALIP) in the bone marrow of myelodysplastic syndromes: current state of knowledge and future directions. In *Leukemia research* 15 (7), pp. 627–639. DOI: 10.1016/0145-2126(91)90032-o.

Marnell, Christopher S.; Bick, Alexander; Natarajan, Pradeep (2021): Clonal hematopoiesis of indeterminate potential (CHIP): Linking somatic mutations, hematopoiesis, chronic inflammation and cardiovascular disease. In *Journal of molecular and cellular cardiology* 161, pp. 98–105. DOI: 10.1016/j.yjmcc.2021.07.004.

Maryanovich, Maria; Zahalka, Ali H.; Pierce, Halley; Pinho, Sandra; Nakahara, Fumio; Asada, Noboru et al. (2018): Adrenergic nerve degeneration in bone marrow drives aging of the hematopoietic stem cell niche. In *Nature medicine* 24 (6), pp. 782–791. DOI: 10.1038/s41591-018-0030-x.

Matsuzaki, Yumi; Mabuchi, Yo; Okano, Hideyuki (2014): Leptin receptor makes its mark on MSCs. In *Cell stem cell* 15 (2), pp. 112–114. DOI: 10.1016/j.stem.2014.07.001.

Matteini, Francesca; Mulaw, Medhanie A.; Florian, M. Carolina (2021): Aging of the Hematopoietic Stem Cell Niche: New Tools to Answer an Old Question. In *Front. Immunol.* 12, p. 738204. DOI: 10.3389/fimmu.2021.738204.

Matthews, Elloise; Lanham, Stuart; White, Kate; Kyriazi, Maria-Eleni; Alexaki, Konstantina; El-Sagheer, Afaf H. et al. (2020): Single cell RNA sequence analysis of human bone marrow samples reveals new targets for isolation of skeletal stem cells using DNA-coated gold nanoparticles (preprint).

Mattiucci, Domenico; Maurizi, Giulia; Izzi, Valerio; Cenci, Lorenzo; Ciarlantini, Marco; Mancini, Stefania et al. (2018): Bone marrow adipocytes support hematopoietic stem cell survival. In *Journal of cellular physiology* 233 (2), pp. 1500–1511. DOI: 10.1002/jcp.26037.

Medyouf, Hind; Mossner, Maximilian; Jann, Johann-Christoph; Nolte, Florian; Raffel, Simon; Herrmann, Carl et al. (2014): Myelodysplastic cells in patients reprogram mesenchymal stromal cells to establish a transplantable stem cell niche disease unit. In *Cell stem cell* 14 (6), pp. 824–837. DOI: 10.1016/j.stem.2014.02.014.

Meggendorfer, Manja; Roller, Andreas; Haferlach, Torsten; Eder, Christiane; Dicker, Frank; Grossmann, Vera et al. (2012): SRSF2 mutations in 275 cases with chronic

myelomonocytic leukemia (CMML). In *Blood* 120 (15), pp. 3080–3088. DOI: 10.1182/blood-2012-01-404863.

Mende, Nicole; Bastos, Hugo P.; Santoro, Antonella; Sham, Kendig; Mahbubani, Krishnaa T.; Curd, Abbie et al. (2020): Quantitative and molecular differences distinguish adult human medullary and extramedullary haematopoietic stem and progenitor cell landscapes.

Méndez-Ferrer, Simón; Lucas, Daniel; Battista, Michela; Frenette, Paul S. (2008): Haematopoietic stem cell release is regulated by circadian oscillations. In *Nature* 452 (7186), pp. 442–447. DOI: 10.1038/nature06685.

Meza-León, Berenice; Gratzinger, Dita; Aguilar-Navarro, Alicia G.; Juárez-Aguilar, Fany G.; Rebel, Vivienne I.; Torlakovic, Emina et al. (2021): Human, mouse, and dog bone marrow show similar mesenchymal stromal cells within a distinctive microenvironment. In *Experimental hematology* 100, pp. 41–51. DOI: 10.1016/j.exphem.2021.06.006.

Mian, Syed A.; Philippe, Céline; Maniati, Eleni; Protopapa, Pantelitsa; Bergot, Tiffany; Piganeau, Marion et al. (2023): Vitamin B5 and succinyl-CoA improve ineffective erythropoiesis in SF3B1-mutated myelodysplasia. In *Science translational medicine* 15 (685), eabn5135. DOI: 10.1126/scitranslmed.abn5135.

Mian, Syed A.; Rouault-Pierre, Kevin; Smith, Alexander E.; Seidl, Thomas; Pizzitola, Irene; Kizilors, Aytug et al. (2015): SF3B1 mutant MDS-initiating cells may arise from the haematopoietic stem cell compartment. In *Nature communications* 6, p. 10004. DOI: 10.1038/ncomms10004.

Midic, Danica; Rinke, Jenny; Perner, Florian; Müller, Violetta; Hinze, Anna; Pester, Frank et al. (2020): Prevalence and dynamics of clonal hematopoiesis caused by leukemia-associated mutations in elderly individuals without hematologic disorders. In *Leukemia* 34 (8), pp. 2198–2205. DOI: 10.1038/s41375-020-0869-y.

Ming Hong; Guangsheng He (2017): The 2016 Revision to the World Health Organization Classification of Myelodysplastic Syndromes. In *Journal of Translational Internal Medicine* 5 (3), p. 139. DOI: 10.1515/jtim-2017-0002.

Mitchell, Carl A.; Verovskaya, Evgenia V.; Calero-Nieto, Fernando J.; Olson, Oakley C.; Swann, James W.; Wang, Xiaonan et al. (2023): Stromal niche inflammation mediated by IL-1 signalling is a targetable driver of haematopoietic ageing. In *Nature cell biology* 25 (1), pp. 30–41. DOI: 10.1038/s41556-022-01053-0.

Mo, Chunyang; Guo, Jingxin; Qin, Jiachen; Zhang, Xiaoying; Sun, Yuxi; Wei, Hanjing et al. (2021): Single-cell transcriptomics of LepR-positive skeletal cells reveals heterogeneous stress-dependent stem and progenitor pools. In *The EMBO Journal* 41 (4). DOI: 10.15252/embj.2021108415.

Monaco, Gianni; Lee, Bernett; Xu, Weili; Mustafah, Seri; Hwang, You Yi; Carré, Christophe et al. (2019): RNA-Seq Signatures Normalized by mRNA Abundance Allow Absolute Deconvolution of Human Immune Cell Types. In *Cell reports* 26 (6), 1627-1640.e7. DOI: 10.1016/j.celrep.2019.01.041.

Moon, Hee-Won; Kim, Bo Hyun; Park, Chul Min; Hur, Mina; Yun, Yeo-Min; Kim, Sung-Yong; Lee, Mark Hong (2011): CD4+CD25highFoxP3+ regulatory T-cells in hematologic diseases. In *The Korean journal of laboratory medicine* 31 (4), pp. 231–237. DOI: 10.3343/kjlm.2011.31.4.231.

Muraro, Mauro J.; Dharmadhikari, Gitanjali; Grün, Dominic; Groen, Nathalie; Dielen, Tim; Jansen, Erik et al. (2016): A Single-Cell Transcriptome Atlas of the Human Pancreas. In *Cell systems* 3 (4), 385-394.e3. DOI: 10.1016/j.cels.2016.09.002.

Napier, Ruth J.; Adams, Erin J.; Gold, Marielle C.; Lewinsohn, David M. (2015): The Role of Mucosal Associated Invariant T Cells in Antimicrobial Immunity. In *Frontiers in immunology* 6, p. 344. DOI: 10.3389/fimmu.2015.00344.

Nath, Anamika; Chattopadhya, Sreya; Chattopadhyay, Utpala; Sharma, Nawal K. (2006): Macrophage inflammatory protein (MIP)1alpha and MIP1beta differentially regulate release of inflammatory cytokines and generation of tumoricidal monocytes in malignancy. In *Cancer immunology, immunotherapy : CII* 55 (12), pp. 1534–1541. DOI: 10.1007/s00262-006-0149-3.

Nguyen, Tuong-Vi; Yao, Shihua; Wang, Yahong; Rolfe, Alan; Selvaraj, Anand; Darman, Rachel et al. (2019): The R882H DNMT3A hot spot mutation stabilizes the formation of large DNMT3A oligomers with low DNA methyltransferase activity. In *The Journal of biological chemistry* 294 (45), pp. 16966–16977. DOI: 10.1074/jbc.RA119.010126.

Nguyen, Yen T. M.; Fujisawa, Manabu; Nguyen, Tran B.; Suehara, Yasuhito; Sakamoto, Tatsuhiro; Matsuoka, Ryota et al. (2021): Tet2 deficiency in immune cells exacerbates tumor progression by increasing angiogenesis in a lung cancer model. In *Cancer Science* 112 (12), pp. 4931–4943. DOI: 10.1111/cas.15165.

Nian, Qing; Li, Jingwei; Han, ZhongYu; Liang, Qi; Liu, Maoyu; Yang, Chan et al. (2022): SPARC in hematologic malignancies and novel technique for hematological disease with its abnormal expression. In *Biomedicine & pharmacotherapy = Biomedecine & pharmacotherapie* 153, p. 113519. DOI: 10.1016/j.biopha.2022.113519.

Nicholls, Jemma; Cao, Benjamin; Le Texier, Laetitia; Xiong, Laura Yan; Hunter, Christopher R.; Llanes, Genesis et al. (2021): Bone Marrow Regulatory T Cells Are a Unique Population, Supported by Niche-Specific Cytokines and Plasmacytoid Dendritic Cells, and Required for Chronic Graft-Versus-Host Disease Control. In *Frontiers in cell and developmental biology* 9, p. 737880. DOI: 10.3389/fcell.2021.737880.

Nie, Yuchun; Han, Yoon-Chi; Zou, Yong-Rui (2008): CXCR4 is required for the quiescence of primitive hematopoietic cells. In *The Journal of experimental medicine* 205 (4), pp. 777–783. DOI: 10.1084/jem.20072513.

Niedźwiecki, M.; Budziło, O.; Zieliński, M.; Adamkiewicz-Drożyńska, E.; Maciejka-Kembłowska, L.; Szczepański, T.; Trzonkowski, P. (2018): CD4+CD25highCD127low/-FoxP3+ Regulatory T Cell Subpopulations in the Bone Marrow and Peripheral Blood of Children with ALL: Brief Report. In *Journal of immunology research* 2018, p. 1292404. DOI: 10.1155/2018/1292404.

Oetjen, Karolyn A.; Bender, Diane E.; Ruzinova, Marianna B.; Fisher, Daniel A.C.; Oh, Stephen T.; Link, Daniel C. (2020): Imaging Mass Cytometry Reveals the Spatial Architecture of Myelodysplastic Syndromes and Secondary Acute Myeloid Leukemias. In *Blood* 136 (Supplement 1), pp. 44–45. DOI: 10.1182/blood-2020-142238.

Oetjen, Karolyn A.; Bender, Diane E.; Ruzinova, Marianna B.; Oh, Stephen T.; Link, Daniel C. (2019): Interrogating the Spatial Architecture of Human Bone Marrow Via Imaging Mass Cytometry. In *Blood* 134 (Supplement_1), p. 3728. DOI: 10.1182/blood-2019-127460.

Okano, Masaki; Bell, Daphne W.; Haber, Daniel A.; Li, En (1999): DNA Methyltransferases Dnmt3a and Dnmt3b Are Essential for De Novo Methylation and Mammalian Development. In *Cell* 99 (3), pp. 247–257. DOI: 10.1016/S0092-8674(00)81656-6.

Papa, Luena; Djedaini, Mansour; Hoffman, Ronald (2019): Mitochondrial Role in Stemness and Differentiation of Hematopoietic Stem Cells. In *Stem cells international* 2019, p. 4067162. DOI: 10.1155/2019/4067162.

Parmentier, Stefani; Kramer, Michael; Weller, Swetlana; Schuler, Ulrich; Ordemann, Rainer; Rall, Gabi et al. (2020): Reevaluation of reference values for bone marrow differential counts in 236 healthy bone marrow donors. In *Annals of Hematology* 99 (12), pp. 2723–2729. DOI: 10.1007/s00277-020-04255-4.

Pauken, Kristen E.; Shahid, Osmaan; Lagattuta, Kaitlyn A.; Mahuron, Kelly M.; Luber, Jacob M.; Lowe, Margaret M. et al. (2021): Single-cell analyses identify circulating anti-tumor CD8 T cells and markers for their enrichment. In *The Journal of experimental medicine* 218 (4). DOI: 10.1084/jem.20200920.

Peng, Xiaohuan; Zhu, Xiaofeng; Di, Tianning; Tang, Futian; Guo, Xiaojia; Liu, Yang et al. (2022): The yin-yang of immunity: Immune dysregulation in myelodysplastic syndrome with different risk stratification. In *Frontiers in immunology* 13, p. 994053. DOI: 10.3389/fimmu.2022.994053.

Peng, Yi; Wu, Song; Li, Yusheng; Crane, Janet L. (2020): Type H blood vessels in bone modeling and remodeling. In *Theranostics* 10 (1), pp. 426–436. DOI: 10.7150/thno.34126.

Petraglia, F.; Sacerdote, P.; Cossarizza, A.; Angioni, S.; Genazzani, A. D.; Franceschi, C. et al. (1991): Inhibin and activin modulate human monocyte chemotaxis and human lymphocyte interferon-gamma production. In *The Journal of clinical endocrinology and metabolism* 72 (2), pp. 496–502. DOI: 10.1210/jcem-72-2-496.

Pietras, Eric M. (2017): Inflammation: a key regulator of hematopoietic stem cell fate in health and disease. In *Blood* 130 (15), pp. 1693–1698. DOI: 10.1182/blood-2017-06-780882.

Pinho, Sandra; Frenette, Paul S. (2019): Haematopoietic stem cell activity and interactions with the niche. In *Nature reviews. Molecular cell biology* 20 (5), pp. 303–320. DOI: 10.1038/s41580-019-0103-9.

Pollyea, Daniel A.; Kim, Hyun Min; Stevens, Brett M.; Lee, Frank Fang-Yao; Harris, Chelsea; Hedin, Brenna R. et al. (2021): MDS-associated SF3B1 mutations enhance proinflammatory gene expression in patient blast cells. In *Journal of leukocyte biology* 110 (1), pp. 197–205. DOI: 10.1002/JLB.6AB0520-318RR.

Poulos, Michael G.; Ramalingam, Pradeep; Gutkin, Michael C.; Llanos, Pierre; Gilleran, Katherine; Rabbany, Sina Y.; Butler, Jason M. (2017): Endothelial transplantation rejuvenates aged hematopoietic stem cell function. In *The Journal of clinical investigation* 127 (11), pp. 4163–4178. DOI: 10.1172/JCI93940.

Pruneri, G.; Bertolini, F.; Soligo, D.; Carboni, N.; Cortelezzi, A.; Ferrucci, P. F. et al. (1999): Angiogenesis in myelodysplastic syndromes. In *British journal of cancer* 81 (8), pp. 1398–1401. DOI: 10.1038/sj.bjc.6693515.

Pülhorn, Heinke; Herrmann, Martin; Harms, Harry; Jung, Andreas; Baumann, Irith (2012): Apoptotic cells and clonally expanded cytotoxic T cells in bone marrow trephines of

patients with myelodysplastic syndrome. In *Histopathology* 61 (2), pp. 200–211. DOI: 10.1111/j.1365-2559.2012.04209.x.

Qian, Junbin; Olbrecht, Siel; Boeckx, Bram; Vos, Hanne; Laoui, Damya; Etlioglu, Emre et al. (2020): A pan-cancer blueprint of the heterogeneous tumor microenvironment revealed by single-cell profiling. In *Cell research* 30 (9), pp. 745–762. DOI: 10.1038/s41422-020-0355-0.

Quirici, Nadia; Soligo, Davide; Bossolasco, Patrizia; Servida, Federica; Lumini, Cristina; Deliliers, Giorgio Lambertenghi (2002): Isolation of bone marrow mesenchymal stem cells by anti-nerve growth factor receptor antibodies. In *Experimental hematology* 30 (7), pp. 783–791. DOI: 10.1016/s0301-472x(02)00812-3.

Raaijmakers, Marc H. G. P.; Mukherjee, Siddhartha; Guo, Shangqin; Zhang, Siyi; Kobayashi, Tatsuya; Schoonmaker, Jesse A. et al. (2010): Bone progenitor dysfunction induces myelodysplasia and secondary leukaemia. In *Nature* 464 (7290), pp. 852–857. DOI: 10.1038/nature08851.

Ranzoni, Anna Maria; Tangherloni, Andrea; Berest, Ivan; Riva, Simone Giovanni; Myers, Brynelle; Strzelecka, Paulina M. et al. (2021): Integrative Single-Cell RNA-Seq and ATAC-Seq Analysis of Human Developmental Hematopoiesis. In *Cell stem cell* 28 (3), 472-487.e7. DOI: 10.1016/j.stem.2020.11.015.

Rasmussen, Hannah K.; Wong, Frankie; Tate, Tiffany; Scadden, David T.; Hoggatt, Jonathan (2015): Oncostatin M Enhances Hematopoietic Stem Cell Homing and Engraftment. In *Blood* 126 (23), p. 31. DOI: 10.1182/blood.V126.23.31.31.

Reber, Laurent; Da Silva, Carla A.; Frossard, Nelly (2006): Stem cell factor and its receptor c-Kit as targets for inflammatory diseases. In *European journal of pharmacology* 533 (1-3), pp. 327–340. DOI: 10.1016/j.ejphar.2005.12.067.

Rinker, Elizabeth B.; Dueber, Julie C.; Qualtieri, Julianne; Tedesco, Jason; Erdogan, Begum; Bosompem, Amma; Kim, Annette S. (2016): Differential expression of ribosomal proteins in myelodysplastic syndromes. In *Journal of clinical pathology* 69 (2), pp. 176–180. DOI: 10.1136/jclinpath-2015-203093.

Rivera, Lee B.; Bradshaw, Amy D.; Brekken, Rolf A. (2011): The regulatory function of SPARC in vascular biology. In *Cellular and molecular life sciences : CMLS* 68 (19), pp. 3165–3173. DOI: 10.1007/s00018-011-0781-8.

Roversi, Fernanda Marconi; Bueno, Maura Lima Pereira; Pericole, Fernando Viera; Saad, Sara Teresinha Olalla (2021): Hematopoietic Cell Kinase (HCK) Is a Player of the Crosstalk Between Hematopoietic Cells and Bone Marrow Niche Through CXCL12/CXCR4 Axis. In *Frontiers in cell and developmental biology* 9, p. 634044. DOI: 10.3389/fcell.2021.634044.

Russler-Germain, David A.; Spencer, David H.; Young, Margaret A.; Lamprecht, Tamara L.; Miller, Christopher A.; Fulton, Robert et al. (2014): The R882H DNMT3A mutation associated with AML dominantly inhibits wild-type DNMT3A by blocking its ability to form active tetramers. In *Cancer cell* 25 (4), pp. 442–454. DOI: 10.1016/j.ccr.2014.02.010.

Sage, H. (1986): Culture shock. Selective uptake and rapid release of a novel serum protein by endothelial cells in vitro. In *The Journal of biological chemistry* 261 (15), pp. 7082–7092.

Sage, H.; Johnson, C.; Bornstein, P. (1984): Characterization of a novel serum albumin-binding glycoprotein secreted by endothelial cells in culture. In *The Journal of biological chemistry* 259 (6), pp. 3993–4007.

SanMiguel, Jennifer M.; Young, Kira; Trowbridge, Jennifer J. (2020): Hand in hand: intrinsic and extrinsic drivers of aging and clonal hematopoiesis. In *Experimental hematology* 91, pp. 1–9. DOI: 10.1016/j.exphem.2020.09.197.

Santini, Valeria (2016): Treatment of low-risk myelodysplastic syndromes. In *Hematology: the American Society of Hematology Education Program* 2016 (1), pp. 462–469. DOI: 10.1182/asheducation-2016.1.462.

Schofield, R. (1978): The relationship between the spleen colony-forming cell and the haemopoietic stem cell. In *Blood cells* 4 (1-2), pp. 7–25.

Schürch, Christian M.; Riether, Carsten; Ochsenbein, Adrian F. (2014): Cytotoxic CD8+ T cells stimulate hematopoietic progenitors by promoting cytokine release from bone marrow mesenchymal stromal cells. In *Cell stem cell* 14 (4), pp. 460–472. DOI: 10.1016/j.stem.2014.01.002.

Sekeres, Mikkael A.; Taylor, Justin (2022): Diagnosis and Treatment of Myelodysplastic Syndromes: A Review. In *JAMA* 328 (9), pp. 872–880. DOI: 10.1001/jama.2022.14578.

Serriari, N-E; Eoche, M.; Lamotte, L.; Lion, J.; Fumery, M.; Marcelo, P. et al. (2014): Innate mucosal-associated invariant T (MAIT) cells are activated in inflammatory bowel diseases. In *Clinical and experimental immunology* 176 (2), pp. 266–274. DOI: 10.1111/cei.12277.

Shahi, Payam; Kim, Samuel C.; Haliburton, John R.; Gartner, Zev J.; Abate, Adam R. (2017): Abseq: Ultrahigh-throughput single cell protein profiling with droplet microfluidic barcoding. In *Sci Rep* 7 (1). DOI: 10.1038/srep44447.

Shi, Lei; Zhao, Youshan; Fei, Chengming; Guo, Juan; Jia, Yan; Wu, Dong et al. (2019): Cellular senescence induced by S100A9 in mesenchymal stromal cells through NLRP3 inflammasome activation. In *Aging (Albany NY)* 11 (21), pp. 9626–9642. DOI: 10.18632/aging.102409.

Singh, Amit; Veeriah, Vimal; Xi, Pengjun; Labella, Rossella; Chen, Junyu; Romeo, Sara G. et al. (2019): Angiocrine signals regulate quiescence and therapy resistance in bone metastasis. In *JCI insight* 4 (13). DOI: 10.1172/jci.insight.125679.

Singh, Pratibha; Mohammad, Khalid S.; Pelus, Louis M. (2020): CXCR4 expression in the bone marrow microenvironment is required for hematopoietic stem and progenitor cell maintenance and early hematopoietic regeneration after myeloablation. In *Stem cells (Dayton, Ohio)* 38 (7), pp. 849–859. DOI: 10.1002/stem.3174.

Sivaraj, Kishor K.; Adams, Ralf H. (2016): Blood vessel formation and function in bone. In *Development (Cambridge, England)* 143 (15), pp. 2706–2715. DOI: 10.1242/dev.136861.

Smith, Molly A.; Choudhary, Gaurav S.; Pellagatti, Andrea; Choi, Kwangmin; Bolanos, Lyndsey C.; Bhagat, Tushar D. et al. (2019): U2AF1 mutations induce oncogenic IRAK4 isoforms and activate innate immune pathways in myeloid malignancies. In *Nature cell biology* 21 (5), pp. 640–650. DOI: 10.1038/s41556-019-0314-5.

Solomou, Elena E.; Tsanaktsi, A.; Fertakis, V.; Dallas, K.; Karambina, S.; Tiniakou, M. et al. (2008): Overexpansion of Th17 and Th1/17 Cells in Patients with Myelodysplastic Syndrome. In *Blood* 112 (11), p. 2698. DOI: 10.1182/blood.V112.11.2698.2698.

Stalmann, Ursula S. A.; Banjanin, Bella; Snoeren, Inge A. M.; Nagai, James S.; Leimkühler, Nils B.; Li, Ronghui et al. (2022): Single-cell analysis of cultured bone marrow stromal cells reveals high similarity to fibroblasts in situ. In *Experimental hematology* 110, pp. 28–33. DOI: 10.1016/j.exphem.2022.03.010.

Steensma, David P. (2018): Myelodysplastic syndromes current treatment algorithm 2018. In *Blood cancer journal* 8 (5), p. 47. DOI: 10.1038/s41408-018-0085-4.

Steensma, David P.; Bejar, Rafael; Jaiswal, Siddhartha; Lindsley, R. Coleman; Sekeres, Mikkael A.; Hasserjian, Robert P.; Ebert, Benjamin L. (2015): Clonal hematopoiesis of indeterminate potential and its distinction from myelodysplastic syndromes. In *Blood* 126 (1), pp. 9–16. DOI: 10.1182/blood-2015-03-631747.

Storan, Melonie J.; Heazlewood, Shen Y.; Heazlewood, Chad K.; Haylock, David N.; Alexander, Warren S.; Neaves, Rebecca J. et al. (2015): Brief Report: Factors Released by Megakaryocytes Thrombin Cleave Osteopontin to Negatively Regulate Hematopoietic Stem Cells. In *Stem cells (Dayton, Ohio)* 33 (7), pp. 2351–2357. DOI: 10.1002/stem.2038.

Stucker, Sina; Chen, Junyu; Watt, Fiona E.; Kusumbe, Anjali P. (2020): Bone Angiogenesis and Vascular Niche Remodeling in Stress, Aging, and Diseases. In *Frontiers in cell and developmental biology* 8, p. 602269. DOI: 10.3389/fcell.2020.602269.

Suda, Toshio; Takubo, Keiyo; Semenza, Gregg L. (2011): Metabolic regulation of hematopoietic stem cells in the hypoxic niche. In *Cell stem cell* 9 (4), pp. 298–310. DOI: 10.1016/j.stem.2011.09.010.

Sun, Shu; Jin, Chen; Si, Jia; Lei, Ying; Chen, Kunying; Cui, Yueli et al. (2021): Single-cell analysis of ploidy and the transcriptome reveals functional and spatial divergency in murine megakaryopoiesis. In *Blood* 138 (14), pp. 1211–1224. DOI: 10.1182/blood.2021010697.

Szilard, L. (1959): ON THE NATURE OF THE AGING PROCESS. In *Proceedings of the National Academy of Sciences of the United States of America* 45 (1), pp. 30–45. DOI: 10.1073/pnas.45.1.30.

Tao, Jinglian; Li, Lijuan; Wang, Yingshuai; Fu, Rong; Wang, Huaquan; Shao, Zonghong (2016): Increased TIM3+CD8+T cells in Myelodysplastic Syndrome patients displayed less perforin and granzyme B secretion and higher CD95 expression. In *Leukemia research* 51, pp. 49–55. DOI: 10.1016/j.leukres.2016.11.003.

Tavassoli, M.; Aoki, M. (1989): Localization of megakaryocytes in the bone marrow. In *Blood cells* 15 (1), pp. 3–14.

Thol, Felicitas; Kade, Sofia; Schlarmann, Carola; Löffeld, Patrick; Morgan, Michael; Krauter, Jürgen et al. (2012): Frequency and prognostic impact of mutations in SRSF2, U2AF1, and ZRSR2 in patients with myelodysplastic syndromes. In *Blood* 119 (15), pp. 3578–3584. DOI: 10.1182/blood-2011-12-399337.

Thurston, Gavin (2002): Complementary actions of VEGF and angiopoietin-1 on blood vessel growth and leakage. In *Journal of Anatomy* 200 (6), pp. 575–580. DOI: 10.1046/j.1469-7580.2002.00061.x.

Tikhonova, Anastasia N.; Aifantis, Iannis (2021): Pain-sensing neurons mobilize blood stem cells from bone marrow. In *Nature* 589 (7843), pp. 520–521. DOI: 10.1038/d41586-020-03577-7.

Tikhonova, Anastasia N.; Dolgalev, Igor; Hu, Hai; Sivaraj, Kishor K.; Hoxha, Edlira; Cuesta-Domínguez, Álvaro et al. (2019): The bone marrow microenvironment at single-cell resolution. In *Nature* 569 (7755), pp. 222–228. DOI: 10.1038/s41586-019-1104-8.

Tormin, Ariane; Li, Ou; Walsh, Stuart; Ehinger, Mats; Brune, Jan Claas; Scheding, Stefan (2009): CD146 Expression in Primary Bone Marrow MSC Progenitor/Stem Cells Is Dependent On Their In Vivo Location. In *Blood* 114 (22), p. 251. DOI: 10.1182/blood.V114.22.251.251.

Tosato, Giovanna; Feng, Jing-Xin; Ohnuki, Hidetaka; Sim, Minji (2021): Bone marrow niches in myelodysplastic syndromes. In *Journal of cancer metastasis and treatment* 7. DOI: 10.20517/2394-4722.2021.120.

Toubal, Amine; Nel, Isabelle; Lotersztajn, Sophie; Lehuen, Agnès (2019): Mucosal-associated invariant T cells and disease. In *Nat Rev Immunol* 19 (10), pp. 643–657. DOI: 10.1038/s41577-019-0191-y.

Tratwal, Josefine; Rojas-Sutterlin, Shanti; Bataclan, Charles; Blum, Sabine; Naveiras, Olaia (2021): Bone marrow adiposity and the hematopoietic niche: A historical perspective of reciprocity, heterogeneity, and lineage commitment. In *Best practice & research. Clinical endocrinology & metabolism* 35 (4), p. 101564. DOI: 10.1016/j.beem.2021.101564.

Travlos, Gregory S. (2006): Normal structure, function, and histology of the bone marrow. In *Toxicologic pathology* 34 (5), pp. 548–565. DOI: 10.1080/01926230600939856.

Tricot, G.; Wolf-Peeters, C. de; Hendrickx, B.; Verwilghen, R. L. (1984): Bone marrow histology in myelodysplastic syndromes. I. Histological findings in myelodysplastic syndromes and comparison with bone marrow smears. In *British journal of haematology* 57 (3), pp. 423–430. DOI: 10.1111/j.1365-2141.1984.tb02916.x.

Trischler, Jordis; Shiomi, Takayuki; Turner, Damian L.; Sklepkiewicz, Piotr L.; Goldklang, Monica P.; Tanaka, Kenji F. et al. (2016): Immune Modulation of the T Cell Response in Asthma through Wnt10b. In *American journal of respiratory cell and molecular biology* 54 (4), pp. 584–593. DOI: 10.1165/rcmb.2014-0425OC.

Turner, Russell T.; Martin, Stephen A.; Iwaniec, Urszula T. (2018): Metabolic Coupling Between Bone Marrow Adipose Tissue and Hematopoiesis. In *Current osteoporosis reports* 16 (2), pp. 95–104. DOI: 10.1007/s11914-018-0422-3.

Tzeng, Yi-Shiuan; Li, Hung; Kang, Yuan-Lin; Chen, Wen-Cheng; Cheng, Wei-Cheng; Lai, Dar-Ming (2011): Loss of Cxcl12/Sdf-1 in adult mice decreases the quiescent state of hematopoietic stem/progenitor cells and alters the pattern of hematopoietic regeneration after myelosuppression. In *Blood* 117 (2), pp. 429–439. DOI: 10.1182/blood-2010-01-266833.

Valent, Peter (2019): ICUS, IDUS, CHIP and CCUS: Diagnostic Criteria, Separation from MDS and Clinical Implications. In *Pathobiology : journal of immunopathology, molecular and cellular biology* 86 (1), p. 30. DOI: 10.1159/000489042.

van der Leun, Anne M.; Thommen, Daniela S.; Schumacher, Ton N. (2020): CD8+ T cell states in human cancer: insights from single-cell analysis. In *Nature reviews. Cancer* 20 (4), pp. 218–232. DOI: 10.1038/s41568-019-0235-4.

van Eden, Willem; van der Zee, Ruurd; Prakken, Berent (2005): Heat-shock proteins induce T-cell regulation of chronic inflammation. In *Nature reviews. Immunology* 5 (4), pp. 318–330. DOI: 10.1038/nri1593.

Vandoorne, Katrien; Rohde, David; Kim, Hye-Yeong; Courties, Gabriel; Wojtkiewicz, Gregory; Honold, Lisa et al. (2018): Imaging the Vascular Bone Marrow Niche During Inflammatory Stress. In *Circulation research* 123 (4), pp. 415–427. DOI: 10.1161/CIRCRESAHA.118.313302.

Vercauteren, Suzanne M.; Starczynowski, Daniel T.; Sung, Sandy; McNeil, Kelly; Salski, Chris; Jensen, Clara-Lynn et al. (2012): T cells of patients with myelodysplastic syndrome are frequently derived from the malignant clone. In *British journal of haematology* 156 (3), pp. 409–412. DOI: 10.1111/j.1365-2141.2011.08872.x.

Volarevic, Vladislav; Al-Qahtani, Ahmed; Arsenijevic, Nebojsa; Pajovic, Sladjana; Lukic, Miodrag L. (2010): Interleukin-1 receptor antagonist (IL-1Ra) and IL-1Ra producing mesenchymal stem cells as modulators of diabetogenesis. In *Autoimmunity* 43 (4), pp. 255–263. DOI: 10.3109/08916930903305641.

Wang, Shan; Mo, Miaohua; Wang, Jinmei; Sadia, Sobia; Shi, Bihua; Fu, Xiaobing et al. (2018): Platelet-derived growth factor receptor beta identifies mesenchymal stem cells with enhanced engraftment to tissue injury and pro-angiogenic property. In *Cellular and molecular life sciences : CMLS* 75 (3), pp. 547–561. DOI: 10.1007/s00018-017-2641-7.

Wang, Wei; Zhong, Yu; Zhuang, Zhenkun; Xie, Jiarui; Lu, Yueer; Huang, Chengzhi et al. (2021): Multiregion single-cell sequencing reveals the transcriptional landscape of the immune microenvironment of colorectal cancer. In *Clinical and translational medicine* 11 (1), e253. DOI: 10.1002/ctm2.253.

Weaver, Casey T.; Harrington, Laurie E.; Mangan, Paul R.; Gavrieli, Maya; Murphy, Kenneth M. (2006): Th17: an effector CD4 T cell lineage with regulatory T cell ties. In *Immunity* 24 (6), pp. 677–688. DOI: 10.1016/j.immuni.2006.06.002.

Webber, Elizabeth; Li, Lian; Chin, Lih-Shen (2008): Hypertonia-associated protein Trak1 is a novel regulator of endosome-to-lysosome trafficking. In *Journal of molecular biology* 382 (3), pp. 638–651. DOI: 10.1016/j.jmb.2008.07.045.

Weickert, Marie-Theresa; Hecker, Judith S.; Buck, Michèle C.; Schreck, Christina; Rivière, Jennifer; Schiemann, Matthias et al. (2021): Bone marrow stromal cells from MDS and AML patients show increased adipogenic potential with reduced Delta-like-1 expression. In *Scientific reports* 11 (1), p. 5944. DOI: 10.1038/s41598-021-85122-8.

Welsh, Raymond M.; Bahl, Kapil; Marshall, Heather D.; Urban, Stina L. (2012): Type 1 interferons and antiviral CD8 T-cell responses. In *PLoS pathogens* 8 (1), e1002352. DOI: 10.1371/journal.ppat.1002352.

Williams, S. J.; Farrell, G. C. (1986): Inhibition of antipyrine metabolism by interferon. In *British journal of clinical pharmacology* 22 (5), pp. 610–612. DOI: 10.1111/j.1365-2125.1986.tb02943.x.

Wobus, Manja; Mies, Anna; Asokan, Nandini; Oelschlägel, Uta; Möbus, Kristin; Winter, Susann et al. (2021): Luspatercept restores SDF-1-mediated hematopoietic support by MDS-derived mesenchymal stromal cells. In *Leukemia* 35 (10), pp. 2936–2947. DOI: 10.1038/s41375-021-01275-5.

Wolock, Samuel L.; Krishnan, Indira; Tenen, Danielle E.; Matkins, Victoria; Camacho, Virginia; Patel, Sweta et al. (2019): Mapping Distinct Bone Marrow Niche Populations and Their Differentiation Paths. In *Cell reports* 28 (2), 302-311.e5. DOI: 10.1016/j.celrep.2019.06.031.

Woods, Kevin; Guezguez, Borhane (2021): Dynamic Changes of the Bone Marrow Niche: Mesenchymal Stromal Cells and Their Progeny During Aging and Leukemia. In *Frontiers in cell and developmental biology* 9, p. 714716. DOI: 10.3389/fcell.2021.714716.

Wu, Yuenv; Aanei, Carmen Mariana; Kesr, Sanae; Picot, Tiphanie; Guyotat, Denis; Campos Catafal, Lydia (2017): Impaired Expression of Focal Adhesion Kinase in Mesenchymal Stromal Cells from Low-Risk Myelodysplastic Syndrome Patients. In *Frontiers in oncology* 7, p. 164. DOI: 10.3389/fonc.2017.00164.

Xie, Hui; Cui, Zhuang; Wang, Long; Xia, Zhuying; Hu, Yin; Xian, Lingling et al. (2014): PDGF-BB secreted by preosteoclasts induces angiogenesis during coupling with osteogenesis. In *Nature medicine* 20 (11), pp. 1270–1278. DOI: 10.1038/nm.3668.

Xing, Tong; Lyu, Zhong-Shi; Duan, Cai-Wen; Zhao, Hong-Yan; Tang, Shu-Qian; Wen, Qi et al. (2022): Dysfunctional bone marrow endothelial progenitor cells are involved in patients with myelodysplastic syndromes. In *Journal of translational medicine* 20 (1), p. 144. DOI: 10.1186/s12967-022-03354-2.

Xu, Chunliang; Gao, Xin; Wei, Qiaozhi; Nakahara, Fumio; Zimmerman, Samuel E.; Mar, Jessica; Frenette, Paul S. (2018): Stem cell factor is selectively secreted by arterial endothelial cells in bone marrow. In *Nature communications* 9 (1), p. 2449. DOI: 10.1038/s41467-018-04726-3.

Yamashita, Masayuki; Passegué, Emmanuelle (2019): TNF-α Coordinates Hematopoietic Stem Cell Survival and Myeloid Regeneration. In *Cell stem cell* 25 (3), 357-372.e7. DOI: 10.1016/j.stem.2019.05.019.

Yamazaki, Satoshi; Ema, Hideo; Karlsson, Göran; Yamaguchi, Tomoyuki; Miyoshi, Hiroyuki; Shioda, Seiji et al. (2011): Nonmyelinating Schwann cells maintain hematopoietic stem cell hibernation in the bone marrow niche. In *Cell* 147 (5), pp. 1146–1158. DOI: 10.1016/j.cell.2011.09.053.

Yoon, D. S.; Choi, Y.; Lee, J. W. (2016): Cellular localization of NRF2 determines the self-renewal and osteogenic differentiation potential of human MSCs via the P53-SIRT1 axis. In *Cell death & disease* 7 (2), e2093. DOI: 10.1038/cddis.2016.3.

Zaiss, Dietmar M. W.; van Loosdregt, Jorg; Gorlani, Andrea; Bekker, Cornelis P. J.; Gröne, Andrea; Sibilia, Maria et al. (2013): Amphiregulin enhances regulatory T cell-suppressive function via the epidermal growth factor receptor. In *Immunity* 38 (2), pp. 275–284. DOI: 10.1016/j.immuni.2012.09.023.

Zhang, Jia-Min; Feng, Fei-Er; Wang, Qian-Ming; Zhu, Xiao-Lu; Fu, Hai-Xia; Xu, Lan-Ping et al. (2016): Platelet-Derived Growth Factor-BB Protects Mesenchymal Stem Cells (MSCs) Derived From Immune Thrombocytopenia Patients Against Apoptosis and Senescence and Maintains MSC-Mediated Immunosuppression. In *STEM CELLS Translational Medicine* 5 (12), pp. 1631–1643. DOI: 10.5966/sctm.2015-0360.

Zhang, Pan; Li, Xiang; Pan, Chengwei; Zheng, Xinmin; Hu, Bohan; Xie, Ruiheng et al. (2022a): Single-cell RNA sequencing to track novel perspectives in HSC heterogeneity. In *Stem cell research & therapy* 13 (1), p. 39. DOI: 10.1186/s13287-022-02718-1.

Zhang, Yudi; Wu, Junying; Qin, Tiejun; Xu, Zefeng; Qu, Shiqiang; Pan, Lijuan et al. (2022b): Comparison of the revised 4th (2016) and 5th (2022) editions of the World Health Organization classification of myelodysplastic neoplasms. In *Leukemia* 36 (12), pp. 2875–2882. DOI: 10.1038/s41375-022-01718-7.

Zhao, Ende; Xu, Huanbin; Wang, Lin; Kryczek, Ilona; Wu, Ke; Hu, Yu et al. (2012): Bone marrow and the control of immunity. In *Cellular & molecular immunology* 9 (1), pp. 11–19. DOI: 10.1038/cmi.2011.47.

Zhao, Meng; Perry, John M.; Marshall, Heather; Venkatraman, Aparna; Qian, Pengxu; He, Xi C. et al. (2014): Megakaryocytes maintain homeostatic quiescence and promote post-injury regeneration of hematopoietic stem cells. In *Nature medicine* 20 (11), pp. 1321–1326. DOI: 10.1038/nm.3706.

Zhou, Bo O.; Yue, Rui; Murphy, Malea M.; Peyer, James G.; Morrison, Sean J. (2014): Leptin-receptor-expressing mesenchymal stromal cells represent the main source of bone formed by adult bone marrow. In *Cell stem cell* 15 (2), pp. 154–168. DOI: 10.1016/j.stem.2014.06.008.

Zhu, Jiang; Garrett, Russell; Jung, Younghun; Zhang, Yi; Kim, Nacksung; Wang, Jingcheng et al. (2007): Osteoblasts support B-lymphocyte commitment and differentiation from hematopoietic stem cells. In *Blood* 109 (9), pp. 3706–3712. DOI: 10.1182/blood-2006-08-041384.

Zioni, N.; Bercovich, A.; Chapal-Ilani, N.; Solomon, A.; Kopitman, E.; Sacma, M. et al. (2022): Inflammatory signals from fatty bone marrow supports the early stages of DNMT3a driven clonal hematopoiesis (77).

Zou, Linhua; Barnett, Brian; Safah, Hana; Larussa, Vincent F.; Evdemon-Hogan, Melina; Mottram, Peter et al. (2004): Bone marrow is a reservoir for CD4+CD25+ regulatory T cells that traffic through CXCL12/CXCR4 signals. In *Cancer research* 64 (22), pp. 8451–8455. DOI: 10.1158/0008-5472.CAN-04-1987.